4-18-2011 12:00 AM

Biological Nutrient Removal from Municipal and Industrial Wastewater Using a Twin Circulating Fluidized Bed Bioreactor

Mehran Andalib
University of Western Ontario

Supervisor
Professor Jesse Zhu
The University of Western Ontario Joint Supervisor
Professor George Nakhla
The University of Western Ontario

Graduate Program in Chemical and Biochemical Engineering
A thesis submitted in partial fulfillment of the requirements for the degree in Doctor of Philosophy

Biological Nutrient Removal from Municipal and Industrial Wastewater Using a Twin Circulating Fluidized Bed Bioreactor

(Spine title: Biological Nutrient Removal Using a TCFBBR)
(Thesis format: Integrated Article)

by

Mehran Andalib

Graduate Program in Engineering Science
Department of Chemical and Biochemical Engineering

A thesis submitted in partial fulfillment
of the requirements for the degree of
Doctor of Philosophy

The School of Graduate and Postdoctoral Studies
The University of Western Ontario
London, Ontario, Canada

THE UNIVERSITY OF WESTERN ONTARIO
School of Graduate and Postdoctoral Studies

CERTIFICATE OF EXAMINATION

Joint-Supervisors

_____
Dr. George Nakhla

_____
Dr. Jesse Zhu

Examiners

_____
Dr. Sudhir Murthy

_____
Dr. Ernest Yanful

_____
Dr. Amarjeet Bassi

_____
Dr. Mita Ray

The thesis by

Mehran Andalib

entitled:

Biological Nutrient Removal From Municipal And Industrial Wastewater Using A Twin Circulating Fluidized Bed Bioreactor

is accepted in partial fulfillment of the
requirements for the degree of
Doctor of Philosophy

_____
Date

_____
Chair of the Thesis Examination Board

Abstract

Biological nutrient removal (BNR) refers to removal of carbon (C), nitrogen (N) and phosphorus (P) from wastewater (WW) by the aid of various microorganisms. Because of the public concern for the environment C, N and P effluent standards have become stricter. Different BNR processes such as suspended growth and attached growth have been studied during the last three decades in order to meet the increasingly stringent discharge standards.

In this work, two novel processes called Twin Fluidized Bed Bioreactor (TFBBR) and Twin Circulating Fluidized Bed Bioreactor (TCFBBR) were developed and tested for BNR from municipal WW. Both TFBBR and TCFBBR comprise of an anoxic column and an aerobic column with particle recirculation between the two reactors achieved mechanically (TFBBR) and hydraulically (TCFBBR). Moreover, a newly developed system called Anaerobic Fluidized-Circulating Fluidized Bed Bioreactor (AF-CFBBR) was developed and tested to accomplish BNR from high strength industrial WW. AF-CFBBR comprises of an anaerobic, an anoxic and an aerobic columns. In all three aforementioned systems, fine carrier media are employed for biofilm attachment. After the development of biofilm, the particles are called biofilm-coated particles.

TFBBR and TCFBBR were operated at organic, nitrogen and phosphorus loading rates (OLR, NLR and PLR) of up to 2.8 kg COD/m^3·d and 4.5 kg COD/m^3·d, 0.3 kg N/m^3·d and 0.5 kg N/m^3·d and 0.041 kg P/m^3·d respectively to study the performance of the system with respect to biological nutrient removal. The nitrification rates based on biofilm surface area in TFBBR and TCFBBR were 0.91 g N/m^2·d and 1.26 g N/m^2·d respectively and the denitrification rates based on biofilm surface area in TFBBR and TCFBBR were 0.65 g N/m^2·d and 1.32 g N/m^2·d respectively. Both systems removed >96% organic matter, 84%-88% nitrogen and 12%-50% phosphorus at overall hydraulic retention time of (HRT) 2h. TFBBR and TCFBBR achieved long SRTs of 72-108 d and 37-40 d respectively, which rationalized the very low observed yield of 0.06-0.07 g VSS/g COD and 0.09-0.1 g VSS/g COD. The AF-CFBBR demonstrated 99.7% COD removal, 84% nitrogen removal, with a very low sludge yield of 0.017 g VSS/g COD while treating a wastewater containing 10700 mg COD/L and 250-300 mg NH_3-N/L. The system was operated at an organic loading rate (OLR) of 35 kg COD/m^3·d based on the AF volume and 1.1 kg N/m^3·d based on the CFBBR

at an overall HRT of less than 12 h in the AF-CFBBR. The nitrification, denitrification and organic removal rates based on aerobic, anoxic and anaerobic biofilm surface area in AF-CFBBR respectively were 2.6 g $N/m^2 \cdot d$, 9.03 g $N/m^2 \cdot d$ and 12.1 g $COD/m^2 \cdot d$. Additionally, the inhibitory effect of nitrate on methanogenic activities in a high rate anaerobic fluidized bed with organic loading rate of above 35 kg $COD/m^3 \cdot d$ was studied in order to evaluate the feasibility of simultaneous denitrification and methanogenic activities (SDM) in a high rate anaerobic system.

Terminal settling velocity and bed expansion of biofilm-coated particles as the two main hydrodynamic criteria in a fluidized bed, were studied. Archimedes was superior to Reynolds number for drag coefficient and bed expansion definitions. A new equation for determining drag force on fluidized bed bio-film coated particle (F_d) as an explicit function of terminal settling velocity was generated based on Archimedes numbers (Ar) of the biofilm coated particle. The proposed equation adequately predicted the terminal settling velocity of other literature data with an accuracy of >90%. A new equation based on Archimedes number was proposed to calculate bed expansion index of biofilm-coated particles, which predicted the existing experimental data with less standard error than all other literature equations that related bed expansion to Reynolds number.

A two-phase and three-phase predictive fluidization model based on the characteristics of a system such as media type and size, flow rates, and reactor cross sectional area was proposed to calculate bed expansion, solid, liquid and gas hold up, specific surface area of the biofilm particles. The model was subsequently linked to 1d AQUIFAS APP software (Aquaregen*)* to model two and three phase fluidized bed bioreactors. The model was validated for biological nutrient removal using the experimental data from a Twin Circulating Fluidized Bed Bioreactors (TCFBBR) treating synthetic and municipal wastewater. Two-sided t-tests showed that there were no statistically significant difference between the experimental and the modeled TCOD, SCOD, NH_3-N, NO_x-N.

Key Words: Twin circulating fluidized bed bioreactor, Twin circulating fluidized bed bioreactor, biofilm-coated particles, drag coefficient, biological nutrient removal, terminal settling velocity, bed expansion index, mathematical modeling

Co-Authorship Statement

Chapter 4: Terminal Settling Velocity and Drag Coefficient of Biofilm-coated Particles at High Reynolds Number

Andalib M, Zhu, J, Nakhla G.

Published in *AICHE* 2010; 56-10:2598-2606

The primary author of this chapter was M. Andalib under supervision of Professor Nakhla and Professor Zhu

Chapter 5: New Definition of Bed Expansion Index for Fluidized Biofilm-coated Particles

Andalib M, Zhu J, Nakhla G.

Under peer review *Chemical Engineering Journal* 2011

The primary author of this chapter was M. Andalib under supervision of Professor Nakhla and Professor Zhu

Chapter 6: Biological Nutrient Removal Using a Novel Laboratory-scale Twin Fluidized Bed Bioreactor (TFBBR)

Andalib M, Nakhla G, Zhu J.

Published in *Chemical Engineering and Technology* 2010; 33-7:1125-1136

The primary author of this chapter was M. Andalib under supervision of Professor Nakhla and Professor Zhu

Chapter 7: Dynamic Testing of Twin Circulating Fluidized Bed Bioreactor (TCFBBR) for Nutrient Removal from Municipal Wastewater

Andalib M, Nakhla G, Zhu J.

Published in *Chemical Engineering Journal* 2010; 162-2:616-625

The primary author of this chapter was M. Andalib under supervision of Professor Nakhla and Professor Zhu

Chapter 8: Evaluation of Biological Nutrient Removal from Wastewater by Twin Circulating Fluidized Bed Bioreactor (TCFBBR) Using a Predictive Fluidization Model and AQUIFAS APP

Andalib M, Nakhla G, Sen D, Zhu J.

Published in *Bioresource Technology* 2011; 102-3:2400-2410

The primary author of this chapter was M. Andalib under supervision of Professor Nakhla and Professor Zhu

Chapter 9: Comparative Modeling of Biological Nutrient Removal from Landfill Leachate Using a Circulating Fluidized Bed Bioreactor

Eldyasti A, Andalib M, Hafez H, Nakhla G, Zhu J.

Published in *Hazardous Material* 2011

M. Andalib was the secondary author of this chapter and responsible for the AQUIFAS simulation. The work was under supervision of Professor Nakhla and Professor Zhu.

Chapter 10: Simultaneous Denitrification and Methanogenesis (SDM): Review of Two-decade Research

Andalib M, Nakhla G, McIntee E, Zhu J.

Under peer review *Desalination*

The primary author of this chapter was M. Andalib under supervision of Professor Nakhla and Professor Zhu

Chapter 11: High Rate Biological Nutrient Removal from High Strength Wastewater Using Anaerobic-Circulating Fluidized Bed Bioreactor (AF-CFBBR)

Andalib M, Nakhla G, Zhu J.

Under peer review *Environmental Science and technology*

The primary author of this chapter was M. Andalib under supervision of Professor Nakhla and Professor Zhu

Acknowledgments

This thesis would not have been possible without the help, support and patience of my supervisors, Prof. George Nakhla and Prof. Jesse Zhu, not to mention their advice and unsurpassed knowledge. The good advice, support and friendship of my supervisors have been invaluable on both an academic and a personal level, for which I am extremely grateful. I was extraordinarily fortunate in having Professor George Nakhla and professor Jesse Zhu as my supervisors. Thank you.

I offer my regards and blessings to my supervisor from my MSc., Dr. Farshad Nourai, and my colleagues, Ahmed Eldyasti, Ming Li, Sayed Elbeshbishi, Hisham Hafez and Pegah Saremi who supported me in every respect during the completion of this project. I would like to thank Joanna Blom, Mr. Wen, Michael Zhu, George Zhang, Mike Gaylard and Soheil Afara for their timely support.

I would like to thank the University of Western Ontario, Natural Sciences and Engineering Research Council of Canada (NSERC), Ontario Centre of Excellence (OCE), The Government of Ontario and Trojan Technologies, London, Ontario for their financial support toward my studies and research.

I am extremely thankful to my cousins Kavoos and Kiomars Soofi and family who supported me throughout this journey.

I would like to express my deepest appreciation to my wife, Sarah MacKenzie, for her understanding and love during the past few years. Her support and encouragement was in the end what made this dissertation possible.

Dedication

To

My wife, Sarah who bore with me

My dear dad, Dr. Mahmoud Andalib and
my dear mom Hadiseh Soofi, who inspired me

Table of Contents

List of Tables

List of Figures

List of Abbreviations and Symbols

A	column cross sectional area (L^2)
Ar	Archimedes number
BOD	biochemical oxygen demand (ML^{-3})
d_c	the diameter of column (L)
d_m	the volumetric equivalent diameter of the bare media (L)
d_p	the volumetric equivalent diameter of the biofilm coated particles (L)
C_d	drag coefficient for an isolated particle
COD	chemical oxygen demand (ML^{-3})
d	downer (when it is used as subscript)
D	effective diffusivity of substrate in the liquid phase (L^2T^{-1})
D_e, D_F	effective diffusivity of substrate in biofilm (L^2T^{-1})
F_b	buoyant force (MLS^{-2})
F_d	drag force on an isolated particle (MLS^{-2})
F_G	gravity force on an isolated particle (MLS^{-2})
f_d	fraction of biomass that remains as cell debris
g	gravitational constant (LS^{-2})
G	hydrodynamic shear coefficient (0-5)
h	height of expanded bed in a fluidized bed (L)
H_c	height of the columns (L)
H_{re}	estimated height of the expanded bed in the riser (L)
H_{de}	estimated height of the expanded bed in the downer (L)
H_r	height of the expanded bed in the riser (L)
H_d	height of the expanded bed in the downer (L)
HRT	hydraulic retention time (T)

k	Mean wake-to-bubble ratio
k_{d_r}	detachment rate coefficient in the downer (T^{-1})
k_{d_d}	detachment rate coefficient in the downer (T^{-1})
k_o	Intrinsic zero order rate constant ($MM^{-1}T^{-1}$)
k_d	biomass decay-rate coefficient ($MM^{-1}T^{-1}$)
$J_{F,i}$	mass flux of substrate of "I" into the biofilm ($ML^{-2}T^{-1}$)
M_d	mass of dry particles in the downer (M)
M_r	mass of dry particles in the riser (M)
N_d	number of particles in the downer
N_r	number of particles in the riser
NLR	nitrogen loading rate ($ML^{-3}T^{-1}$)
M, M_m	total weight of bare particle weight (M)
n	bed expansion index
Mn	media structure coefficient (0-5)
OLR	organic loading rate ($ML^{-2}T^{-1}$)
Re_t	Reynolds number at terminal settling velocity
r	riser (when it is used as subscript)
r_c	substrate penetration depth (L)
r_m	carrier media radius (L)
r_p	biofilm-coated particle radius (L)
$r_{F,i}$	rate of reaction for substrate i in the biofilm (MT^{-1})
S_r	the total surface area of the particles in the riser (L^2)
S_d	the total surface area of the particles in the downer (L^2)
S_r^*	specific surface area of the particles in the riser ($L^2 L^{-3}$)
S_d^*	specific surface area of the particles in the downer ($L^2 L^{-3}$)
S	Substrate concentration (ML^{-3})

S_b bulk liquid substrate concentration (ML^{-3})

S_0 concentration of initial SCOD in the SDNR batch test (ML^{-3})

$S_{in,i}$ inlet concentration of substrate "i" in the element (ML^{-3})

$S_{out,i}$ outlet concentration of substrate "i" in the element (ML^{-3})

SNR specific nitrification rate ($ML^{-3}d^{-1}$)

SDNR specific denitrification rate ($ML^{-3}d^{-1}$)

SMA specific methanogenic activity ($ML^{-3}d^{-1}$)

SRT sludge retention time (T)

t time (T)

TSS total suspended solids (ML^{-3})

u_l superficial liquid velocity in a fluidized bed (LS^{-1})

u_g superficial gas velocity in the downer (LS^{-1})

u_{mf} minimum fluidization velocity (LS^{-1})

u relative velocity of fluid and particle (LS^{-1})

u_t terminal settling velocity (LS^{-1})

U_d superficial liquid velocity in the downer (LS^{-1})

U_g superficial gas velocity in the downer (LS^{-1})

U_r superficial liquid velocity in the riser (LS^{-1})

V_m volume of wet particles (L^3)

V_r volume of expanded bed in the riser (L^3)

V_d volume of expanded bed in the downer (L^3)

V_L volume of liquid in each cell (L^3)

V_p particle volume (L^3)

VSS volatile suspended solids (ML^{-3})

X dry mass of biofilm / media diameter (MM^{-1})

X_o average attached biomass (mg) per volume reactor (ML^{-3})

X_{waste} average biomass wasted per day (MT^{-1})

X' biomass volumetric concentration (ML^{-3})

X'_r Biomass concentration in the riser (ML^{-3})

X'_d Biomass concentration in the downer (ML^{-3})

X_i Concentration of particulate "i" in the element (mg/L)

Y biomass true yield (MM^{-1})

Y_{obs} biomass observed yield (MM^{-1})

Q flow rate (L^3T^{-1})

Greek letters

α, β constant coefficients

ε voidage

ε_l liquid holdup

ε_g gas holdup

ε_s solid holdup

ε_{mf} voidage at minimum superficial liquid velocity

δ biofilm thickness (L)

γ biofilm-coated particle diameter / media diameter = d_p / d_m

μ_l liquid dynamic viscosity ($M\ L^{-1}S^{-1}$)

ρ_a true dry density of bacteria (ML^{-3})

ρ_b fluidized bed suspension density= $= \rho_P \times (1-\varepsilon) + \rho_l \times \varepsilon$ (ML^{-3})

ρ_m true density of media (ML^{-3})

ρ_d biofilm dry density (ML^{-3})

ρ_p biofilm coated particle effective density (ML^{-3})

ρ_l liquid density (ML^{-3})

ρ_w biofilm wet density (ML^{-3})

ρ_{pr} biofilm coated particle density in the riser (ML^{-3})

ρ_{pd} biofilm coated particle density in the downer (ML^{-3})

ρ_{mt} true particle density (ML^{-3})

ρ_{mw} wet particle density (ML^{-3}) $= \rho_{mt} \times (1 - \psi_i) + \rho_l \times \psi_i$

ρ_{md} dry bulk density (ML^{-3})

η_0 bioparticle zero-order effectiveness factor

Φ_{0m} modified zero-order Thiele modulus

ϕ_s Sphericity of particles

ψ_t total porosity of the bare particles (i.e. 0.62)

ψ_i internal porosity of the bare particles (i.e. 0.18)

1 Introduction

1.1 Rationale

In response to increasingly stringent effluent nutrient criteria as a result of deteriorating surface water quality, biological nutrient removal (BNR) processes have become increasingly popular recently. [1, 2] In addition, since only 10% of potable water currently used for domestic purpose, water experts worldwide are trying to conserve potable water by recycling water in industrial and agricultural applications. [3]

Biological nutrient removal (BNR) processes are modifications of the activated sludge process that incorporate aerobic with anoxic and /or anaerobic zones to provide nitrogen and/or phosphorus removal. BNR processes are known to offer several advantages over the conventional activated sludge processes, namely superior effluent quality, a significant reduction in aeration energy requirements due to utilization of formed nitrates to reduce organic matter, improved sludge settling characteristics, a reduction in sludge quantities due to lower bacterial yields in the anoxic tanks, and the elimination/minimization of chemical sludge. Consequently these BNR processes offer significant savings in both capital and operation/maintenance cost, in addition to the technical advantages of BNR over conventional activated sludge systems, and their ability to meet stringent total nitrogen and phosphorous effluent criteria. Incomplete denitrification and low food to microorganisms (S/X) ratio have been observed to cause filamentous bulking conditions in BNR activated sludge systems. [4] In some cases, external sources of carbon may be required to achieve phosphorus and nitrogen removal, because of low concentrations of readily biodegradable organics. In view of the aforementioned shortcomings of the suspended growth BNR processes, there is a need to develop more effective wastewater treatment processes for biological nutrient removal.

There have been few studies to integrate biological nutrient removal (BNR) processes with attached growth processes such as fluidized bed bioreactors. [5-7] The BNR capability of airlift technology has also been studied. [7] Research on Biofilm Airlift

Suspension (BAS) reactors in the late 1980s led to the concept of CIRCOX® airlift reactor which was also integrated for nitrogen removal. [9-10]

An extensive use of fluidized bed-bioreactors in various biotechnology processes e.g. fermentation, production of enzymes, production of primary and secondary metabolites, production of antibiotics and bioconversions have been reported for the following advantages. [11-14]

I. Compact reactors with lower volumes, i.e. much smaller "footprint" than suspended growth systems. Typically, the fluidized bed bioreactors occupy about 10-30% of the space required by continuously stirred tank reactors of similar capacities
II. The process can be operated at high biomass concentration and mass transfer area resulting in high conversion capacities. These systems facilitate biomass concentrations, ranging from 15,000 mg/L in aerobic fluidized bed to 40,000 mg/L in anoxic fluidized bed
III. Due to high biomass retention, the system can better handle dynamic loading conditions than activated sludge
IV. Lower sludge production; this is significant in light of the high sludge management costs. It should be noted that sludge handling costs account for 50%-60% of the overall treatment costs
V. Fluidization overcomes operating problems such as bed clogging and high pressure drop which would occur if small media were employed in biofilm reactors
VI. Secondary clarification can be reduced or may even become unnecessary since excess waste sludge is removed from the waste system.

The circulating fluidized bed bioreactor (CFBBR) involving biofim-coated particle recirculation between the anoxic and aerobic bioreactors, was introduced and developed by Nakhla and his colleagues [7, 15-18] to combine the advantages of BNR and biofilm reactors in both lab and pilot scales. While the CFBBR has successfully incorporated fluidized bed systems with BNR, the required height of 5.5 m makes it difficult to retrofit an existing plant. Therefore, a new twin fluidized bed bioreactor (TFBBR) and a new

twin circulating fluidized bed bioreactor (TCFBBR) have been developed wherein both the riser and downer with the same size operated in a conventional fluidization mode and particle recirculation was achieved mechanically thus eliminating of a riser separator in the CFBBR.

1.2 Objectives

This research was conducted to study the possibility of retrofitting the existing wastewater treatment plants by liquid solid circulating fluidized bed bioreactor (LSCFB) technology, previously patented by Nakhla and his co-workers and studied in this research group. LSCFB was comprised of a riser and downer equipped with two separators on top of each column. The configuration of LSCFB as well as the height of the riser were not conducive to easily retrofit rectangular tanks. Twin circulating fluidized bed (TFBBR) and Twin circulating fluidized bed comprise rectangular columns with the same height were developed to investigate biological nutrient removal (BNR) capability from municipal wastewater. In addition, a new system consisting of a conventional strict anaerobic fluidized bed and circulating fluidized bed (AF-CFBBR) was developed to study BNR from high strength industrial wastewater streams. While the focus of this work was predominantly on process development, in order to further process understanding, the experimental progress was complemented by both hydrodynamic testing of biofilm-coated particles and process modeling for various wastes. Thus, the specific objectives of this work were: Process development (I, II, VI), hydrodynamics (III, IV) and modeling (V, VII)

I. To first study biological nutrient removal capability and further to investigate retrofitting existing wastewater treatment plants by a newly developed TFBBR for the purpose of biological nutrient removal from municipal wastewater as well as to investigate the fate of nutrients in the system

II. To demonstrate a TCFBBR in biological nutrient removal from municipal wastewater as well as study the sustainability of TCFBBR, in terms of nitrification-denitrification, tested at a hydraulic peaking factor of 4 for 3 hours, and to a carbon shock test

III. To study the existing correlations of drag coefficients in the literature for biofilm-coated particles with high terminal settling velocity Reynolds number and propose a new equation

IV. To examine the proposed equations in the literature for bed expansion index of biofilm-coated particles and propose a new equation based on Archimedes number

V. To develop a predictive fluidization model and link it to AQUIFAS APP, a diffusional simulation software to predict biological nutrient removal in particulate biological systems.

VI. To examine a newly developed anaerobic fluidized-CFBBR for BNR purposes from high strength industrial wastewater

VII. To develop, calibrate and compare BNR simulation from landfill leachate by BioWin and AQUIFAS considering biofilm diffusion and kinetics to further use if to predict the process performance

1.3 Thesis Organization

After the introductory chapter 1, a comprehensive literature review on hydrodynamics of liquid-solid and gas-liquid-solid fluidization and particularly on hydrodynamics of biofilm-coated particles, biological nutrient removal, conventional and innovative nitrogen removal as well as comparative study of different attached-growth technologies is presented in chapter 2. In chapter 3, the detailed descriptions of materials and methodology used throughout this work are explained.

Chapter 4 discusses the terminal settling velocity and drag coefficient of biofilm-coated particles at higher Reynolds number than what had been proposed in the literature. In this chapter the authors demonstrate that drag coefficient for falling particles should be defined rather as a function of Archimedes number than Reynolds. In this chapter a new correlation for drag coefficient for biofilm-coated particles was proposed which could predict all other experimental data in the literature with a statistical error of less than 10%. Following chapter 4, the bed expansion index for fluidized biofilm-coated particles

is studied in chapter 5, where it is demonstrated that bed expansion index should be defined as a function of Ar as well. In this chapter a correlation for bed expansion index is proposed based on Ar, which predicts the existing experimental data in the literature with 90% precision.

In chapter 6, the performance of twin fluidized bed bioreactor (TFBBR) is presented for biological nutrient removal from synthetic wastewater at different organic and nutrient loading rates to determine the optimum process design loadings. Chapter 7 focused on investigating the BNR capacity of twin circulating fluidized bed bioreactor (TCFBBR) from both synthetic and municipal wastewater and to examine the sustainability of the system against dynamic loading and carbon shock loadings.

Chapters 8 and 9 concentrate on mathematical modeling and simulation of biological nutrient removal using the aforementioned technologies by the most used simulation software in the market for fixed-film processes, BioWin and AQUIFAS. Since none of these simulators are capable of simulating fluidized bed systems, a predictive fluidization model was developed in chapter 8 based on the proposed correlation of biofilm-coated particle drag coefficient by this work. This model could numerically calculate the specific surface area and volume of each biological cell based on the operational and physical characteristics of the system. The output of the model was used directly in AQUIFAS to model BNR and a new biofilm thickness which was used further in the predictive fluidization model to run the loop to converge. In chapter 9, however, the focus of the work was mainly on the incorporation of the complexity of leachate characteristics into the two different simulators and investigate whether they can model BNR from leachate in a LSCFBR system.

Chapter 10 studies over 74 references on simultaneous denitrification and methanogenesis (SDM) in a single strict anaerobic system to investigate the feasibility of SDM in real wastewater plants. A newly developed system called anaerobic fluidized-circulating fluidized bed bioreactor (AF-CFBBR) was designed and developed to study high rate biological nutrient removal from high strength industrial wastewater. Chapter 11 shows the BNR performance of AF-CFBBR in different phases with different organic

and nitrogen loading rates. In this chapter simultaneous denitrification and methanogenesis was studied in a high rate anaerobic fluidized bed at an organic loading rate of > 35 kg COD/m^3·d.

Chapter 12 presents a general discussion of this study on observed results and experiments. Finally, chapter 13 summarizes the major findings of this study with recommendations for continuous improvement of this novel technology.

1.4 Thesis Format

This thesis is prepared in an Integrated-Article manuscript format as specified in Thesis Regulation Guide by the School of Postgraduate Studies at the University of Western Ontario. Chapter 4 of this thesis in which M. Andalib was the primary author was published in AICHE 2010; 56-10:2598-2606. Chapter 5 in which M. Andalib was the primary author has been submitted to Chemical Engineering Journal. Chapter 6 of this work in which M. Andalib is the primary author was published in Chemical Engineering and Technology 2010; 33-7:1125-1136. Chapter 7 in which M. Andalib was the primary author was published in Chemical Engineering Journal 2010; 162-2:616-625. Chapter 8 of this thesis in which M. Andalib was the primary author was published Bioresource Technology 2011; 102-3:2400-2410. Chapter 9 was published in Hazardous Material 2011. M. Andalib was the secondary author of chapter 9. Chapter 9 in which M. Andalib was the primary author has been submitted to Desalination. Chapter 11, in which M. Andalib was the primary author has been prepared to be submitted to Environmental Science and Technology.

1.5 Reference

[1] van Loosdrecht MCM, Smolders GJF, Kuba Y, Heijnen JJ. Metabolism of microorganisms responsible for enhanced biological phosphorus removal from wastewater. Use of dynamic enrichments cultures. *Ant. Van Leeuwenhoek* 1997; 71, 109-116.

[2] Wentzel MC, Dold P, Ekama GA, Marais GVR. Kinetics of biological phosphorus release. *Water Sci. Technol*. 1985; 15:51-71.

[3] Metcalf, Eddy. Water Reuse: Issues, Technologies, and Applications. 1st Ed. McGraw-Hill, New York, 2007.

[4] Musvoto EV, Casey TG, Ekama GA, Wantzel MG, Marais GVR. The Effect of Incomplete Denitrification on Anoxic-Aerobic (Low F/m) Filament Bulkng in Nutrient Removal Activated Sludge Systems. *Water Sci. Technol.* 1994; 29:295-299.

[5] Borregaard VR. Experience with nutrient removal in a fixed-film system at full-scale wastewater treatment plants. Wat. Sci. Technol. 2000; 36-1:129–137.

[6] Sen P, Dentel SK. Simultaneous nitrification-denitrification in a fluidized bed reactor. Wat. Sci. Technol. 1998; 38:247-254.

[7] Chowdhury N, Nakhla G, Zhu J. Load maximization of a liquid-solid circulating fluidized bed bioreactor for nitrogen removal from synthetic municipal wastewater. Chemosphere 2008; 71:807-815.

[8] Eikelboom D, Kampf R, Van Voorneburg F. Biofilm formation in an airlift reactor for the sewage purification. H_2O_2 1987; 20:388-392.

[9] Nicolella C, van-Loosdrecht MCM, Heijnen JJ. Wastewater treatment with particulate biofilm reactors. J. Biotechnol. 2000; 80:1-33.

[10] Frijters CTMJ, Eikelboom DH, Mulder A, Mulder R. Treatment of municipal wastewater in a CIRCOX airlift reactor with integrated denitrification. Wat. Sci. Technol. 1997; 36-1:173–181.

[11] Fahid K, Rabah J, Dahab MF. Nitrate removal characteristics of high performance fluidized-bed biofilm reactors. *Water Res.,* 2004; 38:3719-3728.

[12] Grady JCPL, Daigger GT, Lim HC. *Biological Wastewater Treatment*. New York: Marcel Dekker, 1999; 810-811.

[13] Mulcahy LT, Shieh WK. Fluidization and reactor biomass characteristics of denitrification fluidized bed biofilm reactor (FBBR). *Water Res.* 1987; 21:451-458.

[14] Shieh WK, Keenan DK. Fluidized bed biofilm reactor for wastewater treatment. In: Fiechter, A. (Ed.), Advances in Biochemical Engineering/Biotechnology. Springer-Verlag, Berlin, 1986; 132-168.

[15] Nakhla G, Zhu J, Cui Y. Liquid-solid circulating fluidized bed wastewater treatment system for simultaneous removal of carbon, nitrogen, and phosphorus. US patent no. 6,716,244, Int'l PCT patent awarded Aug. 2005.

[16] Cui Y, Nakhla G, Zhu J, Patel A. Simultaneous carbon and nitrogen removal in anoxic-aerobic circulating fluidized bed biological reactor (CFBBR). Environ. Technol. 2004; 25:699-712.

[17] Patel A, Zhu J, Nakhla G. Simultaneous carbon, nitrogen and phosphorus removal from municipal wastewater in a circulating fluidized bed bioreactor. Chemosphere 2006; 65:1103-1112.

[18] Chowdhury N. Biological nutrient removal from municipal wastewater using a liquid-solid circulating fluidized bed bioreactor. The University of Western Ontario. PhD dissertation 2009.

2 Literature Review

2.1 Introduction

Fluidization technology has a history of almost one century. Studies have long shown that fluidization provides many advantages to the processes, such as significantly enhanced mass and heat transfer rates, improved inter phase contact efficiency, ease in handling large quantity of particles, and a uniform temperature distribution. These characteristics have led to increased productivity and the wide application of fluidized bed reactors. [1] It started with gas-solid fluidization, and then extended to liquid-solid and gas-liquid-solid three-phase fluidization where different applications were encountered. From an industrial point of view, liquid-solid fluidization is becoming more and more important. Liquid-fluidized beds are widely used in hydrometallurgy and food technology, biochemical, water treatment, etc.

Many researchers have studied the conventional fluidization. [2] However there has not been significant research conducted into the effects of biofilms on the hydrodynamics of fluidized particles. It is generally accepted that liquid-solids fluidized bed expand in a homogeneous manner. A number of mathematical flow models have been proposed to predict the flow characteristics. Richardson and Zaki (1954) proposed a correlation, known as the Richardson and Zaki equation, to predict the relationship between the bed voidage and the liquid velocity in the conventional fluidized bed. This correlation has been found to be valid over a wide range of operating conditions, $\varepsilon < 0.85$, by many researchers and served as a "building block" for a number of models developed for liquid-solids fluidization. [2] In conventional liquid-solid particulate fluidization with low superficial liquid velocities, there clearly exists a dense bed region at the bottom and a freeboard region at above, devoid of solids. An increase of superficial liquid velocity causes significant particle entrainment.

Fluidization in the liquid-solid systems is controlled by the liquid flow rate. With increasing liquid flow rate, the liquid-solid system passes through several flow regimes: the fixed bed regime when liquid flow rate is lower than the minimum fluidization velocity, the conventional particulate fluidization regime where a clear boundary between the bottom dense region and the top freeboard region exists, and then the circulating fluidization regime. There is also a transition region from conventional fluidization to circulating fluidization regimes where the boundary between the two phases becomes unclear while the height of the dense phase increases further and some particles are transported out of the bed and it is essential to continuously feed particles into the riser bottom to maintain the bed.

2.2 Biofilm-coated Particles

2.2.1 Definition

A biofilm may be described as an assemblage of bacterial cells that is both enclosed by and attached to a wetted surface by means of an extracellular fibrous polysaccharide-containing matrix. This matrix, termed a glycocalyx [3], is synthesized by bacteria, and it serves, in part, to permanently anchor bacterial cells adsorbed to a substratum. [4] Wastewater biofilms may be more complex, however, than a simple assemblage of firmly attached bacterial cells; they may possess a thick, overlying, less firmly bound, filamentous bacterial component. [5] Development and attachment of biomass on a carrier media result in particles with carrier core covered by biofilm. Biofilm development is the difference between biofilm growth, attachment and detachment processes. In general, due to different physical properties of biofilm, development of biofilm will change physical properties of the particles (initially carrier media) such as size, overall density, and surface roughness. In a fluidized bed bioreactor, which employs biofilm-coated particles for the purpose of wastewater treatment, pollutant removal rates depend on particle properties, control of biofilm thickness, biomass concentrations in the bioreactors, interaction between various microbial groups, and substrate diffusion in biofilms. Stable granular biofilm is one of the perquisites of the efficient fluidized bed bioreactors, which can be ensured by maintaining smooth biofilm on the carrier particles. The balance between biofilm growth and detachment, determines the physical structure of the biofilm,

and thereby the settling and fluidization characteristics. [6] The solid surface on which the biofilm grows is called the substratum, and it normally represents a separate compartment in the biofilm system. The typical substratum is inert and impermeable. Rocks, sand, and plastic biofilm carriers are good examples of inert substrata. Nothing enters or leaves an inert substratum, and it also has no transformations. [7]

2.2.2 Biofilm Structure

Biofilms are very complex, both physically and microbiologically. [8] **Figure 2.1** depicts a biofilm-coated particle comprises of biofilm covered substratum as carrier media. The biofilm grows attached to a solid support, which is usually impermeable. In general, the biofilm can be divided into two zones, the base film and the surface film. Both contain a compilation of microorganisms and other particulate material bound together by a matrix of extracellular polymers, which are excreted by the microorganisms. [9]

The relative thicknesses of the base and surface film depend largely on the hydrodynamic characteristics of the system, but also on the nature of the microorganisms in the biofilm. Consequently, one biofilm may have almost no surface film whereas another may be entirely surface film. There is normally relative motion between the biofilm and the bulk liquid, with the one moving depending upon the configuration of the attached growth process. For example, in packed towers the bulk fluid moves down over the biofilm in a thin sheet, whereas in a rotating disc reactor the biofilm support moves through the bulk liquid. In either case, however, mass transfer from the bulk fluid to the biofilm depends on the hydrodynamic regime. [8]

Components in biofilm are divided into particulate and dissolved. Particulate components are the materials that form the biofilm solid phase, such as cells and EPS. They are physically attached to each other or to the substratum. However, particulate components such as cells can be found also suspended in the bulk liquid. Dissolved components are the dissolved species found in the biofilm liquid phase, such as substrates and metabolites. Dissolved components include substrates, metabolic intermediates, and various products of microbial conversion processes. [7]

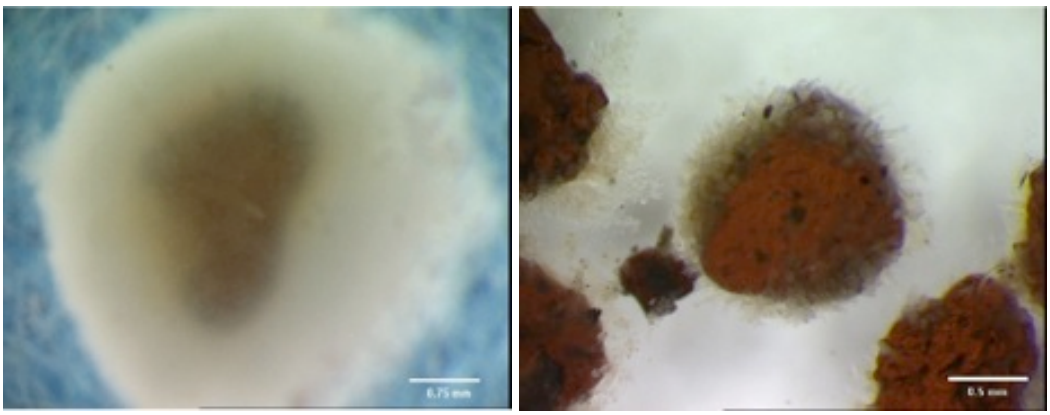

Figure 2.1. Biofilm-Coated Particles (Left: heterotrophic film, right: autotrophic film on Lava rock)

It is assumed that all types of bacteria are available for growth at any point within a biofilm, but that their ultimate distribution is determined by their competition for shared nutrients and space. [10] As substrate can only move into the biofilm by diffusion, a substrate concentration gradient will exist through the biofilm. This means that bacteria near liquid-biofilm interface are growing faster than those in the interior. However, as bacteria in the interior grow, they occupy more space, pushing those that are closer to the liquid-biofilm interface further away from the solid support. In addition, all of the bacteria are subject to decay, regardless of their position in the biofilm, resulting in the accumulation of the biomass debris. The net effect of both processes is to cause a migration of particles from the interior of the film to the exterior where surface shear forces remove them, allowing a biofilm of constant thickness to develop. [11]

2.2.3 Biofilm Formation and Detachment

Biofilm can form in various environments on the condition that a surface, nutrients and water are accessible. Studies show that the principle mode of microbial existence in most natural and synthetic environments is related to surface associated biofilms.

In ideally mixed reactors, formation of biofilm on carriers only takes place when the hydraulic retention time is less than the inverse of the maximum growth rate. [12] Tijhuis et al. (1994) reported a similar finding in their study i.e. formation of heterotrophic aerobic biofilms on small suspended basalt particles in airlift reactors for municipal

wastewater treatment. [13] Biofilm accumulation and detachment are strongly influenced by abrasion processes in the reactor, which are mainly due to particle attrition and interactions.

The influence of carrier type on adhesion and biofilm formation of pure and mixed cultures using suspended carriers were studied (standard, roughened, hydrophobic and positively charged glass beads, sand and basalt grains) in laboratory airlift reactors. [14] This study showed that hydrodynamic conditions and particle collisions control biofilm formation in airlift reactors. Increased surface roughness of the particles promoted biofilm accumulation, whilst the physico-chemical characteristics of the particles proved to be less important. [15]

Biofilm detachment refers to the interphase transport of biomass particles from an attached microbial film to the fluid compartment bathing the film. Although detachment has not been investigated extensively, it is the primary process that balances microbial growth and thereby, determines the steady state accumulation of biofilm and overall biofilm activity. [16]

The biofilm detachment rate is a complicated function of many variables, including hydrodynamics of the liquid flow, biofilm morphology, and support characteristics. [17] Biofilm detachment is a critical biofilm-loss mechanism that has been mostly quantified by a first-order rate coefficient, b_s. In principle, the function can be expressed in terms of the fundamental biofilm, support, and hydrodynamic variable likely to affect detachment:

$$b_s = f(\tau, X_f, \delta, \mu_t, C_p, \mathrm{Re}\ldots) \qquad (2.1)$$

where b_s is the biofilm detachment rate coefficient (day $^{-1}$), τ is the liquid shear stress (dyne /cm^2), δ is biofilm thickness (cm), X_f biofilm density (mg VS/cm^3), μ_t is the biofilm true growth rate (day^{-1}), C_p is the particle concentration (g/L), and Re is the Reynolds number. [17]

Based on experimental data and multiple linear regression analysis of X_f and δ against all the other independent variables, Chang et al. (1991) yielded the following two best descriptions:

$$X_f = -113.3 + 0.189\ C_p + 69.1\ \mathrm{Re} \qquad (2.2)$$

$$\delta = 131.1 - 0.131\ C_p - 64.4\ \mathrm{Re} \qquad (2.3)$$

The best proposed model by Chang et al. (1991) for describing how b_s varied contains C_p, Re, and τ was **Equation (2.4)**.

$$b_s = -3.14 + 0.0335\ C_p + 19.3\ \mathrm{Re} - 3.46\ \tau \qquad (2.4)$$

Bryers has distinguished five categories of detachment processes: erosion (removal of individual cells or small groups of cells from the surface of the biofilm), sloughing (detachment of relatively large particles of biomass), human intervention, predator grazing and abrasion. Whereas erosion can be viewed as a continuous process occurring uniformly over the surface of a biofilm, sloughing is more plainly a discrete process. [16] Other detachment processes, such as human intervention (e.g., scraping), predator grazing, and abrasion, are clearly the results of external forces acting on the biofilm.

A variety of empirical mathematical expressions to describe detachment rates have been developed. [16] **Equation (2.5)** is one commonly applied detachment model which assumes a first-order dependency of detachment rate on biofilm mass and thickness. [17, 18]

$$r_{di} = b_s \rho_i \delta \qquad (2.5)$$

where ρ_i is the density of component I in the biofilm and r_{di} is the detachment rate of component i.

Others have postulated that detachment rate is a power law or second-order function of biomass: [19]

$$r_{di} = b_s (\rho_i \delta)^2 \qquad (2.6)$$

Wanner and Gujer (1986) used a second-order function of biofilm thickness to model biofilm detachment in numerical simulation of multispecies population dynamics. [20]

$$r_{di} = b_s \rho_i \delta^2 \tag{2.7}$$

Rittmann (1982) developed simple equations for detachment rate coefficient in which shear stress was explicitly incorporated. When the biofilms are thin ($\delta < 30$ μm), b_s is related to the shear stress acting tangentially to the biofilm surface, and can be estimated using **Equation (2.8)** and **Equation (2.5)**.

$$b_s = 8.42 \times 10^{-2} \times \tau^{0.58} \tag{2.8}$$

$$\tau = \frac{\left[\left(\rho_P - \rho_w\right) \times \left(1 - \varepsilon\right) g\right]}{a} \tag{2.9}$$

$$b_s = 8.42 \times 10^{-2} \times \left(\frac{\tau}{1 + 433.2\,(\delta - 0.003)} \right) \tag{2.10}$$

where ρ_p and ρ_w are particle density and water density (g/cm^3), g is gravity (cm^2/s), ε is bed porosity, and a is specific surface area of biofilm carrier (cm^{-1}). In thick biofilm, the bacteria deep inside the biofilm are protected from detachment; b_s can be estimated using **Equation (2.10)**. [18]

A few models of detachment postulate a dependence on cellular physiology. Speitel and DiGiano suggested that growth rate in the biofilm influences detachment rates and have proposed **Equation (2.11)**. [21]

$$r_{di} = \delta\ (b_s + b_s' \mu) \tag{2.11}$$

2.2.4 Biofilm-coated Particle Size and Density

If we consider equivalent biofilm-coated particle diameter, d_p and equivalent clean particle diameter, d_m, the average bio-film thickness is:

$$\delta = \frac{d_p - d_m}{2} \tag{2.12}$$

Effective density of a biofilm-coated particle (ρ_p) can be defined as the average of the carrier media density and the biofilm wet density as below:

$$\rho_p = \frac{V_m \rho_{mw} + V_p \rho_w}{V_m + V_p} \tag{2.13}$$

where V_m and V_p are the volumes of clean and biofilm-coated particles respectively and ρ_{mw} and ρ_w are particles wet density and biofilm wet density.

$$\text{It is obvious that } V_m + V_p = \frac{4\pi}{3}\left(\frac{d_m}{2} + \delta\right)^3 \tag{2.14}$$

Substituting and rearranging the two above equations gives:

$$\rho_p = \rho_m \left(1 + 2\frac{\delta}{d_m}\right)^{-3} + \rho_w \left[1 - \left(1 + 2\frac{\delta}{d_m}\right)^{-3}\right] \tag{2.15}$$

Nicolella et al. (1999) suggested that the density of wet biomass can be estimated by adding the density of water (ρ_l) and the biofilm dry density (ρ_d) and ignoring the contribution of dry biofilm to the total volume. [22]

$$\rho_w \frac{g\left(VSS + H_2O\right)}{cm^3\, VSS} = 1.0 \frac{g\, H_2O}{cm^3\, VSS} + \rho_d \frac{g\, VSS}{cm^3\, VSS} \tag{2.16}$$

It has been experimentally found by different researchers that the density of dry biomass is a function of biofilm thickness, δ. Mulcahy and LaMotta (1978) proposed the following correlations: [23]

$$\begin{aligned} &\rho_d (mg/cm^3) = 65 && for\ \ 0 < \delta \le 300\,\mu m \\ &\rho_d (mg/cm^3) = 96.8 - 0.106\,\delta && for\ \ 300 < \delta \le 630\,\mu m \\ &\rho_d (mg/cm^3) = 30 && for\ \delta > 630\,\mu m \end{aligned} \tag{2.17}$$

Boaventura and Rodrigues (1988) fitted their experimental data and offered the following equations to calculate biofilm dry density: [24]

$$\begin{aligned} &\rho_d(mg/cm^3) = 104.3 - 0.1245\delta \quad for\ \ \delta < 620\,\mu m \\ &\rho_d(mg/cm^3) = 26.9 \qquad\qquad\ \ for\ \ \delta > 620\,\mu m \end{aligned} \tag{2.18}$$

Hermanowicz and Cheng (1990) proposed the following Equations: [25]

$$\begin{aligned} &\rho_{bd}(mg/cm^3) = 120\left(\frac{L_f}{180}\right)^{3.7} \qquad for\ \ L_f < 180\,\mu m \\ &\rho_{bd}(mg/cm^3) = 120\left(\frac{L_f}{180}\right)^{-1.8} \qquad for\ \ L_f > 180\,\mu m \end{aligned} \tag{2.19}$$

Chang et al. (1991) suggested the following equation with two main assumptions: first, cells contain 80% volatile solids and 20% nonvolatile solids, second, the volume of the solids negligibly reduces the volume of water contained in the biofilm. [17]

$$\rho_f \frac{g\left(VSS + H_2O\right)}{cm^3} = 1.0\frac{g\,H_2O}{cm^3\,VSS} + \frac{\rho_{bd}}{0.8}\frac{g\,VS/cm^3}{g\,VS/g\,cells} \tag{2.20}$$

Based on multiple experimental data, Chang et al. (1991) suggested **Equations (2.21)** and **(2.22)** in order to calculate the density of dry cells as well as biofilm thickness:

$$\rho_d = -113.3 + 0.189\,C_c + 69.1\,\mathrm{Re} \tag{2.21}$$

$$\delta = 131.1 - 0.131\,C_c - 64.4\,\mathrm{Re} \tag{2.22}$$

where C_c (g/L) is the local clean particle concentration and ε is the bed voidage.

$$C_c = \left(1-\varepsilon\right)\frac{V_m}{V_m + V_p}\rho_{mw} \tag{2.23}$$

Another experimental equation was proposed to calculate biofilm dry density by Coelhoso et al. (1992). [26]

$$\rho_d(mg/cm^3) = 191.4 - 0.224\delta \quad for\ \delta < 593\mu m$$
$$\rho_d(mg/cm^3) = 58.6 \quad for\ \delta > 593\mu m \qquad (2.24)$$

2.3 Hydrodynamics of Fluidization

2.3.1 Fluid-Particle Interaction Forces and Terminal Settling Velocity, u_t

When a single particle is falling in a liquid, there are three forces acting on it: gravity, Archimedes buoyancy force and drag force. In general when the velocity of a falling particle becomes constant, the summation of the drag force and buoyancy force equals the gravity force, thus the dynamic force balance in a fluidized bed can be written as **Equation (2.25)**.

$$F_d = F_G - F_b \qquad (2.25)$$

Gravity force is equal to:

$$F_G = \frac{\pi}{6} d_p^3 \rho_p g \qquad (2.26)$$

With the assumption of an aerodynamic equivalent sphere with diameter d_p for non-spherical particles. Archimedes buoyancy force is equal to:

$$F_b = V_p \rho_l g = \frac{\pi}{6} d_p^3 \rho_l g \ . \qquad (2.27)$$

Sir Isaac Newton (1643-1724) derived the general equation for the resistance force on a sphere moving through a gas while investigating the ballistics of cannon balls. Newton theorized that a sphere must push aside a volume of gas equal to the projected area of the sphere multiplied by its velocity. The general form of Newton's resistance equation is as **Equation (2.28)**:

$$F_d = \frac{1}{2} C_d \rho_l A u_t^2 = \frac{1}{2} C_d \rho_l \left(\frac{\pi d_p^2}{4} \right) u_t^2 = \frac{\pi}{8} C_d d_p^2 \rho_l u_t^2 \qquad (2.28)$$

Solving **Equation (2.25)** derives **Equation (2.29)** where u_t is called terminal settling velocity. u_t is the notation of the particle settling velocity after it becomes constant.

$$u_t = \left[\frac{4gd\left(\rho_p - \rho_l\right)}{3C_D \rho_l} \right]^{0.5} \qquad (2.29)$$

The drag coefficient, C_d, is dependent upon Reynolds number (Re). For flow around a sphere, there are three regions for the drag coefficient: the Stoke's Law region $\mathrm{Re} \le 1$, the Transition region $1 < \mathrm{Re} \le 1000$, and Newton's Law region $1000 < \mathrm{Re} \le 2 \times 10^5$.

In 1851, George Gabriel Stokes (1819-1903) derived an expression, now known as Stokes' law, for drag force, also called the frictional force, exerted on spherical objects with very small Reynolds numbers (e.g., very small particles) in a continuous viscous fluid (**Equation 2.30**). Stokes' law is derived by solving the Stokes flow limit for small Reynolds numbers, $\mathrm{Re} \le 1$, of the generally unsolvable Navier-Stokes equations:

$$F_d = 3\pi \mu d_p u_t \qquad (2.30)$$

where the drag coefficient is $C_D = \frac{24}{\mathrm{Re}}$

According to Stokes, for the creeping flow, $\mathrm{Re} \le 1$, **Equation (2.29)** becomes:

$$u_t = \frac{8d^2\left(\rho_p - \rho_l\right)}{18\mu} \qquad (2.31)$$

Based on non-linear regression of experimental data, various researchers have proposed different drag coefficient as a function of Re and in different range of *Re*.

Perry and Green (1997) proposed the following simple equation for smooth and rigid spherical particles for Re < 10^5: [27]

$$C_D = 18.5\,\mathrm{Re}_t^{-0.6} \tag{2.32}$$

Even though the drag correlations are mostly offered as a function of Reynolds number, Karamanev (1996) showed that the best way to calculate the drag coefficient and the terminal velocity of particles in an infinite fluid is by describing the drag coefficient as a function of Archimedes number as below: [28]

$$C_D = \frac{432}{Ar}\left(1 + 0.0470\,Ar^{2/3}\right) + \frac{0.517}{1 + 154\,Ar^{-1/3}} \tag{2.33}$$

Equation (2.33) is valid for entire region of Ar below the critical point (Ar =2.2×10^{10} corresponding to Re= 2.5×10^5)

There is a major disagreement in the literature on the correct expression to use for the buoyancy force, F_b, in a fluidized bed system. The conventional formula for F_b as **Equation (2.27)** is simply the buoyant force under static (no-flow) conditions. [29] This is based on the Archimedes buoyancy force principle for a single particle in a fluid.

The counterargument, presented among others by Gibilaro et al. (1987), posits that $F_b = V_p \rho_b g$ where ρ_b is the fluidized bed suspension density given by $\rho_b = \rho_P (1-\varepsilon) + \rho_l \varepsilon.$

After solving the force conservation equation, the drag force is as follows: [30]

$$F_d = V_p \left(\rho_p - \rho_l\right) g\,\varepsilon \tag{2.34}$$

This drag force is less than drag force derived above by the factor of voidage. V_p is the volume of a representative particle in a homogeneously fluidized bed.

Researchers on both sides of the argument agree that the frictional pressure gradient, $-\frac{dp_f}{dz}$, of the fluidized bed must be given by the specific weight of the suspension corrected for hydrostatic head. [29] In other words, for the solid particle to be fluidized, the total interaction force exerted on it by the surrounding fluid must match its weight.

$$-\frac{dp_f}{dz} = \rho_b g - \rho_l g = \left[\rho_P (1-\varepsilon) + \rho_l \varepsilon\right] g - \rho g = (1-\varepsilon)(\rho_p - \rho_l) g \qquad (2.35)$$

By definition, dynamic pressure loss is the ratio of drag force on representative particle to volume of bed associated with representative particles or volume of liquid associated with representative particles.

Since V_p is the volume of representative particle, the volume of the bed associated with representative particle is $\frac{V_P}{1-\varepsilon}$ and the volume of liquid in the bed is

$$\frac{V_p}{1-\varepsilon} - V_P = \frac{V_P \varepsilon}{1-\varepsilon} \qquad (2.37)$$

Therefore:

$$-\frac{dp_f}{dz} = \frac{F_D}{\left(\frac{V_P \varepsilon}{1-\varepsilon}\right)} = (1-\varepsilon)(\rho_p - \rho_l) g \qquad (2.38)$$

The frictional pressure drop in a column containing liquid and particles, is zero before any liquid velocity is imparted. In this state, the only pressure difference along the column is hydro static pressure. When liquid is injected into the system the frictional pressure drop resumes increasing until it reaches a constant value after the minimum fluidization point.

2.3.2 Biofilm-coated Particle Terminal Settling Velocity

As it has been mentioned, the terminal settling velocity of a single spherical particle in a fluid can be calculated by **Equation (2.29).**

Biofilm coated particles are nearly spherical and **Equation (2.29)** can be used to determine their u_t. However, they are neither smooth nor rigid and consequently the proposed C_d for smooth rigid particles could not be used. As a result, other equations relating C_d to Re_t, were developed for biofilm coated particles by different researchers in predominantly two forms of ($\alpha \mathrm{Re}_t^{\beta}$) and ($24\mathrm{Re}_t^{-1} + \alpha \mathrm{Re}_t^{\beta}$). All proposed equations had one thing in common: they are all functions of Re_t and consequently implicit in the terminal settling velocity. The suggested equations were defined in a certain range of $\mathrm{Re}_t < 100$ as mentioned in **Table 2.1**, equations (a) to (f). Thus far, there has been no evidence showing the accuracy of these equations for a $Re_t > 100$.

Nicolella et al. (1999) found that the ratio of drag coefficient for biofilm particles to drag coefficient for smooth rigid solid is independent of biofilm thickness, and concluded that particle deformability has a negligible effect on C_d. They also showed that as the Reynolds number decreases (up to 0.001), the experimental measurements for C_d become closer to the correlation for rigid smooth particles, thereby indicating that the surface roughness indeed plays a dominant role in in the determination of C_d.[22] It was previously suggested that surface roughness is the main reason for the increases in the drag coefficient of biofilm particles [31, 32].

Nicolella et al. (1999) estimated the terminal settling velocity of particles used in their work and those reported by other authors with an average error of 10%: [22]

$$\frac{(C_D)_{bio-covered}}{(C_D)_{clean}} = 1.6 \qquad (2.39)$$

Based on the above ratio Nicolella et al (1999) suggested **Equation (2.40)** for the Reynolds range of below 100. [22] They, however, mentioned that for Re=2300, this equation is valid with prediction average error of 15%.

$$C_D = \left(\frac{6.1}{\mathrm{Re}_t^{0.5}} + 0.8 \right)^2 \qquad (2.40)$$

Table 2.1. Proposed drag coefficient for biofilm-coated particles

Reference	Re_t	equation	C_d
Hermanowicz et al. (1983)	50-100	(a)	$17.1\,\mathrm{Re}_t^{-0.47}$
Mulcahy et al. (1987)	40-90	(b)	$36.66\,\mathrm{Re}_t^{-0.67}$
Ro et al. (1990)	15-87	(c)	$24\,\mathrm{Re}_t^{-1} + 21.55\,\mathrm{Re}_t^{-0.518}$
Chang et al. (1991)		(d)	$C_d = 24\,\mathrm{Re}_t^{-1} + 3.6\,\mathrm{Re}_t^{-0.33}$
Yu and Rittmann (1997)	40-90	(e)	$24\,\mathrm{Re}_t^{-1} + 14.55\,\mathrm{Re}_t^{-0.48}$
Nicolella et al. (1999)	7-90	(f)	$\left(0.8 + 6.1\mathrm{Re}_t^{-0.5}\right)^2$
Nicolella et al. (2000)	7-90	(g)	$29.6\,\mathrm{Re}_t^{-0.6}$

Many experimental studies were conducted for a single particle system in an infinite flow field. Chang et al. (1991), in a multi-particle system, postulated that the drag force acting on one particle is affected the presence of other particles, or the voidage of the bed. Richardson and Zaki (1984) and Wen and Yu (1966) have suggested the use of a voidage function, $f(\varepsilon)$, to quantify the affects of other particles: [2, 33]

$$F_d' = F_d f(\varepsilon) \quad \text{or} \quad C_d' = C_d f(\varepsilon) \qquad (2.41)$$

Therefore, the dynamic force balance in a fluidized bed, **Equation (2.25)**, for multiple particles should be modified to the following correlation:

$$F_D f(\varepsilon) = F_G - F_B \qquad (2.42)$$

Substitution of the expressions for the forces into the above equation provides **Equation (2.43)** for the voidage function:

$$f(\varepsilon) = \frac{Ga}{18\,\mathrm{Re} + 2.7\,\mathrm{Re}^{1.687}} \tag{2.43}$$

where Ga is the Galileo number $= \dfrac{d_b^3 \rho_l (\rho_b - \rho_l) g}{\mu^2}$ (2.44)

And d_b is biofilm-colonized particle diameter (cm), μ is the viscosity of fluid (g/cm.s) and g is the gravitational acceleration coefficient (980 cm/s^2).

Wen and Yu (1966), further evaluated the experimental data and correlations from their works and previous works of others and found the voidage function is a function of porosity only and can be expressed approximately as below: [17, 33]

$$f(\varepsilon) = \varepsilon^{-4.7} \tag{2.45}$$

Equations (2.43) and **(2.45)** can be combined to give **Equation (2.46)**.

$$\varepsilon = \left[\frac{18\,\mathrm{Re} + 2.7\,\mathrm{Re}^{1.687}}{Ga}\right]^{\frac{1}{4.7}} \tag{2.46}$$

This correlation is valid in the following ranges: [34]

0.0015 cm < d_p < 0.635 cm; 1.06 g/cm^3 <ρ_b < 11.25 g/cm^3;

0.818 g/cm^3 < ρ_w < 1.135 g/cm^3; 0.01 g/cm.s < μ < 0.1501 g/cm.s

2.3.3 Minimum Fluidization Velocity in Liquid-Solid Fluidization

The minimum fluidization velocity (u_{mf}) represents the transition between the packed/fixed and fluidized states. The value of the u_{mf} depends on the particles properties (shape, size and density) and system. For the design purposes, it is important to be able to calculate the minimum fluidization velocity theoretically. Researchers have developed a number of correlations to calculate the u_{mf}. [29]

Fluidization starts at a point when the bed pressure drop exactly balances the downward forces (gravity minus buoyancy forces) on the bed packing. At the point of incipient fluidization, the frictional pressure gradient can be calculated by **Equation (2.35)** at $\varepsilon = \varepsilon_{mf}$.

Newtonian fluid flow through the corresponding ‘‘loose’’ packed bed, as given by the widely accepted Ergun (1952) equation is as below: [35]

$$-\frac{\Delta p_f}{L} = (1-\varepsilon_{mf})(\rho_p - \rho)g = 150\frac{\mu u_{mf}(1-\varepsilon_{mf})^2}{\varphi_s^2 d_p^2 \varepsilon_{mf}^3} + 1.75\frac{\rho u_{mf}^2(1-\varepsilon_{mf})}{\varphi_s d_p \varepsilon_{mf}^3} \qquad (2.47)$$

The basic approach starts with the very famous theoretical Hagen-Poiseuille equation for pressure drop in a liquid-solid two-phase tube flow at low Reynolds number: [35]

$$\frac{\Delta p}{L} = 150\frac{\mu U\ (1-\varepsilon)^2}{d_p^2 \varepsilon^{\ 3}} \qquad (2.48)$$

For high Reynolds range Burke and Plummer (1928) offered a similar equation: [29]

$$\frac{\Delta p}{L} = 175\frac{\rho U^2\ (1-\varepsilon)}{d_p \varepsilon^{\ 2}} \qquad (2.49)$$

Both constants, 150 and 175, were determined based on fitting experimental data with the equations.

Although at first sight fluid flow in pipes looks very little in common with fluid flow in a packed bed column, Ergun observed those measured values of pressure drops in the intermediate regime and simply added the two equations. [35]

Gibilaro et al. (1986b) improved the Ergun equation, the equation to predict the pressure drop in fixed beds of spheres, over a wide range of both flow and voidage conditions, for fluidized bed operated in intermediate regime to **Equation (2.50)**. [36]

$$\frac{\Delta P}{L} = \frac{\rho u^2 (1-\varepsilon)}{d_p}\left[\left(\frac{17.3}{\mathrm{Re}}\right)^{\alpha} + 0.336^{\alpha}\right]^{\frac{1}{\alpha}} \varepsilon^{-4.8} \qquad (2.50)$$

The dependence on α of ε is well described by the empirical relationship, obtained by numerical fitting of fluidized bed expansion data:

$$\alpha = 2.55 - 2.1\left[\tanh\left(20\times\varepsilon - 8\right)^{0.33}\right]^3 \qquad (2.51)$$

At minimum fluidization conditions the pressure drops for both the fixed and fluidized beds are same.

Algebraic manipulation and rearrangement of **Equation (2.47)** result in **Equation (2.52).**

$$\mathrm{Re}_{mf}^2 + \frac{150}{1.75}.\frac{1-\varepsilon_{mf}}{\phi}.\mathrm{Re}_{mf} - \frac{\phi\varepsilon_{mf}^3 Ar}{1.75} = 0 \qquad (2.52)$$

where, $\mathrm{Re}_{mf} = \dfrac{d_p u_{mf}\rho_l}{\mu}$ and $Ar = \dfrac{d_p^3\rho_l(\rho_p-\rho_l)g}{\mu_l^2}$

The physically realistic solution of quadratic above equation is: [29]

$$\mathrm{Re}_{mf} = \left[C_1^2 + C_2 Ar\right]^{0.5} - C_1 \qquad (2.53)$$

where $C_1 = \frac{150(1-\varepsilon_{mf})}{2\phi(1.75)} = 42.86\frac{(1-\varepsilon_{mf})}{\phi}$ (2.54)

and $C_2 = \frac{\phi\varepsilon_{mf}^3}{1.75} = 0.5714\phi\varepsilon_{mf}^3$ (2.55)

Thus knowing d_p, ρ_p, ρ_f and μ knowledge of both ε_{mf} and ϕ is also required in order to solve above equations.

Wen and Yu (1966) correlated the terms containing ε_{mf} and ϕ_s for $0.0508 < d_p < 50$ mm, $0.385 < \varepsilon_{mf} < 0.935$, $0.136 < \phi_s < 1$, and particle to column diameter ratio from 0.000807 to 0.25: [33]

$$\frac{(1-\varepsilon_{mf})}{\phi_s^{\,2}\varepsilon_{mf}^{\,3}} \cong 11 \quad (2.56)$$

$$\frac{1}{\phi_s\varepsilon_{mf}^{\,3}} \cong 14 \quad (2.57)$$

Using these correlations, Wen and Yu (1966) proposed a simple relation giving Re_{mf} as a function of the Archimedes number (Ar) with two constants C_1 and C_2 being equal to 33.7 and 0.0408. [33]

2.3.4 Minimum Fluidization Velocity in Gas-Liquid-Solid Fluidization

Begovich and Watson, 1978, showed that minimum fluidization velocity in a gas liquid solid is a function of superficial gas velocity as well as superficial liquid velocity. As the gas velocity was increased, the minimum liquid velocity required to achieve fluidization decreased. For a given gas velocity, the minimum liquid fluidization velocity decreases as the liquid viscosity is increased. However, the influence of liquid viscosity appeared to decrease for higher gas velocity. [37]

Begovich and Watson (1978) proposed the following dimensionless equation. However the equation is not valid for zero gas flow rate. [37]

$$\mathrm{Re}_{mf} = a * Ar^{b} * Fr^{c} \qquad (2.58)$$

where
$$a = 5.121 \times 10^{-3} \pm 0.004$$
$$b = 0.662 \pm 0.062$$
$$c = -0.118 \pm 0.048$$

and Froude number $= U_G^2 / g * d_p$ (2.59)

In order to produce a three-phase correlation that degenerates to an acceptable two-phase correlation as the gas flow rate goes to zero, Begovich and Watson (1978) presented the following equation which relates the minimum fluidization velocity for two phase proposed by Wen and Yu (1966) with three phase minimum fluidization velocity. [37]

$$U_{L,mf}^{Three-phase} / U_{L,mf}^{Wen\&Yu} = 1 - U_G^a * \mu_f^b * d_p^c * (\rho_s - \rho_f)^d \qquad (2.60)$$

where
$$a = 0.436 \pm 0.088 \qquad c = 0.589 \pm 0.289$$
$$b = 0.227 \pm 0.058 \qquad d = -0.305 \pm 0.146$$

2.3.5 Bed Expansion and Voidage

Empirical Equations

In 1954, Richardson and Zaki made a significant contribution to the liquid-solid fluidization by proposing a simple relationship between the operating liquid velocity and the bed voidage. This correlation has been found to be valid over a wide range of operating conditions by many researchers and served as a "building block" for a number of models developed for liquid-solids fluidization. For liquid-solid homogeneous batch conventional fluidization, Richardson-Zaki equation is simply: [2]

$$\frac{u_l}{u_t}\left(=\frac{\mathrm{Re}}{\mathrm{Re}_t}\right)=k\varepsilon^n \tag{2.61}$$

where n is defined as bed expansion index.

On the basis of regression analysis of experimental data covering the range Re_t = 0.01-7000 and d_p/d_c=0.001-0.2, the following empirical equation (Khan and Richardson, 1989) is to determine the value of k: [38]

$$\frac{u_i}{u_t}=k=1-1.15(\frac{d_p}{D_c})^{0.6} \tag{2.62}$$

Expansion index (n) can be determined using the following correlations. [39]

$$n=4.65+20\frac{d_p}{d_c} \qquad \text{for } \mathrm{Re}_t<0.2 \tag{2.63}$$

$$n=(4.4+18\frac{d_p}{d_c})\mathrm{Re}_t^{-0.03} \qquad \text{for } 0.2<\mathrm{Re}_t<1 \tag{2.64}$$

$$n=(4.4+18\frac{d_p}{d_c})\mathrm{Re}_t^{-0.1} \qquad \text{for } 1<\mathrm{Re}_t<200 \tag{2.65}$$

$$n=4.4\,\mathrm{Re}_t^{-0.1} \qquad \text{for } 200<\mathrm{Re}_t<500 \tag{2.66}$$

$$n=2.4 \qquad \text{for } \mathrm{Re}_t>500 \tag{2.67}$$

The index n for spheres was originally correlated by the above five empirical equations relating this index to Re_t and the wall effect ratio, d_p/d_c. [2] However, the wall effect on n has not been confirmed by subsequent investigators [40], and several investigators have proposed a single equation relating n to either Re_t [41, 42, 43] or Ar [38], Garside and Al-Dibouni (1977), proposed that when Richarson and Zaki's equation is utilized, n should be calculated from this equation which produces values of n some 10% greater than those of the corresponding Richarsdon and Zaki correlation. [43]

$$\frac{5.1-n}{n-2.7} = 0.1\mathrm{Re}_t^{0.9} \qquad (2.68)$$

Rowe (1987) suggested that the division of the curve into four different equation was not necessary, and proposed a single relationship applicable to the entire flow range: [41]

$$\frac{4.7-n}{n-2.35} = 0.175\mathrm{Re}_t^{0.75} \qquad (2.69)$$

The equation of Khan and Richardson (1989), which has been carefully adjusted to the available data, is: [38]

$$\frac{4.8-n}{n-2.4} = 0.043Ar^{0.57} \qquad (2.70)$$

Equations (2.68), **(2.69)** and **(2.70)** reflect the fact that the upper limit of n, for spheres in the Stokes region ($\mathrm{Re}_t < 0.2$, Ar < 4), is somewhere between 4.6 and 4.9, while the lower limit, for spheres in the Newton region (Ret > 500, Ar > 85,000), falls between 2.3 and 2.4.

The advantage of the latter being that Ar, unlike Re_t, can be calculated directly without further ado if the particle and liquid properties are known.

Pressure Drop and Voidage in Gas-Liquid-Solid Fluidized bed

The pressure drop within the dense bed region, ΔP_1, can be measured by a differential pressure transducer or simply a manometer connected to two pressure taps located at the top and bottom of the measuring section.

The expanded bed height (h) can be determined by visual observation or by locating the minimum point in the dynamic pressure gradient versus height curve. [44] Since the settled bed height (h_0) is known before fluidization, the solid hold-up can be calculated from:

$$1-\varepsilon_s=[h-h_0(1-\varepsilon_{pack})]/h \tag{2.71}$$

By a pressure balance, the measured pressure drop per unit length of the bed should be equal to the bed density, ρ_{bed}. The following equations [45] have typically been used to determine the volume fraction (hold-up) of each phase in a three phase fluidized bed:

$$\frac{\Delta P_1}{H_1 g}=\rho_{bed}=\varepsilon_s\rho_s+\varepsilon_l\rho_l+\varepsilon_g\rho_g \tag{2.72}$$

$$\varepsilon_s+\varepsilon_l+\varepsilon_g=1 \tag{2.73}$$

$$\varepsilon_s=\frac{M_s}{\rho_s A H_t} \tag{2.74}$$

These equations are obtained either visually or from the measured pressure gradient. [45]

Where ΔP_1, is the pressure drop across the measured section of the bed and H_1 is the bed height of measured section within the dense bed. Because ρ_g is about two orders of magnitude smaller than either ρ_f or ρ_s, the last term in equation above can be dropped. With the density of the three-phases given, the liquid phase hold-up can be obtained from **Equation (2.75)**.

$$\varepsilon_l\cong(\frac{\Delta P_1}{H_1 g}-\varepsilon_s\rho_s)/\rho_l \tag{2.75}$$

The gas phase hold-up can then be calculated by:

$$\varepsilon_g=1-\varepsilon_l-\varepsilon_s \tag{2.76}$$

According to Begovich and Watson (1978) at high flow rates, this method is not satisfactory because the indistinct bed height makes visual measurements extremely subjective, while the measured pressure gradient yields a bed height based on an unrealistic homogeneous bed. [37]

Based on the literature data Begovich and Watson (1978) offered the following dimensional correlations:

$$1-\varepsilon_s = a * u_l^b * u_G^c * (\rho_s - \rho_l)^d * d_p^e * \mu_l^h * d_c^k \qquad (2.77)$$

where

$a = 3.93 \pm 0.18$
$b = 0.271 \pm 0.011$
$c = 0.041 \pm 0.005$
$d = -0.316 \pm 0.011$
$e = -0.268 \pm 0.01$
$h = 0.055 \pm 0.008$
$k = -0.033 \pm 0.013$

Bed Expansion and Voidage in Fluidized Bed Biofilm Reactors

One of the industrial applications of fluidization is in biological treatment of wastewater. Aerobic as well as anaerobic fluidized bed biofilm reactors (FBBRs) have received increasing attention for being an effective technology to treat water and wastewater. [46] The bed voidage in such reactors is important to evaluate a biofilm specific surface area; however, no satisfactory means exist so far for prediction of bed voidage in a three-phase FBBR. This could be attributed to the complexity of three-phase fluidization as well as the complex manner by which fluidization characteristics and biofilm characteristics are interrelated. [47]

Different researchers derived equations based on experimental data by Hermanowicz and Cheng, 1990; Mulcahy and Shieh, 1987; Ngian and Martin, 1980; Nicolella et al., 1999; Abdul-Aziz and Asolekar, 200; Csikor, 1994. However there has been some evidence that indicated that Richarson and Zaki equation provides a satisfactory description of biological beds. [22] Yu and Rittmann (1997) also indicated that the Richarson and Zaki equation was reasonable in the lower Re region, although the range was not specified by the authors, but it severely under-estimates n for larger Re. [47]

Table 2.2. Proposed Bed Expansion Index for Fluidized Biofilm-Coated Particles

Reference	Re_t	equation	n
Mulcahy et al. (1978)	1000 < Ga < 15000	(a)	$47.36\,Ga^{-0.2576}$
Mulcahy and Shieh (1987)	40-90	(b)	$10.35\,\mathrm{Re}_t^{-0.18}$
Harada et al. (1987)	10-50	(c)	$8.733\,\mathrm{Re}_t^{-0.341}$
Thomas et al. (1983)		(d)	$30\,\mathrm{Re}_t^{-0.505}$
Nieuwstad et al. (1984)	2-100	(e)	$4.26 - 0.73\log \mathrm{Re}_t$
Hermanowicz et al. (1990)	40-81	(f)	$(9.11 + d/D)\mathrm{Re}_t^{-0.21}$
Yu et al. (1997)	2-190	(g)	$4.526\,\mathrm{Re}_t^{0.0126}$

Considering mono-size sphere particles as core supports with average diameter d_p and density ρ_p in an FBBR, where each particle gets covered with a uniform thickness of biofilm over a period of time leading to a wide size distribution of bio-particles with overall diameters d_{bp} and densities ρ_{bp} .

2.4 Mass Transfer in Fluidized Bed

2.4.1 Gas-Liquid Mass Transfer

The volumetric gas-liquid mass transfer coefficient plays an important role in the design and operation of three-phase biofilm reactors and has been the subject of much research interest. In a gas-liquid-solid system the volume fraction of gas has a strong influence on the performance of pneumatic biofilm reactors. The residence time of the gas in the liquid, the gas–liquid contact area for mass transfer and the design volume of the reactor depend on the gas hold-up, which occurs under given operating conditions. In

addition, the gas hold-up in conjunction with the mean bubble diameter allows the determination of the interfacial area and consequently the mass transfer rate between gas-liquid phases. [48]

The influence of the presence of solids on hydrodynamics and mass transfer has been reported for various types of particles including glass beads [49], plastic beads [50], polystyrene cylinders [51], activated carbon particles [52], Raney nickel particles [53], calcium alginate beads [54], and basalt [22]. Ryhner et al. (1988) reported that the gas–liquid volumetric mass transfer coefficient in a three phase biofilm fluidized sand bed reactor decreased (in the range 0.02–0.04 s^{-1}) with increasing amounts of clean sand and was almost independent of the sand fraction with biofilm-covered sand. [55]

Solid size affects the particle terminal settling velocity (u_t), which has a direct influence on the difference in solid holdup between the riser and the downer. Again, this difference strongly influences the hydrodynamics of the system: if the solid hold-up in the up-flow column is larger than in the down-flow column, the presence of solids lowers the driving head of the system, and thereby the liquid circulation rate and the gas recirculation. [56] The terminal settling velocities of basalt particles varied in a wider range (1.9–12.9 cm/s) than those of biofilm coated particles (3.0–4.9 cm/s), and the influence of particle size was more noticeable in the first case than in the latter. [22] In both cases, the gas hold-up decreased with increasing particle-settling velocity.

2.4.2 Liquid-Solid and Gas-Liquid-Solid Mass Transfer

Liquid-solid mass transfer coefficient, described as Sherwood number (*Sh*), is originated from the boundary layer theory, which leads to a correlating **Equation (2.78)**:

$$Sh = 2.0 + C\,\mathrm{Re}^{n}\,Sc^{m} \qquad (2.78)$$

where, Sh is the Sherwood number ($Sh = k_f d_p / D_m$) , Re is the particles Reynolds number ($\mathrm{Re}_p = d_p U_{slip} \rho / \mu$), Sc is the Schmidt number ($Sc = \mu / \rho D_m$), k_f is the film mass transfer co-efficient and D_m is the molecular diffusion co-efficient.

Many studies have been carried out regarding the mass transfer in the fluidized bed system.

Fan et al. (1960) correlated the fluidized beds mass transfer data as a function of bed voidage and particles Reynolds number (Re_p) for spherical particles and $5 < Re_p < 130$: [57]

$$Sh = 2 + 1.03((1-\varepsilon)\mathrm{Re}_p)^{1/2}(Sc)^{1/3} \quad (2.79)$$

For lower Reynolds numbers ($0.0015 < Re_p < 55$), Wilson- Geankoplis equation is used to estimate the film mass transfer co-efficient: [57]

$$Sh = \frac{1.09}{\varepsilon}\mathrm{Re}_p^{1/3}\,Sc^{1/3} \quad (2.80)$$

In problems involving liquid–solid mass transfer in three-phase suspension the Reynolds number is frequently defined according to Kolmorgoff's theory of turbulence:

$$\mathrm{Re} = \frac{\varepsilon d_S^4}{v^3} \quad (2.81)$$

where ε is the energy dissipation rate. One approach to analyzing the mass transfer data is to assume that the biofilm reactor may be treated as having essentially uniform energy dissipation rates throughout the entire volume. The energy dissipation rate is calculated by **Equation (2.82)**.

$$\varepsilon = u_G g \quad (2.82)$$

Kolmorgoff's theory has been used extensively in correlating mass transfer data for bubble columns [58, 59], fluidized beds [60, 61] and airlift reactors. [22]. An exponent of 1/3 in **Equation (2.80)** is often chosen for the Schmidt number. The liquid-solid mass-transfer coefficients measured for particle-supported biofilms were found to be smaller (by a factor of approximately 15%) than the values reported for rigid particles, and it was therefore concluded that liquid-solid mass transfer should be regarded as the critical process in biofilm systems.

2.4.3 Inter-particle Mass Transfer

Biofilm reactors are characterized by microorganisms attached onto a solid surface in the form of a biofilm, through which substrates have to be transported for biochemical reaction to occur. Mass transport takes place by molecular diffusion, which is a slow process. In practice it is observed that the removal is limited by diffusion, constituting one of the major disadvantages of biofilm reactors. [62]

Available substrate in a biofilm is determined by the substrate conversion process and diffusion. In general, the effective diffusion coefficient is 80–90% of the diffusion coefficient in water. The substrate flux at the biofilm surface (if the concentration is well above the substrate affinity coefficient, which is often the case for biofilm processes) can be calculated by considering two distinct reaction regions with an abrupt transition in the order of the reaction. [63] This transition is characterized by **Equation (2.83)**.

$$\beta = \sqrt{\frac{2D_e C_f^i}{k_o \delta^2}} \tag{2.83}$$

$$\beta > 1 \Rightarrow N_S = k_O \delta \tag{2.84}$$

$$\beta < 1 \Rightarrow N_S = \sqrt{2D_e k_O C_f^i} \tag{2.85}$$

$$k_O = \mu_{\max} X_f / Y \tag{2.86}$$

where, D_e is the diffusion coefficient (m^2/s), C_f is the substrate concentration in the film (mg/L), δ is the biofilm thickness (mm), and k_0 is the zero-order reaction rate constant ($kg/m^3/s$). **Equation (2.14)** can be used for $\beta > 1$, the biofilm is fully penetrated by the substrate and the substrate flux (N_S) is zero order with respect to the substrate concentration at the biofilm surface. In case of $\beta < 1$, the biofilm is partially penetrated by the substrate and the substrate flux is half order with respect to the substrate concentration at the biofilm surface.

2.5 Biological Nutrient Removal

Since wastewater treatment using activated sludge was invented by Arden and Lockett in 1914 in England, the activated sludge process and its variations have been used worldwide for domestic and industrial wastewater treatment. In the past decades, nitrogen removal technologies using activated sludge process have been developed and optimized. Because of the public concern for environmental aspects, the effluent standards have become stricter. In order to fulfill the increasingly stringent discharge standards, new technologies and operational strategies have been elaborated for the removal of nitrogen from wastewater. According to the EU Standards, the most important requirement is that the wastewater treatment plants (WWTPs) larger than 100.000 PE must have a nitrogen concentration in effluent less than or equal to 10 mg/l of total nitrogen or 70 – 80 % of nitrogen elimination. [64]

Thus, activated sludge processes have been modified to accomplish biological nutrient removal (BNR) to fulfill nitrogen and phosphorus requirements in the effluent. This modification incorporates anoxic-anaerobic and aerobic zones to provide nitrogen and phosphorus removal. In aerobic zones, oxygen is predominantly the electron acceptor; in anoxic zones, nitrogen oxides are the electron acceptors; and in anaerobic zones, organic matter is both the electron acceptor and donor. The division of the bioreactor to provide these alternative biochemical environment is the distinguishing feature of a BNR system. The aerobic zone is a necessary component of all BNR systems, while the anaerobic zone is necessary to accomplish phosphorus removal, and the anoxic zone is necessary for nitrogen removal. [65]

2.5.1 Conventional Biological Nitrogen Removal

Conventional biological nitrogen removal refers to the biological conversion of ammonia to nitrite (nitritation) and then nitrite to nitrate (nitratation) in two sequential oxidation steps called nitrification and subsequently biological conversion of nitrate to nitrogen gas, which is called denitrification. Biological denitrification involves the biological oxidation of organic substrates in wastewater treatment using nitrate and nitrite as the electron acceptor instead of oxygen. [66]

Nitrification

Figure 2.2 depicts the combination of nitrogen cycle adapted from different references. [66, 67] The reactions occurring in **Figure 2.1** have been summarized in **Table 2.3**.

As mentioned the biological nitrification consists of two sequential stages of nitritation and nitratation. Each stage is performed by different bacterial genera, which use ammonia or nitrite as an energy source and molecular oxygen as an electron acceptor. Both bacterial groups are autotrophic, which require inorganic carbon sources. However they are distinctly different. The most commonly recognized genus of bacteria that carries out ammonia oxidation, known as ammonia oxidizing bacteria (*AOBs*), to nitrite is *Nitrosomonas*. However, *Nitrosococcus*, *Nitrosopira, Nitrosorobrio,* and *Nitrosolobus* are also able to oxidize ammonium to nitrite. [66]

In the nitrification process, ammonia is first oxidized into nitrite (NO_2^-) by several genera of autotrophic bacteria, known as ammonia oxidizing bacteria (A*OBs*), the most important being *Nitrosomonas.* [68] Nitrite is then oxidized to the much less toxic nitrate (NO_3^-) by several other genera of bacteria including *Nitrococcus*, *Nitrobacter*, *Nitrospira*, *Nitrospina*, and *Nitroeystis*. For Nitrite oxidation in activated sludge, *Nitrococcus* was found quite prevalent. [69]

Theoretically, based on Equation (3) **Table 2.3**, for each g of ammonia nitrogen (as N) converted, 4.57 g of O_2 are utilized of which 3.43 g O_2 is for the nitritation step and 1.14 g O_2 for the second step, nitratation. However the oxygen required to oxidize 1.0 g of ammonia nitrogen to nitrate (4.25 g) is less than the theoretical value of 4.57 g computed using Equation (7) **Table 2.3** where the ammonia for cell synthesis was considered in the overall nitrification reaction as well.

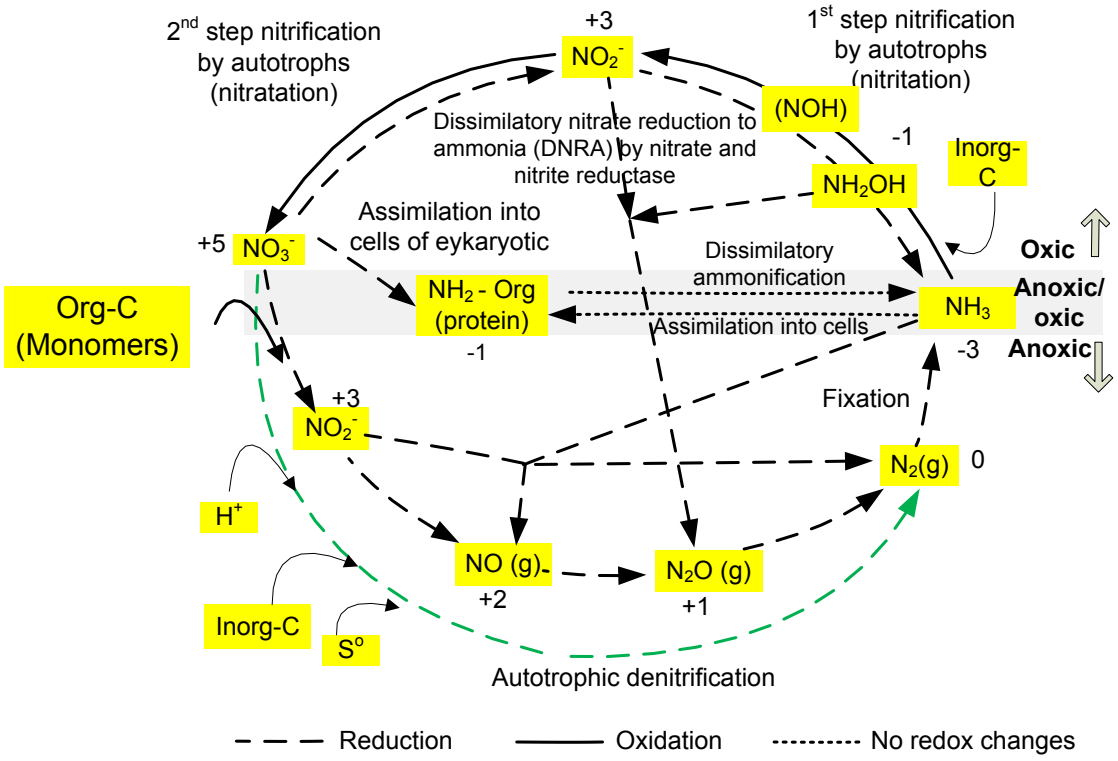

Figure 2.2. Biological Nitrogen Cycle [66, 67]

In conventional nitrification process, for each g of ammonia nitrogen (as N) converted, 4.25 g of O_2 are utilized, 0.16 g of new cells of formed, 7.07 g of alkalinity as $CaCO_3$, with considering the conversion of some of the ammonia to cellular nitrogen in Equation (7) **Table 2.3**, are removed. [66] According to Equation (4) **Table 2.3**, however, the theoretical alkalinity requirement is 7.14 g of alkalinity as $CaCO_3$ for each g of ammonia nitrogen converted without accounting for the ammonia conversion into the cellular nitrogen. Energy released from the above conversions is used by *Nitrosomonas* and *Nitrobacter* to drive their life processes. In addition, these reactions require oxygen, produce hydrogen ions (lowering pH) and produce nitrite as an intermediate product. Nitritation and nitratation reactions with cell synthesis in consideration are denoted as Equation (5) and Equation (6) **Table 2.3**. [74]

As mentioned earlier, overall synthesis and oxidation reactions in nitrification process can be represented as Equation (7) **Table 2.3**. [66] Based on Equation (5) and Equation (6)

Table 2.3, yields for *AOBs* and *NOBs* are 0.15mg cells/mg NH_4-N oxidized and 0.02 mg cells/ mg NO_2-N oxidized, respectively.

Table 2.3. Biological Nitrogen reactions

No	Reactions	[II]ΔG^o	Ref.
	Nitrification (Nitritation and Nitratation)		
1	$NH_4^+ + 1.5O_2 \rightarrow NO_2^- + 2H^+ + H_2O$	-277.68	[70]
2	$NO_2^- + 0.5O_2 \rightarrow NO_3^-$	-74.14	[70]
3	$NH_4^+ + 2O_2 \rightarrow NO_3^- + 2H^+ + H_2O$ (overall without cell and alkalinity)	-349	[66]
4	$NH_4^+ + 2HCO_3^- + 2O_2 \rightarrow NO_3^- + 2CO_2 + H_2O$ (overall with alkalinity)	-349	[66]
5	$NH_4^+ + 1.381O_2 + 1.981\ HCO_3^- \rightarrow 0.981NO_2^- + 1.89H_2CO_3 + 1.0363H_2O + 0.0181C_5H_7NO_2$ (Overall nitritation with cell synthesis and alkalinity)		
6	$NO_2^- + 0.0025NH_4^+ + 0.01\ H_2CO_3 + 0.487O_2 \rightarrow NO_3^- + 0.0075H_2O + 0.0025C_5H_7NO_2$ (Overall nitratation with cell synthesis and alkalinity)		
7	$NH_4^+ + 1.863O_2 + 0.098\ CO_2 \rightarrow 0.098NO_3^- + 1.98H^+ + 0.0941H_2O + 0.0196C_5H_7NO_2$ (Overall reaction with cell synthesis and alkalinity)	-349	[66]
8			
9			
	Denitrification (Heterotrophs)		
10	$5H_2 + 2NO_3^- + 2H^+ \rightarrow 6H_2O + N_2(g)$	-224	[71]
11	$NO_2^- + 4H^+ + 3e^- \rightarrow 2H_2O + 0.5N_2(g)$	277	[70]
12	$5CH_3COO^- + 8NO_3^- + 8H^+ \rightarrow 9H_2O + 5CO_2 + 5HCO_3^- + 4N_2(g)$	-797	[71]
13	$5CH_3CH_2COO^- + 14NO_3^- + 14H^+ \rightarrow 17H_2O + 10CO_2 + 5HCO_3^- + 7N_2(g)$	-1398	[71]
14	$5C_6H_{12}O_6 + 24NO_3^- + 24H^+ \rightarrow 42H_2O + 30CO_2 + N_2(g)$	-2657	[72]
15	$C_6H_{12}O_6 + 8NO_2^- + 8H^+ \rightarrow 10H_2O + 6CO_2 + 4N_2(g)$	-3144	[72]
16	$5CH_3OH + 6NO_3^- \rightarrow 3N_2 + 5CO_2 + 6OH^- + 7H_2O$		
17	$C_{10}H_{19}O_3 + 10NO_3^- \rightarrow 5N_2 + 10CO_2 + 3H_2O + NH_3 + 10OH^-$		[66]
	Denitrification (Autotrophs)		
18	$8NO_3^- + 5MeS + 6H_2O \rightarrow 2H^+ + 4N_2(g) + 5SO_4^{2-} + 5Me(OH)_2$		
19	$NO_3^- + H^+ + 2.5\ H_2 \rightarrow 0.5N_2(g) + 3H_2O$	-560.3[I]	[73]
20	$3NO_3^- + 5NH_4^+ \rightarrow 4N_2(g) + 9H_2O + 2H^+$	-297	
	DNRA (Heterotrophs)- Respiratory ammonification		
21	$4H_2 + 2NO_3^- + 4H^+ \rightarrow 6H_2O + 2NH_4^+$	-150	[71]
22	$CH3COO^- + NO_3^- + 2H^+ \rightarrow CO_2 + HCO_3^- + NH_4^+$	-500	[71]
23	$8CH_3CH_2COO^- + 14NO_3- + 28H_+ \rightarrow 2H_2O + 16CO_2 + 8HCO_3^- + 14NH_4^+$	-878	[71]
24	$C_6H_{12}O_6 + 3NO_3^- + 6H^+ \rightarrow 3\ NH_4^+ + 3H_2O + 6CO_2$	-1767	[72]
25	$C_6H_{12}O_6 + 12NO_3^- \rightarrow 12\ NO_2^- + 6H_2O + 6CO_2$	-1767	[72]
26	$C_6H_{12}O_6 + 4NO_2^- + 8H^+ \rightarrow 4\ NH_4^+ + 2H_2O + 6CO_2$	-1713	[72]
	Aerobic deammonification		
27	$NH_2OH + NO_2^- \rightarrow N_2O(g)$		[67]
	Nitrogen Fixation		
28	$N_2 + 8H^+ + 8e^- + 16ATP \rightarrow 2NH_3 + H_2 + 16ADP + 16Pi$		[67]
	Anoxic ammonia oxidation		
29	$NO_2- + NH_4^+ \rightarrow NO(g)$		
	Anaerobic ammonia oxidation (Anommox)		
30	$1.3NO_2^- + NH_3^+ \rightarrow 1.02N_2(g) + 0.26\ NO_3^- + 2H_2O$	-357	

[I] kJ/reaction

[II] kJ/mol e donor

Nitrogen Pathway and Denitrification

The detection of new organisms is making the nitrogen cycle increasingly complicated, to the point that traditional descriptions of nitrification (ammonia is oxidised to nitrate via nitrite), denitrification (conversion of nitrate and nitrite to nitrogen gas), and nitrogen fixation are rather simplistic and insufficient for explanation of nitrogen pathways in real life. [67]

As depicted in **Figure 2.2**, the nitrate may be denitrified, reduced to the form of ammonia or converted to organic nitrogen. The biological nitrate reduction can be either a respiratory pathway, which is also called dissimilatory ammonification, or assimilatory ammonification, which denotes the reduction of nitrate to ammonia for the biosynthesis of nitrogenous compounds. These two pathways differ: 1- The enzymes of the respiratory pathways dissimilatory nitrate reduction to ammonia (DNRA) are integrated in cytoplasmic membranes or located in the periplasm (a space between the inner cytoplasmic membrane and external outer membrane of Gram-negative bacteria or the equivalent space outside the inner membrane of Gram-positive bacteria and their synthesis is repressed by oxygen, whereas 2- The biosynthesis pathways use soluble enzymes, the synthesis of which is repressed by ammonia. [4] According to Tiedje et al. (1988), DNRA is a major nitrate pathway in anaerobic digesters in which the nitrate reductase enzymes are within the cytoplasm. [75] Several other researchers have also concluded that added nitrate in a strict anaerobic environment was mainly reduced to ammonia, while only a minor fraction was recovered as nitrogen gas. [35] A number of obligate and facultative anaerobic, and microaerophilic, bacteria perform dissimilatory nitrate reduction to ammonium; mainly in carbon rich and low electron acceptor environments such as nitrate. Relative abundance of fermentative and obligate anaerobes such as ammonium formers, discovered in anaerobic environments is responsible for DNRA. [36] Assimilatory nitrate reduction occurs directly to eukaryotes, as shown in **Figure 2.2**. Also, organic nitrogen may be used further by bacteria and fungi to form ammonia (ammonification). Several authors have shown that high carbon to nitrogen ratios which are normally found in anaerobic digesters favour dissimilatory nitrate

reduction to ammonia, [1] while others found that a high COD/NO_3 did not favour dissimilatory reduction of nitrate to ammonia. [76] Rustrian et al. (1997) reported that the reduction of nitrate to ammonia was dominant at low nitrate loads (high COD/NO_3-N ratios: 361, 220 and 130) with 50% assimilation of nitrogen in biomass at COD/NO_3-N of 361.

The biological reduction of nitrate to nitric oxide, nitrous oxide, and nitrogen gas, termed denitrification, is generally performed by heterotrophic bacteria under anoxic conditions. The oxidized nitrogen compounds (NO_2 and NO_3) are reduced to nitrogen gas by heterotrophic microorganisms that use nitrite and nitrate instead of oxygen as electron acceptors and organic matter such as methanol, ethanol, glucose and volatile fatty acids as carbon and energy source. The reactions are listed in **Table 2.3**. As shown in **Table 2.3**, bacteria capable of denitrification are both heterotrophic and autotrophic. The heterotrophic organisms include *Archromobacter*, *Acinetobacter*, *Agrobacterium*, *Alcaligens*, *Arthrobacter*, *Bacillus*, *Chromobacterium*, *Corynebacterium*, *Moraxella*, *Flavobacterium*, *Pseudomonas*, *Vibrio*, *Spirillum* [66] of which *Pseudomonas* species are the most common and widely distributed of all the denitrifiers, and have been shown to use a wide range of organic compounds such as hydrogen, methanol, carbohydrates and VFAs. [76] Most of the aforementioned species are facultative aerobic organisms with the ability to use oxygen, nitrate, and nitrite.

In all heterotrophic denitrification reaction listed in **Table 2.3**, one equivalent of alkalinity is produced per equivalent of NO_3-N reduced, which equates to 3.57 g of alkalinity (as CaCO3) production per g of NO_3-N reduced. [66] The amount of bsCOD needed to provide a sufficient amount of electron donor for nitrate removal depends on the system operating conditions and the type of electron donor. According to Metcalf and Eddy (2003), this amount can be calculated by **Equation (2.87)**.

$$\frac{g\ bsCOD}{g\ NO_3 - N} = \frac{2.86}{1 - 1.42Y_n} \qquad (2.87)$$

where Y_n is the observed yield.

Simultaneous Nitrification Denitrification (SND)

Simultaneous nitrification-denitrification (SND) is the conversion of the ammonium ion to nitrogen gas in a single bioreactor. There are two different types of SND processes:

1- Autotrophic nitrification and heterotrophic denitrification occur within microbial biofilms and flocs due to the oxygen gradient that is established across the biomass (von Munch et al., 1996). Nitrifiers are active in the areas of high dissolved oxygen (DO) concentration in the outermost zone of biofilm or flocs whereas denitrifiers are active in the low DO concentration areas, mostly at the core of the flocs of biofilm. The uneven DO distribution inside the biomass allows simultaneous proliferation of nitrifying and denitrifying bacteria. Ammonium is hydroxylated to hydroxylamine by ammonium monooxygenase under aerobic conditions and subsequently, hydroxylamine is oxidized to nitrite. Finally, nitrite is directly transformed into N_2 based on Equation (11) (**Table 2.3)**. Complete oxidation of ammonia to nitrate in the outermost of the biofilm and subsequently the conversion of nitrate to nitrogen gas can also occur in the biofilm, which is considered a SND process too.

2- Denitrification can occur under aerobic conditions by heterotrophic nitrifying bacteria such as *Paracoccus pantotropha*, *Alcaligenes and Thiosphera pantotropha.* [66, 77] These bacteria are capable of performing SND by using organic substrates aerobically as sources of carbon and energy to convert ammonium (NH_4) aerobically into nitrogen gas. Investigation on the efficiency of nitrogen removal wastewaters by SND-based sequencing batch reactors (SBR) by Pochana and Keller (1999) showed that higher DO concentrations enhances nitrification rates but inhibited denitrification process, causing an accumulation of nitrite and nitrate in the reactor. On the other hand, limited DO slowed down the nitrification process and enhanced denitrification process. Hence, the DO level is a critical factor to the SND process and it must be maintained at an appropriate level, DO concentrations as low as 0.5 mg/L [66], in the SND reactor in order to reach balanced equilibrium between nitrification and denitrification processes. [65]

2.5.2 Innovative Nitrogen Removal

Various novel biological nitrogen removal processes such as short-cut nitrification and denitrification, anaerobic ammonium oxidation (ANAMMOX), completely autotrophic nitrogen removal over nitrite (CANON) process and oxygen-limited autotrophic nitrification-denitrification (Oland) process, bioaugmentation batch enhanced treatment (BABE) and single reactor for high activity ammonia removal over nitrite (SHARON) have been developed exclusively. [78]

Partial Nitrification

Nitrification is a sequential biological oxidation process, which involves two different groups of bacteria. The first step of nitrification is the oxidation of ammonia to nitrite over hydroxylamine (NH_2OH), involving the membrane- bound ammonia mono-oxygenase (AMO) and the hydrox-ylamine oxidoreductase (HAO), and is carried out by ammonia-oxidizing bacteria (AOB); the second group, nitrite-oxidizing bacteria (NOB), further oxidizes nitrite to nitrate. [79] Under normal conditions, the reaction of ammonia oxidation to nitrite is a velocity-limiting step; in contrast, nitrite is oxidized rapidly to nitrate, so nitrite is seldom accumulated in nitrifying reactors. In partial nitrification process, however, nitrite accumulation is required, and the second step must be restrained so as to accumulate AOB and washout NOB. [80] Partial nitrification process is based on the fact that nitrite is an intermediary compound in both nitrification and denitrification steps: a partial nitrification up to nitrite is performed followed by nitrite denitrification (Ferhan 1996; Fdz- Polanco et al. 1996), as shown in **Figure 2.3**. Chung et al., (2007) showed the benefits of shortcut nitrogen removal by comparing the stoichiometries for O_2 and CH_2O (representing the organic electron donor) in **Equation (2.89)** and **(2.90)** (conventional BNR) to **Equations (2.91)** and **(2.92)** (shortcut BNR). [81]

Conventional BNR:

$$NH_4^+ + 2O_2 \text{ (ammonium and nitrite oxidizers)} \rightarrow NO_3^- + H_2O + 2H^+ \qquad (2.89)$$

$$NO_3^- + 1.25CH_2OH \rightarrow 0.5N_2 + 1.25HCO_3^- + 1.25\ H^+ \qquad (2.90)$$

Shortcut BNR:

$NH_4^+ + 1.5O_2$ (ammonium oxidizers) → $NO_2^- + H_2O + 2H^+$ (2.91)

$NO_2^- + 0.75CH_2OH \rightarrow 0.5N_2 + 0.75HCO_3^- + 0.75\ H^+$ (2.92)

Partial nitrification to nitrite and nitrite denitrification was reported to be technically feasible and economically favorable, especially when wastewater with high ammonium concentrations or low C/N ratios with high temperature is treated. [79]

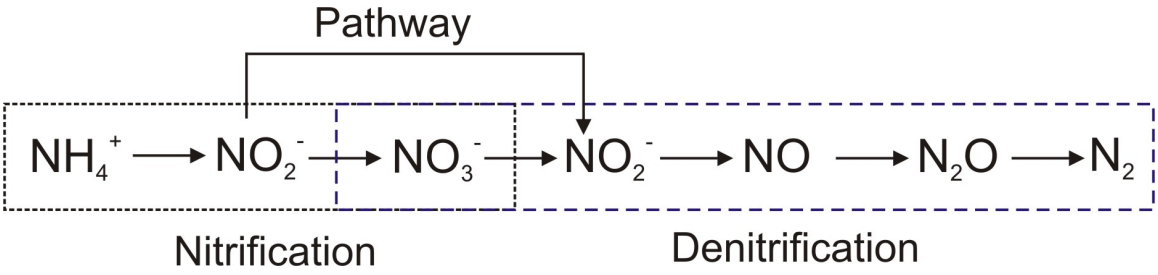

Figure 2.3. Shortcut nitrogen removal

Compared to traditional nitrification denitrification via nitrate, the main advantages of partial nitrification with respect to complete nitrification were reported as followed: [82, 83, 84]

I. 25% lower oxygen consumption in the aerobic stage implies 60% energy savings
II. In the anoxic stage the electron donor requirement is lower (up to 40%)
III. Nitrite denitrification rates are 1.5 to 2 times higher than with nitrate;
IV. 20% CO_2 emission reduction
V. 33～35% less sludge production in nitrification process and 55% in denitrification process.

Methods to Maintain Partial Nitrification

Researchers have developed many control methods and strategies to achieve partial nitrification. The main objective of these methods and approaches was to accumulate *AOB* and washout *NOB* through different activation energies, different sludge ages,

different dissolved oxygen half-saturation coefficients, and different anti-toxic capacities of *AOB* and *NOB*. [79]

Raising temperature cannot only promote the growth rates of *AOB*, but can also expand the differences of specific growth rates between *AOB* and *NOB*. [79] From the aspect of specific growth rate, only at temperatures above 25 °C is it possible for the ammonium oxidizers to effectively out- compete the nitrite oxidizers. [85] But the opposite was the case at temperature below 15 °C.

Based on experiences from full-scale operation, van Kempen et al. (2001) suggested maintaining SRT between 1 day to 2.5 days to washout *NOBs* while retain *AOBs*. However, Peng and Zhu (200) and Pollice et al. (2002) reported partial nitrification to nitrite under oxygen limitation, independent of sludge age at SRT of 10, 14 and 40 days. [79, 86, 87]

The dissolved oxygen half-saturation coefficients of *AOB* and *NOB* are 0.2–0.4 mg/L and 1.2–1.5 mg/L, respectively. [88] Therefore, low DO concentration is more restrictive for the growth of *NOB* than *AOB*, which will result in nitrite accumulation. [79] Garrido et al. (1997) found that both ammonium oxidation rate and nitrite accumulation reached maximum when DO was 1.5 mg/L. Below 0.5 mg/l of DO ammonium was accumulated and over 1.7 mg/L complete nitrification to nitrate was achieved [89]. On the other hand, it should be noticed that lower DO will lower nitrification rate and cause filamentous bulking sludge. Considering ammonia oxidation rate and nitrite accumulation, DO concentration should be maintained about 1.0–1.5 mg/L. [79] Use of intermittent aeration was in favor of implementation of nitrite accumulation. [86, 87]

Autotrophic Nitrification

Autotrophic nitrifying bacteria, such as *Nitrosomonas europaea*, can use nitrite to oxidized ammonia with the production of nitrogen gas when dissolved oxygen is not present. [90] However, these bacteria oxidize the ammonia with oxygen as electron acceptor when oxygen is present. [66] This distinguishes autotrophic nitrification from ANOMMOX process.

ANOMMOX

The bacteria in the ANOMMOX (**AN**aerobic **AMM**onium **OX**idation) process are different than the autotrophic nitrifying bacteria. ANOMMOX cannot use oxygen for ammonia oxidation. [91] Under the anaerobic conditions the ammonia oxidation rate by Anommox, Equation (30) **Table 2.3**, was shown to be 6 to 10 times faster than that for *Nitrosomonas europaea.* [66, 91]

Side Stream Nitrogen Removal

Side streams including the reject streams from the membrane, dewatering process and supernatant liquid from sludge digesters also contain a significant load of nutrients. Estimates of the nitrogen load from this side stream return range between 15% and 30% of the total nitrogen load on a process. [92] As mentioned before, several relatively new processes have been developed to remove nitrogen in high-concentration side streams from biosolids processing prior to recycling to the headwork of the publicly owned treatment works (POTWs); SHARON® (**S**ingle reactor system for **H**igh activity **A**mmonium **R**emoved **O**ver **N**itrite), ANAMMOX®, CANON® (**C**ompletely **A**utotrophic **N**itrogen removal **O**ver **N**itrite), InNitri® (**In**expensive **Nitri**fication) [93], and BABE® (**B**io-**A**ugmentation **B**atch **E**nhanced) [67]. The schematic of the aforementioned processes are depicted in **Figure 2.3**. In SHARON® process (known as nitrogen removal over nitrite) ammonia oxidizing bacteria (*AOB*) are encouraged and nitrite oxidizing bacteria (*NOB*) hindered by operating at higher temperature of 30-35 °C, SRT=HRT of 1-2 d and lower oxygen concentrations of 1-2 mg/L. The products of SHARON® process are approximately 50% ammonia and 50% nitrite to be further denitritified by ammonia as electron donor in ANAMMOX® and CANON® processes or heterotrophic bacteria in SHARON® process. In the ANAMMOX process, also known as fully autotrophic nitrogen removal, nitrite and ammonia acts as an electron donor to convert nitrite to nitrogen gas. Autotrophic ANAMMOX bacteria are very slow growers with μ_{max} of 0.069 1/d, which is significantly lower than nitrifying bacteria with μ_{max} of 0.8 1/d. As a result very long SRT of 30-50 days are needed to facilitate ANAMMOX process. Moreover nitrite > 40 mg/L and free ammonia > 10 mg/L have inhibitory effects on ANAMMOX.

The temperature for ANAMMOX process should be maintained within 30-35 C.

As depicted in **Figure 2.4d**, the BABE® process is comprised of a single batch reactor. Side stream waters high in ammonia content and return activated sludge (RAS) from the main biological treatment process are combined with previously settled sludge in the batch reactor at average temperature of 25 °C. [94] The RAS is used to augment the bacteria in the settled sludge. By utilizing a batch reactor, the long residence times necessary to grow both the nitrifying and denitrifying bacteria are possible. There are five phases to the BABE® process: 1-filling, 2-mixing and aeration, 3-mixing, 4- settling, and 5-settling and decant. [94] The first two steps are done under aerobic conditions. The third involves mixing without aeration to achieve anoxic conditions. This condition is conducive to denitrification. Steps four and five complete the process.

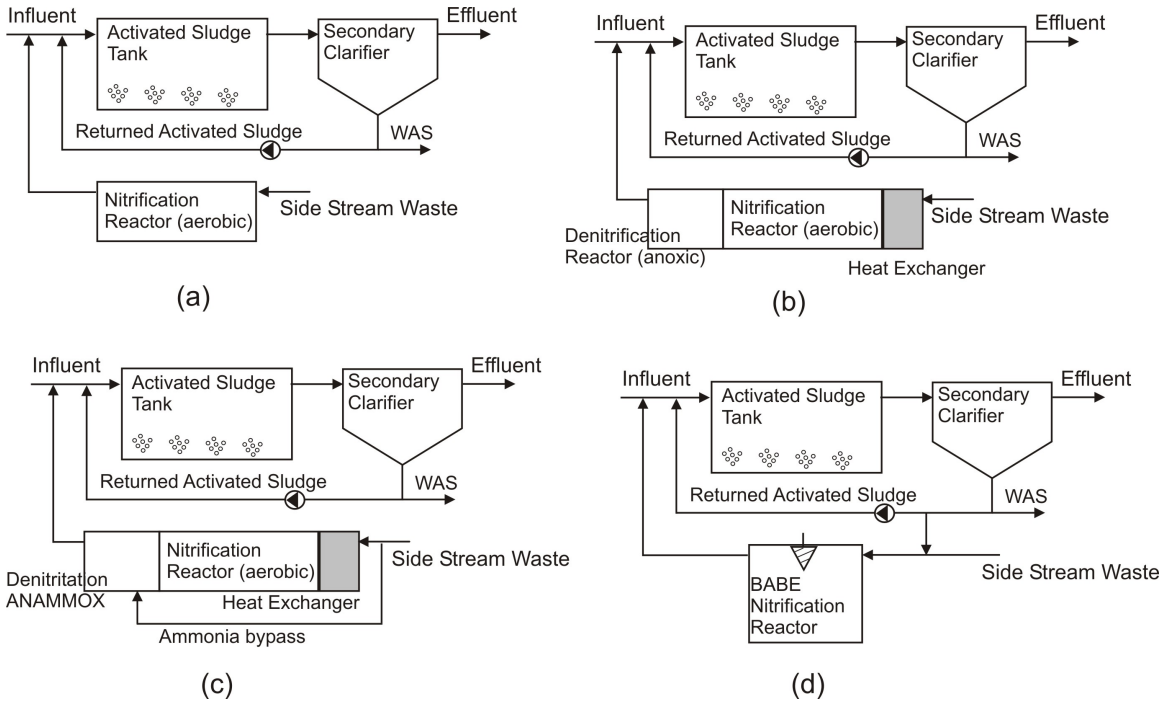

Figure 2.4. Schematic of innovative biological nitrogen removal processes from side stream waste (a) InNitri Process (b) SHARON (c) SHARON/ANAMMOX (d) BABE (Adapted from USEPA 2008)

2.5.3 Biological Phosphorus removal

Biological phosphorus removal is accomplished by creating conditions favorable for the growth of phosphorus accumulating organisms (PAOs), causing the activated sludge community to become enriched with them. [95] As illustrated in **Figure 2.5**, the anaerobic zone provides the selective advantages for the PAOs by allowing them to grow at the expense of other heterotrophic bacteria. Because oxygen and nitrate-N are absent, oxidation of organic matter cannot occur in the time provided, making it impossible for most species of heterotrophic bacteria to transport and store metabolized organic matter, and rather carry out fermentation reactions, forming volatile fatty acids (VFAs). Phosphorus accumulating organisms are able to transport VFAs into the cell and store them as polyhydroxyalkanoates (PHAs) predominantly polyhydroxybutyrates (PHBs) and other carbon storage polymers, using energy from the cleavage of intracellular polyphosphate, releasing inorganic phosphate. The VFAs are then unavailable to the other heterotrophic bacteria when the mixed liquor flows into the aerobic zone. Rather, the stored substrate is used exclusively by the PAOs for growth and to provide energy for reforming polyphosphate from inorganic phosphate in the wastewater. Only the slowly biodegradable substrate is available to the other heterotrophs. As a consequence, PAOs become a significant part of the community. Because of its role in microbial selection, the anaerobic zone is referred to as an anaerobic selector. Since the PAOs generally grow in a flocculent rather than a filamentous form, anaerobic selectors have also been used to control filamentous sludge bulking, providing another method of metabolic selection. [96]

The enrichment of biomass with PAOs, which contain a high concentration of polyphosphate at the end of aerobic zone, provides the mechanism by which phosphorus is removed from the wastewater. The phosphorus content of a typical activated sludge is on the order of 1.5-2% (expressed on the basis of phosphorus to volatile suspended solids in the mixed liquor), whereas when PAOs are present the P/VSS ratio will typically be increased to the 5-7% range, with values as high as 12-15% sometimes observed. [66]

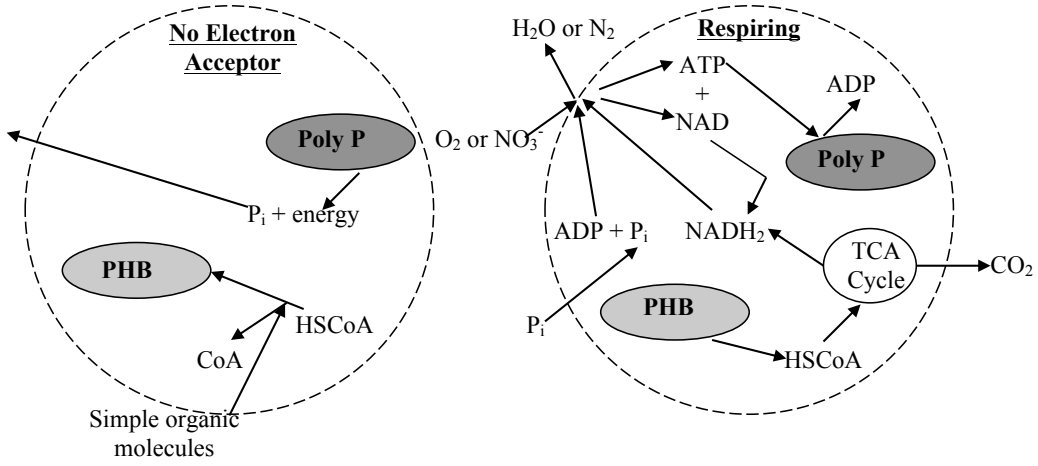

Figure 2.5. Biochemical mechanisms of enhanced biological phosphorus removal [96]

2.6 BNR Processes

In many important waste treatment processes the cells are aggregated either into flocs or biofilms. Some of these processes can be performed as suspended- or attached-growth processes. Suspended-growth processes are the biological treatment processes in which the microorganisms responsible for the conversion of the wastes are maintained in suspension within the liquid. Attached- growth or fixed-film processes are biological processes applied in waste neutralization, in which the microorganisms responsible for the conversion of organic matter or other constituents in the wastewater or air are attached to some inert solid surfaces. Attached-growth biological treatment processes are usually used to remove organic matter found in wastewater. It is also used to achieve biological conversion of nitrogen compounds (nitrification or denitrification). [97]

2.6.1 Suspended Growth Processes

Most wastewater treatment plants are equipped with this type of suspended growth process called “activated sludge”. This process has been adopted worldwide as a secondary biological treatment for domestic wastewaters. This process consists essentially of an aerobic treatment that oxidizes organic matter to CO_2, H_2O, and new cell

biomass where air is provided by using diffused or mechanical aeration. Aerobic oxidation of organic matter is carried out in this tank. At the same time, primary effluent is introduced and mixed with return activated sludge (RAS) to form the mixed liquor, which contains 2000–3000 mg/L of suspended solids. In the activated sludge process, a large portion of the biomass is recycled, thus decoupling the mean cell residence time (i.e., sludge age) from the hydraulic retention time and making the former much greater than the latter to facilitate biomass growth. This practice helps maintain a large number of microorganisms that effectively oxidize organic compounds in a relatively short time. The hydraulic detention time in the aeration basin varies between 4 and 8 hours. The microbial cells form flocs that are allowed to settle in a clarification tank. Technologically, the function of the settling tank is to separate the phases and recycle part of the biomass. However, this conventional process has the disadvantages of large area requirements, high biomass production, and low sludge age and with low treatment capacity. [98] Some suspended growth BNR processes with layouts depicted in **Figure 2.6**, are described in **Table 2.4**.

Table 2.4. Suspended growth processes for wastewater treatment [65]

Process	**Description**
Ludzack-Ettinger	Ludzack and Ettinger was introduced with preanoxic BNR in 1962, which was an anoxic-aerobic operating sequence. The influent wastewater was fed to an anoxic zone, which was followed by an aerobic zone. The process relies on the nitrate formed in the aerobic zone being returned via the RAS to the anoxic zone. Because the only nitrate fed to the anoxic zone is that in the RAS, denitrification is limited greatly by the RAS recycle ratio.
Modified Ludzack-Ettinger (MLE)	MLE is one of the most widely used BNR processes. Barnard (1973) improved the original Ludzack-Ettinger design by providing the internal recycle to feed more nitrate to the anoxic zone directly form the aerobic zone. Both the denitrification rate and overall nitrogen-removal efficiency are increased. The internal recycle flow ratio (recycle flowrate divided by influent flowrate) typically ranges from 2 to 4.

Bardenpho	Bardenpho process was developed and applied at full-scale facilities in South Africa in the mid-1970s, before making its way to the United States in 1978. The detention time of the postanoxic stage is about the same as or larger than that used for the preanoxic zone. During pilot plant testing with higher-strength wastewaters, Barnard (1974) found that biological phosphorus removal occurred as well as nitrogen removal.
University of Cape Town (UCT)	The UCT process was developed at the University of Cape Town (South Africa). It was developed to minimize the effect of nitrate in weaker wastewaters in entering the anaerobic contact zone. The amount of nitrate in the anaerobic zone is critical to the biological phosphorus-removal efficiency. The return activated sludge is recycled to the anoxic stage instead of the aeration stage, and the internal recycle is from the anoxic stage to the anaerobic stage. By returning the activated sludge to the anoxic stage, the introduction of nitrate to the anaerobic stage is eliminated, thereby improving the uptake of phosphorus in the anaerobic stage. The anaerobic recycle rate is typically 2 times the influent flow rate.

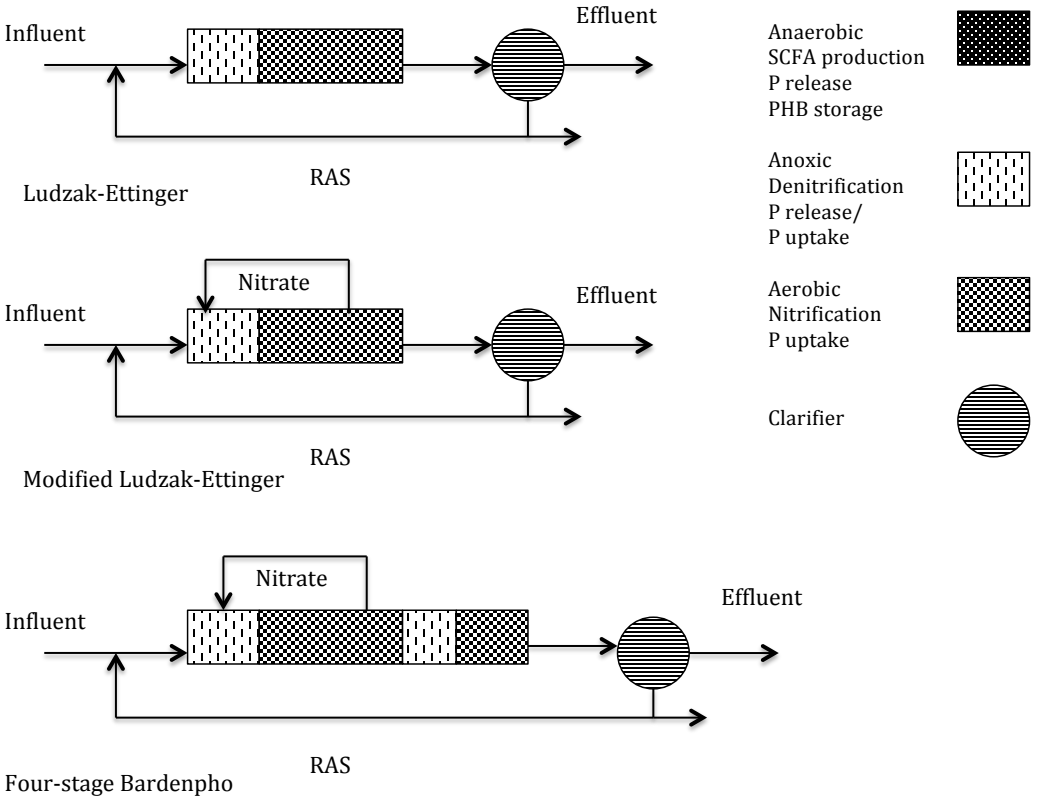

Figure 2.6. Schematic of some common BNR processes

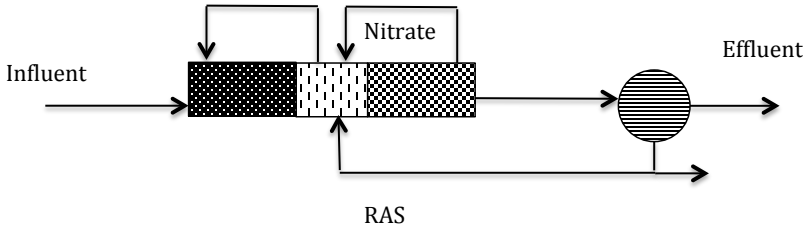

UCT

(MetCalf and Eddy, 2003)

Figure 2.5. Continued

2.6.2 Attached Growth Processes

In an attached growth system also known as fixed-film processes (**Table 2.5**), microorganisms are grown in a biofilm that are attached over the surface of a solid support medium [6] on which the individual microorganisms are immobilized. Wastewater treatment processes are based on the use of two types of attached growth; static biofilms (e.g. in trickling filters), particulate biofilms (e.g. in biofilm fluidized bed reactors, upflow anaerobic sludge blanket reactors and biofilm airlift suspension reactors). The application of biofilm processes for biological wastewater treatment is gaining interest because of the benefits offered by biofilms. Advantages of biofilm processes are primarily due to the active biomass built up and maintained in the reactor through attachment to solid surfaces. Thus, fixed-film processes allow the accumulation of high biomass concentrations, which facilitate large volumetric loadings and maintain good effluent quality. Moreover, biofilm reactors are mainly useful when slow growing microorganisms like nitrifiers have to be kept in a wastewater treatment process. Recently, both nitrification and denitrification have been individually successfully achieved in the biofilm reactor. [99]

Table 2.5. Attached growth processes for wastewater treatment [65]

Process	Description
Trickling Filter	The trickling filter is a non submerged fixed-film biological reactor using rock or plastic packing over which wastewater is distributed continuously. Treatment occurs as the liquid flows over the attached biofilm. Both BOD removal and nitrification can be accomplished at low organic loadings.
RBC	Rotating biological contractors (RBCs) were first installed in West Germany in 1960 and later introduced in the United States. An RBC consists of series of closely spaced circular disks of polystyrene or polyvinyl chloride that are submerged in wastewater and rotate through it. RBC is effective in organic removal and nitrification.
Biofor	The Biofor process, an upflow submerged aerobic attached growth process, is begin used more than 100 installations in Europe and North America. This process has been applied for BOD removal and nitrification, tertiary nitrification, and denitrification.
Packed-bed Reactors	Upflow and downflow packed-bed reactors are used for biological denitrification following secondary nitrification processes to reduce nitrate/nitrite produced. Typically an external carbon source is added to provide an electron donor for nitrate/nitrite reduction.

2.7 Application of Particulate Biofilms in Wastewater Treatment

The main reactor types applicable for the suspension of particulate biofilms in wastewater treatment processes are Biofilm Upflow Sludge Blanket (USB), Fluidized Bed (BFB), Expanded Granular Sludge Blanket (EGSB), Biofilm Airlift Suspension (BAS), and Internal Circulation (IC) reactors (**Figure 2.7**). In USB, BFB and EGSB reactors (**Figure 2.7 a,b,c**, respectively), particles are kept fluidized by the up-flowing influent. In BAS reactors (**Figure 2.7d**) an airlift suspension is obtained by pumping air into the system, whilst in IC reactors (**Figure 2.7e**) the gas produced in the system drives the circulation and mixing of liquid and solids in the reactor. [100]

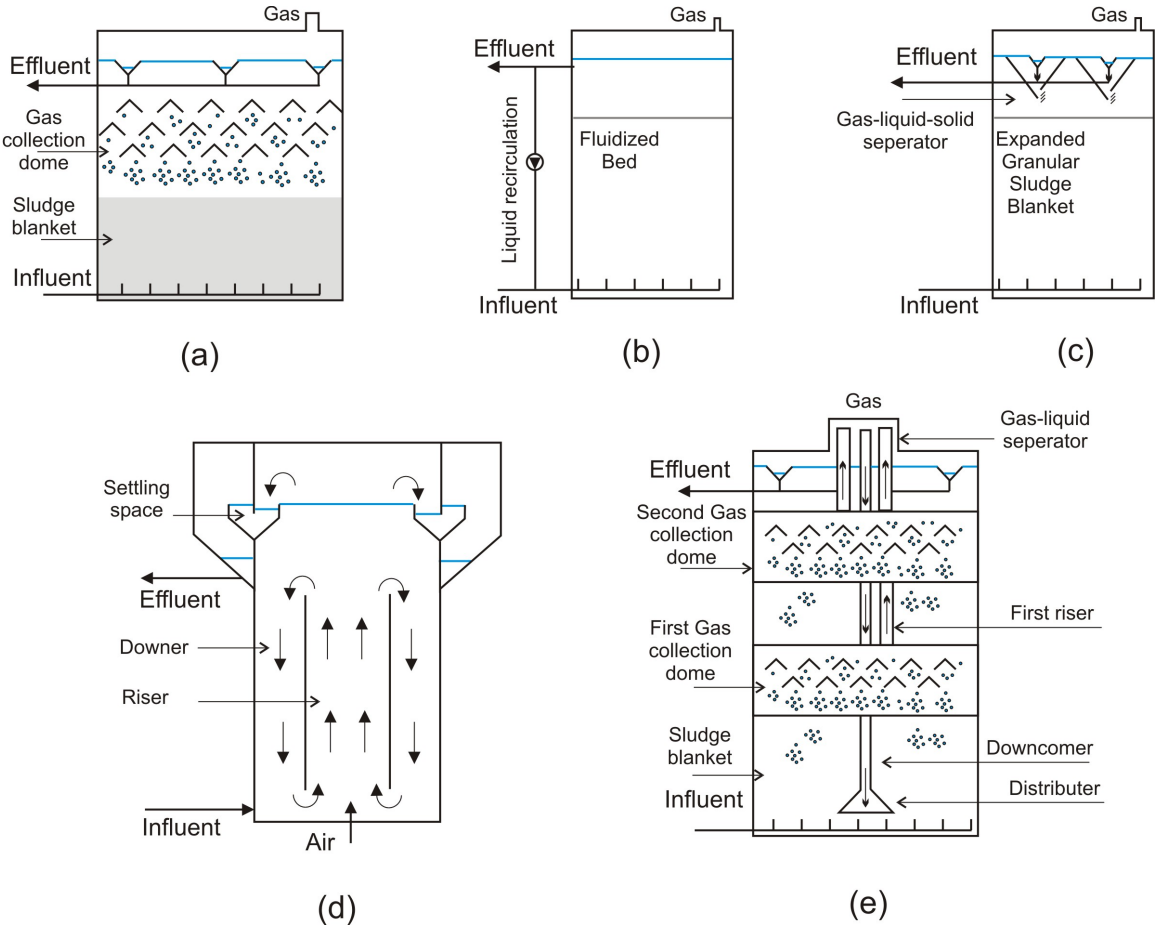

Figure 2.7. Biofilm reactor configurations (a) USB (b) BFB (c) EGSB (d) BAS (e) IC (Adapted from Nicolella et al., 2000)

2.7.1 Biofilm AirLift Suspension (BAS®) Reactor

The BAS technology was originally developed for aerobic purification of anaerobically treated industrial wastewaters. [12, 101, 102] Airlift reactors consist of two connected sections, a riser and a downer. [103] Different configurations are possible, including internal loop and external loop reactors. The principle of operation is the same for both configurations. A gas is sparged at the bottom, moves upward and exits at the top of the riser section. In internal-loop airlift reactors, air may recirculate through the downer section and provide aeration throughout the reactor. The difference in density between riser and downer, due to the difference in gas hold-up, drives the liquid to circulate between the two sections. When the liquid velocity is sufficiently high, small

particles will be suspended and recirculated with the liquid. This results in a thorough mixing of both particles and liquid throughout the reactor. The airlift technique has found two major applications in wastewater treatment processes, the Biofilm Airlift Suspension (BAS) reactor (**Figure 2.7d**) for aerobic treatment and the gas-lift reactor for anaerobic treatment. [100]

Fundamental and applied research on Biofilm Airlift Suspension (BAS®) reactors in the late 1980s [12, 101, 102], including research at Gist-Brocades, TNO (Dutch Organisation for Applied Scientific Research) and Delft University of Technology (The Netherlands), led to the concept of CIRCOX® airlift reactor (**Figure 2.9**), developed and patented by Gist-Brocades and commercialized by Paques. [100] In general, in airlift reactors the biomass is immobalized on small (200-300 μm) carrier particles. [104] The reason why a relatively very small media with average size of 0.09 mm to 0.3 mm is used in airlifts might be due to the limitation of minimum fluidization velocity provided by airlift.

2.7.2 Internal Circulation Reactor (IC®)

In fact the IC® reactor consists of two UASB reactors on top of each other; one high loaded and one low loaded (**Figure 2.8**). Its special feature is the separation of biogas in two stages. The biogas collected in the first stage drives a gas-lift creating an internal circulation, from which the reactor's name has been derived. Figure 1 presents a schematic of the IC® reactor. [105]

The influent (1) is pumped into the reactor via a distribution system, where influent, recycled mixed liquor and effluent are well mixed (2). The first reactor compartment (3) contains an expanded granular sludge bed, where most of the COD is converted into biogas. The biogas produced in this compartment is collected by the lower level phase separator (4) and is used to generate a gas lift by which water and sludge are carried upward via the "riser" pipe (5) to the gas/liquid separator (6) on top of the reactor. Here the biogas (7) is separated from the water/sludge mixture and leaves the system. The water/sludge mixture is directed downwards to the bottom of the reactor via the concentric "downer" pipe (8), resulting in the internal circulation flow. The effluent from the first compartment is post-treated in the second, low loaded compartment (9), where

residual biodegradable COD is removed. The biogas produced in the upper compartment is collected in the top three-phase-separator (10), while the anaerobic treated effluent (11) leaves the reactor via overflow weirs.

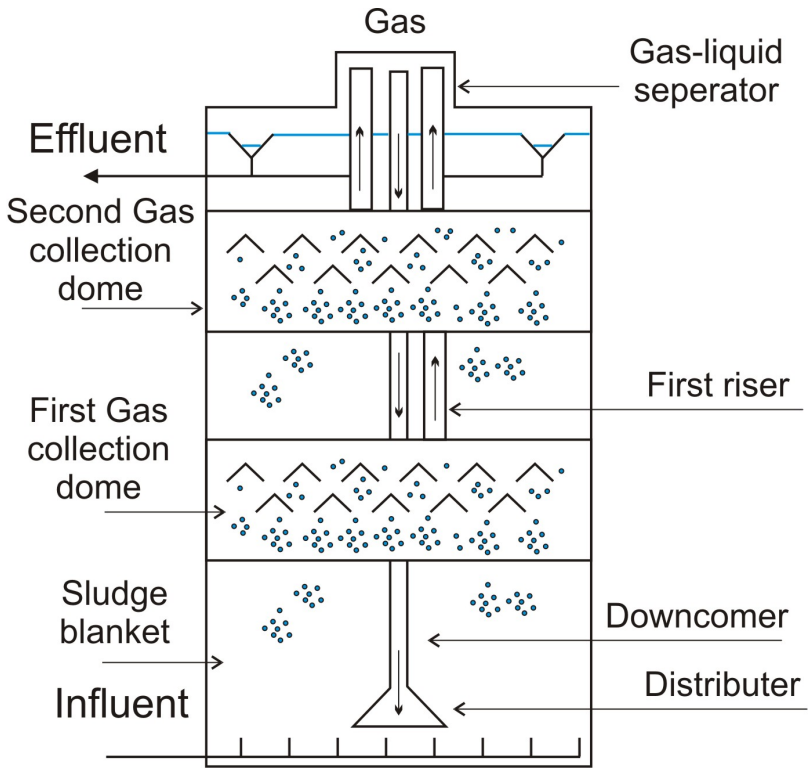

Figure 2.8. Schematic of IC® (Adapoted from Driessen et al., 1997)

In principle the IC® technology is suitable for treatment of all types of effluents that can be treated by the UASB process as it has already been applied on a large variety of industrial effluents. [105]

2.7.3 CIRCOX® AirLift Reactor

A schematic diagram of the CIRCOX® airlift reactor is presented in **Figure 2.9**. The cylindrical bottom part incorporates another cylinder creating a riser and a downer. Air is introduced at the bottom of the reactor into the riser creating an internal circulation of wastewater and biomass going up in the riser and down in the downer. The driving force for this so-called airlift is created by density difference (because of air hold up) between the riser and the downer. The airlift provides the mixing and ensures optimal contact

between wastewater and biomass. The top part of the CIRCOX® consists of a settler in which the biomass is settled and allowed to flow back into the downer.

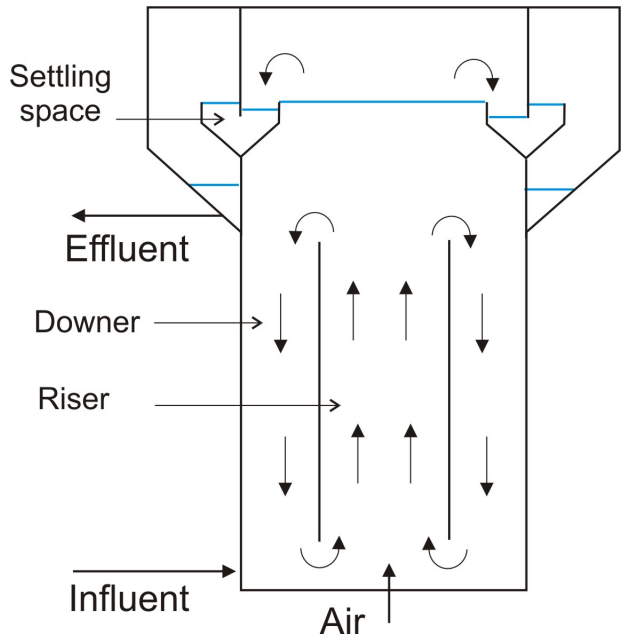

Figure 2.9. Schematic of CIRCOX airlift (Adapted from Mulder 1992)

The CIRCOX® uses biomass on a carrier in the form of basalt grains, which has excellent settling properties. This allows for effective separation of the wastewater and biomass whereas primary suspended solids pass through the system. In this way a very high biomass concentration (10-40 g VSS/L) can be maintained in the reactor. Due to the good sludge retention the sludge age is very high, resulting in minimal excess sludge production. The high sludge age furthermore enables specialized growing micro-organisms to retain in the reactor, making the CIRCOX® technology especially suitable for biological conversion of difficult compounds like ammonia and xenobiotics. [106]

In 1985 the TNO studied the airlift technology at bench scale for the treatment of municipal wastewater. High removal efficiencies for both BOD and Kjeldahl N were obtained. [107] However, in order to meet a more stringent nitrogen effluent concentration (< mg N/L), a CIRCOX® in combination with a denitrifying CIRCOX® reactor (**Figure 2.10**) was used in a pilot-plant scale at Zaandam, The Netherlands. [108] In both

reactors, basalt (Basalt N. V., Schiedam, Holand) was used with the diameter varied from 0.09 to 0.30 mm).

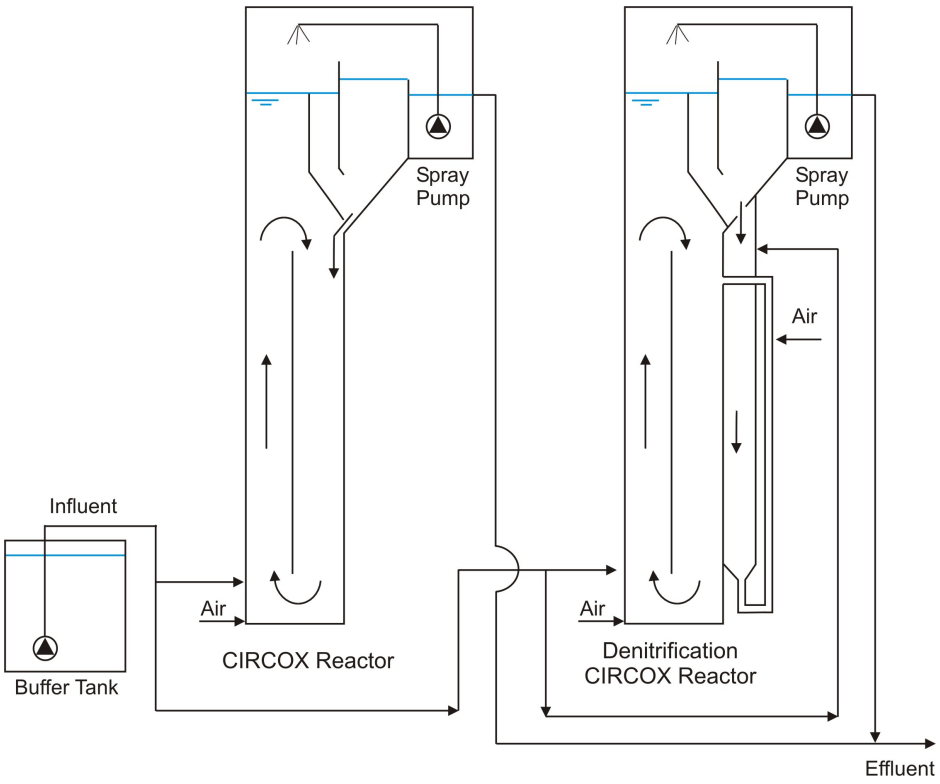

Figure 2.10. schematic diagram of the pilot scale plant set up at Zaandam (Adapoted from Frijters et al., 1997)

Frijters et al. (2000) also proposed a new type of CIRCOX® for a potato processing wastewater. This type of airlift reactor with biofilms on carrier is an airlift reactor extended with an anoxic compartment to obtain total nitrogen removal as sketched in **Figure 2.11**. [109]

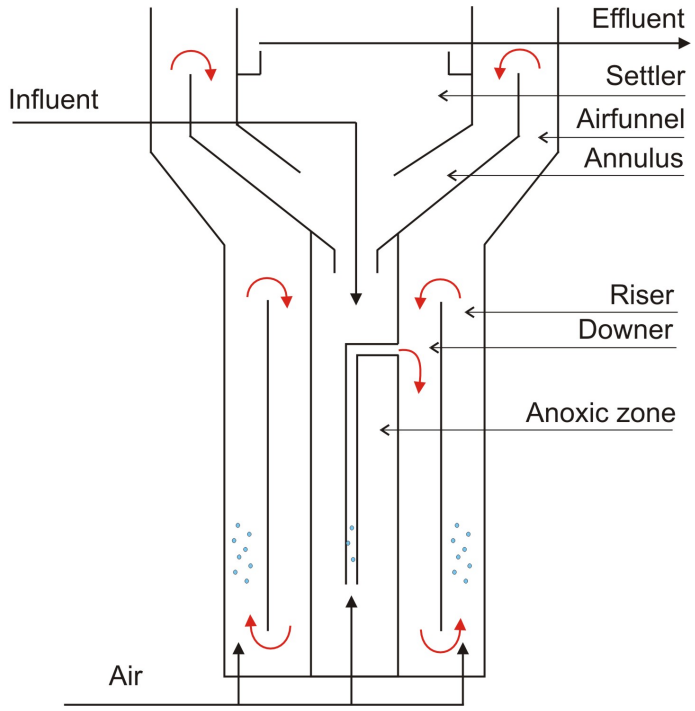

Figure 2.11. CIRCOX reactor with integrated anoxic compartment (Adapted from Frijters et al., 2000)

The above configuration was claimed to achieve complete nitrification and 90% denitrification with a HRT of 3-4.3 hrs.

The circulating floating bed reactor (TURBOFLO) is another form of BAS biofilm reactor for secondary and tertiary wastewater treatment developed by Cie Lyonnaise des Eaux (France) using the concept of an internal circulating airlift reactor [110] (**Figure 2.12**). The reactor comprises a rectangular column filled with high density polyethylene granules (size: 0.5–2.5 mm; density 860 kg/m^3). An industrial-scale reactor was operated at a wastewater treatment plant at Evry (France). [100]

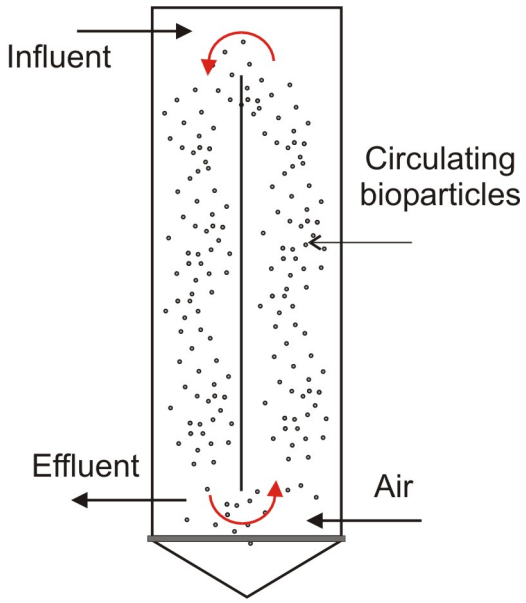

Figure 2.12. Industrial-scale circulating floating bed configuration (Adapted from Lazarova and Manem 1996)

In 1994 a combined anaerobic/aerobic wastewater treatment plant comprising BIOPAQ®-IC and CIRCOX® technology (**Figure 2.13**) was used at the Grolsch brewery, Enschede, The Netherlands. [105] The plant also consisted of buffering and pre-acidification tanks in prior to the aforementioned reactor combination. The flow rate of the brewery wastewater was 4200 m3/d with TCOD of 2500 mg/l, TSS of 750 mg/l, average temperature of 32 C and average pH of 6.8. [105] BIOPAQ®-IC and CIRCOX® are relatively tall slender tanks with heights of respectively 20m and 19 m and with hydraulic retention times of 2.2h and 1.3 h respectively. [105, 111] Driessen et al. (1997) reported overall TCOD and SCOD removal efficiencies average 80% and 94% respectively. Excess bio-solid production was estimated to be less than 0.01 kg TS/kg COD. However, due to lack of information regarding the effluent VSS in the article, estimation of the actual observed yield seems to be unfeasible. It should be mentioned that no further study for biological nutrients removal was conducted for the combination of BIOPAQ®-IC and CIRCOX®.

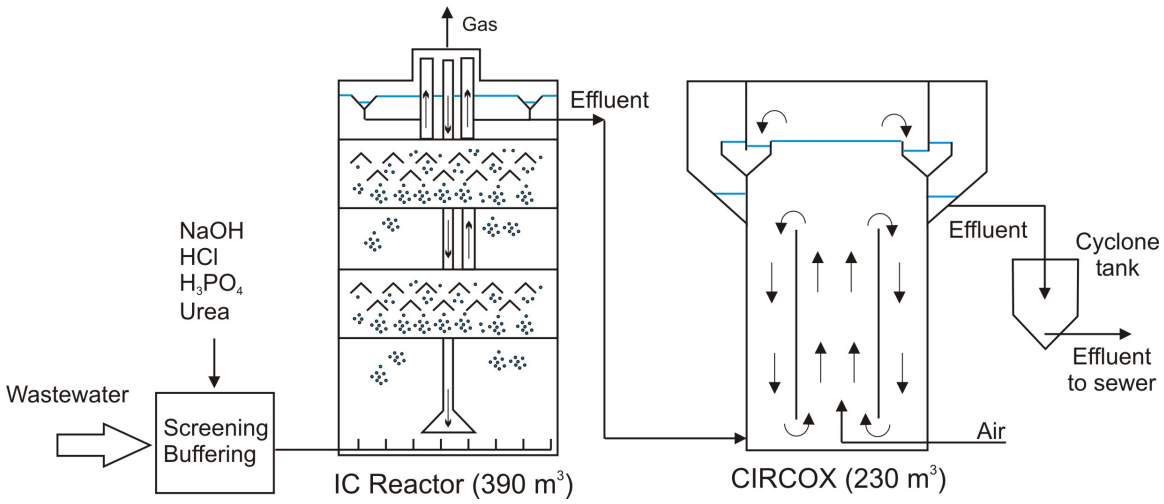

Figure 2.13. Schematic of process flow diagram of IC and CIRCOX (Adapted from Driessen et al., 1997)

2.7.4 Fluidized Bed Bioreactors

Fluidized bed bioreactors have emerged in recent years as one of the most promising devices for biological wastewater treatment. [100, 112] In such reactors, organic or inorganic pollutants in wastewater are removed by microbes immobilized on the surface of the fluidized particles. The particles coated with biofilm are termed as biofilm-coated particles. Biological wastewater treatment using fluidized bed bioreactors involves both aerobic and anaerobic processes.

The use of immobilized living cells on particle in an expanded bed or a fluidized bed for wastewater treatment was conceived as early as the 1930's [113]. However, engineering work utilizing immobilized cells in a mobile state, or more precisely a fluidized bed bioreactor, as a sole means of biodegradation in wastewater treatment was not attempted until the late 1960's. Among early investigators, Weber and his coworkers studied the physicochemical treatment of raw sewage using granular activated carbon in a fluidized bed bioreactor. [114] Jesis (1977) employed a fluidized bed bioreactor to treat ammonia-rich wastewater using sand as a career media and observed that the ammonia removal efficiency depends on the total sand concentration in the fluidized bed. The first industrial

application of the fluidized bed technology was reported by Jeris (1983) when an Ecolotrol HY-FLO system was installed at a soft drink bottling plant in Birmingham (USA). [115] Since the early 1980s, fluidized bed bioreactors are being used for industrial and municipal wastewater treatment. **Table 2.6** shows some full-scale applications of fluidized bed bioreactors in wastewater treatment.

Table 2.6. Applications of the particulate bioreactors for wastewater treatment [63]

Commercial names	Development	Examples of full –scale applications	Design parameters	References
BFB ANAFLUX, Degremont, France	Upflow anaerobic BFB using a mineral support (BIOLITE R280) as fluid bed media to treat a variety of brewery, food-processing and paper industry wastewater	Starch factory, Habourdin, France (1993)	V_L: 200 m^3; OLR: 12,000 kg COD/d; RC: 60 kg COD/(m3.d)	Holst et al. (1997)
BFB OXYTRON, ANYTRON, Dorr-Oliver, USA	Carbonaceous oxidation, nitrification, denitrification and anaerobic reduction of municipal and industrial (automotive industry, coke-making operations) wastewater using sand activated carbon as fluid bed media	By-product coke plant, ON, Canada (1996)	V_L: 540 m^3; OLR: 6,690 kg COD/d; RC: 10.5 kg COD/(m3.d)	Sutton et al. (1999)

V_L = reactor volume; OLR = organic loading rate; RC = reactor capacity

2.7.5 Circulating Fluidized Bed Bioreactor (CFBBR)

The circulating fluidized bed bioreactor (CFBBR) technology consists of two fluidized bed columns, **Figure 2.14**, that utilize attached microbial films on a carrier media for BNR, was introduced and patented in 2005. [116] As depicted in **Figure 2.14**, the column with smaller surface area acts as an anoxic column where denitrification occurs and the right column with greater surface area is predominantly for nitrification as well as aerobic utilization of organics. Lava rock particles with an average size of 700 micron were used as the carrier media in this technology in both columns, which provided up to 4000 m^2/m^3 specific surface area after development of biofilm. This specific surface area can only be provided when using a very porous and fine particle, which cannot be easily handled in other technologies. This technology was a promising "fixed-film" nutrient removal which

has demonstrated 95% carbon, 85% nitrogen and 70% phosphorus removal in both lab and pilot scales (a pilot-scale CFBBR has been established at the Adelaide wastewater treatment plant in London, Canada in cooperation with Ontario Centre of Excellence (OCE), Trojan Technology and the City of London) with an overall retention time of less than 2.7 h and a very low sludge yield of 0.1 g VSS/g COD. [65, 117, 118]

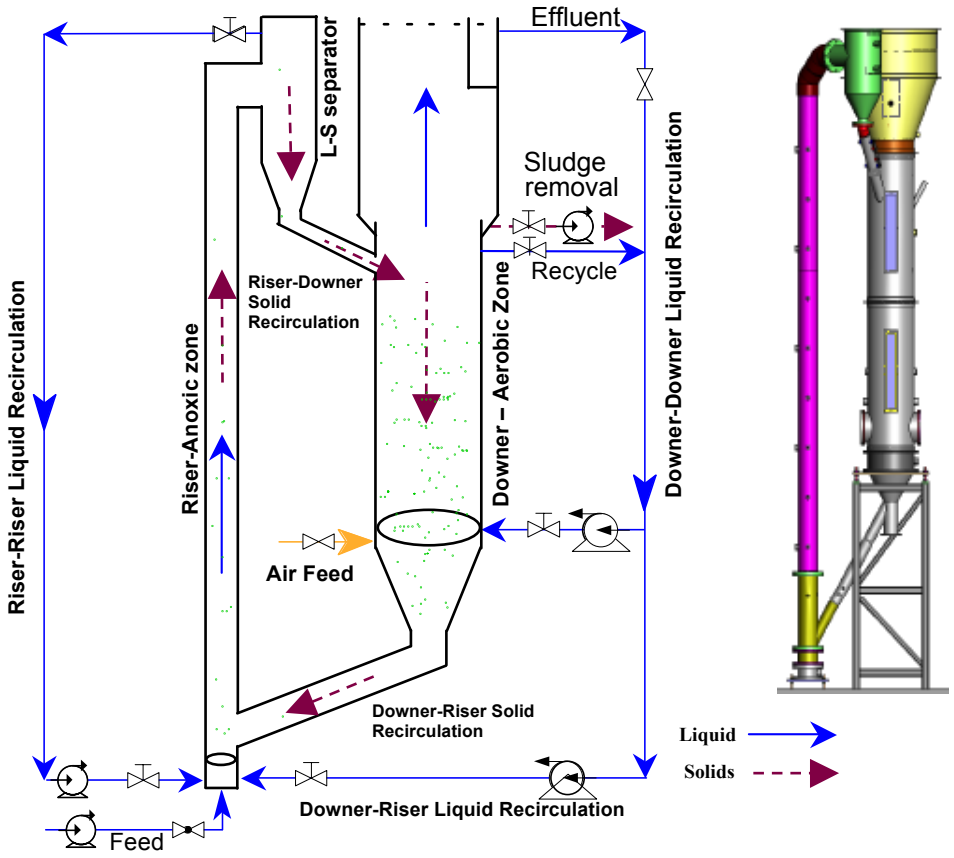

Figure 2.14. Schematic of CFBBR

2.8 Kinetic Models of Nitrification and Denitrification

The classical microbial growth kinetics model termed the Monod model is a simple empirical model that introduces the concept of a growth-controlling substrate. For nitrification systems operated at temperatures below 28°C, ammonia-oxidation kinetics versus nitrite-oxidation kinetics are rate limiting, so that designs are based on saturation kinetics for ammonia oxidation as given below: [66]

$$\mu_n = \frac{\mu_{n,\max} N}{K_N + N} - k_{dn} \qquad (2.93)$$

where μ_n is specific growth rate of nitrifying bacteria (g new cells/g cells.d), $\mu_{n,max}$ is maximum specific growth rate of nitrifying bacteria (1/d) and K_n is half saturation coefficient, and k_{dn} is endogenous decay coefficient for nitrifying organisms (g VSS/g VSS.d).

Due to the presence of inhibitory substances and variations in experimental techniques, a wide range of maximum nitrification growth rates has been reported, 0.25-0.77 g VSS/g VSS.d at 20°C. In an event $\mu_{n,max}$ values for nitrifying organisms are much lower than the corresponding values for heterotrophic organisms, requiring much longer SRT values for nitrifying systems, 10-20 d at 10°C and 4-7 d at 20°C. [66]

Based on the aforementioned equation and mass balance over an ideal Chemostat process, Henze et al., (2008) derived **Equation (2.94)** for theoretical minimum sludge age for nitrification:

$$SRT_m = \frac{1}{\left(1 + \frac{K_{NT}}{N_{ai}}\right)\mu_{n,\max,T} - k_{dn,T}} \qquad (2.94)$$

where $\mu_{n,max,\,T}$ is maximum specific growth rate of nitrifying bacteria at temperature T (g new cells/g cells.d), K_{NT} is half saturation coefficient for nitrifiers at T(°C), N_{ai} is nitrogen ammonia concentration in the influent, and $k_{dn,T}$ is endogenous decay coefficient for nitrifying organisms at T(°C)(g VSS/g VSS.d).

Nitrification rates are affected by the liquid DO concentration. To account for the effect of DO, the expression for the specific growth rate is modified as follows: [66]

$$\mu_n = \frac{\mu_{n,\max} N}{K_N + N} \frac{DO}{K_o + DO} - k_{dn} \qquad (2.95)$$

where K_o is half-saturation coefficient for DO

At low DO concentrations (<0.5 mg/L) where nitrification rates are greatly inhibited, the low DO inhibition effect has been shown to be greater for *Nitrobacter* than for *Nitrosomonas.* [66]

Nitrate serves as an electron acceptor in the same way as oxygen from a biokinetics perspective and thus the nitrate utilization rate (denitrification rate) is proportional to the substrate utilization rate. To apply biokinetic expressions for denitrification, the substrate utilization rate expression (r_{su}) is modified to account for the fact that only a portion of the biomass is active in the anoxic zone.

$$r_{su} = -\frac{kXS\eta}{K_s + S} \qquad (2.96)$$

where η is the fraction of denitrifying bacteria in the biomass (g VSS/g VSS)

Dissolved oxygen can inhibit nitrate reduction by repressing the nitrate reduction enzyme [66] which can be expressed by the following bokinetic form:

$$r_{su} = -\left(\frac{kXS}{K_s + S}\right)\left(\frac{NO_3}{K_{s,NO3} + NO_3}\right)\left(\frac{K_O}{K_O + DO}\right)\eta \qquad (2.97)$$

where K_O is DO inhibition coefficient for nitrate reduction (mg/L) and $K_{s,NO3}$ is half velocity coefficient for nitrate limited reaction (mg/L).

Values of 0.1-0.2 mg/L and 0.1 have been proposed for K_O and $K_{s,NO3}$, respectively.

2.9 References

[1] Zhu JX, Zheng Y, Karamanev DG, and Bassi AS. (Gas-)Liquid-Solid Circulating Fluidized Beds and their Potential Applications to Bioreactor Engineering", *Can. J. Chem. Eng.*, 2000; **78**-2:82-94.

[2] Richardson JF, and Zaki WK. Sedimentation and fluidization: Part I. Trans. Instn. Engrs. 1954; 32:35-53.

[3]. Costeron, J. W., R. T. Irvin, and K.-J. Cheng. 1981. The role of bacterial surface structures in pathogenesis. Crit. Rev. Microbiol. 8:303-338.

[4] Fletcher M, and Floodgate GD. An electronmicroscopic demonstration of an acidic polysaccharide involved in the adhesion of a marine bacterium to solid surfaces. J. Gen. Microbiol. 1973; 74:325-334.

[5] Alieman JE, Veil JA, and Canaday JT. Scanning electron microscope evaluation of rotating biological contactor biofilm. Water Res. 1982; 16:543-550.

[6] van Loosdrecht MCM, Eikelboom D, Gjaltema A, Mulder A, Tijhus L, Heijnen JJ. Biofilm structures. *Water Sci. Technol*., 1995; 31:163-171.

[7] Wanner O, Eberl HJ, Morgenorth E, Noguera DR, Picioreanu C, Rittmann BE, van Loosdrecht MCM. Mathematical modeling of biofilms. IWA Task Group on Biofilm Modeling 2006 • ISBN: 9781843390879

[8] Characklis WG, Marshall KC. eds., *Biofilms*, Wiley, New York. 1990; 59.

[9] Grady JCPL, Daigger GT, Lim HC. *Biological Wastewater Treatment*. New York: Marcel Dekker, 1999; 810-811.

[10] Gujer W, Wanner O. Modeling mixed population biofilms. In *Biofilms*, Characklis, W.G., Marshall, K.C., eds. Willey, New York, 1990; 397-443.

[11] Zhang TC, Bishop PL. Experimental determination of the dissolved oxygen boundary layer and mass transfer resistance near the fluid-biofilm interface. *Water Sci. Technol.,* 1994, 30, 47-58.

[12] Heijnen JJ. Biological industrial wastewater treatment minimizing biomass production and maximizing biomass concentration. Ph.D. Thesis, 1984, Delft University of Technology, Delft, Netherland.

[13] Tijhuis L, van Loosdrecht MCM, Heijnen JJ. Formation and growth of heterotrophic aerobic biofilms on small suspended particles in airlift reactors. *Biotechnol. Bioeng*. 1994; 55:595-608.

[14] Gjaltema A, Arts PAM, van Loosdrecht MCM, Kuenen JG, Heijnen JJ. Heterogeneity of biofilms in rotating annular reactors: occurrence, structure, and consequences. *Biotechno. Bioeng.,* 1994; 44:194-204.

[15] Tijhuis L, Hijman B, van Loosdrecht MCM, Heijnen JJ. Influence of detachment, substrate loading and reactor scale on formation of biofilms in airlift reactors. *Appl. Microbiol. Biotechnol.,* 1995; 45:7-17.

[16] Stewart PS. A model of biofilm detachment. Biotechnol. Bioeng. 1993; 41:111-117.

[17] Chang HT, Rittmann BE, Amar D, Heim R, Ehlinger O, and lesty Y. Biofilm detachment mechanisms in a liquid-fluidized bed. Biotech. Bioeng. 1991; 38:499-506.

[18] Rittmann BE. The effect of shear stress on biofilm loss rate. Biotechnol. Bioeng. 1982; 24:501-506.

[19] Characklis WG, Turakhia MH, Zelver N. Transport and interfacial transfer phenomena. In: Characklis WG, and Marshall KC. (eds.), Biofilms. Wiley, New York. 1990; 265-340.

[20] Wanner O, Gujer W. A multispecies biofilm model. Biotechnol. Bioeng. 1986; 28:314-328.

[21] Speitel GE, DiGiano FA. Biofilm shearing under dynamic conditions. Biotechnol. Bioeng. 1991; 37:778-789.

[22] Nicolella C, Van Loosdrecht MMC, Di Felice, R, Rovatti M. Terminal settling velocity and bed-expansion characteristics of biofilm coated particles. Biotechnol Bioeng. 1999; 62:62-70.

[23] Mulcahy LT, LaMotta EJ. Mathematical model of the fluidized bed biofilm reactor. Processing of the 51 st annual conference of the Water Pollution control federation, Anheim, CA, USA.1978.

[24] Boaventura RA, Rodrigues AE. Consecutive reactions in fluidized-bed biological reactors: Modeling and experimental study of wastewater denitrification. Chem Engng Sci. 1988; 43:2715-2728.

[25] Hermanowicz SW, and Cheng YW. Biological fluidized bed reactor: hydrodynamics, biomass distribution and performance. Wat. Sci. Technol. 1990; 22-1:193-202.

[26] Coelhoso I, Boaventura R, Rodrigues A. Biofilm reactors: An experimental and modeling study of wastewater denitrification in fluidized-bed reactors of activated carbon particles. Biotecnol Bioeng. 1992; 40:625-633.

[27] Perry RH, Green DW. Chemical Engineer's Handbook (7th Edition). NewYork: McGrawHill Inc., 1997.

[28] Karamanev DG. Equations for calculation of the terminal velocity and drag coefficient of solid spheres and gas bubbles. Chem. Eng. Comm. 1996; 147:75-84.

[29] Yang WC. Handbook of fluidization and fluid-particle systems. Taylor and Francis 2005 Chapter 26 Liquid-solid fluidization by Epstein N.

[30] Gibilaro LG, Di Felice R, Waldram SP, Foscolo PU. Authors' reply to Clift et al. Chem Eng Sci 1987; 42:194–196.

[31] Hermanowicz SW, and Ganczarczyk JJ. Some fluidization characteristics of biological beds. Biotech. Bioeng. 1983; XXV:1321-1330.

[32] Mulcahy LT, and Shieh WK. Fluidization and reactor biomass characteristics of the denitrification fluidized bed biofilm reactor. Wat. Res. 1987; 21-4 :451-458.

[33] Wen CH, Yu YH. Mechanics of fluidization. Chem Eng Prog Symp Ser 1966; 62-62:100–111, 1966.

[34] Shieh WK, Sutton PM, Kos P. Predicting reactor biomass concentration in a fluidized-bed system. J. WPCF 1982; 53-11:1574-1584.

[35] Ergun S. Fluid flow through packed columns. Chem Eng Prog 1952; 48:89–94.

[36] Gibilaro LG, Hossain I, Foscolo PU. Aggregate behaviour of liquid fluidised beds. Can J Chem Eng 1986b; 64:931–938.

[37] J.M. Begovich and J.S. Watson , An electroconductivity technique for the measurement of axial variations of holdups in three-phase fluidized beds. *A.I.Ch.E. J.* 1978; 24:351–354.

[38] Khan AR, Richardson JF. Fluid-particle interactions and flow characteristics of fluidized beds and settling suspen- sions of spherical particles. Chem Eng Commun. 1989; 78:111–130.

[39] Couderc JP. Incipient fluidization and particulate systems. In: Davidson JF, Clift R, Harrison D, eds. Fluidization. 2d ed. London: Academic Press, 1985; 1–46.

[40] Di Felice R, Parodi E. Wall effects on the sedimentation velocity of suspensions in viscous flow. AIChE J 1996; 42:927–931.

[41] Rowe PN. A convenient empirical equation for estimation of the Richardson–Zaki exponent. Chem Eng Sci 1987; 42:2795–2796.

[42] Wallis GB. One-Dimensional Two-Phase flow. New York: McGraw-Hill, 1969.

[43] Garside J, Al-Dibouni MR. Velocity–voidage relationships for fluidization and sedimentation in solid-liquid systems. Ind Eng Chem Process Des Dev 1977; 16:206–214.

[44] Fan LS, Gas–Liquid–Solid Fluidization Engineering. Stoneham, MA: Butterworth, 1989.

[45] Bhatia VK, Epstein N. Three phase fluidization: a general wake model. In: Angelino H, Couderc JP, Gibert H, Laguerie C, eds. Fluidization and Its Applications. Toulose: Cepadues-editions, 1974; 372–392.

[46] Shieh WK, Keenan DK. Fluidized bed biofilm reactor for wastewater treatment. In: Fiechter, A. (Ed.), Advances in Biochemical Engineering/Biotechnology. Springer-Verlag, Berlin, 1986; 132-168.

[47] Yu H, and Rittmann BE. Predicting bed expansion and phase holdups for three-phase fluidized-bed reactors with and without biofilm. Wat. Res. 1997; 31-10:2604-2616.

[48] Heijnen JJ, van Riet K. Mass transfer and heat transfer phenomena in low viscosity bubble column reactors. *Chem. Eng. J*., 1984; 28:21-42.

[49] Koide K, Horibe K, Kawabata H, Ito S. Gas holdup and volumetric liquid-phase mass transfer coefficient in solid-suspended bubble column with draught tube. *J. Chem. Eng. Jpn.*, 1985; 18:248-254.

[50] Miyahara T, Kawate O. Hydrodynamics of a solid-suspended bubble column with a draught tube containing low-density particles. *Chem. Eng. Sci.*, 1993; 48:127-133.

[51] Hwang SJ, Lu WJ. Gas-liquid mass transfer in an internal loop airlift density particles. *Chem. Eng. Sci.* 1997; 853-857.

[52] Muroyama K, Fan LS. Fundamentals of gas-liquid-solid fluidization. *AIChE J*., 1985; 31:1-34.

[53] Gavroy D, Joly-vuillemin C, Cordier G, Delmas H. Gas hold-up, liquid circulation and gas-liquid mass transfer in slurry bubble columns. *Chem. Eng. Res. Des.*, 1995; 73:637-642.

[54] Lu WJ, Hwang SJ, Chang CM. Liquid velocity and gas holdup in three-phase internal loop airlift reactors with low-density particles. *Chem. Eng. Sci*. 1995; 50: 1301-1310.

[55] Ryhner G, Petrozzi S, Dunn IJ. Operation of a three-phase biofilm fluidized sand bed reactor for aerobic wastewater treatment. *Biotechnol. Bioeng*., 1988; 32:677-688.

[56] Heijnen JJ, Hols J, van der Lans RGJM, van Leewen HLJM, Mulder A, Weltevrede R. A simple hydrodynamic model for the liquid circulation velocity in a full-scale two and three phase internal airlift rector operating in the gas recirculation regime. *Chem. Eng. Sci*., 1997; 52:2527-2540.

[57] Fan LT, Yang YC, Wen CY. Mass transfer in semiflui- dized beds for solid-liquid system. AIChE J 1960; 6:482–487.

[58] Sano Y, Yamaguchi N, Adachi T. Mass transfer coefficients for suspended particles in agitated vessels and bubble columns. *J. Chem. Eng. Jpn*., 1974; 7:179-186.

[59] Sanger P, Deckwer WD. Liquid-solid mass transfer in aerated suspensions. *Chem. Eng. J*., 1981; 22:179-186.

[60] Arters DC, Fan LS. Solid-liquid mass transfer in a gas-liquid-solid fluidized bed. *Chem. Eng. Sci.*, 1986; 41:107-115.

[61] Livingston AG, Chase SF. Liquid-solid mass transfer in a three-phase draft tube fluidized bed reactor. *Chem. Eng. Commun*. 1990; 92:225-244.

[62] Harremoes P, Henze M. Biofilters In: Henze, M., Harremoes, P., Jansen, J.C., Arvin, E. (Eds.), *Wastewater Treatment*. Springer, Berlin, 1995; 143-192.

[63] Harremoes P. *Biofilm Kinetics*. In: Mitchell, R. (Ed.), Water Pollution Microbiology, vol. 2. Wiley, New York, 1978; 71-109.

[64] Rosenwinkel KH, Beier M, Phan LC, and Hartwig P. Conventional and advanced technologies for biological nitrogen removal in Europe. Wat. Prac. Technol. 2209; 4-1:1-8.

[65] Chowdhury N. BIOLOGICAL NUTRIENT REAMOVAL FROM Municipal Wastewater using a Liquid-solid Circulating Fluidized Bed Bioreactor. The University of Western Ontario. PhD Thesis 2009

[66] Metcalf and Eddy, Wastewater Engineering: Treatment and reuse. 4th ed., McGraw-Hill (2003).

[67] M. Henze, M.C.M. Van Loosdrecht, G.A. Ekama, and D. Brdjanovic, Biological wastewater treatment: Principle, modeling and design. IWA publishing. ISBN: 1843391880. (2008)

[68] Ahn YH. Sustainable nitrogen elimination biotechnologies: A review. *Process Biochem*. 2006; 42:1709-1721.

[69] Teske A, Alm E, Regan JM, Toze S, Rittman BE, and Stahl DA. Evolutionary relationship among ammonia and nitrite-oxidizing-bacteria. J. Bactrio. 1994; 176:6623-6630.

[70] Gao D, Peng Y, and Wu W. Kinetic model for biological nitrogen removal using shortcut nitrification-denitrification process in sequencing batch reactor. Environmental Science and Technology. 2010; 44:5015-5021.

[71] Tugtas, A.E., (2007). Effect of nitrate reduction on the methanogenic fermentation: Process interactions and modeling. phD thesis. Georgia Institute of Technology.

[72] Lengeler JW, Drews G, Schlege HG. Biology of the prokaryotes. ISBN: 3-13-108411-1. 1999.

[73] Q. Banihani, R. Sierra-Alvarez, and J.A. Field, Nitrate and nitrite inhibition of methanogenesis during denitrification in granular biofilms and digested domestic sludges. Biodegradation. 20 (2009) 801–812.

[74] USEPA. *Process design manual of nitrogen control*. 1993, EPA 625/r-93/010, Cincinnati, Ohio.

[75] Tiedje JN, Biology of Anaerobic Microorganisms, by Zehnder, A.J.B. Wiley Publishing:New York, (1988) Ed.179-244.

[76] Payne WJ. Denitrification. Wiley. New York 1981.

[77] Chiu YC, Lee LL, Chang CN, Chao AC. Control of carbon and ammonium ratio for simultaneous nitrification and denitrification in a sequencing batch bioreactor. *Int. Biodeterioration Biodegradation*, 2007; 59:1-7.

[78] Verstraete W, Philips S. Nitrification–denitrification processes and technologies in new contexts. Environ. Pollut. 1998; 102:717–726.

[79] Peng Y, Zhu G. Biological nitrogen removal with nitrification and denitrification. Appl. Microbiol. Biotechnol. 2006; 73:15-26.

[80] Laanbrock HJ, Gerards S. Competition for limiting amounts of oxygen between *Nitrosomonas europaea* and *Nitrobacter winog- radsky* grown in mixed continuous cultures. Arch Microbiol 1993; 159:453–459.

[81] Chung J, Bae W, Lee YW, Rittmann BE. Shortcut biological nitrogen removal in hybrid biofilm/suspended growth reactors. Process Biochems 2007; 42:320-328.

[82] Beccari M, Marani E, Ramadori R, Tandoi V. Kinetic of dissimilatory nitrate and nitrite reduction in suspended growth culture. J. Water Pollut Control Fed. 1983; 55:58–64.

[83] Turk O, Mavinic DS. Benefits of using selective inhibition to remove nitrogen from highly nitrogenous wastes. Environ. Technol. Lett. 1987; 8:419–426

[84] van Kempen R, Mulder JW, Uijterllnde CA, van Loosdrecht MCM. Overview: full scale experience of the SHARON process for treatment of rejection water of digested sludge dewatering. Water Sci. Technol. 2001; 44:145–152.

[85] Brouwer M, van Loosdrecht MCM, Heijnen JJ. One reactor system for ammonium removal via nitrite. STOWA Report. 96–01. STOWA, Utrecht, The Netherlands. (ISBN

90 74476 55 4) 1996.

[86] Pollice A, Tandoi V, Lestingi C. Influence of aeration and sludge retention time on ammonium oxidation to nitrite and nitrate. Wat. Res. 2002a; 36-10:2541–2546.

[87] Pollice A, Valter T, Carmela L. Influence of aeration and sludge retention time on ammonium oxidation to nitrite and nitrate. Wat. Res. 2002b; 36:2541–2546.

[88] Picioreanu C, van Loosdrecht MCM, Heijnen JJ. Modelling of the effect of oxygen concentration on nitrite accumulation in a biofilm airlift suspension reactor. Water Sci. Technol. 1997; 36:147–156.

[89] Ruiz G, Jeison D, Chamy R (2003) Nitrification with high nitrite accumulation for the treatment of wastewater with high ammonia concentration. Wat. Res. 2003; 37-6:1371–1377.

[90] Bock E, Schmidt I, Stuven R, Zart D. Nitrogen loss caused by denitrifying *Nitrosomonas* cells using ammonium or hydrogen as electron donors and nitrites as electron acceptor. Arch. Microbiol. 1995; 163:16-20.

[91] Jetten MSM, Strous M, van de Pas-Schooen KT, Schalk J, van Dongen UGJM, van de Graaf AA, Logemann S, Muyzer G, van Loosdrecht MCM, and Kuenen JG. The anaerobic oxidation of ammonium. FEMS Microbiol. Rev. 1999; 22:421-437.

[92] Solley D. Upgrading of large wastewater treatment plant for nutrient removal. Churchill Fellowship 2000 report. The Winston Churchill Memorial trust of Australia 2000.

[93] Warakomski A, van Kempen R, and Kos P. Microbiology/Biochemistry ofNitrogen Cycle Innovative Process Applications. International Water Association proceedings, Moncton, New Brunswick, Canada 2006.

[94] STOWA (Dutch Foundation for Applied Water Rsearch). 2006.SHARON and SHARON ANOMMOX Process Sheets.

[95] Ekama GA, Siebritz IP, Marais GVR. Considerations in the process design of nutrient removal activated sludge processes. *Water Sci. Technol.,* 1983; 15:283-288.

[96] Rittmann BE, McCarty PL. *Environmental Biotechnology: Principles and Applications*, 2001, McGraw-Hill Companies Inc.

[97] Gavrilescu M, Macoveanu M. Attached-growth engineering in wastewater treatment. Bioprocess Eng. 2000; 23:95-106.

[98] Keinath TM, Ryckman MD, Dana CH, Hofer DA. Activated sludge-unified system design and operation. *J. Environ. Technol.*, 1977; 103:829-835.

[99] Borregaard VR. Experience with nutrient removal in fixed film system at full scale wastewater treatment system. *Water Sci. Technol.,* 1997; 36:129-137.

[100] Nicolella C, Van Loosdrecht MMC, Heijnen JJ. Wastewater treatment with particulate biofilm reactors. J Biotechnol. 2000; 82:1-33.

[101] Heijnen JJ, Mulder A, Weltevrede R, Hols PH, van Leeuwen HLJM. Large-scale anaerobic/aerobic treatment of complex industrial wastewater using immobilized biomass in fluidized bed and airlift suspension reactors. Chem. Eng. Tech. 1990; 13:202-208.

[102] Heijnen JJ, van Loosdrecht MCM, Mulder R, Weltevrede R, Mulder A. Development and scale up of an aerobic biofilm airlift suspension reactor. Water Sci. Technol. 1993; 27:253–261.

[103] Chisti MY. Airlift Reactors. Elsevier, Amsterdam. 1989.

[104] Roessink R, Eikelboom DH. Characterization of suspended solids in/out airlift biofilm-reactors. Wat. Sci. Technol. 1997; 36-1:237-245.

[105] Driessen W, Habets L, Vereijken T. Novel anaerobic and aerobic process to meet strict effluent plant requirements. Ferment Vol. 10, No. 4, August 1997; 243 – 250.

[106] Mulder R. Airlift technology in practice. Haus der Technik - Seminar on Biotechnological Wastewater Treatment, Maastricht, The Netherlands. 1992.

[107] Eikelboom D, Kampf R, and van Voorneburg F. Biofilm formation in an airlift reactor for the sewage purification, H_2O_2 1987; 20:388–392.

[108] Frijters CTMJ, Eikelboom DH, Mulder A, Mulder R. Treatment of municipal wastewater in a Circox airlift reactor with integrated denitrification. Water Sci. Technol. 1997; 36:173–181.

[109] Frijters CTMJ. Extensive nitrogen removal in a new type of airlift reactor. *IAWQ/IWQ Conference on biofilm systems*, D59, New York 1999.

[110] Lazarova V, Manem J. An innovative process for wastewater treatment: the circulating bed floating reactor. Water Sci. Technol. 1996; 34:89–99.

[111] Gorur S, Vereijken T, Tielbaard M. Strict effluent treatment design criteria at brewery met with novel anaerobic-aerobic process. Presented at WEFTEC Conference , U.S.A. 1995.

[112] Bolton J, Tummala A, Kapadia C, Dandamudi M, Belovich MJ. Procedure to quantify biofilm activity on carrier used in wastewater treatment systems. *J. Environ. Eng.,* 2006; 132:1422-1430.

[113] Miller G, Kolar A, Zakkay V, Hakim S. Bed expansion studies and slugging characteristics in a pressurized fluidized bed of large particles. *AIChE Symposium Series*, 1981; 205:166-173.

[114] Weber RB. Oxygenation system for accelerated sewage treatment. *American Society of Mechanical Engineers,* 1973; 73 -ENAs-13.

[115] Jesis JS, Owen RW, Biological fluid-bed treatment for BOD and nitrogen removal. *J. Water Pollution Control Fed.,* 1977; 49:816-821.

[116] Nakhla G, Zhu J, Cui Y. Liquid-solid circulating fluidized bed wastewater treatment system for simultaneous removal of carbon, nitrogen, and phosphorus. US patent no. 6,716,244, Int'l PCT patent awarded Aug. 2005.

[117] Chowdhury N, Nakhla G, and Zhu J. Load maximization of a liquid–solid circulating fluidized bed bioreactor for nitrogen removal from synthetic municipal wastewater. *Chemosphere*, 2008; 71:807-815.

[118] Chowdhury N, Nakhla G, Zhu J, Islam M. Pilot-scale Experience with Biological Nutrient Removal and Biomass Yield Reduction in a Liquid-Solid Circulating Fluidized Bed Bioreactor, Water Environ. Res, 2010.

[119] Ro KS, Neethling JB. Biofilm density for biological fluidized beds. Res J Water Pollut Control Fed. 1991; 63(5):815-18.

[120] Ro KS, Neethling JB. Terminal settling velocity of bioparticles. Res J Water Pollut Control Fed. 1990; 62:901–906.

[121] Ngian K, and Martin WRB. Bed expansion characteristics of liquid fluidized particles with attached microbial growth. Biotech. Bioeng. 1980; XXII:1843-1856.

[122] Ruiz G, Jeison D, Rubilar O, Cuidad G, Chamy R. Nitrification-denitrification via nitrite accumulation for nitrogen removal from wastewater. Biores. Technol. 2006; 97:330-335.

[123] Csikor Z, Mihaltz P, Czako L, Hollo J. New interpretation of expansion in biofilm-coated particle fluidization. Appl Microbiol Biotechnol. 1994; 41:608–614.

[124] Garrido JM, van Benthem W, van Loosdrecht MCM, Heijnen JJ. Influence of dissolved oxygen concentration on nitrite accumulation in a biofilm airlift suspension reactor. Biotechnol. Bioeng. 1997; 53:168–178.

[125] van Kempen R, Mulder JW, Uijterllnde CA, van Loosdrecht MCM. Overview: full scale experience of the SHARON process for treatment of rejection water of digested sludge dewatering. Water Sci. Technol. 2001; 44:145–152.

[126] Municipal nutrient removal technologies reference document Volume 1, Technical report, US Environmental Protection Agency 2008)

3 Materials and Methods

In this chapter, the materials and methodology used throughout this research work will be introduced.

3.1 Materials

3.1.1 Wastewater Feed

Two different low strength and high strength synthetic wastewater (SMW, HSSW) were prepared and used in this work as well as real municipal wastewater with the characteristics shown in **Table 3.1**.

The low strength synthetic municipal wastewater (SMW) was prepared from tap water combined with concentrated CH_3COONa (as carbon source), NH_4Cl (as nitrogen source), and KH_2PO_4 (as phosphorus source) stock solutions as well as a mineral stock solution at volumetric ratios of 1:0.0025, 1:0.001, 1:0.001 and 1:0.002 respectively. The concentrated stock solutions contained 125 g CH_3COONa/L; 100 g NH_4Cl/L; 20 g KH_2PO_4/L and the mineral salt stock solution contained: 75 mg $NiCl.6H_2O$/L; 75 mg $CoCl_2{\cdot}6H_2O$/L; 200 mg $CuCl{\cdot}2H_2O$/L; 125 mg Zn Cl_2/L; 1250 mg $MnCl_2{\cdot}4H_2O$/L; 750 mg $FeCl_3{\cdot}6H_2O$/L; 200 mg $(NH_4)_6Mo_7O_{24}{\cdot}4H_2O$/L; 125 mg H_3BO_3/L; 40 g Mg $SO_4{\cdot}H_2O$/L; 6 g $CaCl_2.H_2O$/L. Technical grade chemicals with minimum purity of 99.0% were used. All chemicals were supplied by VWR International and produced by EMD Chemicals and Alfa Aesar (NJ, USA).

In order to prepare the high strength wastewater used in the anaerobic FBR tests, 9.5 mL CH_3COOH, 0.93 g NH_4Cl, 0.1 g K_2HPO_4, 0.03 g $MgSO_4{\cdot}7H_2O$, 0.03 g $CaCl_2{\cdot}2H_2O$, 0.03 g yeast extract, 5.8 g $NaHCO_3$ and 1 mL of trace element were dissolved in one litre of tap water. The composition of trace element solution as follows: 2000 mg $FeCl_2{\cdot}4H_2O$/L, 500 mg $MnCl_2{\cdot}4H_2O$/L, 50 mg $ZnCl_2$/L, 30 mg $CuCl_2$/L, 50 mg $AlCl_3$/L, 50 mg $CoCl_2{\cdot}6H_2O$/L and 50 mg $NiCl_2$/L. Technical grade chemicals

with minimum purity of 99.0% were used. All chemicals were supplied by VWR International and produced by EMD Chemicals and Alfa Aesar Co (NJ, USA).

Table 3.1. Characteristics of different feed used in this work

Parameter	Synthetic Municipal	Raw Sewage	HSSW
pH	6.9-7.1	6.7-7.5	4.5-4.7
Alkalinity**	235±12	250±10	-
COD (mg/L)	262±13	398±52	10600±270
SCOD (mg/L)	234±13	118±24	10600±270
NH_4-N (mg/L)	26.1±1.7	30±4.5	255
NO_3-N (mg/L)	0.7±0.4	0.8±0.3	2±0.4
TN (mg/L)	29.5±2.1	48±5.8	260±9
PO_4-P (mg/L)	3.9±0.4	3.4±0.7	26±0.3
TP (mg/L)	4.4±0.5	6.5±1.4	-
TSS (mg/L)	27±14	214±41	-
VSS (mg/L)	19±15	183±30	-
SBOD (mg/L)	193±11	72±14	-
C:N:P	12:1:0.19	8:1:0.12	-

3.1.2 Twin Fluidized Bed Bioreactor (TFBBR)

The TFBBR, depicted in **Figure 3.1**, comprised two identical plexi-glass columns with a height of 3.6 m each, operated as two ***conventional*** anoxic (riser) and aerobic (downer) FBRs. In order to evaluate the TFBBR potential to retrofit the existing rectangular wastewater treatment tanks, the columns were made rectangular (5 cm x 8.5 cm). The riser was maintained under anoxic conditions, where denitrification and phosphorus release were the main reactions in the presence of readily biodegradable substrates, available in the influent wastewater. Anoxic conditions were attained by recirculating nitrate from the downer liquid-solid separator and maintaining a dissolved oxygen (DO) concentration of <0.5 mg/L. Proper denitrification and phosphorus release were attained by injecting influent wastewater in the anoxic zone (riser). The aerobic downer column where nitrification, organic oxidation, excess phosphorus uptake were the main reactions was operated in a conventional fluidization regime (by recirculating the liquid from the

downer liquid-solid separator) where a counter-current flow of liquid and solid was attained as liquid moves upward and solids downward. The particles coming from the riser liquid-solid separator settled at the bottom of the downer and flowed back to the riser through a connecting pipe equipped with an electro-impeller to allow continuous particle circulation in the riser column from the downer column. The aerobic condition in the downer column was maintained by injecting air at the bottom of the downer. The superficial liquid velocities (u_l) for bare particles with an average diameter of 680 μm and for the biofilm coated particles with attached biofilm thickness of 400 μm were maintained between the minimum fluidization velocities (u_{mf}) of 0.36 and 0.28 cm/s and terminal settling velocity (u_t) of 10 and 6.7 cm/s respectively. The lower liquid velocity in the riser required a thicker biofilm to reach the u_t, which resulted in a much higher biomass retention time.

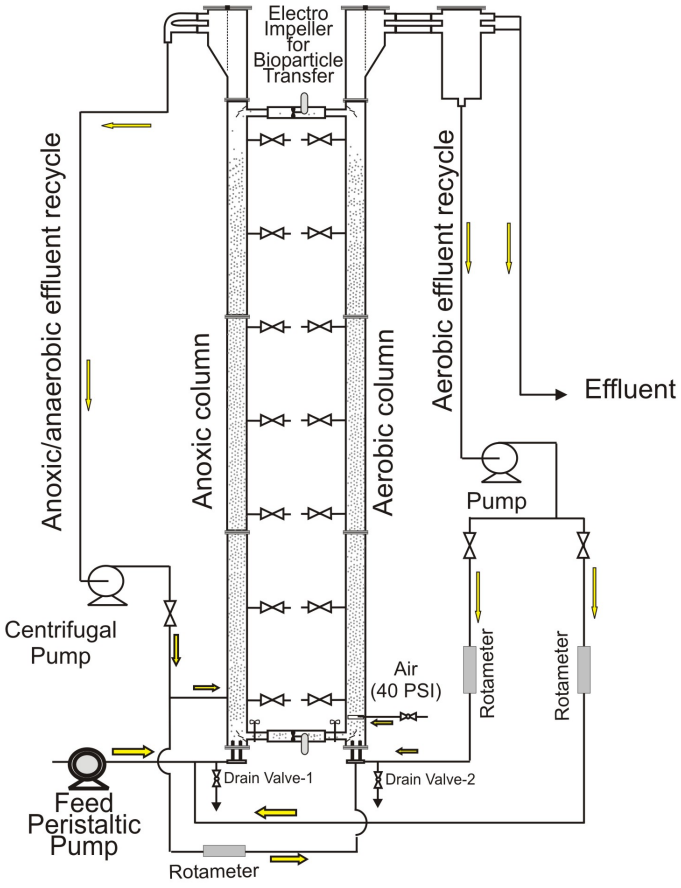

Figure 3.1. Schematic of TFBBR

The amount of particles used in the anoxic/anaerobic and aerobic columns in different phases were 2.2-4.7 and 2.5-5.4 respectively. The aforementioned particle masses were estimated based on the specific nitrification rates (SNRs) [5] of 0.09-0.14 g NH_4-N/g VSS·d, specific denitrification rates (SDNRs) [5] of 0.033-0.243 g NO_x-N/g VSS·d and the attached biomass per g media of 5-20 mg VSS/g media, reported in the literature for the CFBBR. [5-8] Riser-riser and downer-downer to feed recirculation ratios of 6-8.3 and 9.2-11 were provided to fluidize the beds throughput different phases. All recirculation flows were maintained using two centrifugal pumps (IWAKI MD-40RT-115NL, IWAKI CO., Ltd. Japan) and monitored by rotameters (OMEGA FL-812 and OMEGA FL-5331G, Omega Engineering, Inc., Canada).

Particle Transfer Method

The two columns were interconnected through two horizontal connecting pipes (ID=5 cm, see **Figure 3.2**) equipped with two three-blade electro-propellers (ID=3cm, 6-800 rpm, 120 V, 60 Hz, 1/8 hp, Talboys, Tromemner. LLC, NJ, USA). Particle transfer between the columns occurred periodically. Particles from the bottom dense phase of the downer with a thin biofilm (< 30 μm) are transferred to the riser. In the riser, heterotrophic bacteria grow on the media and the biofilm becomes thicker. At a certain biofilm thickness (800 μm), the biofilm coated particles reach the height where the propeller is located. The 60-rpm propeller slowly transfers the particles to the downer. The biofilm may be destroyed during transfer. Besides, after being exposed to the high shear force in the gas-liquid-solid phase in the downer, the biofilm detaches and leaves the system along with the effluent. The downer to riser particle transfer occurred once every three weeks with the aid of a propeller (300 rpm) to make up the particles in the riser. Four water jets (the downer to riser and riser to riser circulation streams) provided a dilute phase in the transferring tube for the 15-minute of particle transfer time from the downer to the riser.

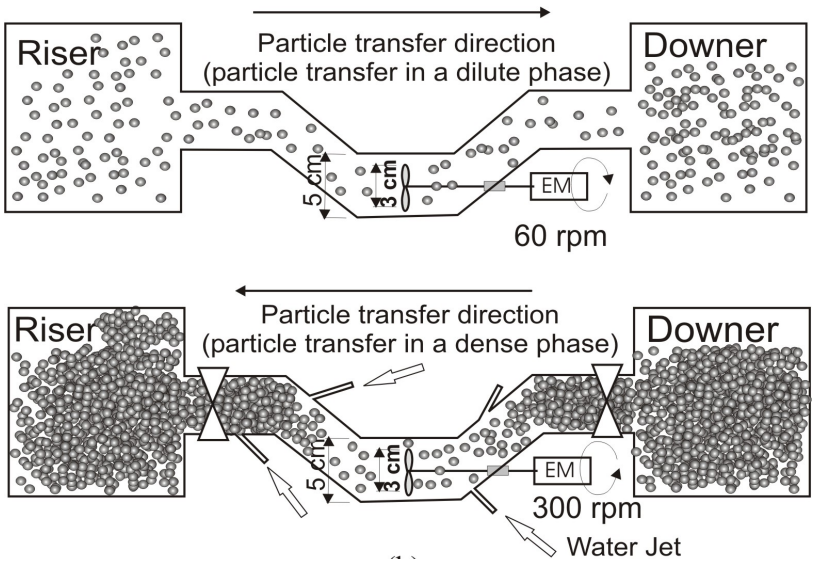

Figure 3.2. Plan view of the horizontal connecting pipes between the downer and riser

3.1.3 Twin Circulating Fluidized Bed Bioreactor (TCFBBR)

The TCFBBR (**Figure 3.2)** is comprised of two plexi-glass columns operated as anoxic and aerobic FBRs with a height of 3.6 m each. The columns were made rectangular (aerobic: 5 cm x 8.5 cm, and anoxic: 5 cm x 5 cm) to investigate the system potential for retrofitting conventional wastewater treatment tanks. The main difference between the TCFBBR and TFBBR was the smaller riser with cross sectional area, 60% of the riser cross sectional area in TFBBR and the particle transfer technology between risers and downers. The smaller cross sectional surface area resulted in a shorter sludge and a hydraulic retention time. Moreover the particle transfer system in TCFBBR was through inclined pipes and with the aid of gravity whereas particle transfer system in TFBBR was mechanically. Lava rock particles were used in both columns with an average diameter (d_m) of 850-1125 μm. The design empty bed contact times (EBCTs) were 0.22 hr in the anoxic column and 0.71 h in the aerobic column in different phases. In the riser, heterotrophic bacteria grow on the media and the biofilm becomes thicker.

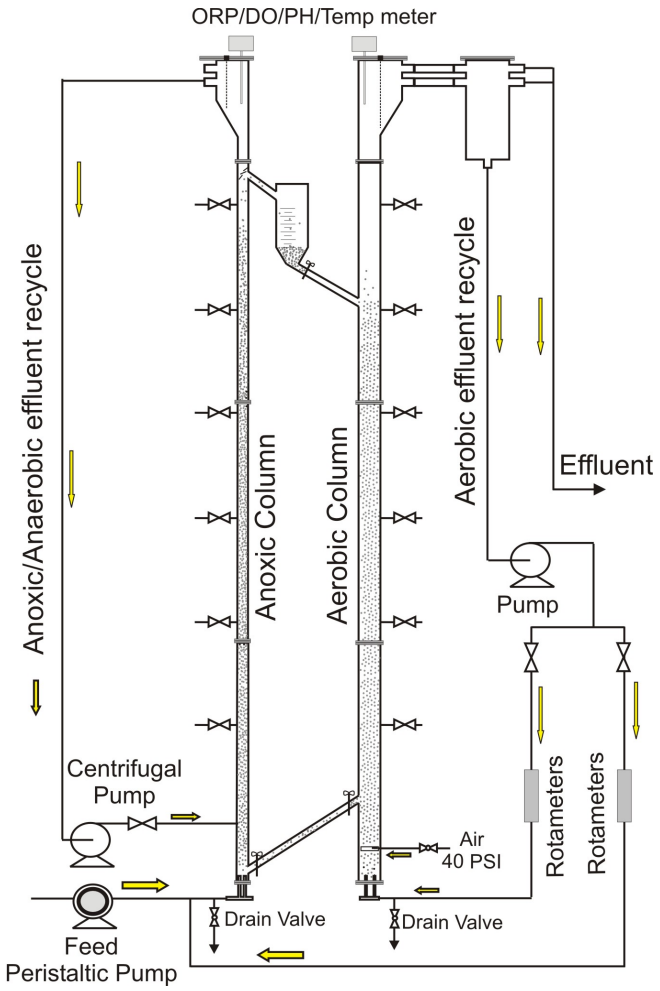

Figure 3.3. Schematic of TCFBBR

Particle Transfer Method

As mentioned earlier, particle transfer between the riser and downer of TCFBBR took place through two inclined connecting pipes between the two columns by gravity rather than mechanically as in the TFBBR described earlier. At a certain biofilm thickness in the riser, depending on the superficial liquid velocity, the biofilm-coated particles reach the height where they can be transferred to the downer through the inclined pipe. However, an intermediate graduated container was placed between the two columns, as shown in **Figure 3.2,** to monitor the particle transfer rate. After exposure to the high shear force in the gas-liquid-solid phase in the downer, the biofilm detaches and leaves

the system along with the effluent. Particles from the bottom dense phase of the downer with a thin biofilm (< 40 μm) are transferred back to the riser manually to make up the particles in the riser.

3.1.4 Anaerobic Fluidized-CFBBR (AF-CFBBR)

As depicted in **Figure 3.4**, the AF-CFBBR is comprised of a conventional strict anaerobic fluidized bed (AF) with overall height of 3.6 m followed by a CFBBR comprising an anoxic and aerobic fluidized bed bioreactors FBRs with heights of 2 m and 3.6 m respectively. Particle recirculation between the riser column and downer carried out similar to what in TCFBBR by gravity. High strength wastewater was initially divided to two parts of 95% and 5% and the 95%-feed was injected to the anaerobic column where methane as biogas was produced. Subsequently the treated anaerobic effluent joined the remaining 5% of feed to enter into the bottom of the anoxic riser where the organic matter contributed in the second cycle of nitrogen removal (denitrification). Nitrification process took place in the aerobic downer and the produced nitrate was recycled to the riser for denitrification similar to previous systems, TFBBR and TCFBBR. Natural zeolite particles (3 kg) with an average diameter (d_m) of 425-610 μm were used as carrier media in the anaerobic column and 3 kg zeolite particles with average diameter of 610-825 μm, were circulated between the aerobic and anoxic fluidized bed columns of CFBBR. The particle weight hold up in the aerobic column of the CFBBR was maintained at 2.4 kg continuously. In the riser, heterotrophic bacteria grow on the media and the biofilm becomes thicker. At a certain biofilm thickness, depending on the superficial liquid velocity, the biofilm-coated particles reach the height where they can be transferred to the downer through the inclined pipe. However, similar to the TCFBBR, an intermediate graduated container was placed between the two columns, as shown in **Figure 3.4,** to monitor the particle transfer rate. After exposure to the high shear force in the gas-liquid-solid phase in the downer, the biofilm detaches and leaves the system along with the effluent. Particles from the bottom dense phase of the downer with a thin biofilm (< 100 μm) are transferred back to the riser manually to make up the particles in the riser.

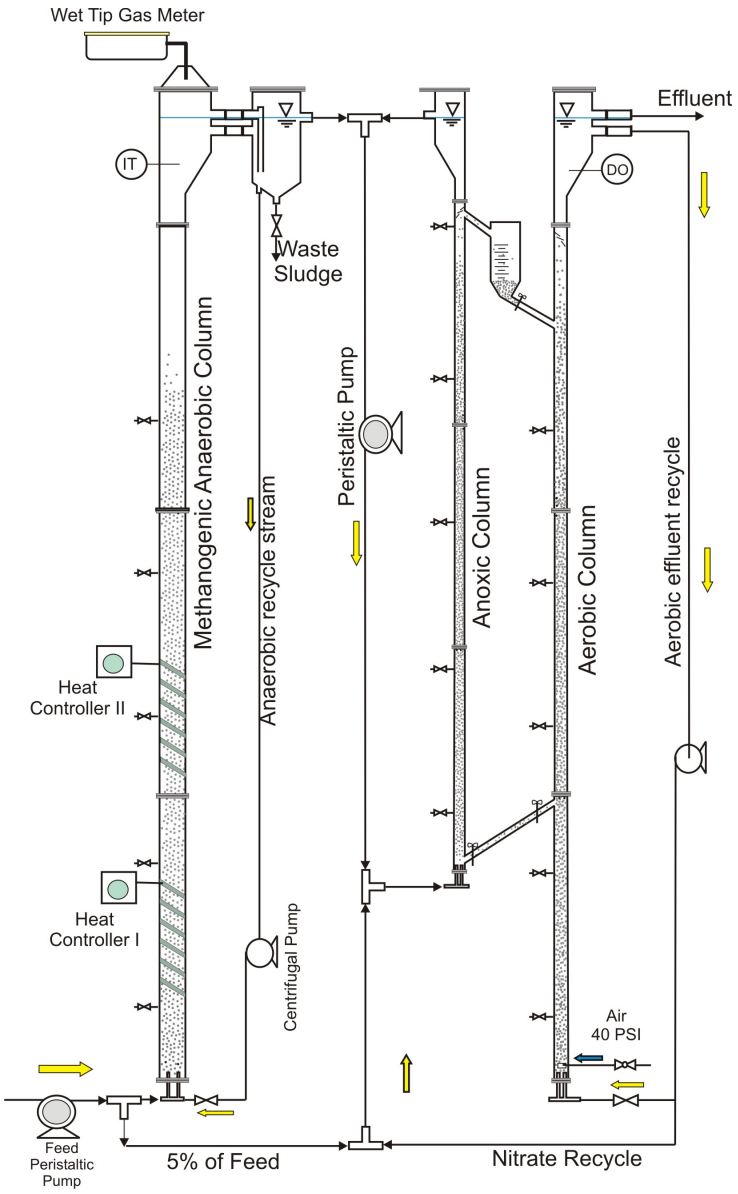

Figure 3.4. Schematic of AF-CFBBR

The dimensions, characteristics of the aforementioned processes and operational conditions are summarized in **Table 3.2**.

3.1.5 Carrier Media

Lava Rock

Lava rock particles were used with an average diameter (*d*) of 680 μm, a total porosity of 62% (44% external and 18% internal), a particle dry bulk density of 1,012 kg/m^3, a particle true density of 2,628 kg/m^3 and a specific surface area determined by BET (Micromeritics ASAP 2010, Micromeritics Co., USA) of 0.48 m^2/g. The final result of the BET test can be found in Appendix A. The particle masses were estimated based on the specific nitrification rates (SNRs), specific denitrification rates (SDNRs) and the attached biomass per g media, reported in the literature for the CFBBR and FBR.

Natural Zeolite

Zeolite particles with an average diameter (d_m) of 425-610 μm were also used as carrier media with an average diameter of 610-825 μm in anaerobic, aerobic and anoxic columns. The amounts of particles were initially estimated based on the specific nitrification rates (SNRs), specific denitrification rates (SDNRs), and specific methanogenesis activity (SMA. Zeolite characteristics were determined as follows: a total porosity (ψ_T) of 61% (44% external and 17% internal), a dry bulk particle density (ρ_{md}) of 885 kg/m^3, a true particle density (ρ_{mt}) of 2360 kg/m^3 and an external specific surface area and uniformity coefficient determined by BET (Micromeritics ASAP 2010, Micromeritics Co., USA) of 26.5 m^2/g and 1.85, respectively. The final result of the BET test can be found in Appendix A.

Table 3.2. Comparison between TFBBR, TCFBBR and AF-CFBBR

		TFBBR	TCFBBR	AF-CFBBR
Height (m)	Aerobic	3.6	3.6	3.6
	Anoxic	3.6	3.6	2.1
	Anaerobic	NA	NA	3.6
Sectional area (cm×cm)	Aerobic	8.5×5	8.5×5	5×5
	Anoxic	8.5×5	5×5	2.8×2.8
	Anaerobic	NA	NA	8.5×5
Particle transfer method (Anoxic⇔Aerobic)		Electro impeller (1/8 hp, 120 V)	2" Inclined tubes (45°)	2" Inclined tubes (45°)
Particle type		Lava rock	Lava rock	Natural Zeolite
Particle amount (kg)	Aerobic	4.7	5.5	2.7
		850-1125	850-1125	610-825
	Anoxic	2.2	2.2	0.3
Particle size range (μm)		850-1125	850-1125	610-825
	Anaerobic	NA	NA	3
				425-610
Superficial liquid velocity (cm/s)	Aerobic	1.0 → 0.7	1.1 → 0.7	1.7 → 1.0
	Anoxic	0.9 → 0.6	1.3 → 0.8	1.3 → 0.7
	Anaerobic	NA	NA	1.4 → 0.5
Attached film (mg VSS/ g media)	Aerobic	6± 1	5 ± 1	20 ± 1
	Anoxic	48 ± 1	29 ± 5	55 ± 10
	Anaerobic	NA	NA	33± 0.5
Total attached biomass (g VSS)	Aerobic	15	28	48
	Anoxic	100	145	47
	Anaerobic	NA	NA	99
HRT (h)	Aerobic	1.4	1.4	4
SRT (d)		13	7	(28)
	Anoxic	1.4	0.8	0.9
		70	31	(28)
	Anaerobic	NA	NA	7.5
				32
EBCT (h)= $V_{compact}/Q_{in}$	Aerobic	0.53	0.71	1.3
	Anoxic	0.45	0.22	0.26
	Anaerobic	NA	NA	1.6
Biofilm detachment rate (1/d)	Aerobic	0.18	0.18-0.2	0.04
	Anoxic	0.02-0.04	0.06-0.08	0.035
	Anaerobic	NA	NA	0.02
Air flow rate (mL/min) DO (mg/L)	Aerobic	2200	2060	2200
		6.3 ± 0.4	4.3 ± 0.5	5.3 ± 0.2
	Anoxic	0.1 ± 0.1	0.3 ± 0.1	0.6 ± 0.2
	Anaerobic	NA	NA	NA
Estimated average biofilm thickness (μm)	Aerobic	25	30	100
	Anoxic	400	300	380
	Anaerobic	NA	NA	320

* There is a 40 cm headspace in addition to the heights of the columns

3.2 Methodology

3.2.1 Water Quality Analytical Methods

Liquid samples were collected from the feed tank, anaerobic and anoxic column top and the effluent. The analyses were either done the day of sampling or the samples were refrigerated at 4 °C prior to analysis. Total suspended solids (TSS), volatile suspended solids (VSS) and biochemical oxygen demand (BOD) were analyzed in accordance with Standard Methods 2540D, 2540E and 5210 [1] respectively. DO and ORP were measured onsite using an Oakton DO 6 meter, and an Oakton ORPTestr 10 (Oakton, Singapore). HACH methods and testing kits (HACH Odyssey DR/2800) were used to analyze total and soluble chemical oxygen demand (TCOD and SCOD), total and soluble nitrogen (TN and STN) and total phosphorus (TP), NH_4-N, NO_2-N, NO_3-N, and PO_4. Alkalinity was measured by titration with 0.01 N H_2SO_4 in accordance with the Standard Method no 2320. [1] Sulfate (SO_4^{2-}) was measured using the ion chromatography (IC, Dionex 600, USA) equipped with CS16-HC and AS9-HC columns. Sodium carbonate solution, 9 mM, was applied as an eluent at a flow rate of 1 mL/min for 30 minutes, with sulfate detected 20 minutes following injection.

Both dissolved and total metals were measured following the standard method 3120 using ICP (Vista-Pro, VARIAN). [1] The soluble metals were measured by doing the analysis on the filtered sample (0.45µm filter paper) and the total was obtained by digesting the sludge samples followed by filtration through a 0.45µm filter paper prior to analysis using ICP. For major metals (Ca, Na, K, and Mg) and most of the trace metals (Fe, Cu, Cr, Al, Co, Ni, Zi, and Mn) the digestion method was followed according to method 3030D of Standard Methods. [1]

The rate of biogas produced in the anaerobic methanogenic column was measured by a gas wet tip gas meter (Rebel wet-tip gas meter company, Nashville, TN, USA) connected to the top of anaerobic column. Methane, nitrogen gas, hydrogen gas were determined by injecting 0.5 mL of the biogas composition into a gas chromatograph (Model 310, SRI Instruments, Torrance, CA) equipped with a thermal conductivity detector (TCD) and a molecular sieve column (Molesieve 5A, mesh 80/100, 182.88×0.3175 cm). The

temperatures of the column and the TCD detector were 90 and 105^{o}C, respectively. Argon was used as carrier gas at a flow rate of 30 mL/min.

3.2.2 Fed-Batch Experiments

Batch tests were carried out to test the maximum specific nitrification rate (SNR), specific denitrification rate (SDNR) and specific methanogenic activities (SMA) of the attached biomass in the aerobic, anoxic and anaerobic aforementioned systems. Batch reactors (0.5 L working volume) equipped with magnetic stirrers were used for nitrification by injecting air or for denitrification by avoiding intrusion of air. To reduce the effect of substrate mass transfer limitation into the biofilm, the biofilm was removed from 30-40 g of media using sonication and then placed into the reactors. The biomass in the SDNR and the SNR tests were in the range of 1500-4000 mg VSS/L and 240-500 mg VSS/L respectively, considering the amount of biofilm in the anoxic and aerobic column, 25-50 mg VSS/g media and 4-6 mg VSS/g media. The initial acetate COD in the denitrification batch tests was set at 350-450 mg/L while the initial alkalinity used in the nitrification test was 250-350 mg/L as $CaCO_3$. For the SNR tests, the initial ammonia concentrations were 35-55 mg/L, added as ammonium chloride.

The biofim-coated particles from anaerobic column were used for specific methanogenic activity (SMA) at 37°C, using 250 mL bottle capped with Teflon septum. Approximately 10 g anaerobic biofilm coated particles and 0.3-0.6 mL acetic acid were added together into the 125 mL-bottles containing 0.2 mL of nutrients (2000 mg/L $FeCl_2{\cdot}4H_2O$, 50 mg/L H_3BO_3, 50 mg/L $ZnCl_2$, 30 mg/L $CuCl_2$, 500 mg/L $MnCl_2{\cdot}4H_2O$, 50 mg/L $AlCl_3$, 50 mg/L $CoCl_2{\cdot}6H_2O$) and 3000 mg alkalinity per litre as $CaCO_3$. All the bottles were sealed after purging the headspace with nitrogen to eliminate the present of oxygen/air. The experiment was continued until the bottles stopped producing biogas. Daily biogas was measured by inserting needle attached to a 100-ml syringe (Hamilton, Nevada, USA). Methane composition was measured using Gas Chromatography (GC) SRI 310 °C with a packed column.

3.2.3 Bacterial Community Analysis

Samples were taken from bottom and top of anoxic, anaerobic and aerobic columns. The total genomic DNA was extracted from each sample using the UltraClean Soil DNA Isolation Kit (MO BIO Labratories, Carlsbad, CA, USA). PCR amplification of a region of the 16S rRNA gene was performed with universal the primer set 349f-GC (5'-CGCC CGCC GCGC GCGG CGGG CGGG GCGG GGGC ACGG GGGG CCTA CGGG AGGC AGCA G-3') and 907rM (5'-CCGT CAAT TCMT TTGA GTTT-3', where M=A+C) [2] using a MyCycler thermal cycler (BioRad, Hercules, CA, USA). The PCR products were applied directly to a 6% (w/v) polyacrylamide gel with 20-50% denaturing gradient (100% denaturing gradient corresponds to 70M urea and 40% (v/v) formamide). Electrophoresis was run at a constant voltage of 130V at 58 °C for 6 h. The DNA templates from the bands of interest were re-amplified and the PCR products were purified with the QIAquick PCR purification Kit (QIAGEN Sciences, MD, USA). The fragments were sequenced at the Sequencing Facility at the Robarts Research Institute (The University of Western Ontario, London, Ontario, Canada) and compared with available sequences from the GenBank database using the Basic Local Alignment Search Tool (BLAST) program. [9]

3.2.4 Attached Biomass

The attached biomass on the carrier media was measured and expressed as mg VSS/g clean particles, based on Standard Method no 2540. [1] Approximately 10-20 g biofilm-coated particles were taken from columns and suspended in a 100 mL vial and sonicated for 3 h at 30°C in an Aquasonic sonicator (SK 1200H Kupos, China) with a rated power of 45 Watts. After sonication, the TSS and VSS content of the detached biomass was determined following Standard Methods no 2540D and 2540E [1] and the values were divide by the weight of the dry clean particles.

3.2.5 Biofilm Thickness Measurement

Biofilm coated particles were periodically taken from sampling ports along the columns for the purpose of measuring the biofilm thickness. The sampling took place by a syringe at the same pressure inside each column to minimize disturbances to the biofilm

structure. Each particle was then transferred to a small container filled with water. Using a microscope (MITUTOYO, Sakada, Japan) with 50X magnification coupled with a camera (LEICA DC300, Germany) each particle was photographed and then transferred to its container. The volumetric equivalent particle diameter (d_p) and the volumetric equivalent media diameter (d_m) were measured with the VISIONGAUGE software (Flexbar Machine Co, New York, USA) synchronized to the camera. In order to maximize the accuracy of the measurements, all the measurements were periodically checked with the microscope's Standard Measurement Ruler.

3.2.6 Dry and Wet Biofilm Densities

In order to measure biofilm dry density, **Equation (3.1)**, Proposed by Ro and Neethling (1990), was used. [3] Samples were taken and photographed to measure d_p and d_m and then sonicated (Aquasonic SK 1200H Kupos, China) for three hours at 30°C to remove the biofilm from the media. Since the biofilm sizes were not completely identical in each sample, average values for diameters were considered. Each sampling took place at a different stage of biofilm development and also hydrodynamic conditions such as superficial liquid velocity. As a result, different biofilm thicknesses were obtained at different times but the thicknesses of the biofilms were relatively equal in each sampling.

$$\rho_d = \frac{X \rho_m}{\gamma^3 - 1} \qquad (3.1)$$

where ρ_d is the biofilm dry density, ρ_m is the media true density, X is the ratio of dry mass of biofilm to dry mass of media, and γ is d_p/d_m

A hydrostatic method was developed to measure the wet biofilm density accurately. The experimental data verified the most accurate equation to calculate this value. Samples were taken, photographed for measuring the biofilm thickness and then sonicated to remove the biofilm from the media. Different concentrations of sodium acetate were dissolved in deionised water in order to make liquids with different densities of 1060, 1065, 1070, 1075, 1080, 1085, 1090 and 1095 kg/m^3. The density of liquid in each vial was measured and verified by hydrometers. Eight 100-mL glass cylinders were

filled with the provided liquids. The biofilm without carrier media was placed inside the vials and then well shaken to lessen the size of bio-particles in order to make the effect of buoyancy force uniform. After two hours bio-particles in one vial did neither float nor settle. Since the gravity force equaled to the buoyancy force, the density of bio-particles, wet density, was considered equal to the density of the liquid.

3.2.7 Carrier Media Size Determination

The size of the bare and biofilm coated particles was measured using a Mastersizer 2000 laser analyzer (Malvern Instruments Inc., UK).

3.2.8 Pressure Gradient and Axial Distribution of Solids

Eight manometers (4 for each aerobic and anoxic column) connected to an air collector were used to measure the pressure difference along columns. Thereafter, axial distribution of solids in a three-phase fluidized bed with heavy particles was determined from the pressure gradient along the column. Axial void fraction (ε), solid hold-up (ε_S), and solids concentrations were calculated using on-line pressure transducers data along the columns and following Equations: [4]

$$-\Delta p_S = L \times (1-\varepsilon) \times (\rho_P - \rho) \times g \qquad (3.2)$$

$$\varepsilon_S = 1 - \varepsilon \qquad (3.3)$$

$$\frac{M}{AL} = \rho_P \times (1-\varepsilon) \qquad (3.4)$$

where, L, A, g, Δp_S, ρ, and ρ_p are length of the section (m), cross sectional area (m^2), acceleration of gravity (m/s^2), additional pressure drop (kPa) due to the presence of solids, liquid density (kg/m^3), and particle density (kg/m^3) respectively.

3.2.9 Statistical Analysis

The student t-test was used to test the hypothesis of equality at a 95% confidence level. The null hypothesis was defined to be no difference between the two groups tested versus the alternative hypothesis that there is a statistical difference between the two

groups. Non-linear regression was done by Matlab (MathWorks, Massachusetts USA) and all other data was analyzed using SigmaPlot and Excel 2007.

3.3 References

[1] APHA; AWWA; WEF. Standard methods for the examination of water and wastewater. 20th Edition, American Public Health Association, Washington D.C. 1998.

[2] Muyzer G, de Waal EC, Uitterlinden AG. Profiling of complex microbial populations by denaturing gradient gel electrophoresis analysis of polymerase chain reaction-amplified genes coding for 16S rRNA. Appl. Environ. Microbiol. 1993; 59: 695-700.

[3] Ro KS, Neethling JB. Terminal settling velocity of bioparticles. Res J Water Pollut Control Fed. 1990; 62:901–906.

[4] Epstein, N. *Liquid-solids fluidization*: Handbook of fluidization and fluid-particle systems. 2003, Marcel Dekker, New York, 707-708.

[5] Chowdhury N, Nakhla G, Zhu J. Load maximization of a liquid-solid circulating fluidized bed bioreactor for nitrogen removal from synthetic municipal wastewater. Chemosphere 2008; 71:807-815.

[6] Cooper PF, Williams SC. High-rate nitrification in a biological fluidized bed. Wat. Sci. Technol. 1990; 22:431–442.

[7] Hermanowicz SW, Cheng YW. Biological fluidized-bed reactor: hydrodynamics, biomass distribution and performance. Wat. Sci. Technol. 1990; 22:193–202.

[8] Nicolella C, Di Felice R, Rovatti M. Biomass concentration in fluidized bed biological reactors. Wat. Res. 1996; 31:936-940.

[9] www.blast.ncbi.nlm.nih.gov/blast.cgi

4 Terminal Settling Velocity and Drag Coefficient of Biofilm-Coated Particles

4.1 Introduction

For the last twenty years, liquid-solid fluidized bed technology has been used for biological processes such as wastewater treatment. Due to the complexity of the hydrodynamic behavior, the design and modeling of liquid-solid fluidized bed bioreactors (LSFBBR) are still being studied and there is still much to be discovered. In an LSFBBR, there are many processes that lead to the formation and attachment of biofilm to the carrier media. An increase in the thickness of the biofilm is a function of the attachment and growth rates while a decrease in its thickness depends on the decay and detachment rates. Changes in the biofilm thickness can vary the hydrodynamic behavior of fluidized beds significantly. Obviously the design of a fluidized bed bioreactors (FBBR) depends strongly on hydrodynamics such as the minimum fluidization velocity (u_{mf}), terminal settling velocity (u_t), bed expansion index and particle effective density (ρ_p). Moreover, this technology has been used for different wastewater treatment applications such as nitrification and denitrification which produce biofilm coated particles with different physical characteristics.

There have been a few studies of drag coefficient (C_d) and u_t of biofilm-coated particles but predominantly for $\mathrm{Re}_t \leq 100$. Primarily because such liquid-solid fluidized bioreactors need to operate at low liquid velocity, which calls for small particle sizes. Biofilm particles are in the intermediate flow regime ($1 < \mathrm{Re}_t < 100$) for the vast majority of cases when sand (0.5-1 mm) or similar material is used as an inert biofilm support. [1] With the new liquid-solid fluidized bed bioreactors developed by our group [2], much higher liquid velocities and bigger particles can be used, thus providing the opportunity to study the flow properties of biofilm-coated particles as well as C_d and u_t at much higher Re_t.

4.2 Previous Works

4.2.1 Terminal Settling Velocity of Biofilm Covered Particles

In general when the velocity of a falling particle becomes constant, the summation of the F_d and buoyancy force (F_b) equals the gravity force so that the solution of the dynamic-force balance results in **Equation (4.1)**.

$$u_t = \left[\frac{4gd_p\left(\rho_p - \rho_l\right)}{3C_d\rho_l}\right]^{0.5} \qquad (4.1)$$

Based on non-linear regression of experimental data, various researchers have proposed different C_d correlations at different Re_t. These correlations have been widely developed for smooth and rigid spherical particles and other conditions such as non-spherical porous particles. [3] One of the most common in use and at the same time the simplest equations for smooth rigid spherical particles in the intermediate region, $0.3< Re_t < 1000$, was suggested by Dallon and Christiansen (1968): [4]

$$C_D=18.5\ Re_t^{-0.6} \qquad (4.2)$$

Biofilm coated particles are nearly spherical and **Equation (4.1)** can be used to determine their u_t. However, they are neither smooth nor rigid and consequently the proposed C_d for smooth rigid particles could not be used. As a result, other equations relating C_d to Re_t, were developed for biofilm coated particles by different researchers in predominantly two forms of (αRe_t^{β}) and ($24Re_t^{-1} + \alpha Re_t^{\beta}$). All proposed equations had one thing in common: they are all functions of Re_t and consequently implicit in the terminal settling velocity. The suggested equations were defined in a certain range of $Re_t < 100$ as mentioned in **Table 4.1**, equations (a) to (f). Thus far, there has been no evidence showing the accuracy of these equations for a $Re_t > 100$.

Table 4.1. Correlations for C_d for biofilm-coated particles, dry and wet biofilm densities

Reference	Re_t	Equation	C_d
Hermanowicz et al. (1983)	50-100	(a)	$17.1\ Re_t^{-0.47}$
Mulcahy et al. (1987)	40-90	(b)	$36.66\ Re_t^{-0.67}$
Ro et al. (1990)	15-87	(c)	$24\ Re_t^{-1} + 21.55\ Re_t^{-0.518}$
Yu et al. (1997)	40-90	(d)	$24\ Re_t^{-1} + 14.55\ Re_t^{-0.48}$
Nicolella et al. (1998)	7-90	(e)	$(0.8 + 6.1\ Re_t^{-0.5})^2$
Nicolella et al. (1999)	7-90	(f)	$29.6\ Re_t^{-0.6}$
Reference		Equation	Dry biofilm density
Mulcahy et al. (1987)		(g)	$\begin{cases} \rho_d = 65\ mg/cm^3 & for\ \ 0 < \delta \le 300\ \mu m \\ \rho_d = 98.6 - 0.106\,\delta\ mg/cm^3 & for\ \ 300 < \delta \le 630\ \mu m \\ \rho_d = 30\ mg/cm^3 & for\ \ \delta > 630\ \mu m \end{cases}$
Boaventura et al. (1988)		(h)	$\begin{cases} \rho_d = 104.3 - 0.1245\,\delta\ mg/cm^3 & for\ \ \delta \le 620\ \mu m \\ \rho_d = 26.9\ mg/cm^3 & for\ \ \delta > 630\ \mu m \end{cases}$
Hermanowicz et al. (1990)		(i)	$\begin{cases} \rho_d = 120(\delta/180)^{3.7}\ mg/cm^3 & for\ \delta \le 180\ \mu m \\ \rho_d = 120(\delta/180)^{-1.8}\ mg/cm^3 & for\ \ \delta > 180\ \mu m \end{cases}$
Coelhoso et al. (1992)		(j)	$\begin{cases} \rho_d = 191.4 - 0.224\,\delta\ mg/cm^3 & for\ \ \delta \le 593\ \mu m \\ \rho_d = 58.6\ mg/cm^3 & for\ \ \delta > 593\ \mu m \end{cases}$
Rabah et al. (2004)		(k)	$\rho_d = 0.43\delta^{-0.26}\ mg/cm^3 \quad for\ 130 \le \delta \le 500\ \mu m$
Reference		Equation	Wet biofilm density (g/ cm^3)
Tsezos et al. (1980)		(l)	$\rho_w = 1.0$
Ngian et al (1980)		(m)	$\rho_w = 1.1$
Hermanowicz et al. (1982)		(n)	$\rho_w = 1.14$
Ro et al. (1991)		(o)	$\rho_w = 2.059\ \rho_d + \rho_l$
Nicolella et al. (1998)		(q)	$\rho_w = \rho_d + \rho_l$

Nicolella et al, (1998) argued that the ratio of C_d for biofilm particles to C_d for smooth and rigid solid particles is independent of biofilm thickness and concluded that particle deformability has a negligible effect on C_d. Although there is sufficient evidence in the literature that the drag coefficient for biofilm-coated particles is higher than rigid smooth particles [5], it has not been firmly proven that the surface roughness is the only dominant factor.

Unlike all previous suggested equations for drag coefficient as functions of Re_t, karamanev (1996) suggested two equations for drag coefficient as functions of Archimedes number for spherical rigid particles and rising spheres.

Karamanev (1996) stated that the analysis of experimental data in the literature and correlations of the motion of falling particles shows that the best way to calculate the drag coefficient and the terminal velocity of particles in an infinite fluid is by describing the C_d as a function of Ar.

where $Ar = \frac{g d_p^3 (\rho_p - \rho_l)\rho_l}{\mu^2}$ (4.3)

Karamanev's equations predicted all reliable existing data [8] with the same accuracy as the equation suggested by Turton and Levenspiel (1986). Furthermore the correlations developed by Karamanev (1996) had the additional advantage of being explicit in terminal settling velocity.

4.2.2 Biofilm Density

Considering the volumetric equivalent diameter for media to be d_m and volumetric equivalent diameter of biofilm-coated particles to be d_p, the effective density of bio-particles can be estimated using **Equation (4.4)**.

$$\rho_p = \left(\frac{d_m}{d_p}\right)^3 \rho_m + \left[1 - \left(\frac{d_m}{d_p}\right)^3\right] \rho_w \quad (4.4)$$

Biofilm thickness is defined as: $\delta = \frac{d_p - d_m}{2}$ (4.5)

The biofilm dry density is defined as the mass of dry biomass VSS per unit wet biofilm volume. Various expressions for calculating biofilm dry density as a function of biofilm thickness have been summarized in **Table 4.1** equations (g) to (k).

Biofilm wet density can be defined as the density of the bulk of biofilm including the mass of dry biomass, the mass of interposing water within the biofilm structure and the water component of bio-cells. The direct measurement of the wet density of non-rigid, porous materials such as biofilm is extremely difficult. [9] Various values suggested by different researchers for calculating biofilm-wet density have been summarized in **Table 4.1** equations (l) to (q). None of those values was derived based on experimental data.

4.3 Materials and Methods

Two different laboratory-scale systems were used for biofilm sampling. As shown in **Figure 4.1** the patented circulating fluidized bed bioreactor (CFBBR, US patent no 7,261,811 B2) consists of an anoxic plexi-glass column as a riser and an aerobic plexi-glass column as a downer. The riser and downer inner diameters were 2 cm and 7.6 cm respectively and heights were 3 m and 2.5 m respectively. The synthetic wastewater flow rate to the system was 48 L/d with the average organic loading of 2.9 kg COD/m^3·d and the average nitrogen loading of 0.33 kg N/m^3·d. The system was running with a superficial liquid velocity of u_l=1.4- 2.0 cm/s in the riser and u_l=0.26 cm/s in the downer. The second system in use was a twin fluidized bed bioreactor (TFBBR) with particle recirculation. The two columns were both 4 m high. Each rectangular area of plexi-glass column was 8.9 cm by 5 cm. The feed flow rate was 180-220 L/d with the average organic loading of 1.5-1.88 kg COD/m^3·d and the average nitrogen loading of 0.18-0.22 kg N/m^3·d. The system was running with u_l= 0.54 cm/s in the aerobic column and a superficial liquid velocity of u_l=0.37-0.64 cm/s in the anoxic column. The carrier media used in both systems was lava rock ranging in size from 400 µm-2000 µm with a true density of 2.63 g/cm^3 and porosity of 0.62. In the TFBBR particle recirculation, was accomplished through a positive displacement particle transfer pump between the twin columns while in the CFBBR biofilm-coated particles were transferred naturally from the

anoxic column to the aerobic column due to a decrease in particle density as a result of biofilm development and consequently reaching the terminal settling velocity.

Synthetic feed was used for both systems, which was prepared using tap water in addition to other chemicals. The chemical oxygen demand (SCOD) of the feed was 250±10 mg/L as a result of dissolving 31.25 g of sodium acetate in 100 L of deionised water and a concentration of 25±2 mg/L NH_3-N as a result of adding 5 g of NH_4Cl to the 100 L of deionised water. A concentration of 3±0.5 mg/L PO_4-P and nutrients were also provided.

Biofilm coated particles were periodically taken from sampling ports along the columns for the purpose of measuring the biofilm dry and wet densities as well as the terminal settling velocity over a period of three months. The sampling took place by a syringe at the same pressure inside each column to minimize disturbances to the biofilm structure. Each particle was then transferred to a small container filled with water. Using a microscope MITUTOYO, Sakada, Japan with magnification 50X coupled with a camera LEICA DC300, Germany, each particle was photographed and then transferred to its container. The volumetric equivalent particle diameter (d_p) and the volumetric equivalent media diameter (d_m) were measured with the VISIONGAUGE software (Flexbar Machine Co, New York, USA) synchronized to the camera. In order to maximize the accuracy of the measurements, all the measurements were periodically checked with the microscope's Standard Measurement Ruler. **Figure 4.1** also shows some estimated measurements of biofilm and media diameters.

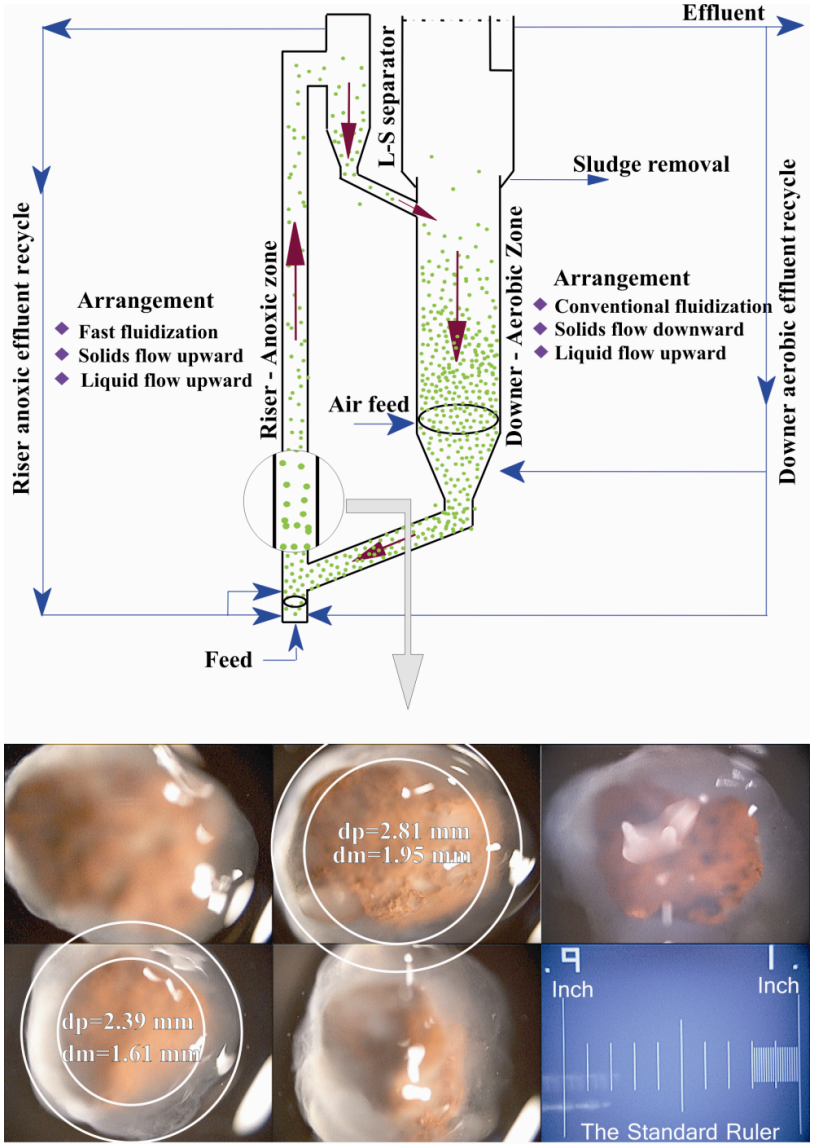

Figure 4.1. Schematic of a liquid-solid circulating fluidized bed used for the experiments and the microscopic pictures of biofilm-coated particles and measurement of biofilm and media diameter

To measure u_t experimentally, biofilm coated particles were sequentially transferred to a third column 6 m high, 32 cm in diameter, Thus nullifying the wall effects due to $d_c >> 50\ d_p$. Clean water was used to fill this column. After letting the particles reach their constant settling velocity (3 m below the top of the column), the travel time between two fixed points (50 cm) was measured. Falling particles with non-straight paths and non-parallel to the centreline were neglected. Non-spherical particles were also neglected.

In order to measure biofilm dry density, **Equation (4.6)** was used. [10] Samples were taken and photographed to measure d_p and d_c and then sonicated (Aquasonic SK 1200H Kupos, China) for three hours at 30°C to remove the biofilm from the media. Since the biofilm sizes were not completely identical in each sample, average values for diameters were considered. Each sampling took place at a different stage of biofilm development and also hydrodynamic conditions such as superficial liquid velocity. As a result, different biofilm thicknesses were obtained at different times but the thicknesses of the biofilms were relatively equal in each sampling.

$$\rho_d = \frac{X \rho_m}{\gamma^3 - 1} \tag{4.6}$$

Since all proposed equations for the wet biofilm density are based on theories without any verification by experimental data, a hydrostatic method was developed to measure the wet biofilm density accurately. The experimental data verified the most accurate equation to calculate this value. Samples were taken, photographed for measuring the biofilm thickness and then sonicated to remove the biofilm from the media. Different concentrations of sodium acetate were dissolved in deionised water in order to make liquids with different densities of 1060, 1065, 1070, 1075, 1080, 1085, 1090 and 1095 kg/m^3. The density of liquid in each vial was measured and verified by hydrometers. Eight 100-mL glass cylinders were filled with the provided liquids. The biofilm without carrier media was placed inside the vials and then well shaken to lessen the size of bio-particles in order to uniform the effect of buoyancy force. After two hours bio-particles in one vial did neither float nor settle. Since the gravity force equaled to the buoyancy force, the density of bio-particles, wet density, was considered equal to the density of the liquid.

4.4 Results and Discussion

Figure 4.2 presents the measured results of dry and wet biofilm densities, along with correlations proposed by different researchers. The experimental dry biofilm density data from this work fit two equations proposed by Boaventura et al. (1988) and Mulcahy et al. (1978), **Table 4.1** equations (h) and (g) respectively, with an overall accuracy of 89% and

93%. Despite the lower accuracy of prediction of dry biofilm density, Boaventura's equation was used in this work to be consistent with Nicolella's study where the same equation was used. [5]

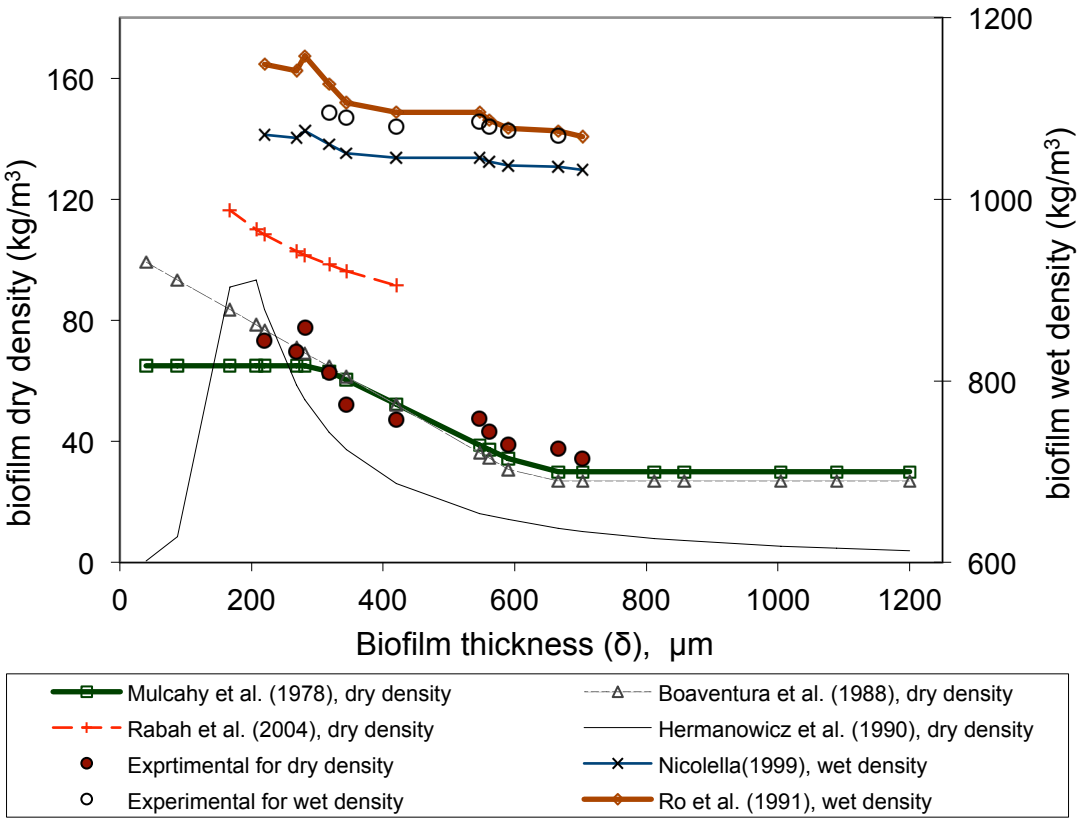

Figure 4.2. Comparison of experimental results of dry and wet densities of attached biofilm with different thicknesses with that predicted by existing correlations

On the other hand, the experimental data of wet biofilm density had a better correlation with the equation proposed by Ro et al. (1991) which was therefore used to estimate the biofilm wet density. It is interesting to note that the proposed equations for dry biofilm density were predominantly based on their experimental data while equations for wet biofilm density were predominantly theoretical due to a lack of a standard experimental method. In this study however the experimental method, described earlier, was developed to measure the wet biofilm density.

The terminal settling velocity tests discussed in this paper were conducted over a period of three months and were based on one hundred data of biofilm coated particles. In order to summarize the experimental data, results from twenty randomly selected experiments out of the one hundred are shown in **Table 4.2**.

Table 4.2. Some terminal-settling velocities out of over one hundred measured data

d_m (mm)	d_p (mm)	ρ_p (kg/m^3)	u_t (mm/s)	Re_t	d_m (mm)	d_p (mm)	ρ_p (kg/m^3)	u_t (mm/s)	Re_t
1.91	2.81	1587.3	83.6	235	1.62	2.39	1598.8	88.3	211
1.71	2.52	1595.3	75.7	191	1.67	2.47	1596.8	73.1	180
1.57	2.31	1601.0	87.7	202	1.91	2.53	1787.0	73.6	186
1.71	2.82	1425.6	68.1	192	1.82	2.57	1664.4	66.6	171
1.92	2.95	1510.6	71.4	210	1.55	2.29	1590.8	80.4	185
1.61	2.51	1512.7	71.9	180.5	1.41	2.32	1443.6	71.5	166
1.70	2.51	1595.2	63.6	160	1.51	2.43	1466.7	70.3	171
1.75	2.63	1556.6	79.0	208	1.65	2.33	1666.7	66.0	154
2.09	2.68	1855.1	74.4	199	2.04	3.00	1592.0	67.0	201
2.01	3.09	1579.6	87.7	271	2.02	3.34	1575.5	85.8	286

As only the relatively spherical particles were counted in this experiment, **Equation (4.1)** was used to estimate the value of experimental drag coefficient C_d. In addition, **Equation (4.7)** was used to estimate the experimental Re_t based on observations of the terminal velocity and particle diameter.

$$\mathrm{Re}_t = \frac{\rho_l u_t d_p}{\mu_l} \qquad (4.7)$$

From the above equation, the experimental Re_t was found to be in the range of 148-281. **Figure 4.3** shows a comparison between all of the proposed equations (as given in **Table 4.1**) for the C_d of biofilm-coated particles and the experimental data from this work. It is apparent from **Figure 4.3** that the proposed equations for $7 < \mathrm{Re}_t < 100$ failed

to predict the drag coefficients at $Re_t > 130$. **Figure 4.3** also compares the experimental data generated by Nicolella et al. (1998) with his suggested equation. The graph shows that at some Re_t, shown by the arrows, there is a deviation of more than thirty percent between his experimental C_d and the predicted C_d from his equation which denies a mono-dependency of drag coefficient on Reynolds number in biofilm coated particles. It is worth mentioning that even at the range of $7 < Re_t < 100$, the deviation between the experimental C_d at the same Re_t exceeded two hundred percent.

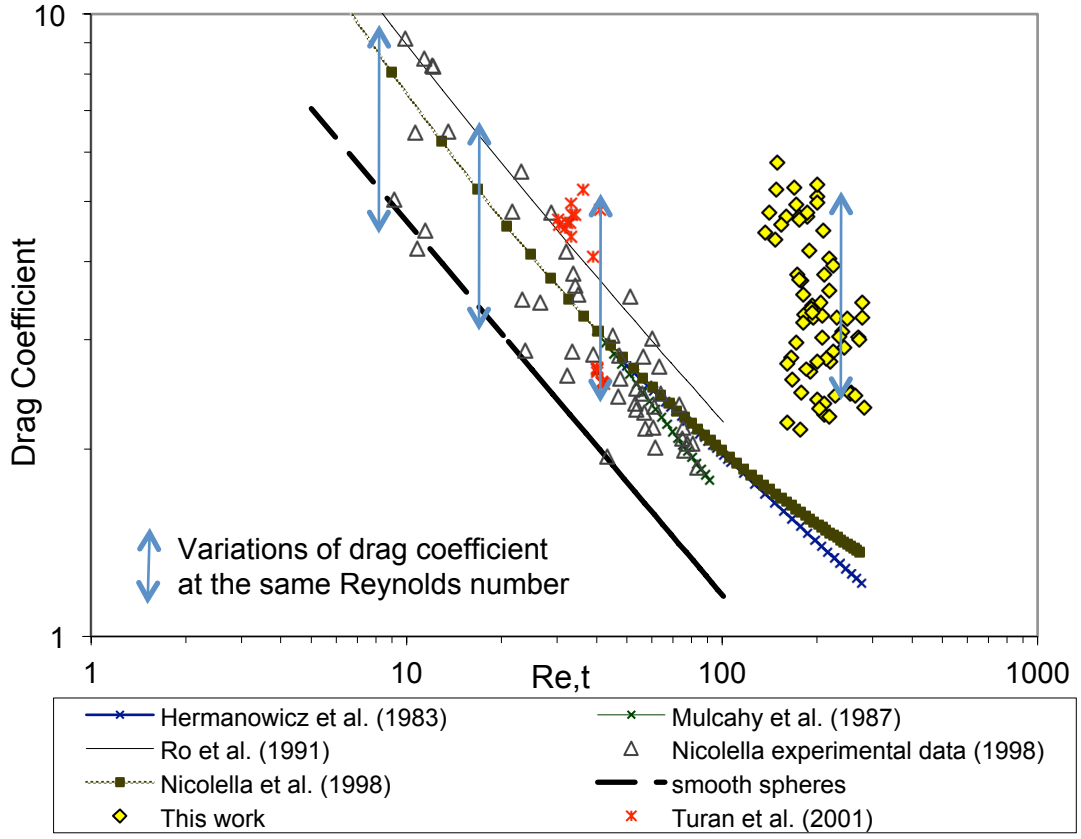

Figure 4.3. Comparison of experimental drag coefficient and that predicted with existing equations for biofilm-coated particles

In order to explain why the biofilm-coated particle Re_t in this work is much higher than the previous works, **Figure 4.4** was produced. In this figure, the values of biofim-coated particle diameters, biofilm thicknesses and biofim-coated particle effective densities of all the existing experimental data were compared. The graph shows that the

equivalent diameters of the biofim-coated particles in this experiment, 2.3 mm to 3.3 mm, were higher than the particle diameters presented in previous works, 0.4 mm to 2.6 mm [5], 0.7 mm to 1.2 mm [14], and 0.8 mm [15] to 1.5 mm. At certain points, there are similar particle diameters to other data even though the values of density at those points were much lower due to the higher biofilm thickness. Since Re_t is a function of diameter $Re_t \propto d_p$ and terminal velocity, and the terminal velocity is a function of body force $u_t \propto \rho_p^{0.5}$, a higher value of Reynolds numbers in this work is logically expected.

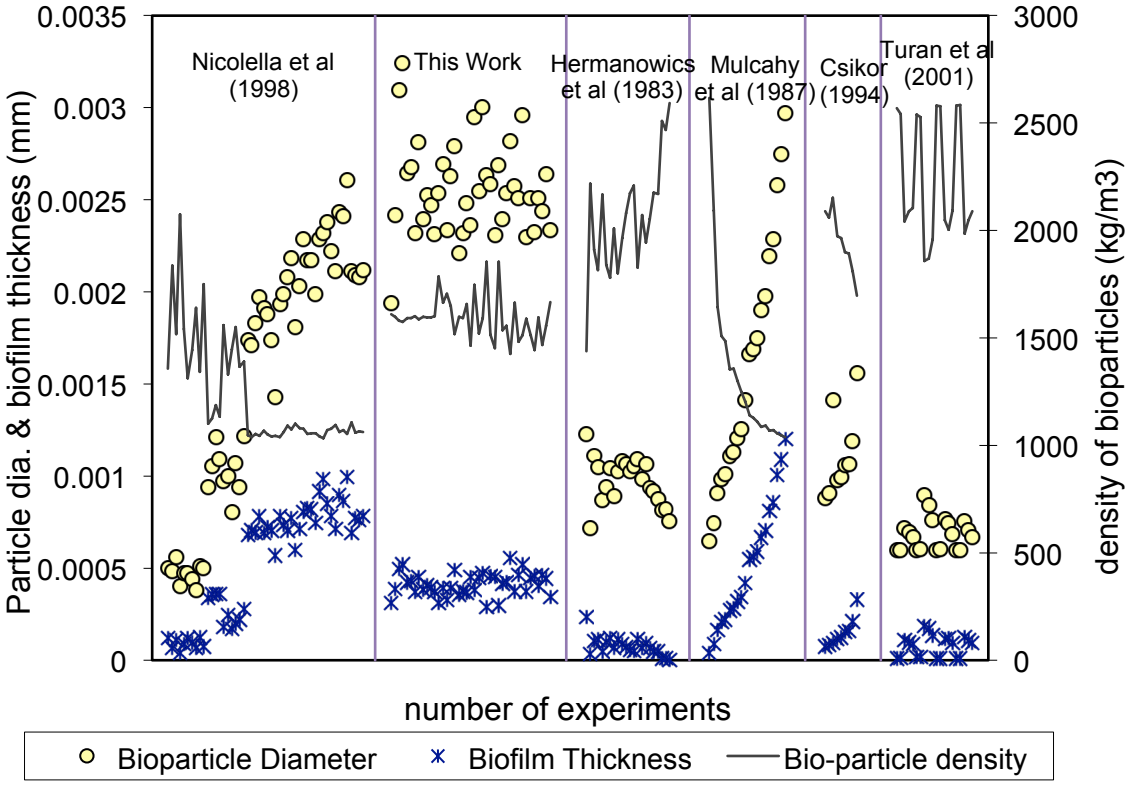

Figure 4.4. Comparison of diameter, thickness and the effective density of the biofilm-coated particles from the literature

Figure 4.5a represents a comparison between the predicted u_t using C_d proposed by Nicolella et al. (1998) and the experimental data existing so far in the literature from five other researchers. The graph shows an acceptable result within 15% average error for

data with $Re_t < 100$. However, when Re_t is above 130, data from this work, there is a significant increased deviation between the experimental data and calculated values.

To check further the suitability of the literature correlations for predicting terminal settling velocity at higher velocities, the following correlations were derived. As mentioned earlier, most equations for drag coefficient of biofilm are written as $\alpha \mathrm{Re}_t^{\beta}$, shown **Table 4.1**, so we can rewrite as:

$$C_d = \alpha.\left(\frac{d_p u_t \rho_l}{\mu_l}\right)^{\beta} = \left[\alpha^{1/\beta}.\frac{\rho_l}{\mu_l}\right]^{\beta}.\left(u_t.d_p\right)^{\beta} \tag{4.8}$$

Combining **Equation (4.8)** with **Equation (4.1)** results:

$$u_t = \left[\frac{4g\mu_l^{\beta}}{3\alpha\rho_l^{\beta+1}}\right]^{1/2+\beta}.\left(\rho_p - \rho_l\right)^{1/2+\beta}.d_p^{1-\beta/2+\beta} \tag{4.9}$$

Assuming the same liquid characteristics, according to **Equation (4.9)**, terminal settling velocity is a function of $\left(\rho_p - \rho_l\right)^{1/2+\beta}$ and $d_p^{1-\beta/2+\beta}$ so the order of change of terminal velocity between two particles (1) and (2) should be:

$$\frac{u_{t,2}}{u_{t,1}} = \left(\frac{\rho_{p,2} - \rho_l}{\rho_{p,1} - \rho_l}\right)^{1/2+\beta}\left(\frac{d_{p,2}}{d_{p,1}}\right)^{1-\beta/2+\beta}. \tag{4.10}$$

According to Nicolella et al. (2000), β equals to -0.6. **Figure 4.5b** shows the values of $\frac{u_{t,i}}{u_{t,1}}\Big|_{i=1\ to\ 50}$ calculated by **Equation (4.10)** for 50 data reported [5] versus the experimental values of $\frac{u_{t,i}}{u_{t,1}}\Big|_{i=0\ to\ 50}$ for the same reported data. The figure demonstrates that the terminal settling velocity calculated by proposed equation [5] has a good agreement with the experimental values at lower settling velocities whereas the accuracy of the predicted terminal settling velocity decreases when the biofilm settling velocity and consequently Re_t increases.

Equation (4.1) can also be written in the dimensionless form of **Equation (4.11)**:

$$Re^2 = \frac{4}{3}\frac{Ar}{C_d} \tag{4.11}$$

Equation (4.11) represents an analytical relationship between three dimensionless parameters of particle settling motion: the Reynolds number, the Archimedes number and the drag coefficient. Based on this equation, the drag coefficient of particles has a linear dependency with the multiplication of their Ar. Re^{-2}. According to **Equation (4.11)** a two-dimensional plot between any two of these three variables can be depicted. [6]

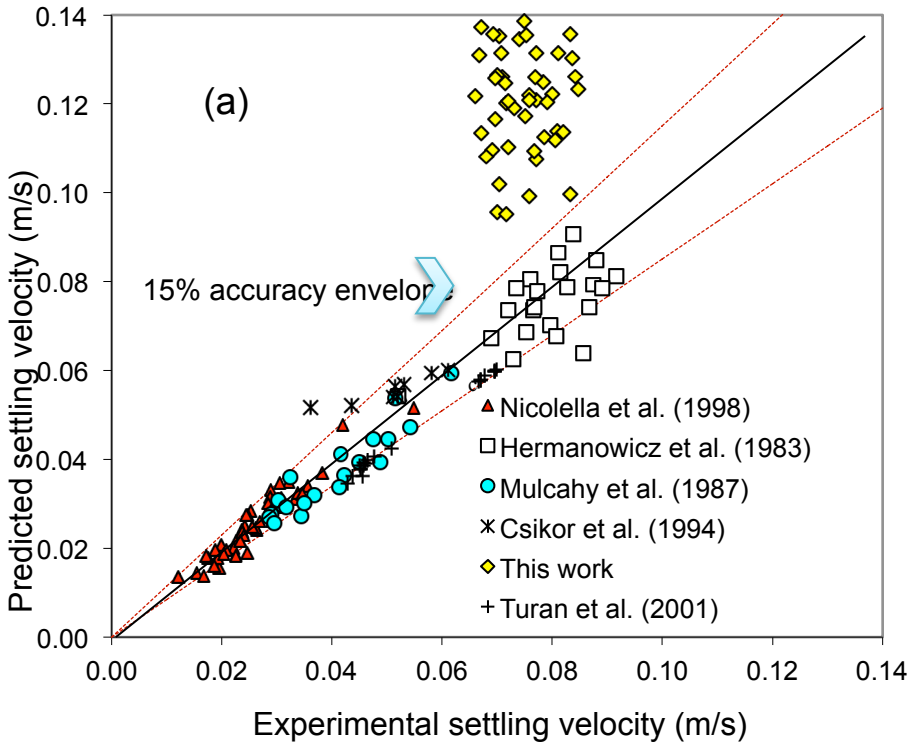

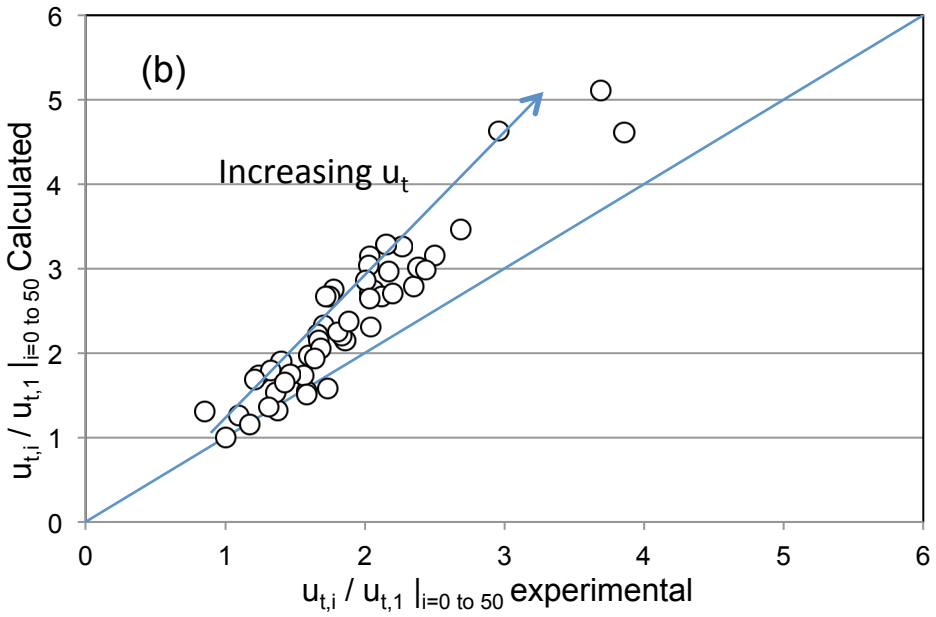

Figure 4.5. (a) Comparison of experimental terminal velocities and the predicted terminal velocities using Nicolella et al. (1998) equation, $C_d = f$ (Re) (b) Comparison of the calculated velocity ratio by **Equation (4.9)** versus experimental ratio

In order to study the experimental relationships between the three mentioned dimensionless parameters of particle motions, Archimedes numbers for experimental data of biofilm-coated particles were drawn versus the experimental Re_t in **Figure 4.6a**. The Archimedes number for each particle was calculated based on **Equation (4.3)**. The best-fitted curve in the format of **Equation (4.11)** was as follows:

$$Ar = 2.6\, Re^2 \qquad for\ \ 310 < Ar < 2.5{\times}10^5\ and\ \ 7 < Re_t < 300 \qquad (4.12)$$

Figure 4.6a shows that biofilm coated particles have the Archimedes values of less than 32,508 in the Reynolds range of less than 97. In this range of Re_t a smaller fluctuation in the Archimedes values was observed. It can also be seen that the Archimedes number increasing rate with increasing Re_t in biofilm-coated particles is higher than the spherical rigid particles.

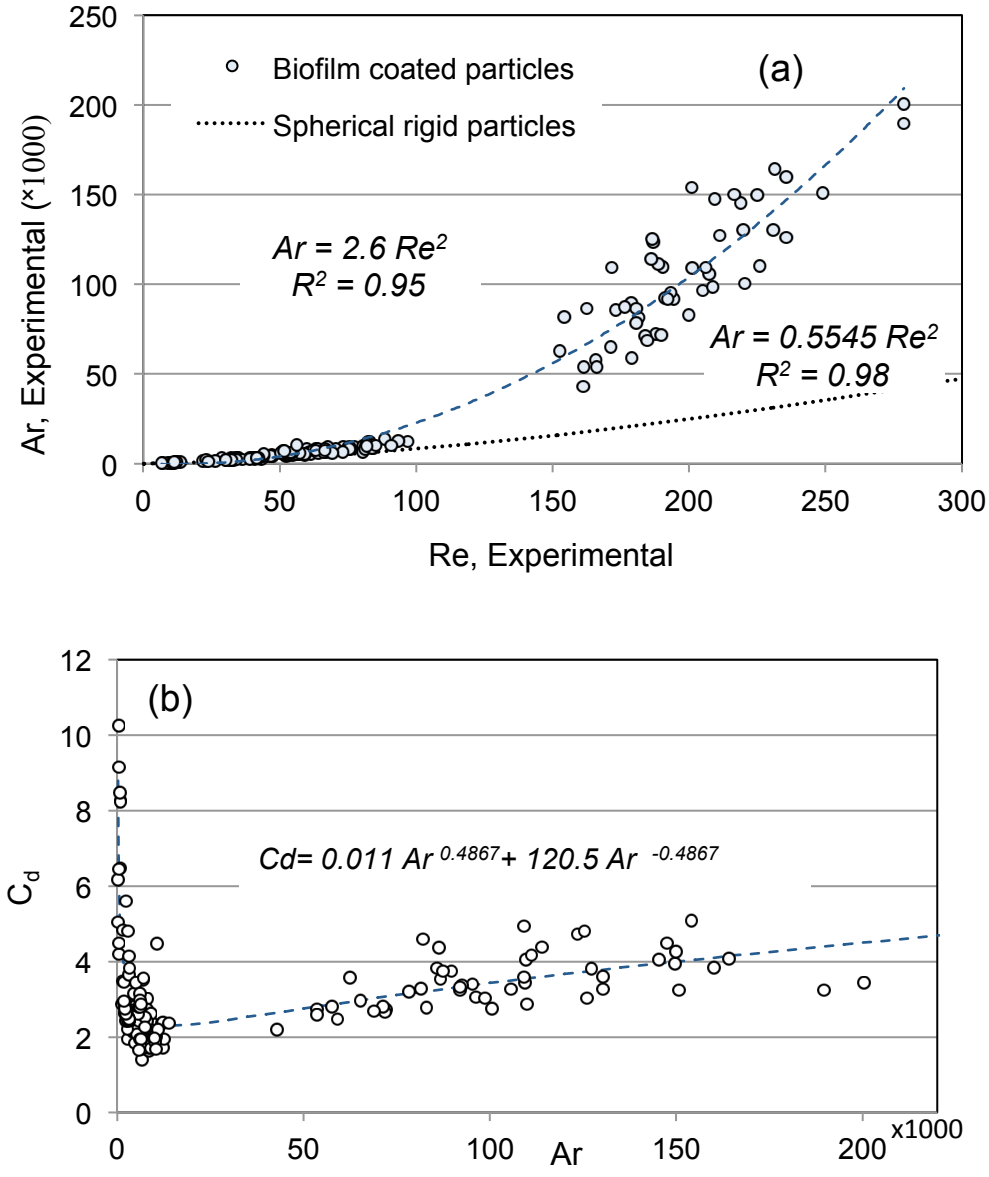

Figure 4.6. (a) Archimedes number as a function of Reynolds number for experimental data of biofilm-coated particles (b) Drag coefficient as a function of Archimedes number for experimental data of biofilm-coated particles

The same concept was applied for the drag coefficient and the Archimedes number and the result is shown in **Figure 4.6b**, which indicates that the maximum drag coefficient of 9~10 occurs when the Ar is in the range of 500~1000 and Re_t is less than 25, also there is a significant decrease in the value of C_d while the Ar increases to 15,000

and Re_t to 100. At higher values of Ar and Re_t, the drag coefficient seems to become constant at the value of 4. Karamanev (1996) also reported a trend for rising particles similar to what was observed for biofilm coated particles where there was a significant decrease in the value of C_d until Ar of 15000 and after that C_d levels out to 0.95. In addition, a comparison between the **Figure 4.6b** and **Figure 4.3** shows that the trend of drag coefficient versus Archimedes number is much more consistent and reliable that the drag coefficient versus Reynolds number. **Equation (4.13)** was found an acceptable fitted curve on the existing biofilm particles experimental data that relates directly the value of the drag coefficient to the Archimedes number.

$$C_d = a\,Ar^b + c\,Ar^{-b} \quad where \begin{cases} a = 0.011 \\ b = 0.487 \\ c = 120.5 \end{cases} \tag{4.13}$$

Using this equation along with **Equation (4.1)**, the terminal settling velocities were calculated implicitly for each particle and depicted versus the terminal velocity experimental data in **Figure 4.7**. In this figure it can be clearly seen that the calculated terminal velocities closely match the experimental data from different researchers. Compared to all experimental data, this equation predicted the terminal velocities with average errors 5.9±4.6%, 11.1±8.4%, 9.5±6.5%, 7.6±5.3%, 8.8±4.8% and 10.8±2.5% for this work, Nicolella [5], Mulcahy [12], Hermaniwicz [14], Csikor [15] and Turan [16] respectively. To compare, equation suggested by Nicolella et al. (1998), as the most previously reliable equation for biofilm particles, predict the terminal velocities with errors of 37.9±7.6%, 8.45±6.6%, 11.2±7.6%, 9.4±9.6%, 9.4±9.5% and 18.1±2.8% for this work, Nicolella [5], Mulcahy [12], Hermaniwicz [14], Csikor [15] and Turan [16] respectively. The above data clearly shows a better prediction of terminal velocity by equation suggested based on Archimedes than the other. Considering the margin of error in experimental data in addition to a lack of standard method for measuring some biofilm particle characteristics, the above equation gives an accurate prediction of drag coefficient in a wide range of $7 < Re_t < 300$ and $310 < Ar < 2.5\times10^5$ for biofilm particle motion.

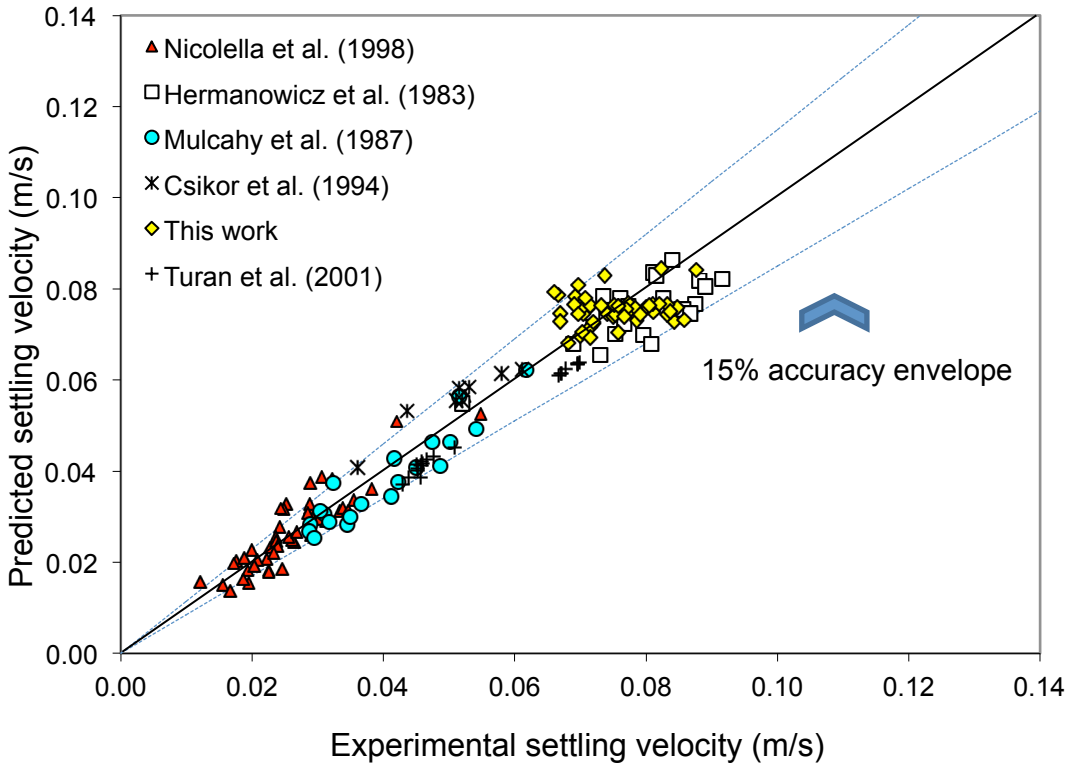

Figure 4.7. Comparison of experimental data for terminal velocity of biofilm-coated particles with the proposed equation, $C_d = f(\mathrm{Ar})$, **Equation (4.13)**

To elaborate on the values of drag coefficient predicted by this work as a function of Archimedes number and work done by Nicolella et al. (1998)[5] as a function of Reynolds, **Figure 4.8** was generated. The figure shows a much better agreement between the calculated values by this work and experimental data than equation proposed by Nicolella et al. (1998).

It is clear that the value of C_d for biofilm-coated particles is higher than smooth spherical particles and different researchers generated equations based on the theoretical assumption of a higher roughness of biofim-coated particle surfaces and deformability. However no further explanation was found to explain the higher drag force of larger biofilm covered particles than what predicted previously.

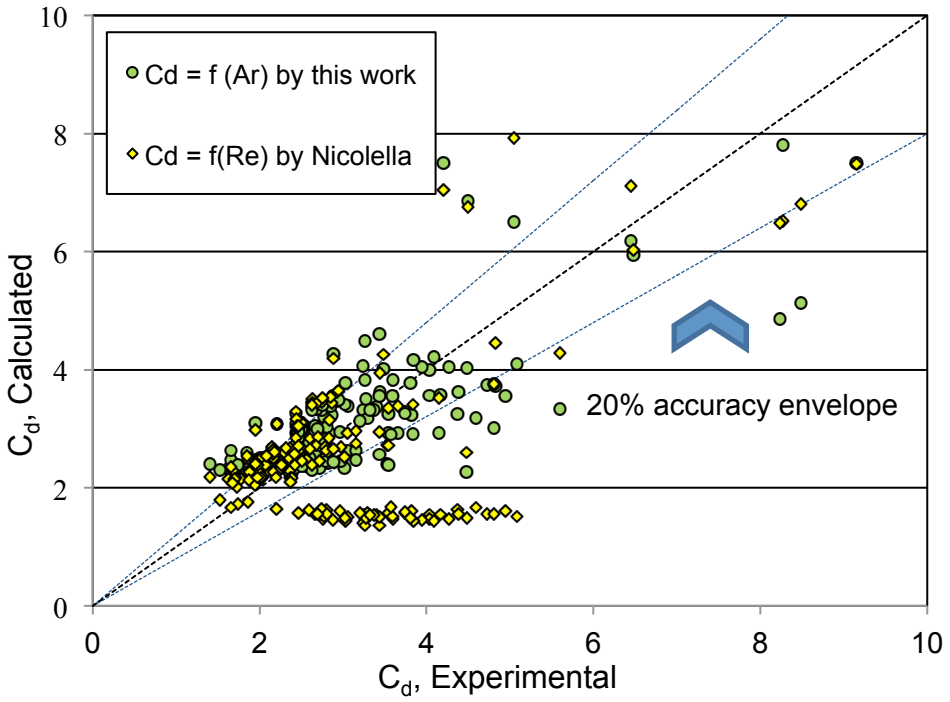

Figure 4.8. Comparison between the predicted values of drag coefficient for biofilm-coated particles by this work and Nicolella et al. (1998) with the experimental data in the literature

4.5 Conclusions

Based on experiment, the proposed equations by Ro [9] and Mulcahy [12] to determine the wet and dry biofilm densities respectively were found the most suitable among the literature equations. A terminal velocity test for biofilm-coated particles was conducted. The Reynolds numbers related to terminal velocity were higher than the literature data due to bigger particle sizes. The literature equations were not adequate for $Re_t > 130$. A new explanation of drag coefficient for a wide range of Re_t and based on a biofilm coated particle Archimedes number, a new equation was generated that was able to predict terminal settling velocity with average error of 5.9±4.6%, 11.1±8.4%, 9.5±6.5%, 7.6±5.3%, 8.8±4.8% and 10.8±2.5% for this work, Nicolella [5], Mulcahy [12], Hermaniwicz [14], Csikor [15] and Turan [16] respectively. This equation is explicit in terminal settling velocity and is valid within $310 < Ar < 2.5\times10^5$ *and* $7 < Re_t < 300$.

4.6 References

[1] Nicolella C, van Loosdrecht MMC, Heijnen JJ. Wastewater treatment with particulate biofilm reactors. J Biotechnol. 2000; 82:1-33.

[2] Patel A, Zhu J, Nakhla G. Simultaneous carbon, nitrogen and phosphorus removal from municipal wastewater in a circulating fluidized bed bioreactor. Chemosphere. 2006; 65:1103-1112.

[3] Haider A. Levenspiel O. Drag coefficient and terminal velocity of spherical and non-spherical particles. Powder tech. 1989; 58:63-70.

[4] Perry HP, Chilton CH. Chemical Engineer's Handbook (5^{th} Edition). NewYork: McGrawHill Inc., 1973.

[5] Nicolella C, van Loosdrecht MMC, Di Felice, R, Rovatti M. Terminal settling velocity and bed-expansion characteristics of biofilm coated particles. Biotechnol Bioeng. 1999; 62:62-70.

[6] Karamanev DG. Equations for calculation of the terminal velocity and drag coefficient of solid spheres and gas bubbles. Chem. Eng. Comm. 1996; 147:75-84.

[7] Turton R, Levenspiel O. A short note on the drag correlation for spheres. Powder Technol. 1986; 47: 83.

[8] Clift R, Grace JR, Weber ME. Bubbles, drops and particles. Academic Press. New York. 1978.

[9] Ro KS, Neethling JB. Biofilm density for biological fluidized beds. Res J Water Pollut Control Fed. 1991; 63(5):815-18.

[10] Ro KS, Neethling JB. Terminal settling velocity of bioparticles. Res J Water Pollut Control Fed. 1990; 62:901–906.

[11] Boaventura RA, Rodrigues AE. Consecutive reactions in fluidized-bed biological reactors: Modeling and experimental study of wastewater denitrification. Chem Engng Sci. 1988; 43:2715-2728.

[12] Mulcahy LT, LaMotta EJ. Mathematical model of the fluidized bed biofilm reactor. Processing of the 51 st annual conference of the Water Pollution control federation, Anheim, CA, USA.1978.

[13] Webb C, Black GM, Atkinson B. Liquid fluidization of highly porous particles. Chem. Eng. Res. Des. 1983; 61:125-134.

[14] Hermanowicz SW, Ganczarczyk JJ. Some fluidization characteristics of biological beds. Biotechnol Bioeng. 1983; 25:1321–1330.

[15] Csikor Z, Mihaltz P, Czako L, Hollo J. New interpretation of expansion in biofilm-coated particle fluidization. Appl Microbiol Biotechnol. 1994; 41:608–614.

[16] Turan M, Ozturk I. Influence of different bioparticles on bed expansion characteristics of anaerobic fluidized bed reactors. J Environ Sci Health. 2001; A36(6):1041-1053.

[17] Coelhoso I, Boaventura R, Rodrigues A. Biofilm reactors: An experimental and modeling study of wastewater denitrification in fluidized-bed reactors of activated carbon particles. Biotecnol Bioeng. 1992; 40:625-633.

[18] Rabah FKJ, Dahab MF. Biofilm and biomass characteristics in high-performance fluidized bed biofilm reactor. Water Res. 2004; 38:4262-4270.

5 A New Definition of Bed Expansion for Fluidized Biofilm-coated Particles

5.1 Introduction

High rate anaerobic biological fluidized beds are becoming of considerable interest due to the rising values of biogas such as methane and hydrogen. **Figure 5.1** presented by Henze et al. (2008), clearly demonstrates the increasing number of full-scale anaerobic treatments applying particulate expanded systems such as fluidized beds (FB) and expanded granular beds (EGB) over up-flow anaerobic sludge blanket (UASB). [2] In the design of a fluidized bed bioreactor (FBBR), it is crucial to know the state of bed expansion in order to design bed volume, solid hold ups and recirculation flows before and after development of biofilm.

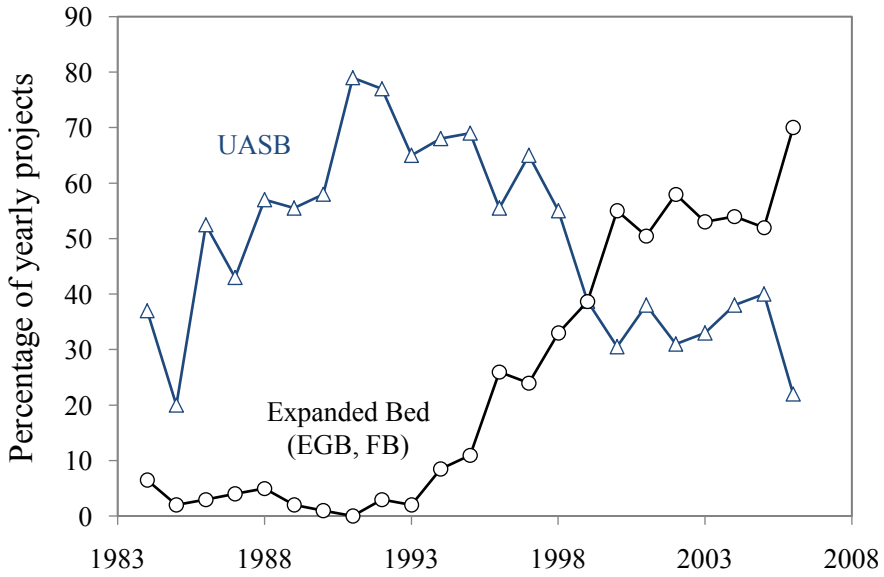

Figure 5.1. Share of UASB and expanded bed systems in the full-scale anaerobic treatment systems installed in the period 1984-2007 (Adapted from Henze et al., 2008, P.440)

For non-biological fluidized beds of homogeneous rigid spherical particles, the Richardson and Zaki model [3] is the most popular among all proposed models to describe bed-expansion characteristics as follow:

$$\varepsilon^n = \frac{u_l}{u_i} \tag{5.1}$$

Where u_i and terminal settling velocity (u_t) can be calculated from the following equations:

$$\log u_i = \log u_t - \frac{d_p}{d_c} \tag{5.2}$$

$$u_t = \left[\frac{4 g d_p \left(\rho_p - \rho_l\right)}{3 C_d \rho_l}\right]^{0.5} \tag{5.3}$$

As apparent from **Equation (5.3)**, u_t is a function of drag coefficient (C_d). Drag coefficient has been proposed as a function of Reynolds number (Re) [3] which itself is a function of u_t, making an implicit correlation to calculate bed expansion index.

As shown in **Table 5.1**, many mathematical expressions have been developed in the literature for bed expansion index (n) of biofilm-coated particles in fluidized beds. As apparent from **Table 5.1**, all the proposed equations were based on Re_t in the range of Re_t<100 and form of $\alpha\, Re_t^{\beta}$, except **Eq. (a)**, **Table 5.1** that was based on Galileo number (Ga) as proposed by Mulcahy and LaMotta (1978). [4]

Galileo number has been defined with the same formula as Ar in the literature. [5]

$$\text{where } Ar = \frac{g d_P^3 \left(\rho_P - \rho_l\right) \rho_l}{\mu^2} \tag{5.4}$$

Unfortunately, these correlations result in different predictions of bed porosity under the same operational conditions and consequently result in considerable difference in biomass concentration prediction in FBBR. [6] In addition, with the new proposed correlation of drag coefficient based on Ar [1], assessment of existing data in the literature

for bed expansion index of biofilm-coated particles using the aforementioned formula was inevitable

Table 5.1. Reported equations for bed expansion index in FBBRs

Eq.	Bed expansion index (n)	Range	Reference[1]	Ref. No
a	$n = 47.36\,Ga^{-0.2576}$	$1000 < Ga < 15000$	Mulcahy and LaMotta (1978)	[4]
b	$n = 4.26 - 0.73\log(\mathrm{Re}_t)$	$10 < \mathrm{Re}_t < 90$	Nieuwstad (1984)	[19]
c	$n = 30\,\mathrm{Re}_t^{-0.505}$	$20 < \mathrm{Re}_t < 100$	Thomas and Yates (1985)	[5]
d	$n = 10.35\,\mathrm{Re}_t^{-0.18}$	$40 < \mathrm{Re}_t < 90$	Mulcahy and Shieh (1987)	[8]
e	$n = 8.733\,\mathrm{Re}_t^{-0.341}$	$10 < \mathrm{Re}_t < 50$	Harada et al. (1987)	[20]
f	$\varepsilon = 1.72\,\mathrm{Re}_t^{0.203}\,Ga^{-0.179}$	-	Setiadi (1989)	[16][2]
g	$n = 9.11\,\mathrm{Re}_t^{-0.21}$	$50 < \mathrm{Re}_t < 100$	Hermanowicz and Cheng (1990)	[21]
h	$n = 4.526\,\mathrm{Re}_t^{-0.0126}$	$40 < \mathrm{Re}_t < 90$	Yu and Rittmann (1997)	[15]
i	$n = 4.45\ \mathrm{Re}_t^{-0.1}$	$10 < \mathrm{Re}_t < 100$	Nicolella et al. (1999)	[9]

[1] The equations are listed based on the proposed year.
[2] Bed expansion was proposed based on voidage in the bed.

Thus a new definition of bed expansion index based on Ar for biofilm-coated particles in FBBR was developed based on data available in the literature which predicted bed voidage precisely.

5.2 Materials and Methods

5.2.1 Experimental data

In order to study the bed expansion of biofilm-coated particles in fluidized bed columns; the existing data in the literature [6, 7, 8, 9, 10, 11, and 12] was employed. The data was sorted in Supplementary Document in the form of Excel sheet. As shown in Supplementary Document, some information in each series of data was not provided and consequently had to be calculated based on the existing information. Drag coefficients in all the seven series of data were calculated using **Equation (5.5)** proposed by Andalib et

al. (2010), proven to be a more reliable correlation to calculate drag coefficient of biofilm-coated particles than other literature models. [1]

$$C_d = 0.011 Ar^{0.487} + 120.5 Ar^{-0.487} \qquad for \quad 310 < Ar < 250000 \quad and \quad 7 < \mathrm{Re} < 300 \quad (5.5)$$

Accordingly **Equation (5.3)**, **Equation (5.2)** and finally **Equation (5.1)** were used to calculate u_t, u_i and n for each test. For the biofilm dry and wet densities, **Equation (5.6)** and **Equation (5.7)** proposed by Mulcahy and Shieh (1987) and Ro and Neethling (1991) respectively were adapted for all seven data series [8, 13]. Total density of biofilm-coated particles was then calculated by **Equation (5.8)**.

$$\begin{cases} \rho_d = 65 \ \ mg \cdot cm^{-3} & for \quad 0 < \delta < 300 \ \mu m \\ \rho_d = 98.6 - 0.106\delta \quad mg \cdot cm^{-3} & for \ 300 < \delta < 630 \ \mu m \\ \rho_d = 30 \ \ mg \cdot cm^{-3} & for \quad 630 < \delta \ \mu m \end{cases} \qquad (5.6)$$

$$\rho_w = 2.059 \rho_d + \rho_l \qquad (5.7)$$

$$\rho_p = \left(\frac{d_m}{d_p}\right)^3 \rho_m + \left[1 - \left(\frac{d_m}{d_p}\right)^3\right] \rho_w \qquad (5.8)$$

For series where the bed expansion was not given as bed voidage but expanded bed heights, the bed voidage was calculated using **Equation (5.9)** proposed by Nicolella et al., 1999. [5]

$$\varepsilon = 1 - \frac{M_m}{Ah\rho_m}\left(\frac{d_p}{d_m}\right)^3 \qquad (5.9)$$

5.2.2 Statistical Analysis

The student t-test was used to test the hypothesis of quality at the 95% confidence level. The null hypothesis was defined to be no difference between the two groups tested

versus the alternative hypothesis that there is a statistical difference between the two groups.

5.3 Results and Discussion

The definition of *Re* denotes the ratio of dynamic pressure to shear stress on a moving particle, whereas the definition of *Ar* denotes the ratio of gravitational force to viscous force times buoyancy force, the three forces directly applied to a free falling particle. Thus, the definitions of drag coefficient and bed expansion index for falling particles, as well as rising bubbles, would be theoretically more rational and scientific to be based on *Ar* rather than *Re*. Karamanev (1996) and Andalib et al. (2010) have confirmed that, through the analyses of experimental data for the motion of rigid spherical and biofilm-coated falling particles respectively in the literature, the best way to correlate C_d for falling particles is by describing it as a function of *Ar* [1, 14]. The following analysis further show that the fluidized bed expansion is also better correlated with *Ar*.

Figure 5.2 shows the experimental bed expansion index for biofilm-coated particles denoted as Series 1 to 7 by Setiadi [7], Mulcahy and Shieh [8], Nicolella et al. [9], Hermanowicz, and Ganczarczyk [10], Shieh et al. [11], Rabah and Dahab [6] and Ngian and Martin [12] respectively versus particle Re_t and *Ar* numbers. The bed expansion index predictions by the proposed equations in the literature (listed in **Table 5.1**) are also depicted in **Figure 5.2**. In **Figure 5.2a and 5.2b,** *n* was considered to be simple power functions of Re_t **(a)** and *Ar* **(b)** with the form of aRe^b or aAr^b respectively, following the original definition of bed expansion for spherical rigid particles by Richardson and Zaki (1954). **Figure 5.2a** clearly shows that while those proposed equations agree in general with the experimental trend, the predictions by all correlations but Eq. (h) deviate significantly from the experimental bed expansion indexes, with Eqs. (b) and (e) overly underestimating the experimental values and with Eqs (c), (d) and (g) severely overestimating at the lower Re_t. Eq. (a), which is the only equation based on *Ar*, over predicts the bed expansion index even more as shown in **Figure 5.2b** at *Ar* below 800. The above demonstrates that the form of proposed equations for *n* was not appropriate.

Even the best predictive correlation by Yu and Rittmann (1997) still underestimates the experimental value at very low *Re*.

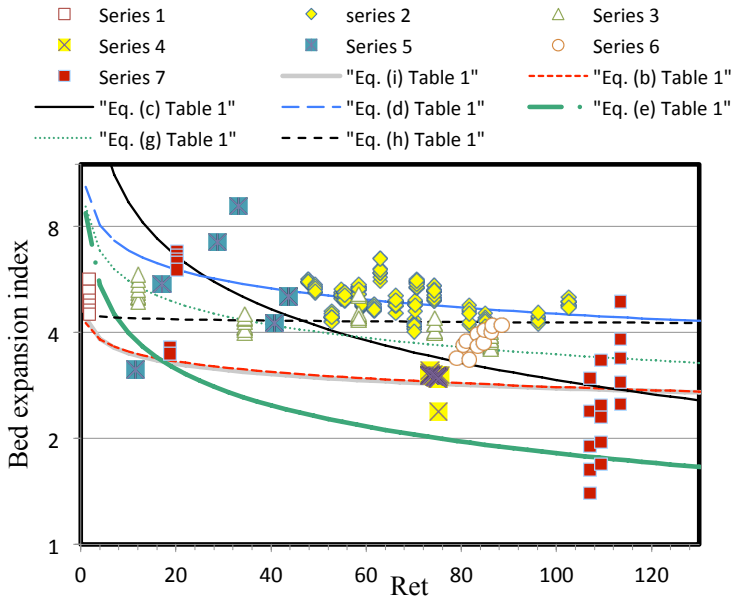

(a)

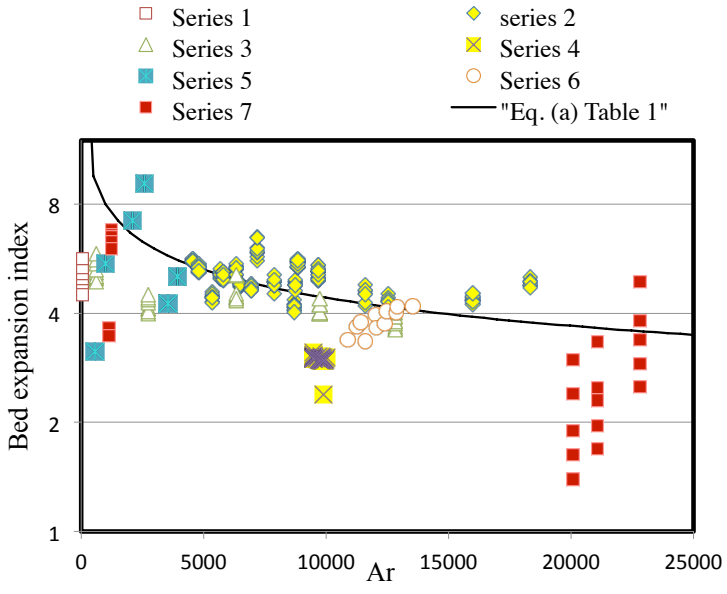

(b)

Figure 5.2. (a) Bed expansion index versus Ret, proposed equations and experimental data (b) Bed expansion index versus Ar, proposed equation and experimental data

Table 5.2 shows the average errors between the predicted bed expansion indexes by different equations listed in **Table 5.1** and the experimental bed expansion indexes (Series 1 to 7). All the values are presented as average error ± standard deviation. In addition, all the proposed equations predict the bed expansion index of Series 7 with an average error of 37% except Harada [20] with an average error of 73%. Among the six-best proposed equations, Eq. (h) proposed by Yu and Rittmann (1997) provides the most precise prediction to the bed expansion index with an average error of 21% for experimental Series 1 to 7.

Table 5.2. Predicted Bed expansion index to experimental n (Series 1 to 7)

		Standard average error ± Standard deviation							
Eq.	Reference	Series 1	Series 2	Series 3	Series 4	Series 5	Series 6	Series 7	Average
(a)	Mulcahy and Lamotta, 1978	72±2	10±8.5	20±15	33±2.3	30±20	10±7	37±18	**30±21**
(b)	Nieuwstad (1984)	21±8	69±15	43±11	4.2±2.5	77±55	33±10	38±34	**41±25**
(d)	Mulcahy and Shieh (1987)	47±3.5	7.3±6	17±6	37±3	28±23	18±16	37±18	**27±14**
(e)	Harada et al. (1987)	12±4	79±18	65±33	38±4.0	33±18	144±7	73±54	**63±42**
(h)	Yu and Rittmann (1997)	10±7.6	16±10	10±8	30±3	37±37	12.6±6	37±18	**21±12**
(i)	Nicolella et al. (1998)	19±8.1	71±15	45±11	5±2	79±59	35±10	38±35	**42±26**
(10)	This work	6±3	8±6.4	10±5.6	36±2	19±16	17±5	37±15	**19±12**

Figure 5.3 represents a comparison between the seven aforementioned experimental bed voidage values and the values predicted by the six-best equations in **Table 5.1**, Eqs. (a), (b), (d), (e), (h) and (i). The statistical errors for those predictions are also in **Table 5.3**. As expected, the Yu and Rittmann's correlation also provides statistically the most precise prediction for the bed voidage with an average standard of 11%.

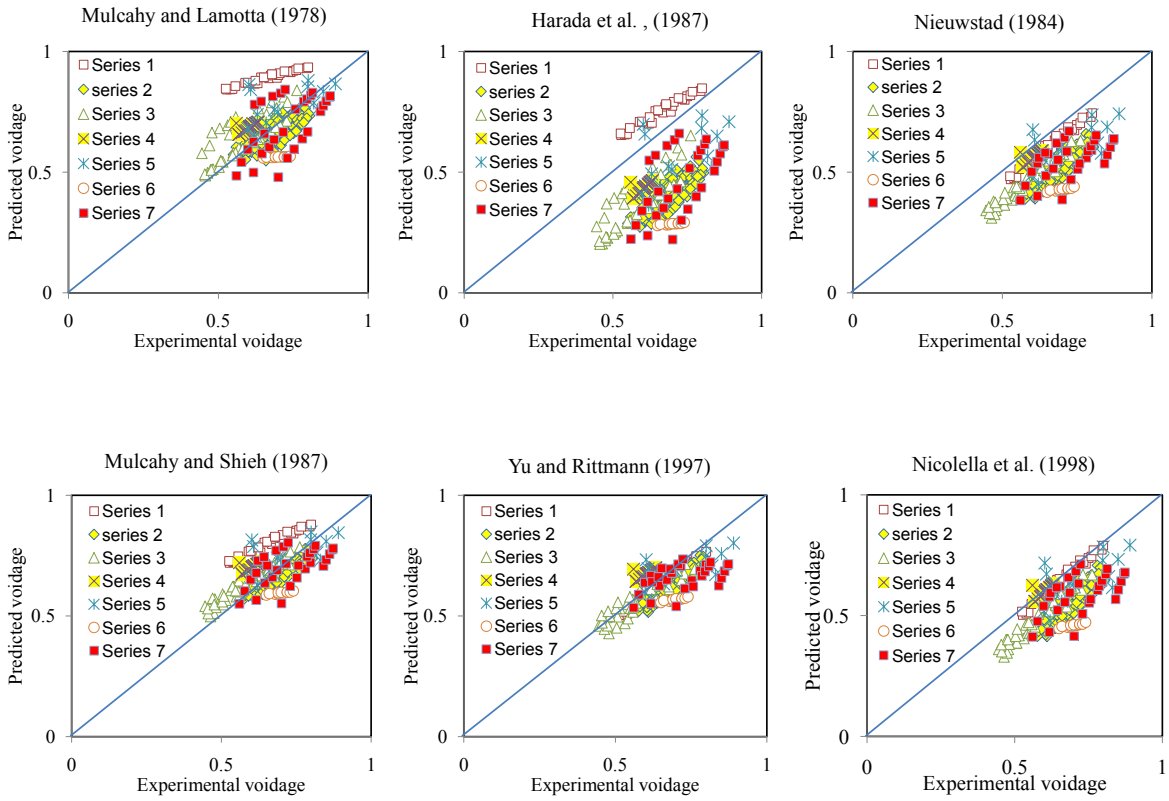

Figure 5.3. Predicted bed voidage by different proposed equation versus experimental data in the literature

Table 5.3. Bed voidage prediction by different equations to experimental ε (Series 1 to 7)

		Standard average error ± Standard deviation							
Eq.	Reference	Series 1	Series 2	Series 3	Series 4	Series 5	Series 6	Series 7	Average
(a)	Mulcahy and Lamotta, 1978	25±6.9	13±2.1	9.4±8	11±1.6	10±8.6	24±4	12±10	**15±6.6**
(b)	Nieuwstad (1984)	9±3.5	40±15	28±7	8±0.9	20±11	63±4	32±17	**28±19**
(d)	Mulcahy and Shieh (1987)	17±5.4	12±20	8±4.4	14±1.6	9±7.4	17±4	1±0.1	**11.1±6**
(e)	Harada et al. (1987)	12±4.3	78±18	65±33	38±4.9	33±19	144±7	70±50	**62±42**
(h)	Yu and Rittmann (1997)	4±2.8	16±19	5.2±3.8	10±1.6	8±7.5	23±3	12±10	**11±6**
(i)	Nicolella et al. (1998)	3±2.7	33±18	20±7.8	10±1.7	14±9.2	52±4	23±15	**22±16**
(11)	This work	2±1.3	8±14.8	5±3.7	10±2.1	8±6.4	16±3	7±4.5	**8±4.3**

As discussed earlier, *Ar* denotes the ratio of gravitational force to viscous force times buoyancy force, which are the three forces directly applied to a free falling particle, whereas *Re* only denotes the ratio of dynamic pressure to shear stress, so that it would be more appropriate to correlate the bed expansion with *Ar*. This is further exemplified by the much large scattering of the experimental data versus *Re* than that versus *Ar*, as shown in **Figures 5.2a** and **5.2b**. Following the aforementioned logic, **Equation (5.10)**

was obtained through non-linear curve fitting to give the best predictions to the bed expansion index:

$$n = \frac{1}{\alpha\, Ar^{\beta}+0.2} \quad where\ \alpha = 9.413\times10^{-6} \quad and\ \beta = 0.7728 \qquad (5.10)$$

Figure 5.4a compares the calculated and experimental bed expansion index from **Equation (5.10)** versus the experimental Ar number of biofilm-coated particles for Series 1 to 7. Compared to the other six-best correlations, the average error for all the seven Series from **Equation (5.10)** is much smaller, at a value of 19%, as shown in **Table 5.2**. In addition, the newly proposed **Equation (5.10)** also predicts the more reasonable mathematical limits for the bed expansion index between 4.47 and 5 for biofilm-coated particles as Ar approaches the two extremes: $\lim_{Ar\to 0} n = 5\ and\ \lim_{Ar\to 25000} n = 4.47$

With **Equation (5.10)**, as well as **Equation (5.1)**, the bed voidage can now be calculated directly from Ar, and are compared to the experimental bed voidage as shown **Figure 5.4b** where the two dash lines represent the model prediction ±10%. As depicted in **Figure 5.4b**, the proposed **Equation (5.10)** well predicts the bed voidage for the seven series of experimental data with less than 10% error. As also shown in **Table 5.3**, the average error between the predicted and experimental bed voidage values is only 8% for the newly proposed correlation, with the average errors ± standard deviations for Series 1 to 7 being 2%±1.3%, 8%±14.8%, 5.0%±3.7%, 10%±2.1%, 8%±6.4%, 16%±3%, and 7%±4.5% respectively. In addition, a two-sided t-test demonstrated that calculated bed voidage agreed with the experimental values at the 95% confidence level.

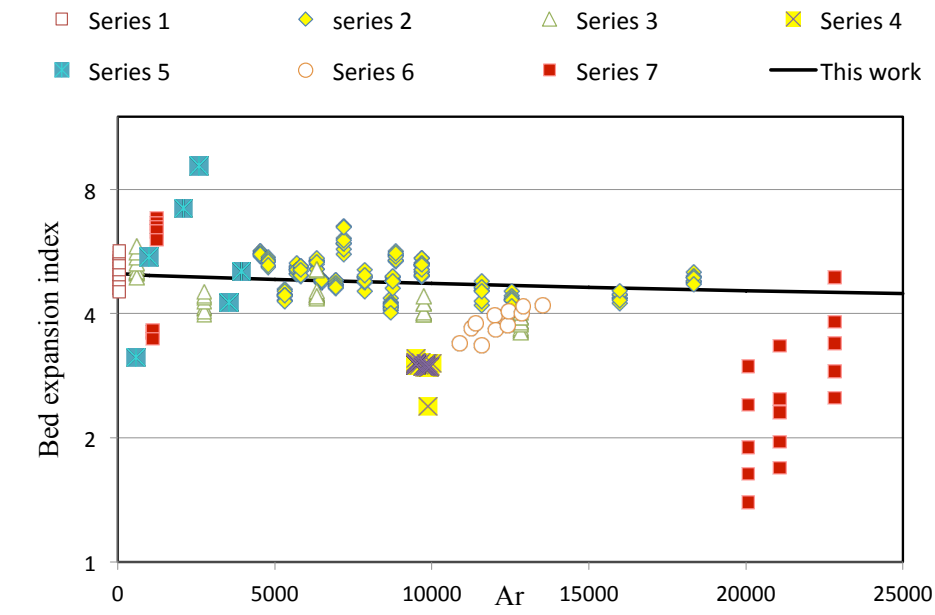

(a)

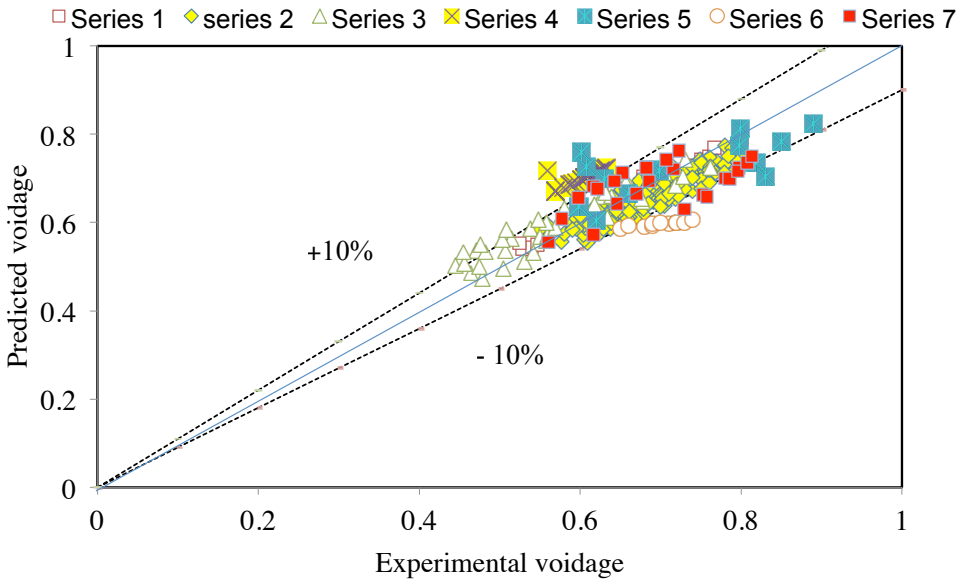

(b)

Figure 5.4. (a) Proposed bed expansion index correlation in this work versus experimental biofilm-coated particle Ar numbers (b) Predicted bed voidage in this work vs experimental voidage

With both drag coefficient and bed expansion index for biofilm-coated particles as functions of *Ar*, the bed voidage can now be directly calculated, without having to first calculate the terminal settling velocity, u_t, and the bed expansion index, n, another advantage of the current approach. When wall effect is negligible ($d_c > d_p$) as $u_i=u_t$, **Equations (5.1)**, **(5.3)**, **(5.5)** and **(5.10)** can be combined to derive a new correlation, **Equation (5.11)** to estimate the bed voidage directly from the physical properties of a biofilm-coated particle such as particle density, particle size, particle Archimedes number and the superficial liquid velocity in the fluidized bed column. It can be seen that the right side of **Equation (5.11)** is also a dimensionless equation and is voidage in the left side of the equation. According to **Equation (5.11)**, the bed voidage is independent of the terminal settling velocity of a biofilm-coated particle. The following correlation is valid when the superficial liquid velocity is greater than the minimum fluidization velocity, u_{mf}.

$$\in = \left[\frac{\rho_l . u_l^2 . (0.033\ Ar^{0.487} + 361.5\ Ar^{-0.487})}{4g . d_p(\rho_p - \rho_l)}\right]^{4.75\times10^{-6} Ar^{0.773} + 0.1} \qquad (5.11)$$

Using **Equation (5.11)**, the average error between the predicted and experimental bed voidage values for all the seven series is reduced to 8% for the average error as shown in **Table 5.3**. This is in comparison to the other six best correlations, which has average errors from 11% - 62%.

In addition [1], the Re_t and *Ar* numbers of biofilm-coated particles reported in the literature [4, 5, 7, 9-12, 15, 17-19] were all below 100 and 25,000, respectively. On the other hand, in a more recent work, Andalib [1] has reported Re_t and *Ar* of up to 250 and 200,000, respectively, for biofilm-coated particles. Taking an *Ar* of 200,000 for biofilm-coated particles, the bed expansion index would be 3.14 based on **Equation (5.10)** whereas the bed expansion index for the same particles with Re_t of 250 and *Ar* of 200,000 would be 2.04, 2.5, 1.8, 3.8, 1.3, 0.59, 2.8, 4.2, 2.56 calculated by Eqs. (a) to (i) of **Table 5.1**, most of them become totally unreasonable.

5.4 Conclusions

A new equation is proposed to correlate the fluidized bed expansion index of the Richardson-Zaki equation for biofilm-coated particles, as a function of *Ar* number, rather than *Re* as in the traditional approach. This was based on a previous finding by the same authors that the drag force can be better correlated to *Ar* than *Re* [1]. The new correlation, **Equation (5.10)**, is found to predict the experimental bed expansion index in the literature much better than the other six best equations reported in the literature. In combination of the Richardson-Zaki equation and our previous correlation that relates particle terminal velocity, u_t, to *Ar* number, the fluidized bed expansion can now be calculated directly from the physical properties of the particles, when the superficial liquid velocity, u_l, is given. The combined equation, **Equation (5.11)**, predicts the fluidized bed expansions to within 10% error for 6 out of 7 Series of best experimental test results, except for Series 6. As this equation is only a function of biofilm-coated particle physical property, trial and error method is not required, which is required as for all other methods that calculate the bed expansion.

5.5 References

[1] Andalib M, Zhu J, Nakhla G. Terminal settling velocity and drag coefficient of biofilm-coated particles at high Reynolds numbers. AIChE J. 2010; 5610:2598-2606.

[2] Henze M, van Loosdrecht MCM, Ekama GA, and Brdjanovic D. Biological wastewater treatment: Principle, modeling and design. IWA publishing. ISBN: 1843391880. 2008.

[3] Richardson JF, and Zaki WK. Sedimentation and fluidization: Part I. Trans. Instn. Engrs. 1954; 32:35-53.

[4] Mulcahy LT, and LaMotta EJ. Mathematical model of the fluidized bed biofilm. Report No. Env. E. 59-78-2, 1978 Department of Civil Engineering, University of Massachusetts at Amherst.

[5] Coulson JM, Richardson JF, Backhurst JR, and Harker JH. Chemical Engineering. Volume 2 4th edition 1991.

[6] Rabah FKJ, Dahab MF. Biofilm and biomass characteristics in high-performance fluidized-bed biofilm reactors. Wat. Res. 2004; 38:4262-4270.

[7] Setiadi T. Predicting the bed expansion of an anaerobic fluidized-bed bioreactor. Wat. Sci. Tech. 1995; 31-9:181-191.

[8] Mulcahy LT, and Shieh WK. Fluidization and reactor biomass characteristics of the denitrification fluidized bed biofilm reactor. Wat. Res. 1987; 21-4 :451-458.

[9] Nicolella C, van Loosdrecht MCM, Di Felice R. Terminal settling velocity and bed-expansion characteristics of biofilm-coated particles. Biotech. Bioeng. 1999; 62-1:62-70.

[10] Hermanowicz SW, and Ganczarczyk JJ. Some fluidization characteristics of biological beds. Biotech. Bioeng. 1983; XXV:1321-1330.

[11] Shieh WK, Sutton PM, Kos P. Predicting reactor biomass concentration in a fluidized-bed system. J. WPCF 1982; 53-11:1574-1584.

[12] Ngian K, and Martin WRB. Bed expansion characteristics of liquid fluidized particles with attached microbial growth. Biotech. Bioeng. 1980; XXII:1843-1856.

[13] Ro KS, and Neethling JB. Biofilm density for biological fluidized beds. J. WPCF. 1991; 63-5:815-819.

[14] Karamanev DG. Equations for calculation of the terminal settling velocity and drag coefficient of solid spheres and gas bubbles. Chem. Eng. Comm. 1996; 147:75-84.

[15] Yu H, and Rittmann BE. Predicting bed expansion and phase holdups for three-phase fluidized-bed reactors with and without biofilm. Wat. Res. 1997; 31-10:2604-2616.

[16] Setiadi T. Liquid mixing and bed expansion in a fluidized-bed reactor with particular reference to gas producing anaerobic systems. PhD thesis, University of Strathclyde, Glasgow. 1989

[17] Csikor Z, Miháltz P, Czakó L, Holló J. New interpretation of expansion in biofilm-coated particle fluidization. Appl. Micro. Biotech. 1994; 41:608-614.

[18] Turan M, and Ozturk I. Influence of different bioparticles on bed expansion characteristics of anaerobic fluidized bed reactors. J. Environ. Sci. Heal. 2001; A36-6:1041-1053.

[19] Nieuwstad TJ. Modeling, optimization and design of fluidized beds for biological denitrification. Wat. Sci. Technol. 1984; 22-2:367-383.

[20] Harada H, Ando H, Momonoi K. Process analysis of fluidized bed biofilm reactor for denitrification. Wat. Sci. Technol. 1987; 19:151-162.

[21] Hermanowicz SW, and Cheng YW. Biological fluidized bed reactor: hydrodynamics, biomass distribution and performance. Wat. Sci. Technol. 1990; 22-1:193-202.

6 BNR Using a Novel Twin Fluidized Bed Bioreactor (TFBBR)

6.1 Introduction

There have been few studies to integrate biological nutrient removal (BNR) processes with fluidized bed bioreactors [1-3] of which some were in sequencing batch mode. [4-6] The BNR capability of airlift technology has also been studied. [7] Research on Biofilm Airlift Suspension (BAS) reactors in the late 1980s led to the concept of CIRCOX® airlift reactor which was also integrated for nitrogen removal. [8-9]

The circulating fluidized bed bioreactor (CFBBR) involving biofim-coated particle recirculation between the anoxic and aerobic bioreactors, was introduced and developed by Nakhla and his colleagues [3, 10-12] to combine the advantages of BNR and biofilm reactors in both lab and pilot scales. Lava rock with d_p of 600-1000 μm was used in CFBBR as a carrier media. More than 90% organic matter, 70-80% total nitrogen and 50-70% phosphorous biological removal were reported with hydraulic retention time (HRT) of 2.5-3 h and with an observed biomass yield of 0.12-0.16 g VSS/g COD. [3, 11, 12]

While the CFBBR has successfully incorporated fluidized bed systems with BNR, the required height of 5.5 m makes it difficult to retrofit an existing plant. Therefore, a new twin fluidized bed bioreactor (TFBBR) has been developed wherein both the riser and downer with the same size operated in a conventional fluidization mode and particle recirculation was achieved mechanically thus eliminating of a riser separator in the CFBBR. The fundamental differences between the CFBBR and TFBBR on one hand, and the CIRCOX® on the other, include the fluidization regime which is conducive to reduce biomass detachment in comparison with the CIRCOX®, media size, sludge retention time (SRT), and circulation of media between the anoxic/anaerobic and aerobic reactors. The lower u_l and consequently a lower biofilm detachment rate cause a much longer (SRT) and a lower observed yield. The purpose of this study is to evaluate the capability of the TFBBR system to treat synthetic municipal wastewater (SMW) with the same

characteristics of a typical municipal wastewater at room temperature (22±2 °C) and investigate its BNR efficiencies.

6.2 Materials and Methods

The SMW was prepared from tap water combined with concentrated CH_3COONa (as carbon source), NH_4Cl (as nitrogen source), and KH_2PO_4 (as phosphorus source) stock solutions as well as a mineral stock solution at volumetric ratios of 1:0.0025, 1:0.001, 1:0.001 and 1:0.002 respectively. The concentrated stock solutions contained 125 g CH_3COONa/L; 100 g NH_4Cl/L; 20 g KH_2PO_4/L and the mineral salt stock solution contained: 75 mg $NiCl.6H_2O$/L; 75 mg $CoCl_2 \cdot 6H_2O$/L; 200 mg $CuCl \cdot 2H_2O$/L; 125 mg $ZnCl_2$/L; 1250 mg $MnCl_2 \cdot 4H_2O$/L; 750 mg $FeCl_3 \cdot 6H_2O$/L; 200 mg $(NH_4)_6Mo_7O_{24} \cdot 4H_2O$/L; 125 mg H_3BO_3/L; 40 g Mg $SO_4 \cdot H_2O$/L; 6 g $CaCl_2.H_2O$/L. Technical grade chemicals were used with the exception of KH_2PO_4, which was reagent grade.

6.2.1 System Description

The TFBBR, depicted in **Figure 6.1a**, comprised two identical plexi-glass columns with a height of 3.6 m each, operated as two conventional anoxic and aerobic FBRs. In order to evaluate the TFBBR potential to retrofit the existing rectangular wastewater treatment tanks, the columns were made rectangular (5 cm x 8.5 cm). The superficial liquid velocities (u_l) for bare particles with an average diameter of 680 μm and for the biofilm coated particles with attached biofilm thickness of 400 μm were maintained between the minimum fluidization velocities (u_{mf}) of 0.36 and 0.28 cm/s and terminal settling velocity (u_t) of 10 and 6.7 cm/s respectively. The lower liquid velocity in the riser required a thicker biofilm to reach the u_t, which resulted in a much higher biomass retention time. The two columns are interconnected through two horizontal connecting pipes (ID=5 cm, see **Figure 6.1b**) equipped with two three-blade electro-propellers (ID=3cm, 6-800 rpm, 120 V, 60 Hz, 1/8 hp, Talboys, Tromemner. LLC, NJ, USA). Particle transfer between the columns occurred periodically. Particles from the bottom dense phase of the downer with a thin biofilm (< 30 μm) are transferred to the riser. In the riser, heterotrophic bacteria grow on the media and the biofilm becomes thicker. At a

certain biofilm thickness (800 μm), the biofilm coated particles reach the height where the propeller is located. The 60-rpm propeller slowly transfers the particles to the downer. The biofilm may be destroyed during transfer. Besides, after being exposed to the high shear force in the gas-liquid-solid phase in the downer, the biofilm detaches and leaves the system along with the effluent. The downer to riser particle transfer occurred once every three weeks with the aid of a propeller (300 rpm) to make up the particles in the riser. Four water jets (the downer to riser and riser to riser circulation streams) provided a dilute phase in the transferring tube for the 15-minute of particle transfer time from the downer to the riser.

Lava rock particles were used with an average diameter (*d*) of 680 μm, a total porosity of 62% (44% external and 18% internal), a particle dry bulk density of 1,012 kg/m^3, a particle true density of 2,628 kg/m^3 and a specific surface area determined by BET (Micromeritics ASAP 2010, Micromeritics Co., USA) of 0.48 m^2/g. The amount of particles used in the anoxic/anaerobic and aerobic columns in Phase I was 2.2 and 2.5 kg respectively increasing to 4.7 and 5.4 kg for Phases II, III and IV. The aforementioned particle masses were estimated based on the specific nitrification rates (SNRs), specific denitrification rates (SDNRs) and the attached biomass per g media, reported in the literature for the CFBBR and FBR. Chowdhury [3] has shown SNR of 0.09-0.14 g NH_4-N/g VSS·d and SDNR of 0.033-0.243 g NO_x-N/g VSS·d whereas Cui [11] has shown SNR and SDNR of 0.026-0.1 g NH_4-N/g VSS·d and 0.016-0.074 g NO_x-N/g VSS·d respectively. A reported value of 5-20 mg VSS/g media for attached biomass was also used. [3, 13-15]

Table 6.1 shows the detailed design parameters and operational conditions of the TFBBR. Air was injected at the bottom of the aerobic column using a perforated tube with an ID of 0.6 cm and a length of 4.6 cm. Air flow was monitored by an air flow meter, OMEGA, FL-3696 ST. The feed solution was pumped into the bottom of the anoxic column with a peristaltic pump (Masterflex I/P, Masterflex AG, Germany). All recirculation flows were maintained using two centrifugal pumps (IWAKI MD-40RT-115NL, IWAKI CO., Ltd. Japan) and monitored by rotameters (OMEGA FL-812 and OMEGA FL-5331G, Omega Engineering, Inc., Canada).

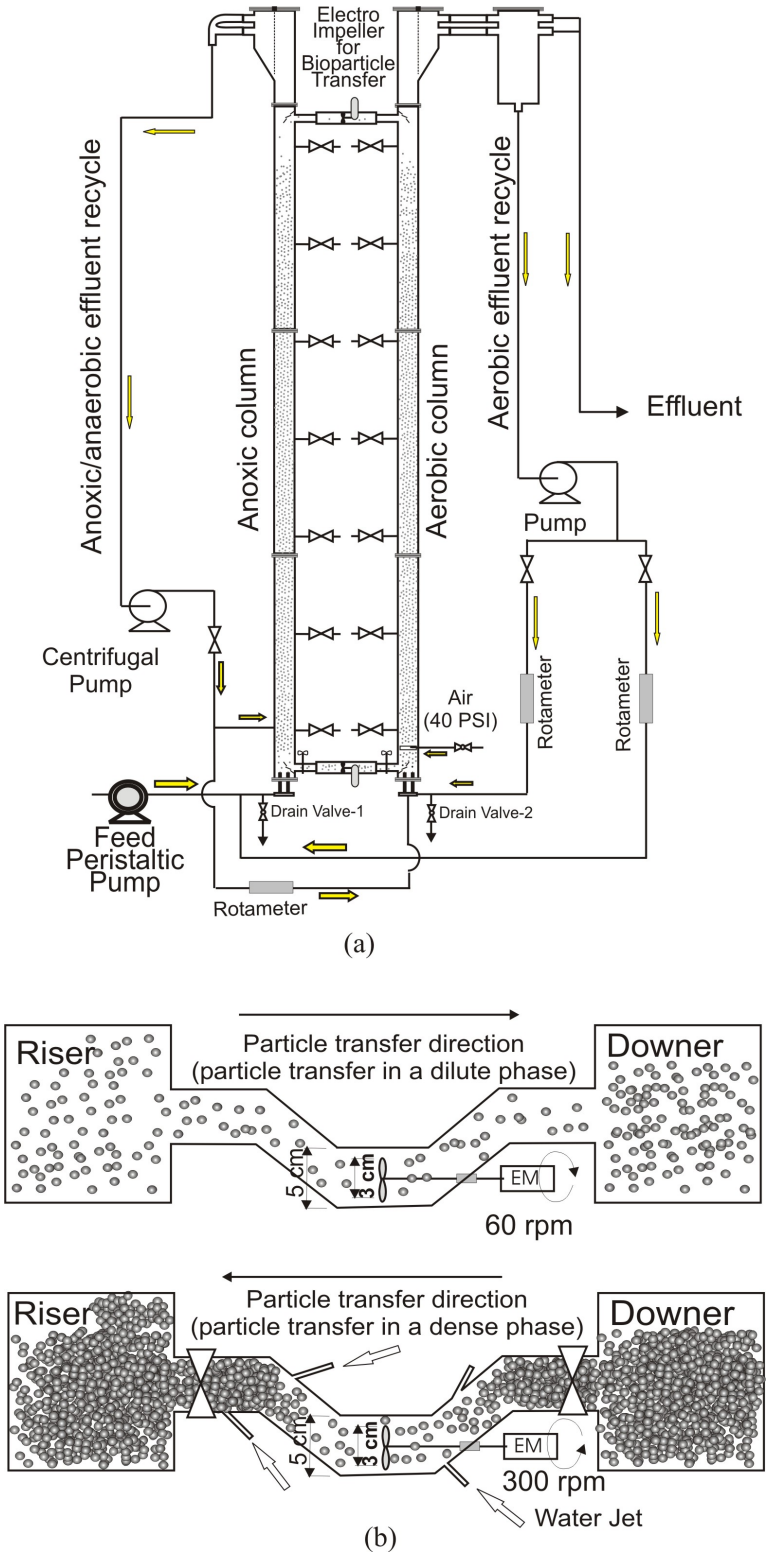

Figure 6.1. (a) Schematic of the TFBBR (b) Plan view of the horizontal connecting pipes between the downer and the riser

Table 6.1. Operating conditions

		Phase I	Phase II	Phase III	Phase IV
Influent flow, Q_{in} (L/d)		150±6	190±7	240±9	290±8
Average organic loading (kg COD/m^3·d)		1.3	1.7	2.3	2.5
Average nitrogen loading (kg N/m^3·d)		0.14	0.18	0.25	0.28
Average phosphorus loading (kg P/m^3·d)		0.024	0.03	0.033	0.04
R-R recirculation ratio ($Q_{r\text{-}r}/Q_{in}$)		7.4	8.3	7.6	6
R-D recirculation ratio ($Q_{r\text{-}d}/Q_{in}$)		0.0	5.6	4.8	3.9
D-R recirculation ratio ($Q_{d\text{-}r}/Q_{in}$)		6.4	5.6	4.7	3.9
D-D recirculation ratio ($Q_{d\text{-}d}/Q_{in}$)		11.7	9.8	8.8	9.2
EBCT (h)= $V_{compact}/Q$	Anoxic	0.35	0.59	0.45	0.38
	Aerobic	0.4	0.67	0.53	0.44
HRT (h)	Anoxic	2.24	1.77	1.34	1.15
	Aerobic	2.24	1.77	1.34	1.15
Air (40 PSIG) flow (mL/min)		2060	2150	2240	2320
DO (mg/L)	*Aerobic*	*6.8±0.4*	*6.3±0.3*	*7±0.3*	*6.4±0.2*
	Anoxic	*0.2±0.1*	*0.2±0.1*	*0.1±0.1*	*0.0*
X (mg VSS/g lava rock)	Anoxic	47.17	27.5	28.18	26.2
	Aerobic	5.83	5.77	5.12	4.3
Biomass (g VSS)	Anoxic	103.3	129.25	132.4	123.1
	Aerobic	14.5	30.58	27.14	24.0
S/X_0 (g COD/g VSS·d)		0.33	0.31	0.37	0.54
Detachment rates (1/d)	Anoxic	0.015	0.016	0.021	0.045
	Aerobic	0.09	0.05	0.07	0.18
Superficial liquid Velocity, u_l (cm/s)	Anoxic	0.55	0.65	0.84	0.82
	Aerobic	0.42	0.62	0.92	0.97
Estimated SRT (d)	Anoxic	62[a]	89	84	79
	Aerobic	12.2	19.0	13	16.6
	Overall	72.2[b]	108	97	95.6
Run time (d)		95	80	40	30

[a] based on **Equation (6.5)**, [b] based on **Equation (6.4)**

Superficial liquid velocities of 0.55-0.84 cm/s and 0.42-0.92 cm/s were maintained in the anoxic and the aerobic columns. Eight manometers (four along each column) were employed to observe the pressure drop along each column.

6.2.2 Reactor Startup

The TFBBR was seeded with enriched nitrifiers, acclimatized in the lab using 12 L returned activated sludge (RAS) from the Adelaide Pollution Control Plant, London, Canada, with TSS and VSS concentrations of approximately 3500 and 2800 mg/L respectively. Meanwhile, the clean media was fluidized in the columns at u_l=0.5 cm/s. The feed was then pumped into the system. In order to transport and trap the bacteria from the bulk liquid on the media surface and the pores, the injected seed sludge was recirculated between the two columns for two days. Thereafter, the continuous feed was initiated at the rate of 1.3 kg COD/m^3·d. Within a period of three weeks, most of the particles in both columns were coated with biomass with average concentrations of 5 and 28 mg VSS/g media, equivalent to 20-100 and 300-800 μm biofilm thicknesses, in the aerobic and anoxic columns respectively.

6.2.3 Batch Tests

Batch tests were carried out to test the SNR, and SDNR of the attached biomass in the system. Batch reactors (0.5 L working volume) equipped with magnetic stirrers were used for nitrification by injecting air or for denitrification by avoiding intrusion of air. To reduce the effect of substrate mass transfer limitation into the biofilm, the biofilm was removed from 30-40 g media using sonication and then placed into the reactors. The biomass in the SDNR and the SNR tests were in the range of 1500-4000 mg VSS/L and 240-500 mg VSS/L respectively, considering the amount of biofilm in the anoxic and aerobic column, 25-50 mg VSS/g media and 4-6 mg VSS/g media. The initial acetate COD in the denitrification batch tests was set at 350-450 mg/L while the initial alkalinity used in the nitrification test was 250-350 mg/L as $CaCO_3$.

6.2.4 Analytical Methods

Samples were collected from the feed tank, anoxic column top and the effluent. The analyses were either done the day of sampling or the samples were refrigerated at 4 °C prior to analysis. Total suspended solids (TSS), volatile suspended solids (VSS) and biochemical oxygen demand (BOD) were analyzed in accordance with Standard Methods 2540D, 2540E and 5210 [16] respectively. DO and ORP were measured onsite using an

Oakton DO 6 meter, and an Oakton ORPTestr 10 (Oakton, Singapore). HACH methods and testing kits (HACH Odyssey DR/2800) were used to analyze total and soluble chemical oxygen demand (TCOD and SCOD), total and soluble nitrogen (TN and STN) and total phosphorus (TP), NH_4-N, NO_2-N, NO_3-N, and PO_4. Alkalinity was measured by titration with 0.01 N H_2SO_4 in accordance with the Standard Method no 2320. [16] Sulfate (SO_4^{2-}) was measured using the ion chromatography (IC, Dionex 600, USA) equipped with CS16-HC and AS9-HC columns. Sodium carbonate solution, 9 mM, was applied as an eluent at a flow rate of 1 mL/min for 30 minutes, with sulfate detected 20 minutes following injection. The size of the bare and biofilm coated particles was measured using a Mastersizer 2000 laser analyzer (Malvern Instruments Inc., UK). and Visiongauge (Flexbar Machine Co, New York, USA) synchronized to a microscope (Mitutoya, Sakada, Japan) coupled with a camera (Leica DC 300, Germany), at a magnification of 50X. Based on Standard Method no 2540G [16], the attached biomass on the carrier media was measured and expressed as mg VSS/g clean particles. Approximately 10-20 g biofilm-coated particles were taken from columns and suspended in a 100 mL vial and sonicated for 3 h at 30°C in an Aquasonic sonicator (SK 1200H Kupos, China) with a rated power of 45 Watts. After sonication, the TSS and VSS content of the detached biomass was determined following Standard Methods no 2540D and 2540E. [16]

6.3 Results and Discussion

6.3.1 Organics Removal

Feed flow rates of 150, 190, 240 and 290 L/d SMW were used to examine the nutrient removal capabilities of the system. **Figures 6.2a**, **6.2b**, and **Figures 6.3a**, **6.3b** and **6.3c** depict the performance of the TFBBR with respect to COD, N and P from the SMW at different nutrient loadings. Average steady-state influent and effluent characteristics, illustrated in **Table 6.2**, show ≥93% TCOD removal in Phases I, II and III at EBCTs of 0.75, 1.27 and 1.0 h respectively. No change in organic removal efficiency was observed with the increase in OLR from 1.3 in Phase I to 2.3 kg COD/m^3·d in Phase III. In Phase IV, at an EBCT 0.78 h, the TCOD removal efficiency decreased slightly to 88% due to the higher amount of effluent VSS (17 mg/L) as a result of a combined high shear coefficient and detached biomass. Detachment rate coefficient (1/d) was calculated by

multiplying the concentration of biomass by the feed flow and then dividing by the total mass of biomass in each column. [12]

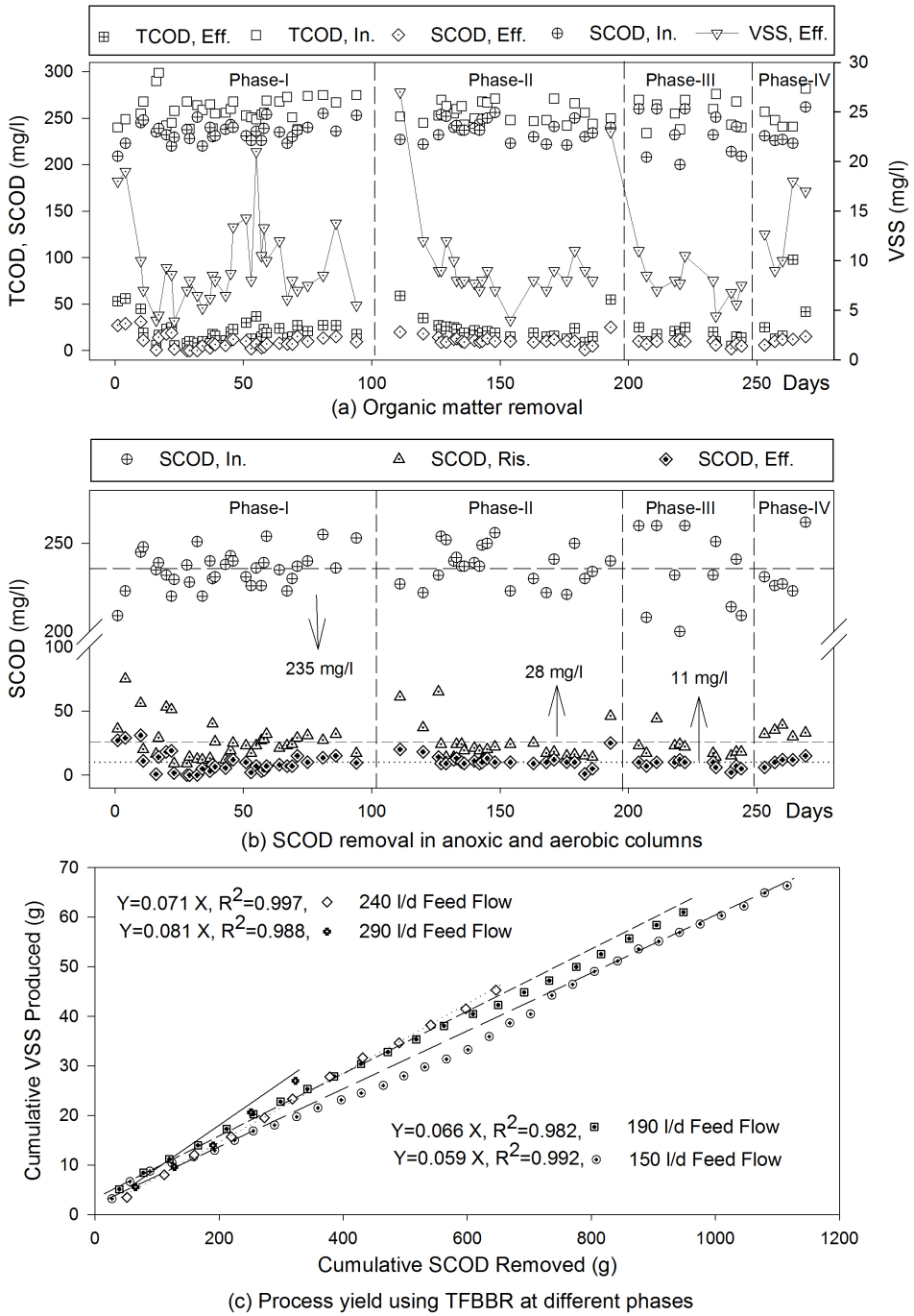

Figure 6.2. (a) Organic matter removal using TFBBR (b) SCOD removal in the anoxic and aerobic columns (c) TFBBR yields in different phases

The increase in the value of detachment coefficient (see **Table 6.1**) with increasing OLRs is consistent with the findings of Chowdhury et al. (2008) and Kwok et al (1997). [3, 17] Particularly, the values of detachment rates in the anoxic column of the TFBBR of 0.016-0.04 1/d are significantly lower than the 0.057-0.16 1/d observed in the lab-scale CFBBR and the 0.129-0.168 1/d for the pilot-scale [3, 12], which resulted in a much longer anoxic SRT of 63-89 d in the anoxic column, as compared with 15-17 d in the CFBBR. [3] Detachment rates in the aerobic column of the TFBBR are quite comparable to the CFBBR. Interestingly, an increase in u_l in both columns up to ≈1 cm/s did not affect the effluent VSS concentrations from Phase I to III.

Although the TFBBR effluent was neither clarified nor filtered, TSS and BOD concentrations of ≤28 mg/L and ≤12 mg/L (**Table 6.2**) meet the US regulations for potable reuse. [18] Due to a higher amount of biomass in the anoxic column of the TFBBR (26 mg VSS/g media) relative to the CFBBR (13 mg VSS/g media) [3], a portion of biofilm was under anaerobic condition, which facilitated the development of sulfate-reducing bacteria (SRB). To investigate this, penetration depths of NO_3-N and SO_4^{2-} as the electron acceptors into the biofilm were calculated as 310 and 330 μm respectively using the proposed **Equations (6.1)** and **(6.2)** by Shieh and Keenan [19], with the measured bulk concentrations of 6 mg/L NO_3-N and 15 mg/L SO_4^{2-} in the liquid phase, and an average biofilm thickness of 400 μm and media diameter of 680 μm.

$$\eta_0 = 1.2712\,\Phi_{0m}^{-1.0} = \frac{3.817}{\left[1-\left(\frac{r_m}{r_p}\right)^3\right]}\left(\frac{D_e}{\rho_d\, k_0\, r_p^2}\right)^{0.5} S_b^{0.5} \tag{6.1}$$

$$\eta_0 = \frac{1-\left(\frac{r_c}{r_p}\right)^3}{1-\left(\frac{r_m}{r_p}\right)^3} \tag{6.2}$$

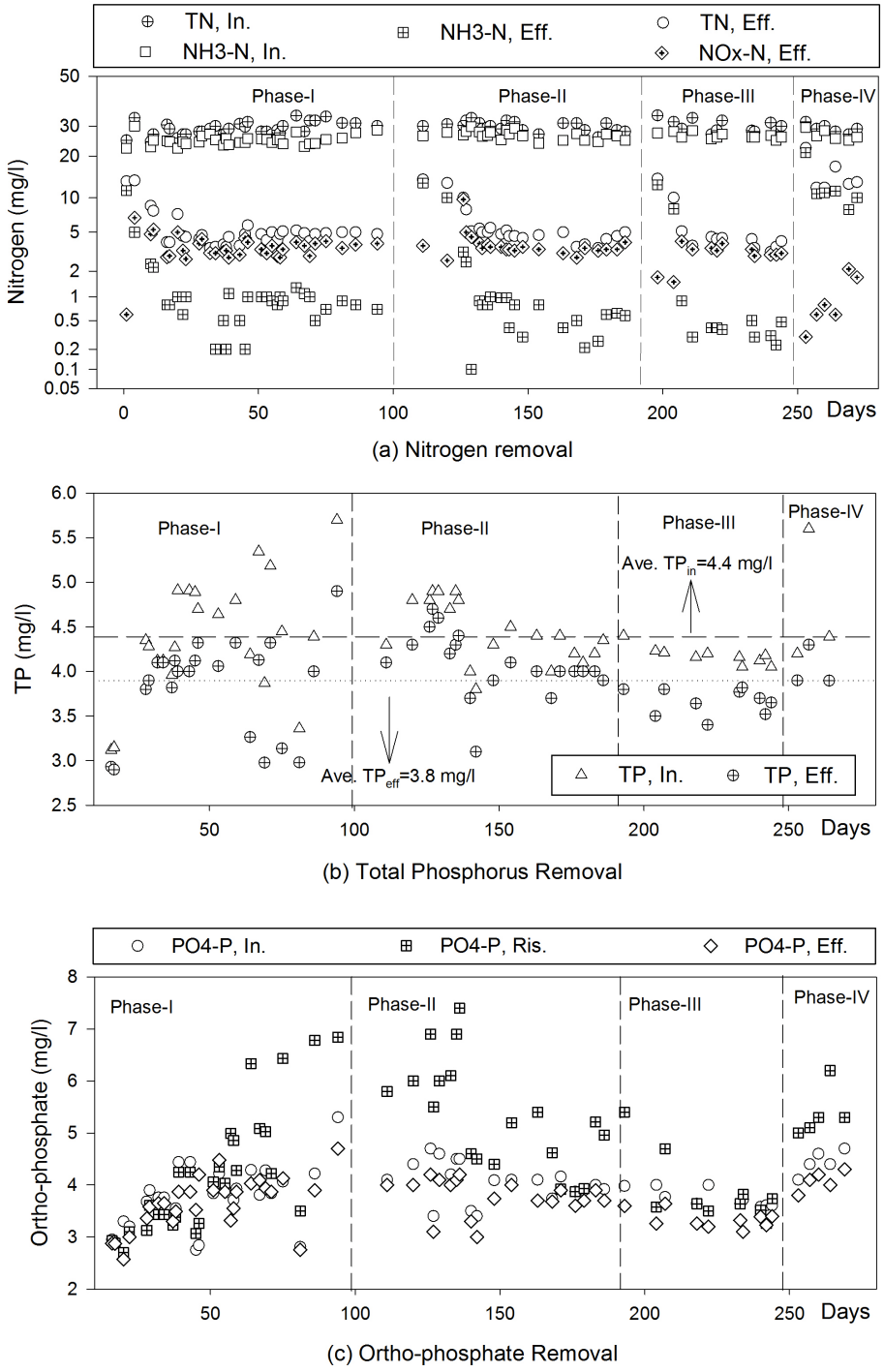

Figure 6.3. (a) Nitrogen removal (b) Total phosphorus removal (c) Ortho-phosphates in the anoxic, aerobic and final effluent

Intrinsic denitrification parameters used to calculate the 310 and 330 μm were, k_0=3.32E-5 1/s, D_e=0.0815 m^2/s and ρ_d=62.1 kg/m^3. [18] $D_{sulfate}$=0.106 m^2/s, D_e=0.8$D_{sulfate}$. Due to the lack of nitrates, there cannot be any denitrification activity beyond 310 μm in the biofilm with sulfate reduction proceeding deeper in the biofilm. Thus **Reaction (6.3)** where eight electrons were transferred from the energy source acetic acid to SO_4^{2-} to produce sulfide occurred. Widdel and Hansen [20] showed that the same reaction also produces 1 mg/L alkalinity as $CaCO_3$ per 1 mg/L sulfate reduced and increases pH. An overall SO_4^{2-} consumption of 36±3 mg/L was observed throughout the runs, which accounts for the excess alkalinity production (**Table 6.3**). A higher pH in the anoxic column of the TFBBR relative to that in the CFBBR was also measured.

$$SO_4^{2-} + CH_3COOH + 2H^+ \rightarrow HS^- + 2\ HCO_3^- + 3\ H^+ \qquad (6.3)$$

An average oxidation-reduction potential (ORP) of -282±28 mV was also observed in the anoxic column. Nagpal et al. (2000) also reported an ORP of -296 mV in a liquid solid sulfate reducing fluidized bed operating at an HRT of 5 h, static bed height of 16.8 cm and attached biomass concentration of 79 mg VSS/g media. [21] Offline batch denitrification experiments using the reactor biomass revealed that 7.2±1.3 g COD is required to denitrify 1.0 g NO_3-N.

Figure 6.3a shows effluent and influent NH_3-N, effluent NO_3-N and effluent and influent (TN) for the different phases. **Table 6.2** shows a negligible value of ≤0.2 mg NO_2-N/L in the influent, anoxic and final effluents. An average TN removal efficiency of 83±1.5% at nitrogen loading rates of 0.14, 0.18 and 0.25 kg N/m^3·d was observed in phases I, II and III respectively. Before the EBCT was decreased to 0.38 and 0.44 h in the anoxic and aerobic columns respectively in Phase IV, the effluent TN was around 5 mg/L less than the tertiary standard limit of 10 mg/L (US EPA, 2004). Nitrification occurred in the aerobic column, with an ambient DO of 5 mg/L, where the average influent 26.1 mg/L

NH_4-N was nitrified to 0.5 mg/L in the effluent in phases I to III. The average SBOD concentration in the aerobic column was <10 mg/L, which facilitated nitrification.

Table 6.2. Influent, riser and effluent water characteristics in different phases

Parameter		**Phase I**		**Phase II**		**Phase III**		**Phase IV**	
	Inf. [a]	**Riser**	**Eff. [a]**	**Riser**	**Eff. [a]**	**Riser**	**Eff. [a]**	**Riser**	**Eff. [a]**
pH	**6.9-7.1**	**7.2-7.7**	**7.4-7.6**	**7.7-8.1**	**7.4-7.8**	**7.6-8.1**	**7.4-7.8**	**7.9-8.3**	**7.9-8.0**
Alkalinity[b]	**235±12**	**221±15**	**188±10**	**220±13**	**178±12**	**229±11**	**190±12**	**239±13**	**220±14**
TCOD (mg/L)	**262±13**	**37±16**	**20±12**	**37±19**	**21±10**	**34±12**	**20±11**	**63±22**	**39±35**
SCOD (mg/L)	**234±13**	**25.7±14**	**9.6±8**	**23±3.8**	**10.6±13**	**23.4±5**	**9.5±10**	**28±3.4**	**11±3.3**
NH_4-N (mg/L)	**26.1±1.7**	**4±1.2**	**0.7±0.4**	**4.5±1.5**	**0.7±0.5**	**3.8±0.8**	**0.5±0.2**	**14.8±4.6**	**12±5.2**
NO_3-N (mg/L)	**0.7±0.4**	**0.7±0.5**	**3.7±1.0**	**0.9±0.4**	**3.9±1.4**	**0.4±0.4**	**3.9±0.7**	**0.5±0.3**	**0.8±0.7**
NO_2-N (mg/L)	**0.05±0.1**	**0.01±0.1**	**0.08±1**	**0.02±0**	**0.23±0**	**0.016**	**0.013**	**0.02**	**1.1±0.5**
TN (mg/L)	**29.5±2.1**	**7.1±2.2**	**5.3±2.2**	**5.9±1.7**	**5.7±2.6**	**5.5±1.2**	**5.4±3.2**	**19.2±5**	**15.3±4.5**
STN (mg/L)	**27.8±2**	**5.9±1.5**	**4.2±0.5**	**5.1±1.4**	**4.6±0.5**	**4.4±1.1**	**4.2±0.6**	**16.8±4.7**	**13.7±4.6**
PO_4-P (mg/L)	**3.9±0.4**	**3.8±0.7**	**3.6±0.5**	**5.3±1.0**	**3.78±0**	**3.8±0.6**	**3.3±0.1**	**5.3±0.4**	**3.8±0.2**
TP (mg/L)	**4.4±0.5**	**--------**	**3.9±0.5**	**--------**	**3.9±0.3**	**--------**	**3.8±0.1**	**--------**	**3.9±0.2**
TSS (mg/L)	**27±14**	**25±2**	**19±3.5**	**22.5±4**	**22±6**	**18.5±3**	**16.3±5**	**31±26**	**28±29**
VSS (mg/L)	**19±15**	**11.1±12**	**8.8±3.6**	**11±4**	**8.2±1.8**	**11±5**	**12±2.9**	**18.5±11**	**10±9**
Biomass wastage (mg/L)		**--------**	**4.4±3.3**	**--------**	**6.1±1.7**	**---------**	**8±1.9**	**---------**	**9.2±1.1**
SBOD (mg/L)	**193±11**	**205±12**	**7.1±5**	**18.3±3**	**7.5±9**	**17±4**	**7.4±8.5**	**25.5±3**	**8.4±3.5**
C:N:P	**12:1:0.19**								

[a] Average±SD number of steady-state data for four phases [b] mg/L as $CaCO_3$

After decreasing the EBCT to 0.44 h in Phase IV (**Table 6.1**), the effluent NH_4-N soared to 12 mg/L, which indicated that, the TFBBR is limited by nitrification as a result of the short aerobic EBCT. The nitrification capacities of the TFBBR, based on the aerobic column volume, and ammonia removal were 0.27, 0.36 and 0.45 kg NH_4-N/m^3·d

in Phases I, II and III and also an average biomass specific nitrification rate of 0.27 g NH_4-N/g VSS·d which was adequately confirmed by the offline batch test results varying from 0.25-0.35 g NH_4-N/g VSS·d. The TFBBR nitrification capacity was in line with the reported values of 0.33-0.61, 0.44-0.45 kg NH_4-N/m^3·d by Chowdhury [3] and Sen [2] respectively for fluidized bed bioreactors. As demonstrated in detail in Appendix E, the nitrification loading rate based on aerobic biofilm surface area in TFBBR was 0.91 g N/m^2·d. Nitrate produced in the aerobic column was recycled to the anoxic column for denitrification with a recirculation to feed ratio of 3.9-6.4 (**Table 6.1**). The effluent concentration of NO_3-N remained constant at 3.4±0.5 mg/L in Phases I-III. The nitrogen-loading rate, based on the anoxic column volume, was 0.24-0.41 kg N/m^3·d consistent with the loadings of 0.25-0.64 kg N/m^3·d reported in the literature. [2, 14, 22, 23]. The denitrification loading rate based on anoxic biofilm surface area in TFBBR was 0.65 g N/m^2·d, as shown in Appendix E. High effluent ammonia concentrations in Phase IV ranging from 6 to 18 mg/L and averaging 12 mg/L confirm that the maximum nitrification capacity of this process at 20 °C is 0.25 kg N/m^3·d and 0.5 kg N/m^3·d based on the total and aerobic reactor volume respectively at an aerobic EBCT of 0.53 h. Biomass SDNR of 0.032-0.045 g NO_3-N/g VSS·d were observed at F/M ratio of 0.31-0.54 g COD/g VSS·d while batch experiments demonstrated a range of 0.1-0.13 g NO_3-N/g VSS·d for SDNR at S_0/X ratio of 0.32-0.41 g COD/g VSS . Due to the large amount of biomass in the anoxic column of the TFBBR, a lower biomass SDNR was observed compared to the CFBBR of 0.15±0.02 g NO_3-N/g VSS·d. [3]

Approximately 11.5±1.5 % phosphorus removal was observed in this study without particle recirculation at EBCTs of 0.75, 1.2, 1.0 and 0.8 h and at average phosphorus loadings of 0.024, 0.03, 0.033 and 0.04 kg P/m^3·d. **Figure 6.3b** and **6.3c** show the trend of phosphorus removal, the influent, and effluent concentration of phosphorus and also the release of ortho-phosphate in the anoxic column of the TFBBR as a result of the activities of phosphorus accumulating microorganisms (PAOs). Phosphorus content of the TFBBR biomass was 3.4 % by weight of VSS slightly above the conventional 1- 2 %. In general, lower phosphorus removal efficiencies were observed in the TFBBR than the 30-70 % reported for CFBBR [3, 12], which might be due to lower biomass transfer from

the anoxic column to the aerobic one in the TFBBR system and longer SRT relative to the CFBBR.

6.3.2 Solids Production and Biomass Yield

The observed sludge yield was calculated as the sum of the effluent biomass, the net change in attached biomass, and biomass wasted divided by the total SCOD consumed. The sludge wastage rates were 0.86, 1.21, 1.8 and 3.02 g/L and the effluent biomass concentrations were 8.8±3.6, 8.2±1.8, 12±2.9 and 10±9 mg VSS/L in Phases I, II, III and IV respectively (**Table 6.2**) corresponding to influent flow of 150, 190, 240 and 290 L/d. However, **Figure 6.2a** shows that the amount of effluent biomass at the beginning of each phase was high, 20-25 mg/L. **Figure 6.2c** demonstrates the linear regression between cumulative biomass and cumulative SCOD removal. Very low observed yields of 0.06, 0.066, 0.071 and 0.081 g VSS/g COD in Phases I to IV was achieved. Although the biomass yield increased with the increase in OLR from 1.3 kg COD/m^3·d in Phase I to 2.5 kg COD/m^3·d in Phase IV, There was not a significant change in the attached biomass in both anoxic and aerobic columns. Using equations (4) and (5), overall SRTs of 74-108 d and anoxic SRT of 62-89 d were calculated throughout the experiments (**Table 6.1**). The long SRT and also up to 64% influent COD consumption in the anoxic column (**Table 6.3**) rationalize the reduced yield in the TFBBR. Accordingly the TFBBR biomass yield is 50% of the 0.12-0.17 g VSS/g COD reported for the CFBBR. [3, 11-12]. Feng [24] also reported an observed yield of 0.06 g VSS/g COD for a fluidized bed BNR process at an OLR of 3 kg COD/m^3·d.

$$SRT_{Total} = \frac{M_{aer} X_{aer} + M_{ano} X_{ano}}{Q_{eff} VSS_{eff} + X_{wast}} \quad (6.4)$$

$$SRT_{ano} = SRT_{Total} \frac{M_{ano} X_{ano}}{M_{aer} X_{aer} + M_{ano} X_{ano}} \quad (6.5)$$

6.3.3 Mass Balances

Table 6.3 presents the detailed mass balances for COD, TN, NH_4-N, NO_3-N, TP, and alkalinity in the anoxic and aerobic column of the TFBBR. The mass balance was based

on pseudo-steady-state experimental data of the influent, anoxic and effluent characteristics and also the sludge wastage. In this study, the obtained average, N and P content of biomass, from linear correlations of particulate N and particulate P versus VSS were 10.4% and 3.4% (not shown, with R^2=0.98 and R^2=0.97) respectively. The amount of TP in the activated sludge seed was also measured in 11 samples and correlated statistically at 1.9% by weight of VSS (R^2=0.98). **Table 6.3** shows mass balances closures of approximately 95.2-98.6% for COD, 85-99% for N, 85.8-95.1% for P and 84.8-93.6% for alkalinity.

Table 6.3 demonstrates that 49.1, 64.6, 64.5 and 55.5% of the overall COD removed in Phases I, II, III and IV took place in the anoxic column by predominantly the three processes of denitrification, sulfate bacteria COD uptake and aerobic utilization due to recirculation of DO from the aerobic column. Based on equation (6) the calculated COD uptake for denitrification were 8.9, 9.7, 11.8 and 3.4 g/d in Phases I, II, III and IV respectively (**Table 6.3**) based on the aforementioned observed yields of 0.059-0.081g VSS/g SCOD (**Figure 6.2c**).

$$\frac{\text{g SCOD}}{\text{g NO}_3 - \text{N}} = \frac{2.86}{1 - 1.42\,Y_{obs}} \frac{\text{gSCOD}}{\text{gNO}_3\text{-N}} = \frac{2.86}{1\text{-}1.42Y_{obs}} \qquad (6.6)$$

An oxygen mass balance based on flow recirculation ratios in the riser and oxygen concentration in the flows (**Table 6.1**) indicates that DO concentration at the bottom of the riser of 3.0-3.3 mg O_2/L. However oxygen concentration was depleted to 0.1 mg/L at the top of the riser. It is estimated that this oxygen concentration and high concentration of COD at the bottom part of the riser, as calculated in **Table 6.3**, affected aerobic COD removal in the anoxic column of 4.3, 12.7, 17.6 g/d in Phases I, II and III as representing 37%, 46% and 38% of the overall anoxic COD consumption.

Table 6.3. Nutrient mass balance

	Mass in influent (g d^{-1})	Mass consumed (g d^{-1})	Mass Utilized (g d^{-1})	Mass in effluent (g d^{-1})	Mass wastage (g d^{-1})	Percent closure (%)
		Anoxic	Aerobic			
Phase I						
TCOD (sCOD)	38.3±1.6 (35.1±1.4)	18.5±4.5 (8.9)[d] (3.5)[e] (7.3)[f]	15.5±5.5	1.9±0.7	0.86[a]±0.01	95.2[1]
TN	4.38±0.2			0.67	0.061[b]±0.0	96.8[2]
NH4-N	3.72±0.2	0.09±0.05 (0.05)[g]	3.45±2.3	0.1±0.01		
NO3-N	0.09±0.03	2.87±0.5	-3.3±0.5	0.55±0.04		
TP	0.67±0.08			0.58±0.07	0.012[c]±0.0	88.4[3]
PO4-P	0.55±0.08	-0.58±1.0	0.59±1.0	0.54±0.06		
Alkalinity	35.2±3.2	-15.8 [h]	24.6 [i]	28.2±3.0		93.6[4]
Phase II						
TCOD (sCOD)	46.7±2.5 (43.3±2.7)	26.9±4.7 (9.7)[d] (4.5)[e] (12.2)[f]	14.71±3.4	2.21±0.3	1.21±0.05	96.6
TN	5.3±0.3			0.84	0.1±0.01	91.2
NH4-N	4.78±0.2	0.08±0.1 (0.065)	4.59±1.1	0.103±0.01		
NO3-N	0.17±0.02	3.09±0.9	-3.76±1.1	0.74±0.04		
TP	0.79±0.05			0.73±0.04	0.02±0.0	95.1
PO4-P	0.74±0.07	-1.72±0.8	1.77±0.9	0.69±0.07		
Alkalinity	44.6±2.9	-18.06	32.7	35.3±2.5		84.8
Phase III						
TCOD (sCOD)	62.2±3.1 (56.4±2.8)	35.1±7.2 (11.8)[d] (5.61)[e] (11.0)[f]	19.3±4.5	3.4±0.6	1.8±0.08	96.1
TN	7.0±0.4			1.1±0.12	0.21±0.05	85.0
NH4-N	6.35±0.3	1.1±0.5 (0.085)	4.7±0.4	0.1±0.04		
NO3-N	0.21±0.07	3.72±0.5	-4.29±0.5	0.81±0.09		
TP	1.04±0.06			0.88±0.02	0.039±0.0	92.1
PO4-P	0.89±0.06	-0.33	0.43	0.79±0.03		
Alkalinity	56.4±3.4	-22.16	32.8	50.5±1.4		90.6
Phase IV						
TCOD (sCOD)	73.9±3.8 (68.9±3.5)	35.3±8.2 (3.4)[d] (6.8)[e] (11.5)[f]	29.8±8.5	5.8±1.1	3.02±0.04	99.5
TN	8.27±0.6			3.65±1.4	0.14±0.003	99.0
NH4-N	7.6±0.5	0.1±1.0 (0.03)	3.9±1.4	3.08±0.4		
NO3-N	0.14v0.08	1.06±0.9	-1.26±1.1	0.33±0.24		
TP	1.39±0.27			1.16±0.07	0.028±0.0	85.8
PO4-P	1.3±0.05	-1.77±0.7	1.87±0.7	1.19±0.04		
Alkalinity	68.1±7.2	-14.51	27.8	62.6±4.3		87.5

a,b,c COD equivalent, Nitrogen (N) and phosphorus (P) content of 1 g biomass were measured 1.5, 0.1 and 0.031 gr respectively.

[d] SCOD consumption through denitrification based on equation (6); for example Phase I $= 2.87 \times \frac{2.86}{1 - 1.42 \times 0.06}$

[e] SCOD consumed by SRB based on stoichiometry of equation (3); for example Phase I

$$= \left(35 \times \frac{\text{mg}}{\text{l}} \text{SO}_4^{2-} \times \frac{59 \text{ g/mol } CH_3COO^-}{96 \text{ g/mol } SO_4^{2-}} \times \frac{1.1 \text{ g COD}}{1 \text{g } CH_3COO^-} \right) \times 150 \frac{\text{l}}{\text{d}}$$

[f] Aerobic SCOD consumption in the riser; for example Phase I

$$= \frac{\Delta O_2}{\Delta t} \times (1 - Y_H)^{-1} = 0.0031 \frac{\text{g } O_2}{\text{l}} \times (7.4 + 1 + 6.4) \times 150 \frac{\text{l}}{\text{d}} \times (1 - 0.66 \times 1.42)^{-1}$$

[g] Nitrogen assimilated for denitrification; for example Phase I

$$= 2.87 \times \frac{2.86}{1 - 1.42 \times 0.06} \times 0.06 \frac{\text{gVSS}}{\text{g SCOD}} \times 0.1 \frac{\text{g N}}{\text{g VSS}}$$

[h] Alkalinity generated in the anoxic column; for example Phase I

$$= 2.87 \text{ g } N_{\text{denitrified}} \times 3.57 \frac{\text{g Alk}_{\text{generated}}}{\text{g N}} + 150 \frac{\text{l}}{\text{d}} \times 0.037 \frac{\text{g}}{\text{l}} \text{alk. as } CaCO_3 \text{ by SRB}$$

[i] Alkalinity consumed in the aerobic column; for example Phase I

$$= 3.45 \text{ g } N_{\text{nitrified}} \times 7.14 \frac{\text{g Alk}_{\text{consumed}}}{\text{g N}}$$

[1] COD % closure $= \frac{18.5 + 15.5 + 1.9 + 0.86}{38.3} \times 100$

[2] Nitrogen % closure $= \frac{0.67 + 0.061 + 0.1 + 0.55 + 2.87}{4.38} \times 100$

[3] Phosphorus % closure $= \frac{0.58 + 0.012}{0.67} \times 100$

[4] Alkalinity % closure $= \frac{35.2 - (24.6 - 15.8)}{28.2} \times 100$

With influent concentrations of 58.3 to 67.5 mg SO_4/L and effluent concentrations of 23.7 to 30.5 mg SO_4/L, a sulfate reduction of 35-37 mg/L was measured throughout phases I to III, which based on **Equation (6.3)**, is estimated to consume 3.5, 4.5, 5.6 and 6.8 g COD/d and generate 5.55, 7.03, 8.88 and 10.73 g alkalinity as $CaCO_3$/d in Phases I to IV respectively. In Phases I-IV, 17.3, 14.7, 19.3 and 29.8 g COD/d were utilized in the aerobic column through oxidation, respectively, from which 1.45, 1.4, 1.55 and 2.13 g COD/d were assimilated into biomass. It must be asserted that for Phases I-III, the estimated anoxic COD removal agreed well with the experimental data (**Table 6.3**). However, due to large fluctuation in effluent ammonia concentrations in Phase IV, as evidenced by the standard deviation of 5.2 mg/L, corresponding to 25% of influent nitrogen, the measured anoxic COD differed substantially from the estimate.

Table 6.3 shows that 2.87-3.72 g NO_3-N/d were removed in the anoxic column, which generate 10.2-13.2 g alkalinity as $CaCO_3$/d. Chowdhury et al., (2008) mentioned that the main reactions in the aerobic column were nitrification, oxidation of accumulated poly-hydroxyalkanoates and organic matter. In the aerobic column, 3.45-4.7 g NH_4-N/d were nitrified and utilized 24.6-33.5 g alkalinity as $CaCO_3$/d while 3.1-4.4 g NO_3-N/d was produced. **Table 6.3** illustrates an alkalinity mass balance closure of 93.6, 84.8, 90.6 and 87.5% in the Phases I to IV with respect to the alkalinity consumption through nitrification and production through denitrification and sulfate reduction processes. In the aerobic column, 0.59-1.57 g PO_4-P/d was consumed, of which approximately 0.02-0.024 g P/d was utilized for cell synthesis considering a yield of 0.06-0.07 g VSS/g COD and 2% phosphorus content by weight of VSS in the sludge). PAOs stored the remaining amount of P in the aerobic column and then were recirculated to both columns. Experimental data indicated phosphorus content of 3.4% by weight of VSS in the sludge, which confirmed the contribution of PAOs in the system, despite the long SRT, which is not conducive to P removal.

6.4 Conclusions

A lab-scale TFBBR was operated at loading rates of 1.3-2.5 kg COD/m^3·d, 0.14-0.28 kg N/m^3·d and 0.024-0.041 kg P/m^3·d to study the performance of the system with respect to biological nutrient removal. The system removed >96% organic matter, 84% nitrogen and 12% phosphorus at EBCT of 0.7, 1.2 and 0.9 h. An average removal of 10% of COD was through an anaerobic sulfate reduction process, which produced 35-37 mg/L as $CaCO_3$ alkalinity. The TFBBR achieved tertiary effluent quality with BOD<6 mg/L, TN < 6 mg/L, NO_3-N < 5 mg/L, NH_4-N < 1 mg/L and TSS < 20 mg/L at an overall HRT of less than 2.9 h. The system achieved long SRT of 72-108 d, which rationalized the very low observed yield of 0.06-0.07 g VSS/g COD. A phosphorus mass balance showed the significant contribution of PAOs even though only 12% of the influent P was removed biologically.

6.5 References

[1] Borregaard VR. Experience with nutrient removal in a fixed-film system at full-scale wastewater treatment plants. Wat. Sci. Technol. 2000; 36-1:129–137.

[2] Sen P, Dentel SK. Simultaneous nitrification-denitrification in a fluidized bed reactor. Wat. Sci. Technol. 1998; 38:247-254.

[3] Chowdhury N, Nakhla G, Zhu J. Load maximization of a liquid-solid circulating fluidized bed bioreactor for nitrogen removal from synthetic municipal wastewater. Chemosphere 2008; 71:807-815.

[4] Rovatti M, Nicolella C, Converti A, Ghigliazza R, Di Felice R. Phosphorus removal in fluidized bed biological reactor (FBBR). Wat. Res. 1995; 29:2627-2634.

[5] Morgenorth E, Wildere PA. Controlled biomass removal-the key parameters to achieve enhanced biological phosphorus removal in biofilm systems. Wat. Sci. Technol. 1999; 39:33-40.

[6] Li J, Xing X, Wang B. Characteristics of phosphorus removal from wastewater by biofilm sequencing batch reactor (SBR). Biochem. Eng. J. 2003; 16:279-285.

[7] Eikelboom D, Kampf R, Van Voorneburg F. Biofilm formation in an airlift reactor for the sewage purification. H_2O_2 1987; 20:388-392.

[8] Nicolella C, van-Loosdrecht MCM, Heijnen JJ. Wastewater treatment with particulate biofilm reactors. J. Biotechnol. 2000; 80:1-33.

[9] Frijters CTMJ, Eikelboom DH, Mulder A, Mulder R. Treatment of municipal wastewater in a CIRCOX airlift reactor with integrated denitrification. Wat. Sci. Technol. 1997; 36-1:173–181.

[10] Nakhla G, Zhu J, Cui Y. Liquid-solid circulating fluidized bed wastewater treatment system for simultaneous removal of carbon, nitrogen, and phosphorus. US patent no. 6,716,244, Int'l PCT patent awarded Aug. 2005.

[11] Cui Y, Nakhla G, Zhu J, Patel A. Simultaneous carbon and nitrogen removal in anoxic-aerobic circulating fluidized bed biological reactor (CFBBR). Environ. Technol. 2004; 25:699-712.

[12] Patel A, Zhu J, Nakhla G. Simultaneous carbon, nitrogen and phosphorus removal from municipal wastewater in a circulating fluidized bed bioreactor. Chemosphere 2006; 65:1103-1112.

[13] Cooper PF, Williams SC. High-rate nitrification in a biological fluidized bed. Wat. Sci. Technol. 1990; 22:431–442.

[14] Hermanowicz SW, Cheng YW. Biological fluidized-bed reactor: hydrodynamics, biomass distribution and performance. Wat. Sci. Technol. 1990; 22:193–202.

[15] Nicolella C, Di Felice R, Rovatti M. Biomass concentration in fluidized bed biological reactors. Wat. Res. 1996; 31:936-940.

[16] APHA; AWWA; WEF. Standard methods for the examination of water and wastewater. 20th Edition, American Public Health Association, Washington D.C. 1998.

[17] Kwok WK, Picioreanu C, Ong SL, van Loosdrecht MCM, Ng WJ, Heijnen JJ. Influence of biomass production and detachment forces on biofilm structures in a biofilm airlift suspension reactor. Biotechnol. Bioeng. 1997; 58:400-407.

[18] U. S. EPA. Guidelines for water reuse. EPA-625/R-04-92-004, U.S. Environment Protection Agency and U.S. Agency for International Development, Washington, DC. 2004.

[19] Shieh WK, Keenan JD. Fluidized bed biofilm reactor for wastewater treatment. Adv. Biochem. Eng. Biotech. 1986; 33:132-167.

[20] Widdel F, Hansen TA. In: Balows, A., Trüper, H. G., Dworkin, M., Harder, W., Schleifer, K.-H., (eds.), The prokaryotes, 2nd. Edn., Springer-Verlag, New York, 1992 pp. 583-624.

[21] Nagpal S, Chuichulcherm S, Peeva L, Livingston A. Microbial sulfate reduction in a liquid-solid fluidized bed reactor. Biotechnol. Bioeng. 2000; 70-4:370-380.

[22] Fdez-Polanco F, Real FJ, Garcia PA. Behavior of an anaerobic/aerobic pilot scale fluidized bed for the simultaneous removal of carbon and nitrogen. Wat. Sci. Technol. 1994; 29:339–346.

[23] Sadic T, Semon J, Palumbo D, Keenan P, Diagger G. Fluidized-bed denitrification. Meeting potential nitrogen limits in Long Island Sound. Wat. Environ. Technol. 1996; 8:81–85.

[24] Feng Q, Yu A, Chu L, Xing XH. Performance study of excess sludge and simultaneous removal of organic and nitrogen by a combination of fluidized – and fixed-bed bioreactors with different structured macroporous carriers. Biochem. Eng. J. 2008; 39:344-352.

7 Dynamic Testing of TCFBBR for Nutrient Removal from Municipal Wastewater

7.1 Introduction

The need for nutrient removal from wastewater discharges to water sources has become evident in many countries through a generally perceived deterioration of surface water quality. Moreover, stringent provincial and federal regulations for tertiary water quality discharge require nutrient removal from waste streams. Extensive research on the mechanisms of biological nutrient removal (BNR) in suspended growth systems during the last two decades has greatly expanded the integration of BNR into advanced wastewater treatment. [1] However, there have been few comprehensive studies to integrate BNR processes with particulate biofilm processes such as fluidized bed bioreactors [2, 3, 4] with and without intermittent feeding and aeration. [5, 6, 7]

In general, the main reactor types applicable for the suspension of particulate biofilms in wastewater treatment processes are categorized into Anaerobic Up-flow Sludge Blanket (UASB), Fluidized Bed Reactors (FBR), Expanded Granular Sludge Blanket (EGSB), Biofilm Airlift Suspension (BAS), and Internal Circulation (IC) reactors. [8] Fluidized bed bioreactors have been investigated for all of the basic secondary and tertiary processes and shown many advantages over other technologies such as conventional suspended growth [9] including: a large specific surface for attached biological growth of 800-1200 m^2/m^3, high biomass concentrations of 8,000-12,000 mg/L for nitrification and 30,000-40,000 mg/L for denitrification [8, 10, 11], long sludge residence times (SRT) and low observed yields which reduce sludge management costs and may result in elimination of secondary clarification requirements. [12]

The BNR capability of another form of particulate biofilm reactors (airlifts) has also been studied at the bench scale level for the treatment of municipal wastewater where high BOD and ammonia removal efficiencies were reported. [13] Research on Biofilm Airlift Suspension (BAS) reactors in the late eighties [14, 15] led to the concept of

CIRCOX® airlift reactor. [8] A CIRCOX® in combination with a denitrifying CIRCOX® reactor achieved effluent nitrogen (< 6 mg N/L) in a pilot-plant scale treating municipal wastewater at Zaandam, The Netherlands. [16]

The Circulating Fluidized Bed Bioreactor (CFBBR), introduced and developed by Nakhla and his colleagues [4, 17, 18, 19, and 20], was tested for BNR from municipal wastewaters in both lab and pilot scales. The CFBBR consists of an anoxic riser and an aerobic downer with fast and conventional fluidization regimes respectively. More than 90% organic, 70%-80% total nitrogen and 50%-70% phosphorous removal were reported at EBCTs of 0.5-1.5 h, HRTs of 2-3 h, with an observed biomass yield of 0.12-0.16 g VSS/g COD. [4, 18, 19] Circulation of the media with the biofilm between anaerobic/anoxic and aerobic columns was reported conducive to enhanced biological phosphorus removal (EBPR) in CFBBRs.

While the CFBBR has successfully incorporated fluidized bed systems with BNR, the required height of 5.5 m makes it difficult for retrofitting existing plants. Thus, a new twin fluidized bed system with rectangular cross sectional area columns, and a height of 3.6 m to facilitate retrofits of existing plants, as well as an anoxic volume of 60% of the aerobic volume was designed, fabricated and tested with synthetic municipal wastewater for 65 days and real municipal wastewater (MWW) for 45 days. Due to the particle transfer through two sloped pipes between the columns, the system was called twin circulating fluidized bed bioreactor (TCFBBR). In contrast to the CFBBR, which employs fast fluidization in the anoxic riser to affect particle recirculation, the fluidization regime in the TCFBBR is conventional in both the riser and downer columns. The responses of the system to the dynamic loading conditions and carbon shock tests were also examined to simulate wet weather condition and the effect of organic shock loads on nitrogen removal.

7.2 Materials and Methods

The synthetic municipal wastewater (SMW) was prepared from tap water combined with concentrated stock solution of CH_3COONa (as carbon source), NH_4Cl (as nitrogen source), and KH_2PO_4 (as phosphorus source) as well as a mineral stock solution at

volumetric ratios of 1:0.0025, 1:0.001, 1:0.001 and 1:0.002 respectively. The concentrated stock solutions contained 125 g CH_3COONa/L, 100 g NH_4Cl/L, 20 g KH_2PO_4/L and the mineral salt stock solution contained 75 mg $NiCl \cdot 6H_2O$/L, 75 mg $CoCl_2 \cdot 6H_2O$/L, 200 mg $CuCl \cdot 2H_2O$/L, 125 mg $ZnCl_2$/L, 1250 mg $MnCl_2 \cdot 4H_2O$/L, 750 mg $FeCl_3 \cdot 6H_2O$/L, 200 mg $(NH_4)_6Mo_7O_{24} \cdot 4H_2O$/L, 125 mg H_3BO_3/L, 40 g $MgSO_4 \cdot H_2O$/L and 6 g $CaCl_2 \cdot H_2O$/L.

7.2.1 System Description

The TCFBBR (**Figure 7.1)** is comprised of two plexi-glass columns operated as anoxic and aerobic FBRs with a height of 3.6 m each. The columns were made rectangular (aerobic: 5 cm x 8.5 cm, and anoxic: 5 cm x 5 cm) to investigate the system potential for retrofitting conventional wastewater treatment tanks. Lava rock particles were used in both columns with an average diameter (d_m) of 850-1125 μm, a total porosity (ψ_T) of 62% (44% external and 18% internal), a dry bulk particle density (ρ_d) of 1012 kg/m, a true particle density (ρ_m) of 2628 kg/m^3 and a specific surface area determined by BET (Micromeritics ASAP 2010, Micromeritics Co., USA) of 0.48 m^2/g. The design EBCTs were 0.22 hr in the anoxic column and 0.71 h in the aerobic column in phases I and II (**Table 7.1**), corresponding to particle masses of 2.5 kg in the riser and 8 kg in the downer which were initially estimated based on the specific nitrification rates (SNRs), specific denitrification rates (SDNRs) and the attached biomass per g media, reported in the literature for the CFBBR, SNR of 0.09-0.14 g NH_4-N/g VSS·d and SDNR of 0.033-0.243 g NO_x-N/g VSS·d, respectively. [4] In the riser, heterotrophic bacteria grow on the media and the biofilm becomes thicker. At a certain biofilm thickness, depending on the superficial liquid velocity, the biofilm-coated particles reach the height where they can be transferred to the downer through the inclined pipe. However, an intermediate graduated container was placed between the two columns, as shown in **Figure 7.1,** to monitor the particle transfer rate. After exposure to the high shear force in the gas-liquid-solid phase in the downer, the biofilm detaches and leaves the system along with the effluent. Particles from the bottom dense phase of the downer with a thin biofilm (< 40 μm) are transferred back to the riser manually to make up the particles in the riser. Particle transfer cycles were observed to occur every 17 days.

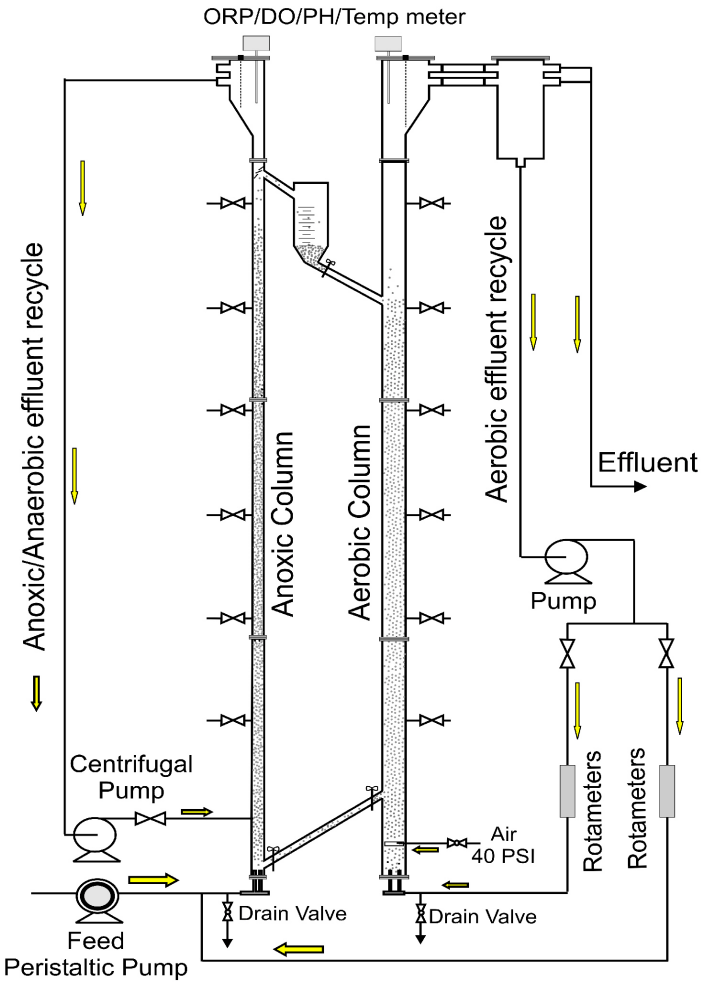

Figure 7.1. Schematic of Twin Circulating Fluidized Bed Bioreactor

Table 7.1 displays the detailed design parameters and operational conditions of the TCFBBR. The feed solution was pumped into the bottom of the anoxic column with a peristaltic pump (Masterflex I/P, Masterflex AG, Germany). To ensure fluidization, riser to riser recirculation flows to feed ratios of 9.4:1-10.7:1 and downer to downer recirculation flows to feed ratios of 16:1-21:1 were provided. Biomass was wasted at the equivalent of 1.2 g VSS/d and 2.1 g VSS/d in phases I and II respectively (**Table 7.1**, **Table 7.2**). All recirculation flows were maintained using two centrifugal pumps (IWAKI MD-40RT-115NL, IWAKI CO., Ltd. Japan) and monitored by rotameters (OMEGA FL-812 and OMEGA FL-5331G, Omega Engineering, Inc., Canada).

Superficial liquid velocities of 1.3-1.9 cm/s and 1.1-1.5 cm/s were maintained in the anoxic and the aerobic columns. Eight manometers (four along each column) were employed to observe the pressure drop along each column. Air, at 40 psi, was injected at the bottom of the aerobic column using a perforated tube. Airflow was monitored around 2.1L/min by an air flow meter, OMEGA, FL-3696 ST.

Table 7.1. Operating conditions

		Phase I	Phase II
Influent flow, Q_{in} (l/d)		262±8.2	260±5
Organic loading (kg COD/(m^3·d))		2.7±0.8	4.3±0.5
Nitrogen loading (kg N/(m^3·d))		0.3±0.1	0.51±0.06
Phosphorus loading (kg P/m^3·d))		0.032	0.06
R-R recirculation ratio ($Q_{r\text{-}r}/Q_{in}$)		10.7±3	9.4±3.1
D-R recirculation ratio ($Q_{d\text{-}r}/Q_{in}$)		4.5±2.1	6±2
D-D recirculation ratio ($Q_{d\text{-}}/Q_{in}$)		16.2±4	21±5
EBCT (h)= $V_{compact}/Q_{in}$	*Anoxic*	0.22	0.22
	Aerobic	0.71	0.71
HRT (h)	*Anoxic*	0.86	0.87
	Aerobic	1.43	1.44
Air flow (ml min^{-1})	(40 psig)	2060	2150
DO (mg/l)	*Aerobic*	5.4±0.7	4.3±0.5
	Anoxic	0.2±0.2	0.3±0.1
X (mg VSS/g lava rock)	*Anoxic*	25.1	29.5
	Aerobic	3.5	4.7
Biomass (g VSS)	*Anoxic*	113	145
	Aerobic	22.3	28.3
F/M ratio (g COD/(g VSS·d))		0.58	0.48
Detachment rates (1/d)	*Anoxic*	0.061	0.086
	Aerobic	0.18	0.2
Superficial liquid	*Anoxic*	1.3-1.9	1.3-1.9
Velocity, u_l(cm/s)	*Aerobic*	1.1-1.5	1.1-1.5
Estimated SRT (d)	*Anoxic*	32[a]	31
	Aerobic	7.6	6.8
	Overal	39.6[b]	37.4
Run time (d)		65	45

[a] based on equation (1), [b] based on equation (2)

7.2.2 Acclimatization and Start-up

A similar approach to CFBBR [4] start-up was undertaken to seed the TCFBBR with enriched nitrifiers, acclimatized in the lab using 15 L of returned activated sludge (RAS)

from the Adelaide Pollution Control Plant, London, Canada, with TSS and VSS concentrations of approximately 3500 and 2800 mg/L respectively. Meanwhile, the clean media was fluidized in both columns at u_f=1.1 cm/s. The seed was pumped into the system and recirculated between the two columns for two days to transport and trap the bacteria from the bulk liquid on the media surface and the pores. Thereafter, the continuous synthetic feed was initiated at a flow rate of 260 L/d corresponding to OLR and NLR of 2.7 kg COD/m^3·d and 0.3 kg N/m^3·d. Within a period of two weeks, most of the particles in both columns were coated with biomass with average concentrations of 5 and 28 mg VSS/g media in the aerobic and anoxic columns respectively.

7.2.3 Analytical Methods

Samples from the feed tank, top of the anoxic column, and the final effluent were collected and refrigerated at 4 °C prior to analysis. Total suspended solids (TSS), volatile suspended solids, (VSS) and 5-day biochemical oxygen demand (BOD) were analyzed in accordance with Standard Methods 2540D, 2540E and 5210 respectively. [21] HACH methods and testing kits (HACH Odyssey DR/2800) were used to analyze total and soluble chemical oxygen demand (TCOD and SCOD), total and soluble nitrogen (TN and STN), total phosphorus (TP), NH_4-N, NO_2-N, NO_3-N, and PO_4. Alkalinity was measured by titration with 0.01 N H_2SO_4 in accordance with the Standard Method no 2320. [21] DO and ORP were measured onsite using an Oakton DO 6 meter, and an Oakton ORPTestr 10 (Oakton, Singapore). The size of the bare and biofilm coated particles was measured using Visiongauge (Flexbar Machine Co, New York, USA) synchronized to a microscope (Mitutoya, Sakada, Japan) coupled with a camera (Leica DC 300, Germany), at a magnification of 50X. Based on Standard Method no 2540G (APHA, 1998), the attached biomass on the carrier media was measured and expressed as mg VSS/g clean particles. Approximately 10-20 g bio-particles were taken from each of the two columns, suspended in a 100 mL vials, and sonicated for 3 h at 30°C in an Aquasonic sonicator (SK 1200H Kupos, China) with a rated power of 45 watts. After sonication, the TSS and VSS content of the detached biomass was determined following Standard Methods no 2540D and 2540E. [21]

7.2.4 Batch Tests

Batch tests were carried out to test the maximum SNR and SDNR of the attached biomass in the system following the methods previously used for the CFBBR. Batch reactors (0.5 L working volume) equipped with magnetic stirrers were used for nitrification by injecting air and alkalinity or for denitrification by avoiding intrusion of air and injecting SCOD. To reduce the effect of substrate mass transfer limitation into the biofilm, the biofilm was removed from 10-40 g media using sonication and then placed into the reactors. The biomass in the SDNR and the SNR tests were in the range of 1500-4000 mg VSS/L and 240-500 mg VSS/L respectively, considering the amounts of biofilm in the anoxic and aerobic column of 25-50 mg VSS /g media and 4-6 mg VSS /g media, respectively. The initial acetate COD in the denitrification batch tests was set at 350-450 mg/L while the initial alkalinity used in the nitrification test was 250-350 mg/L as $CaCO_3$. For the SNR tests, the initial ammonia concentrations were 35-55 mg/L, added as ammonium chloride.

7.2.5 Dynamic Hydraulic and Carbon Shock tests

The impact of dynamic loadings on nutrient removal efficiency of the TCFBBR was tested at different influent flows. While maintaining the same organic and nitrogen loading rates of 4.1 kg COD/m^3·d and 0.39 kg N/m^3·d respectively, the hydraulic loading was gradually increased by adding clean tap water from 260 L/d to 520 L/d and eventually to 1040 L/d at three hour intervals, corresponding to hydraulic retention times (HRTs) of 2.3, 1.16, and 0.58 h respectively in the hydraulic loading test, and subsequently decreased to 520 L/d and 260 L/d at the same intervals. All of the operational conditions were maintained the same during the test.

In order to also test the sensitivity of system nitrification and carbon removal capabilities to organic shock loads, the influent COD was increased from 420 mg/L to 740 mg/L and 1200 mg/L in intervals of three hours while maintaining overall HRT of 2.3 h. Samples from the effluent top of the riser were taken every 0.5 h for measurement of water quality parameters.

7.3 Results and Discussion

7.3.1 Nutrient Removal

In order to ensure attainment of the steady state conditions in the system, the suspended and attached biomass in the aerobic and anoxic columns are measured and depicted in **Figure 7.2a** and **7.2b** respectively. As noticed from the data in the figure, the coefficient of variation (COV) for attached biomass in the aerobic and anoxic columns in phase II are 8.9% and 4.8% respectively. Although it is arguable that suspended VSS concentrations varied more widely, as reflected by COV of 26.4% and 20.7%, this process is indeed a fixed film system and 99.9% of the biomass inventory in the system is in the form of attached biomass. Moreover the nitrification and denitrification activity per gram media depicted in **Figure 7.2a** and **7.2b** respectively demonstrates that the SNR and SDNR coefficients of variation in Phase II are 5.7% and 7.3%. Therefore, the attached biomass and biomass activity reached steady state.

The system was tested at an average flow rate of 260 L/d with synthetic and real municipal wastewater for 65 and 45 days denoted henceforth as phases I and II, respectively. **Figures 7.3a, 7.3b, 7.3c, 7.4a, 7.4b**, and **7.4c** show the performance of the TCFBBR with respect to chemical oxygen demand (COD), suspended solids (SS), nitrogen (N), and phosphorus (P) removal efficiencies. **Figure 7.3c** also shows the VSS to TSS ratio of 0.847 for the detached biomass, which is slightly higher than the conventional suspended biomass. [1]

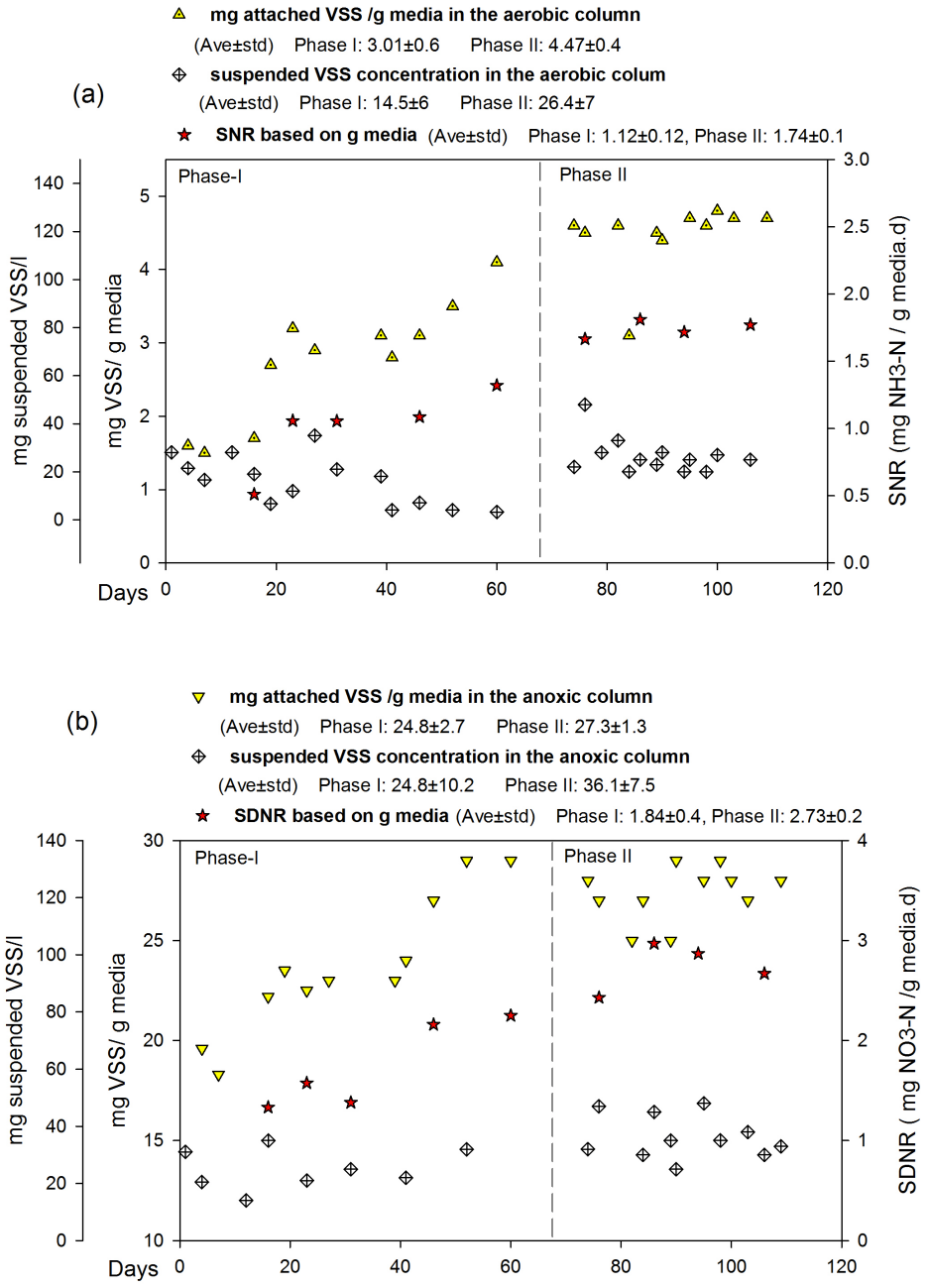

Figure 7.2. (a) Trend of attached and suspended biomass and specific nitrification rate in the aerobic column (b) Trend of attached and suspended biomass and specific denitrification rate in the anoxic column

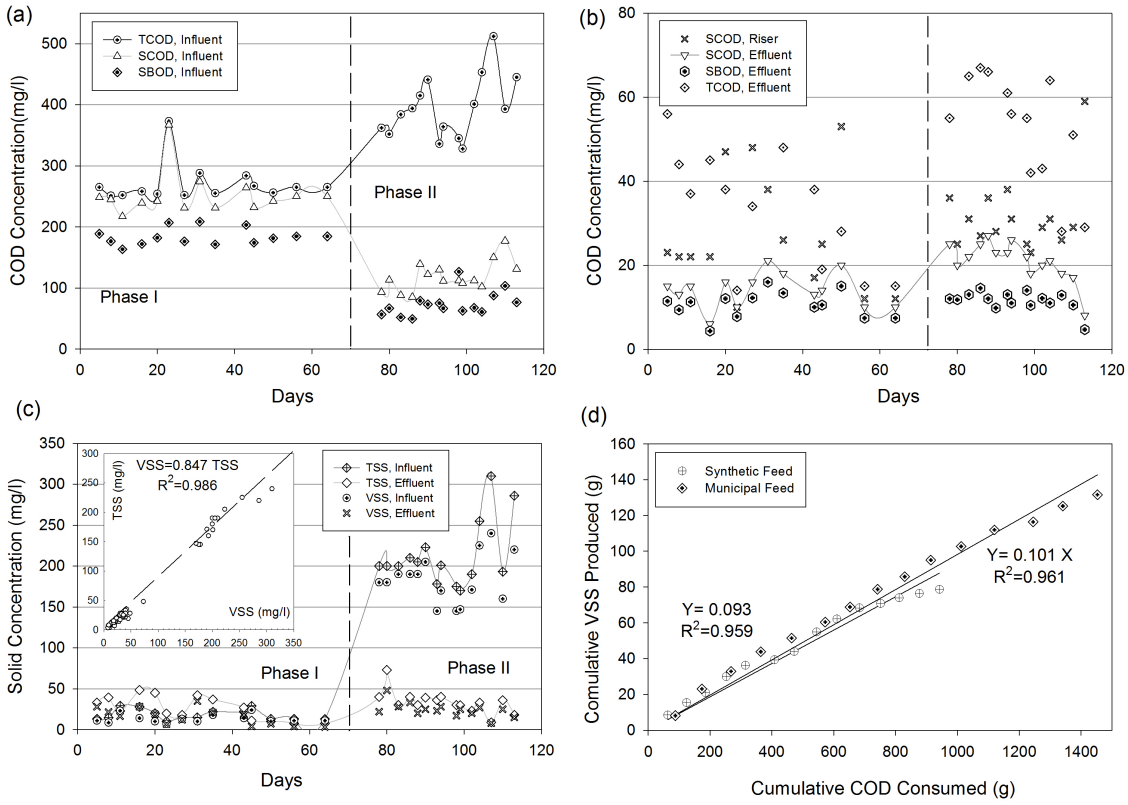

Figure 7.3. (a) TCOD, SCOD and BOD in the influent (b) COD and BOD concentrations in the riser and downer (c) Suspended solids removal in the system (d) Sludge yield during phases I and II

As illustrated in **Table 7.2**, **Figures 7.3a** and **7.3b**, TCOD removal efficiencies of 90% and 87% at a total empty bed contact time (EBCTs) of 0.93 h and organic loading rates (OLR) of 2.7±0.8 kg COD/m^3·d and 4.3±0.5 kg COD/m^3·d were observed in phases I and II respectively. Based on the soluble effluent organic matter, COD removal efficiency would be > 96% in phases I and II. The effluent SBOD during both phases was < 11 mg/L despite operation at an HRT of 2.3 hrs. Even though the influent TSS was relatively high in phase II at 214±40 mg/L, an average effluent TSS of 33 mg/L was achieved, corresponding to suspended solids removal efficiency of 86%, without using a clarifier or filter (**Figure 7.3c**). As shown in **Table 7.1**, biomass first-order detachment rate coefficients calculated, based on Patel et al. (2005) equation were 0.06-0.08 1/d in the anoxic column and 0.18-0.2 1/d in the aerobic column. [22] The observed biomass

detachment rate for the anoxic column was lower than the CFBBR of 0.13-0.17 1/d whereas the detachment rates of CFBBR and TFBBR aerobic columns were comparable. [22, 24]

As shown in **Table 7.2** and **Figure 7.4a**, at nitrogen loading rates (NLR) of 0.3 and 0.51 kg $N/m^3 \cdot d$ in phases I and II respectively, the system achieved 84.5±1.3% TN removal in phases I and II with STN < 4 mg/l in phase I and STN<6.1 mg/L in phase II, which met the tertiary standard limit of 10 mg/L. [23] Effluent TN during phase I and II averaged 5.4 mg/L and 8 mg/L, respectively. Nitrification predominantly occurred in the downer with dissolved oxygen (DO) in the range of 4.3-5.2 mg/L. **Figure 7.4b** depicts the influent and effluent NH_3-N, effluent NO_3-N and effluent NO_2-N. As illustrated in **Figure 7.4b**, the effluent NH_3-N was < 0.9 mg/L throughout phases I and II with average influent NH_3-N concentration of 30 mg/L. The nitrification rate based on the weight of the media were calculated 1.03 mg NH_3-N/g media·d and 1.51 mg NH_3-N/g media·d in phases I and II respectively. To measure the maximum nitrification rate of the biomass, batch tests were conducted which resulted in SNR based on the media weight of 1.12 and 1.74 mg NH_3-N/g media·d in phases I and II (**Figure 7.2a**). It is noteworthy that the aerobic biofilm thickness of <50 μm did not hinder diffusion significantly, thus rationalizing the relative agreement (6-11% discrepancy) between in-line and off-line SNRs in phases I and II. The nitrification rate based on biofilm surface area in TCFBBR was 1.26 g $N/m^2 \cdot d$, as shown in Appendix E. The produced nitrate in the downer was recycled to the riser (anoxic column) with a recirculation flow to the feed flow ratio of 4.5-6. At an empty bed contact time of 0.22 h, effluent NO_x-N concentrations of 3.2 mg/L and 5.2 mg/L were observed in phases I and II with nitrite concentrations of 0.1-0.6 mg/L. The denitrified-nitrogen loading rate based on the anoxic column volume was 0.70 kg $N/m^3 \cdot d$ in phase I and 1.19 kg $N/m^3 \cdot d$ in phase II, corresponding to the biomass specific denitrification rate based on media weight of 1.47 mg NO_3-N/g media·d and 2.27 mg NO_3-N/g media·d in phases I and II respectively. The aforementioned SDNR of TCFBBR are within 20% of offline biomass maximum denitrification rates of 1.84 mg NO_3-N/g media·d and 2.73 mg NO_3-N/g media·d in phases I and II (**Figure 7.2b**), at S_0/X ratio of 0.3-0.4 g COD/g VSS. It must be asserted that the batch test results show

the maximum nitrification and denitrification capacity of the system and may not reflect exactly the TCFBBR rates due to mass transfer limitation. As a result, the 20% difference in the online and offline denitrification rates is due to the nitrate diffusion limitation in the anoxic biofilm with up to 400 μm thickness. The denitrification rate based on anoxic biofilm surface area in TCFBBR was 1.32 g $N/m^2 \cdot d$, as calculated in Appendix E.

Table 7.2. Influent and effluent characteristics in Phases I and II

	Phase I (Synthetic)			Phase II (Municipal)		
	Feed	Riser	Eff.	Feed	Riser	Eff.
PH		7.5±0.3	7.4±0.2		8±0.1	7.7±0.3
ORP (mV)		-88±38	38±41		-21±60	81±37
TCOD (mg/l)	278±31	60±18	31±16	398±52	101±40	50±21
SCOD (mg/l)	252±35	27±14	14±4	118±24	31±8	22±5
SBOD(mg/l)	189±26	20±10	9±5	72±14	18±4	11±3
TN (mg/l)	31±3.1	6.7±1.2	5.4±1.3	48±5.8	11.4±4	8±1.6
STN (mg/l)	29.6±3	4.6±1.2	3.9±0.8	31±5	7.6±2.3	6.1±2.1
NH_3-N (mg/l)	29.1±3	4.1±1.1	0.7±0.4	30±4.5	4.1±0.4	0.9±0.4
NO_3-N (mg/l)	0.5±0.2	0.5±0.2	2.6±0.5	0.8±0.3	3.2±1.9	5.1±1.6
NO_2-N (mg/l)	0.01	0.01	0.6±0.5	0.03	0.3±0.2	0.1±0.1
Alkalinity[a]				250±10	160±15	135±20
TP (mg/l)	3.1±0.3		2.4±0.4	6.5±1.4		3.2±0.6
PO_4-P (mg/l)	2.9±0.3	2.4±0.3	2.3±0.3	3.4±0.7	3±0.5	3±0.5
TSS (mg/l)	18±6	35±17	26±14	214±41	62±30	33±14
VSS (mg/l)	13±5	28±12	16±10	183±30	50±27	24±10
Biomass Wastage (g VSS /d)			1.2			2.1
C:N:P		9:1:0.1			8:1:0.12	

[a] as mg $CaCO_3$ equivalent per liter

Total and ortho-phosphorus (OP) removals in phases I and II are shown in **Figure 7.4c**. Approximately, 18±7% and 55±8% phosphorus removal was observed in phases I and II at phosphorus loading rates of 0.032 and 0.06 kg $P/m^3 \cdot d$ respectively. As apparent from **Figure 7.4c**, OP release in the riser, as the phosphorus accumulating microorganisms (PAO's) activity indicator was insignificant, at 0.1 to 0.13 g/d (as shown in **Table 7.4**) throughout the tests. Phosphorus content of the effluent biomass was

measured as 1.8±0.5% by weight of VSS, which is similar to the conventional sludge phosphorus content of 1%-2%. In general, phosphorus removal in the TCFBBR occurred through biomass synthesis, and precipitation. **Figure 7.4d** depicts the concentrations of alkalinity in phase II in the riser and effluent as mg $CaCO_3$/L that shows 100-120 mg $CaCO_3$/L overall consumption of alkalinity through two stages of nitrification denitrification.

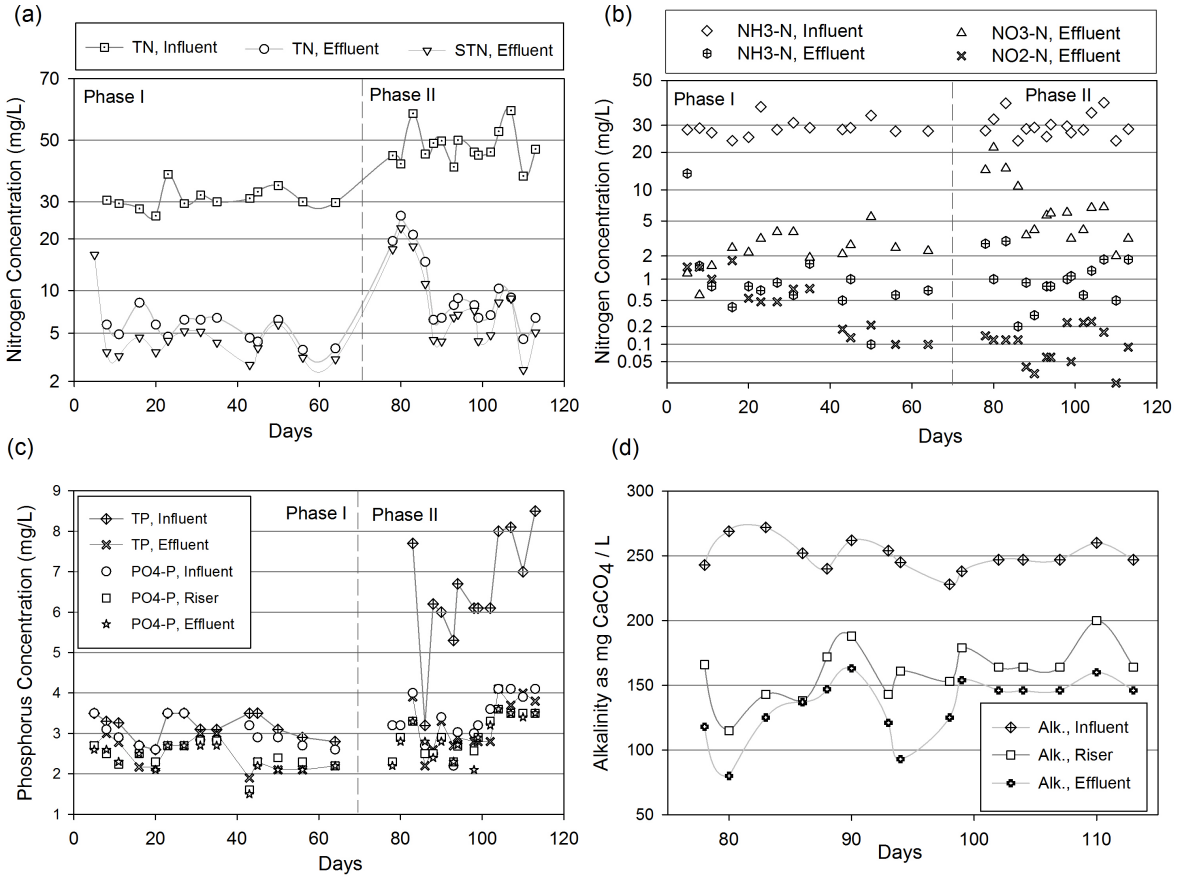

Figure 7.4. (a) Total nitrogen removal during the two phases (b) Ammonia, nitrare and nitrite concentrations in the influent and effluent (c) Total and ortho-phosphate phosphorus removal (d) Alkalinity concentrations in the influent, riser and effluent

7.3.2 Biomass Yield

Figure 7.3d illustrates the linear regression of cumulative VSS produced, based on the sum of the effluent biomass, the net change in attached biomass and biomass wasted,

versus cumulative COD removed. A very low observed yield of 0.093 g VSS/g COD was observed in phase I with an average effluent VSS concentration of 15 mg/L. Although there was a 38% increase in the OLR in phase II to 4.3 kg COD/m^3·d, the observed yield increased marginally to 0.101 g VSS/g COD, a 7.8% increase compared to phase I. As shown in **Table 7.1**, overall sludge retention time (SRT) of 37.8-39.6 d was calculated based on **Equations (6.4)** and **(6.5)**, with anoxic SRTs of 31-32 days.

The long SRT and also up to 54.4-62.7% influent COD consumption in the anoxic column (as shown in **Table 7.4**) rationalize the reduced yield in the TCFBBR. The detailed calculations to justify the experimental observed yields are described as below. The observed sludge yield of 0.093-0.1 in the TCFBBR was 30% lower than the yield reported for CFBBR. [24]

Based on the **Equation (7.1)** [1] and the COD consumption in the riser and downer in each phase, shown in Table 3, the observed yield can be calculated.

$$Y_{obs} = \frac{Y}{1+(k_d)SRT} + \frac{(f_d)(k_d)(Y)SRT}{1+(k_d)SRT} \qquad (7.1)$$

where Y=0.4 g VSS/g SCOD, k_d=0.15 g VSS/g VSS·d and f_d= 0.15 g VSS/g VSS. [1]

Phase I, in the riser:

$$Y_{obs} = \frac{0.85\times0.4\times38.6}{1+0.15\times32} + \frac{0.15\times0.15\times0.85\times0.4\times32}{1+0.15\times32} = 2.302\ \frac{gVSS}{d}$$

Phase I, in the downer:

$$Y_{obs} = \frac{0.4\times22.9}{1+0.15\times7} + \frac{0.15\times0.15\times0.4\times7}{1+0.15\times7} = 4.498\ \frac{gVSS}{d}$$

Overall Yield:

$$Y_{obs} = \frac{2.302 + 4.498}{69.8} = 0.097 \frac{gVSS}{gCOD}$$

The experimental observed yield in phase I is 0.093 g VSS/g COD. For phase II also the same precision can be achieved.

7.3.3 Loading Tests

At the end of the experiment with the real municipal wastewater (phase II), the loading tests including the dynamic loading test as well as the organic shock tests were conducted.

Dynamic Hydraulic Test

The impact of the dynamic loading on the TCFBBR effluent quality and its nutrient removal efficiencies were monitored by simulating wet weather condition at a maximum peaking factor of 4 for 3 hours. The hydraulic loading was gradually increased by the addition of clean tap water from 260 L/d to 520 L/d for 3 h and reached a maximum of 1040 L/d while maintaining all initial recirculation flows at their steady state rates, translating to overall hydraulic retention times (HRTs) of 2.3 h, 1.1 h, and 0.57 h respectively. Although the nutrient loading during the hydraulic loading test was not increased, the overall hydraulic retention time decreased to 1.2 h and 0.6 h which is equivalent to 0.75 h and 0.37 h retention time in the aerobic zone. The main purpose of this dynamic test was to test whether nitrogen removal and specifically nitrification would be hindered at a very low retention time since the biological reaction rates are kinetically limited.

The characteristics of the riser effluent and final effluent are shown in **Table 7.3**. As shown in **Table 7.3** and **Figures 7.5a, 7.5b** and **7.5c**, the effluent concentrations were <0.9 mg NH_3-N/L, < 3 mg NO_3-N/L, < 25 mg SCOD/L, <3 mg PO_4-P/L, <16 mg VSS/L and <20 mg TSS/L after 12 h of the dynamic loading which emphasizes the favorable response of the TCFBBR to the dynamic loadings and the sustainability of performance without loss of nutrient removal capacity and biomass. The system did not show any significant deterioration in terms of nitrification, and denitrification during the test, which

was confirmed by the batch specific nitrification (SNR) and denitrification (SDNR) tests, shown in **Figure 7.5b**.

Table 7.3. Influent and effluent characteristics during dynamic loading tests at different phases D_0 (260 L/d), D_1 (520 L/d) and D_2 (1040 L/d)

Parameter		Phase D_0		Phase D_1		Phase D_2	
	Influent	Riser	Effluent	Riser	Effluent	Riser	Effluent
DO (mg/L)		0.38	4.8	0.35±0.1	5±0.2	0.2±0.0	5.5±0.4
ORP (mV)		-95	4	-103±12	17±12	-85±28	47±10
Alkalinity[a]	270	243	161	213±33	175±14	165±30	144±30
TCOD (mg/L)	393	65	51	53±7	44±10	30±6	31±4
SCOD (mg/L)	177	29	18	25±11	21±3	11±5	18±4
NH_4-N (mg/L)	24.1	2.7	0.6	2.1±0.5	0.6±0.4	1.4±0.2	0.2±0.1
NO_3-N (mg/L)	0.2	0.4	2	0.3±0.1	1.7±0.3	0.2±0.0	0.5±0.1
NO_2-N (mg/L)	0.0	0.0	0.0	0.0	0.01±0.0	0.0	0.01±0.0
TN (mg/L)	37		4.8		3.7±1.1		2.6±0.2
PO_4-P (mg/L)	3.9	3.5	3.4	2.9±0.3	3.0±0.3	1.7±0.6	2.0±0.3
TP (mg/L)	7		3.9		3.3±0.4		2.2±0.3
TSS (mg/L)	193	38	36	35±6	20±3	19±5	11±2
VSS (mg/L)	160	30	25	26±6	16±6	17±2	10±2

[a] as mg $CaCO_3$ equivalent /L

Table 7.4 shows the COD, nitrogen and phosphorus mass removal rates in phases D_1 (520 L/d) and D_2 (1040 L/d). TCOD removal of 78% and 71.6% as well as nitrogen removal of 75.8% and 70.8% were observed in phases D_1 and D_2 respectively which indicated a deterioration of COD and nitrogen removal rates by 10% and 11-15% respectively compared to the steady-state system operation prior to the loading test. After ten hours into the dynamic load, the SNR decreased from 0.31 g NH_3N/g VSS·d to 0.26 g NH_3N/g VSS·d while SDNR decreased from 0.05 g NO_3N/g VSS·d to 0.04 g NO_3N/g VSS·d. The batch tests also indicated 13% and 20% reduction in the activity of the nitrifiers and denitrifiers respectively relative to the steady-state values before the dynamic tests.

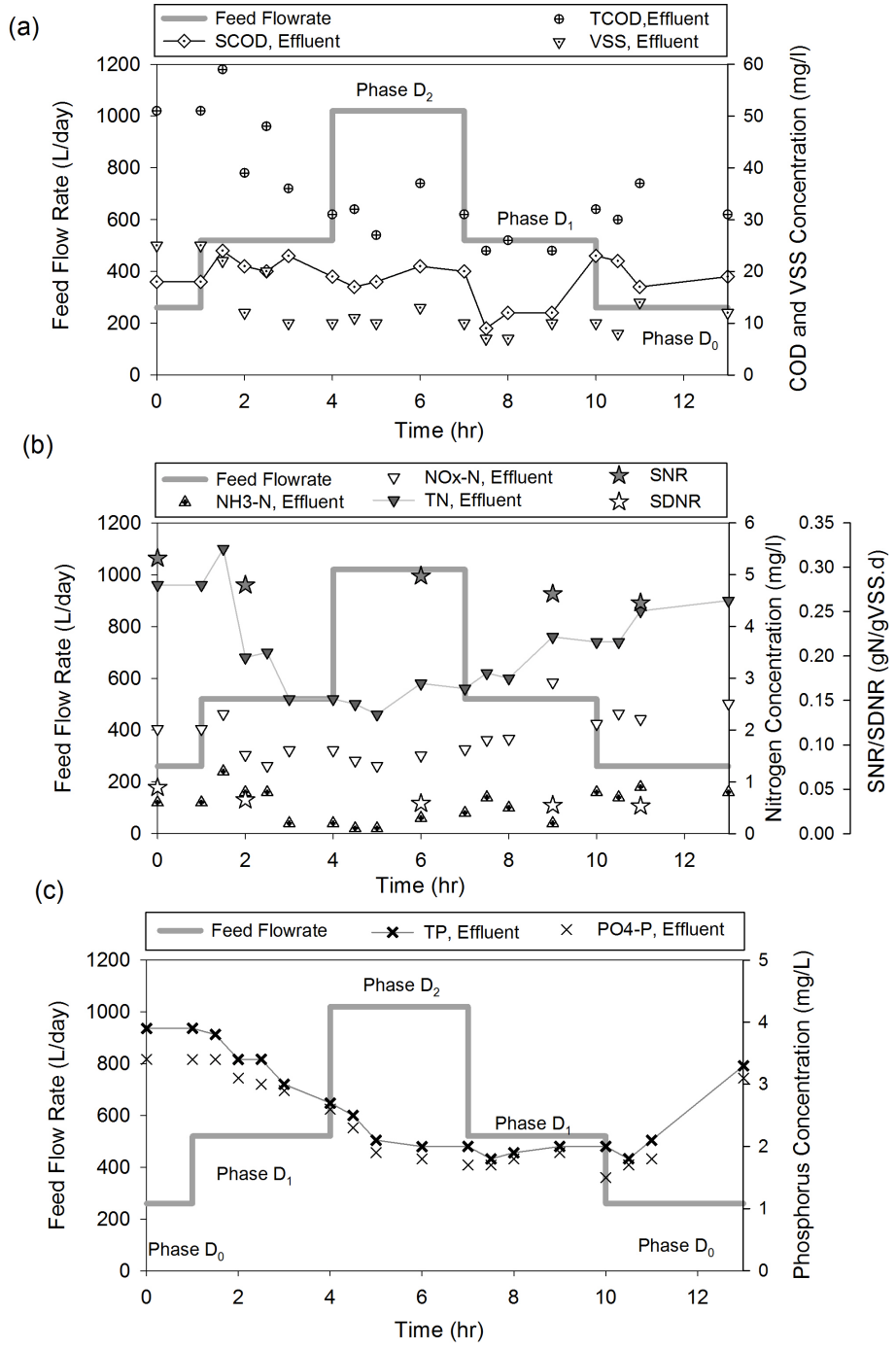

Figure 7.5. Dynamic loading test effect on (a) The effluent COD and VSS (b) The effluent nitrogen (c) The effluent phosphorus

Table 7.4 also shows that phosphorus mass removal significantly decreased from 50% at the beginning of the test to 7% in phase D_1. Interestingly, the effluent soluble phosphorus in phase D_2 was higher than the influent which is attributed to the dissolution of the precipitated phosphorus on the media as a result of the high flow rate and relatively low alkalinity in the diluted wastewater, potentially decreasing pH and solubilizing metal phosphates.

Organic Shock Test

The sensitivity of the system performance in general, and nitrification in particular to organic shocks was tested. Using sodium acetate, the COD of the influent was increased from 420 mg/L to 720 mg/L for 4.5 h and then to 1200 mg/L for 4 h corresponding to an ultimate OLR of 13.2 kg COD/m^3·d. Theoretically, in attached growth systems used for nitrification, most of the BOD must be removed before nitrifying organisms can be established. The heterotrophic bacteria have a higher biomass yield and thus can dominate the surface area of fixed-film systems over nitrifying bacteria. [1] Since the duration of each of the two carbon shock tests was about 2 turnovers of the mean system HRT, it is estimated based on the completely-mixed flow regime that about 87% of the reactor contents would have been displaced at every carbon shock loading. Therefore, it must be asserted that the observed impacts represent short-term effects. As shown in **Figures 7.6a** and **7.6b,** the COD removal efficiency dropped from 93.4% to 64.1% with the effluent SCOD increasing from 18 mg/L prior to the test to as high as 350 mg/L while effluent NH_3-N rose from 1.8 mg/L to 14 mg/L after 9 hrs. It is interesting to note from **Figures 7.6a** and 7.**6b** that the jump in both effluent SCOD and ammonia concentrations started simultaneously at t=1.8 h. As expected, nitrification efficiency in the downer was hindered to 49% from the initial 95% due to dominance of heterotrophs at the outside of the biofilm as well as DO limitations. The concentrations of DO in the riser and downer at the beginning of the test were 0.3 mg/L and 4.9 mg/L respectively but decreased to 0.0 mg/L and 2.5 mg/L after 9 h. **Figure 7.6b** also depicts the results of off-line SNRs test on the decanted aerobic biomass during the carbon shock test with DO of 8 mg/l and SCOD

of 30 mg/l. The average SNR after 10 hours of carbon shock testing was 0.26 g NH_3-N/g VSS·d, 15% lower than prior to the test. Since the SNR is reflective of nitrifiers activity, it is apparent that 15% of the nitrifying population prior test was evidently washed out during the dynamic carbon shock testing. Based on the nitrifying growth rate **Equation (7.2)**, adopted from ASM2, the aforementioned decrease in ambient DO concentration in the aerobic downer as the result of a very high oxygen demand reduces nitrification rate by 11%. It is estimated that the combination of oxygen limitation and nitrifier population reduction would reduce the overall nitrification rate by 25%, well below the observed 44% reduction, clearly emphasizing the sensitivity of nitrifiers to high ambient COD concentration.

$$r_{Nit} = \mu_{aut} \frac{S_{O_2}}{K_{O_2} + S_{O_2}} \cdot X_{aut} \qquad (7.2)$$

Where K_{O2}=0.5 g O_2/m^3

Figure 7.6c shows the effect of carbon shock test on the effluent suspended solids. The VSS in the effluent increased from 14 mg/L to an average value of 55 mg/L after ten hours, which indicated a higher activity and detachment rate of the rapidly growing heterotrophs both in the downer and the riser.

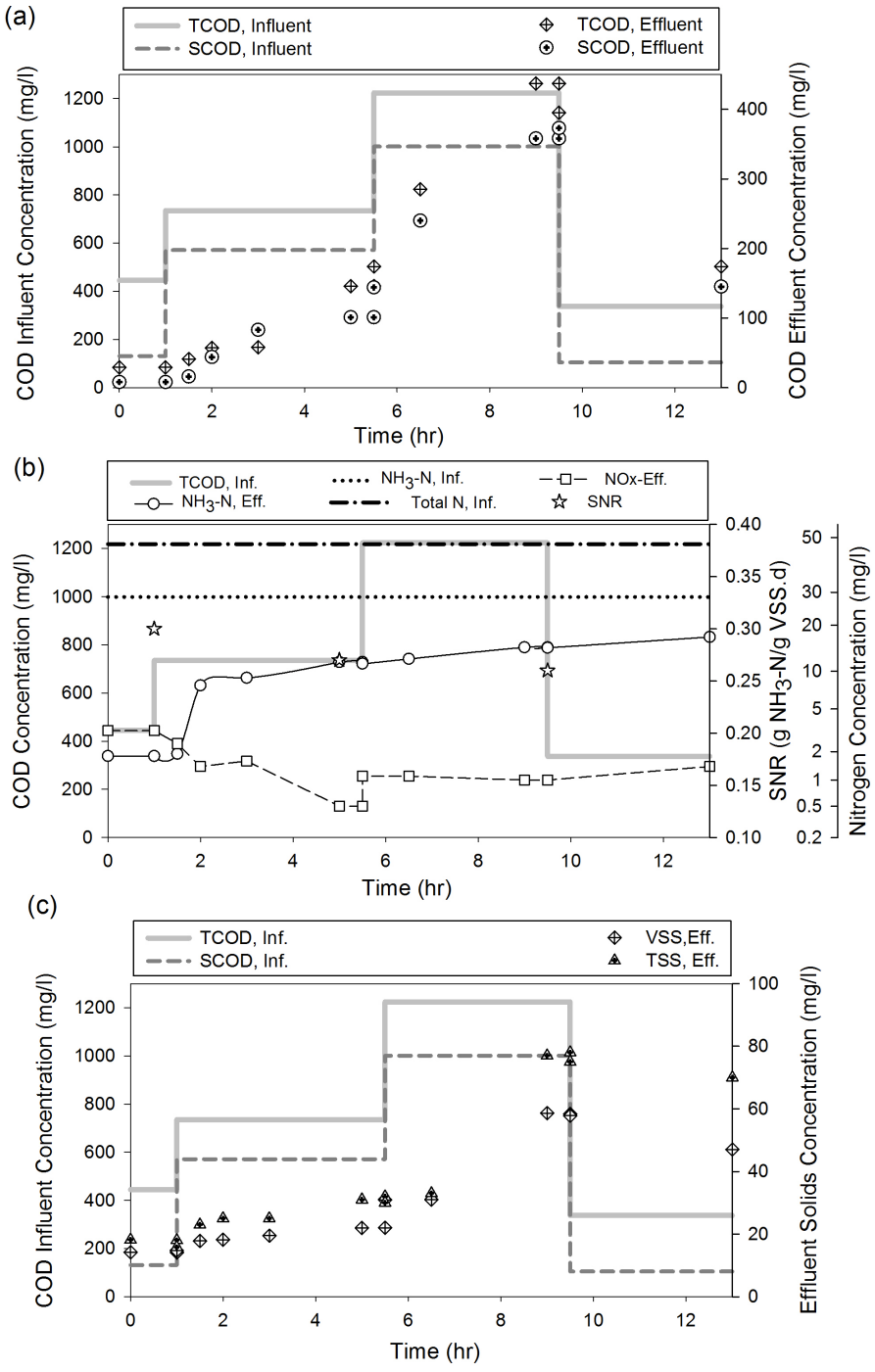

Figure 7.6. Effect of carbon shock test on (a) The COD removal (b) The biological nitrogen removal (c) The effluent solids

7.4 Nutrient Mass Balance

Table 7.4 illustrates the steady state mass balance for COD, TN, NH_3-N, NO_3-N, NO_2-N, TP, PO_4-P and alkalinity for phases I and II and dynamic loading tests at flow rates of 520 and 1040 L/d, where positive values indicate removal and negative values denote generation. The mass balances were based on experimental data of the influent, anoxic and final effluent characteristics, recirculation flows and the sludge wastage for each phase individually. As shown in **Table 7.4**, mass balance closures of 98.0% and 97.8% for COD, 90.6% and 89.6% for nitrogen, 92.7% and 97.8% for phosphorus and 93.3% for alkalinity were observed in phases I and II respectively.

Anoxic COD consumption was observed to account for 53%-58% of overall removal. The COD removal in the anoxic column was due to the denitrification process COD uptake (17.8 g/d, 26.6g/d, 18.1 g/d and 14.8 g/d in phase I, II, D_1 and D_2) as well as aerobic utilization as a result of DO recirculation from the aerobic column (17.5 g/d, 18.5 g/d, 17.5 g/d and 13.1 g/d in phase I, II, D_1 and D_2) whereas the predominant COD removal in the aerobic zone was due to aerobic heterotrophic utilization (22.9 g/d, 42 g/d, 32.4 g/d and 26.9 g/d in phase I, II, D_1 and D_2). The average liquid flow recirculation from the aerobic to anoxic column of 41.6 L/h with DO concentration of 5.5 mg/L mixes with the riser recirculation flow with 1 mg/L DO concentration. Therefore, the DO concentration at the bottom of the riser was 1.6 mg/L, which may have contributed to aerobic COD removal in the riser. For instance in phase I, 14.1 mg/L COD was aerobically degraded in the anoxic zone as shown in the footer of **Table 7.4**. The measured COD consumption in the riser in phases I, II, D_1 and D_2 agree with the calculated COD consumption (d) and (e) within 90.1%-94.5% accuracy.

Ammonia nitrogen was utilized by nitrification in the downer (5.6 g/d, 8.1 g/d, 5.6 g/d and 5 g/d in phases I, II, D_1 and D_2) as well as ammonia nitrogen assimilation through denitrification process in the anoxic zone. There might be an insignificant nitrification zone in the anoxic column, since differences between the experimental ammonia nitrogen consumption and calculated through assimilation were observed (0.9 g NH_3-N/d versus 0.17 g NH_3-N /d in phase I and 1.2 g NH_3-N/d versus 0.26 g NH_3-N/d in phase II). As

apparent from **Table 7.4** in phase I, nitrification mass rates in the riser and downer were respectively 0.73 (0.8-0.12) and 5.6 g NH_4-N/ d. Nitrification in the riser accounted for 11% of the overall nitrification, similarly in phase II, riser nitrification of 0.94 g NH_4-N/d accounted for only 10.6% of the overall system nitrification. As shown in **Table 7.4**, there was nitrite generation in the aerobic column, which was not converted to nitrate, -0.18 g/d in phase I, and also nitrate conversion to nitrogen gas in the anoxic column.

Table 7.4. Nutrient mass balances in Phases I, II, D_1 and D_2

	Mass in influent ($g\ d^{-1}$)	Mass consumed ($g\ d^{-1}$)	Mass Utilized ($g\ d^{-1}$)	Mass in effluent ($g\ d^{-1}$)	Mass wastage ($g\ d^{-1}$)	Percent closure (%)
		Anoxic	Aerobic			
Phase I-Synthetic WW (260 l/d)						
TCOD	69.8±2.5			6±1.4	0.9[a]±0.01	98.0[1]
(sCOD)	64.6±1.1	38.6±3.5 (17.8)[d] (17.5)[e]	22.9±3.1	2.7±1.0		
TN	7.8±0.6			1.45±0.3	0.12[b]±0.0	90.6[2]
NH_4-N	7.6±0.6	0.9±0.6 (0.17)[f]	5.6±0.9	0.15±0.8		
NO_3-N	0.18±0.03	5.4±0.3	-5.5±0.2	0.78±0.3		
NO_2-N	0.0±0.0	0.15±0.02	-0.18±0.03	0.04±0.01		
TP	0.8±0.1			0.66±0.1	0.021[c]±0.01	92.7[3]
PO_4-P	0.74±0.04	-0.1±0.1	2.5±0.7	0.5±0.02		
Phase II-Municipal WW (260 l/d)						
TCOD	108.8±10			12.1±3.4	2.48[a]±0.2	97.8[1]
(sCOD)	33.5±6.9	50.1±9.3 (26.6)[d] (18.5)[e]	42±11.2	5.0±0.5		
TN	11.4±2.1			1.87±0.5	0.21[b]±0.05	89.6[2]
NH_4-N	7.8±1.4	1.2±0.08 (0.26)[f]	8.0±1.1	0.3±0.1		
NO_3-N	0.15±0.07	7.6±0.4	-7.7±0.35	1.1±0.5		
NO_2-N	0.0±0.0	-0.34±0.3	0.3±0.3	0.03±0.02		
TP	1.89±0.3			0.85±0.1	0.034[c]±0.01	50.1[3]
PO_4-P	1.0±0.04	-0.13±0.03	2.4±0.6	0.78±0.03	0.8[j]	89.1[5]
Alkalinity	64±1.4	-26.8[h]±1.3	55.4[i]±8	44±3.7		93.3[4]
Phase D_1-Dynamic loading test (520 l/d)						
TCOD	102.4			22.1±3.3	2.2[a]±0.1	92.2[1]
(sCOD)	46.3	37.5±2.2 (18.1)[d] (17.5)[e]	32.4±4.4	10.4±1.5		
TN	9.26			2.24±0.4	0.22[b]±0.0	84.9[2]
NH_4-N	6.5	0.8±0.08	5.6±1	0.3±16		
NO_3-N	0.05	5.4±0.31	-5.5±0.14	0.8±0.07		
NO_2-N	0.0	0.018±0.0	-0.02±0.0	0.0±0.0		
TP	1.82			1.7±0.06	0.04[c]±0.0	95.6[3]
PO_4-P	1.04	-0.2±0.2	0.57±0.6	1.5±0.1		
Phase D_2-Dynamic loading test (1040 l/d)						
TCOD	102.4			29.3±4.9	2.5[a]±0.1	97.9[1]
(sCOD)	46.3	27±5.8 (14.8)[d] (13.1)[e]	26.9±4.8			
TN	9.26			2.75±0.2	0.3[b]±0.01	93.8[2]
NH_4-N	6.5	0.7±0.4	5±0.17	0.19±0.13		
NO_3-N	0.05	4.7±0.23	-4.8±0.2	1.2±0.15		
NO_2-N	0.0	0.0±0.0	-0.02±0.0	0.01±0.01		
TP	1.82			2.4±0.17	0.06[c]±0.0	75.8[3]
PO_4-P	1.04	-0.28±0.8	1.0±0.3	1.78±0.38		

[a,b,c] COD equivalent, Nitrogen (N) and phosphorus (P) content of 1 g biomass were measured 1.48±0.08, 0.094±0.01 and 0.018±0.05 gr respectively. However, for the COD mass balance a value of 1.42 gCOD / gVSS was used.

[d] SCOD consumption through denitrification based on $\frac{\text{g SCOD}}{\text{g NO}_3\text{-N}} = \frac{2.86}{1-1.42\,Y_{obs}}$ (5) [1]

For example Phase I $= 5.4 \times \frac{2.86}{1-1.42\times 0.093}$

[e] Aerobic SCOD consumption in the riser; for example Phase I

$$= \frac{\Delta O_2}{\Delta t} \times (1-Y_H)^{-1} = 0.0018 \frac{\text{g O}_2}{\text{l}} \times (10.7+1+4.5) \times 260 \frac{\text{l}}{\text{d}} \times (1-0.4\times 1.42)^{-1}$$

[f] Nitrogen assimilated for denitrification; for example Phase I

$$= 5.4 \times \frac{2.86}{1-1.42\times 0.093} \times 0.093 \frac{\text{gVSS}}{\text{gSCOD}} \times 0.1 \frac{\text{g N}}{\text{g VSS}}$$

[h] Alkalinity generated in the anoxic column; for example Phase II

$$= 7.7\,\text{g N}_{\text{denitrified}} \times 3.57 \frac{\text{g Alk}_{\text{generated}}}{\text{g N}}$$

[i] Alkalinity consumed in the aerobic column; for example Phase II

$$= 7.7\,\text{g N}_{\text{nitrified}} \times 7.14 \frac{\text{g Alk}_{\text{consumed}}}{\text{g N}}$$

[j] The value of phosphorus precipitated based on MINTEQ

[1] COD % closure $= \frac{38.6+22.9+6+0.91}{69.8} \times 100$

[2] Nitrogen % closure $= \frac{1.45+5.5+0.12}{7.8} \times 100$

[3] Phosphorus % closure $= \frac{0.66+0.021}{0.8} \times 100$

[4] Alkalinity % closure $= \frac{64-(55.4-26.8)}{44} \times 100$

[5] Phosphorus % closure with precipitation $= \frac{0.85+0.034+0.8}{1.89} \times 100$

Alkalinity was produced in the anoxic column as due to denitrification at 26.8 g/d in phase II, and consumed in the aerobic column as carbon source for autotrophic nitrifiers at 55.4 g/d in phase II.

Phosphorus removal was found to be due mainly to the biomass assimilation. However additional phosphorus removal was observed while treating the municipal wastewater. As a result, the phosphorus mass balance closure in phase II as shown in Table 3 dropped to 50.1%. The additional phosphorus removal was as a result of precipitation by predominantly calcium existing in the wastewater in accordance with **Equation (7.3)**. [1, 24]

$$10\,Ca + 6\,PO_4^{3-} + 2\,OH^- \leftrightarrow Ca_{10}(PO_4)_6(OH)_2 \qquad (7.3)$$

Worth mentioning, no significant changes in total solids and attached biomass of the TCFBBR were noticed in this study. The precipitation of the inorganic metal phosphates

and its strong adherence to media resulted in an accumulation of P in the system, unaccounted for in the mass balance. Assuming the entire unaccounted soluble phosphorus (approximately 1.7 mg/L) was removed by the calcium, based on **Equation (7.3)** it would have generated around 2.3 g of $Ca_{10}(PO_4)_6(OH)_2$ per day, translating to approximately 270 g of solids over the study period or <2.5% of the media mass. The average concentrations of calcium, magnesium and aluminum in the municipal wastewater were measured 59.8 mg/L, 12.9 mg/L and 0.76 mg/L respectively. Considering the aforementioned metal concentrations and ortho-phosphate concentration in the influent with the effluent pH of 7.7±0.3 and temperature of 22 °C (**Table 7.2**, the amount of phosphorus removed by precipitation was calculated as 3.1 mg/L using MINTEQ ver. 2.61 [25], thus improving the phosphorus mass balance closure in phase II to 89.1% from the 50.1% reported above.

7.5 Conclusion

The lab-scale TCFBBR was operated at loading rates of 2.7-4.3 kg COD/m^3·d, 0.3-0.51 kg N/m^3·d, and 0.032-0.06 kg P/m^3·d to study nutrient removal efficiencies of the system at a very short HRT of 2.3 hrs. The principal findings of this study are:

(i) Approximately > 90% organic, >85% nitrogen, and 20%-51% phosphorus removal were experienced using the TCFBBR at nutrient loading rates of 4.3 kg COD/m^3·d, 0.51 kg N/m^3·d, and 0.06 kg P/m^3·d, and an EBCT as low as 1.0 h.

(ii) Effluent TN of <8 mg/L indicates the system efficiently removed nitrogen by nitrification-denitrification.

(iii) Due to precipitation and assimilation 17%-51% of the influent phosphorus was removed without addition of any chemicals.

(iv) As a result of a long SRT of up to 40 days, very low observed yield of 0.093-0.101 g VSS/g COD were observed.

(v) The system did not show any considerable deterioration in nutrient removal efficiency during dynamic testing at a hydraulic peaking factor of 4 for 3 hours.

(vi) A 50% loss of nitrification efficiency was observed during a carbon shock test due to DO limitations, washout of nitrifiers, and high COD concentrations in the aerobic downer.

7.6 References

[1] Metcalf and Eddy, Wastewater Engineering: Treatment and reuse, Fourth ed., McGraw-Hill, 2003.

[2] Borregaard VR. Experience with nutrient removal in a fixed-film system at full-scale wastewater treatment plants. Wat. Sci. Technol. 1997; 36-1:129–137.

[3] Sen P, Dentel SK. Simultaneous nitrification-denitrification in a fluidized bed reactor. Wat. Sci. Technol. 1998;38:247-254.

[4] Chowdhury N, Nakhla G, Zhu J. Load maximization of a liquid-solid circulating fluidized bed bioreactor for nitrogen removal from synthetic municipal wastewater. Chemosphere, 2008;71:807-815.

[5] Rovatti M, Nicolella C, Converti A, Ghigliazza R, Di Felice R. Phosphorus removal in fluidized bed biological reactor (FBBR). Wat. Res. 1995;29:2627-2634.

[6] Morgenorth E, Wildere PA. Controlled biomass removal-the key parameters to achieve enhanced biological phosphorus removal in biofilm systems. Wat. Sci. Technol. 1999; 39:33-40.

[7] Li J, Xing X, Wang B. Characteristics of phosphorus removal from wastewater by biofilm sequencing batch reactor (SBR). Biochem. Eng. J. 2003; 16:279-285.

[8] Nicolella C, van-Loosdrecht MCM, Heijnen JJ. Wastewater treatment with particulate biofilm reactors. J. Biotechn. 2000; 80:1-33.

[9] Hakulinen R, Salkinoja-Salonen M, Saxelin ML. Purification of kraft bleach effluent by an anaerobic fluidized bed reactor and aerobic trickling filter at semitechnical

scale (Enso-Fenox). Proc. Techn. Ass. Pulp Paper Ind. Environ. Conf. TAPPI Press, Atlanta GA, 1981; 197-203.

[10] Shieh WK, Keenan JD. Fluidized bed biofilm reactor for wastewater treatment, Adv. Biochem. Eng. Biotechnol. 1986; 33:131-169.

[11] Cooper PF, Sutton PM. Treatment of wastewaters using biological fluidized beds.

Chem. Eng. 1983; 392-395.

[12] Sutton PM, Mishra PN. Fluidized bed biological wastewater treatment: Effects of scale-up on system performance. Wat. Sci. Technol. 1990; 22:419-430.

[13] Eikelboom D, Kampf R, Van Voorneburg F. Biofilm formation in an airlift reactor for the sewage purification. H_2O_2 1987; 20:388-392.

[14] Heijnen JJ, Mulder A, Weltevrede R, Hols J, van Leeuwen HLJM. Large scale anaerobic– aerobic treatment of complex industrial waste water using biofilm reactors. Wat. Sci. Technol. 1991; 23:1427–1436.

[15] Heijnen JJ, van Loosdrecht MCM, Mulder R, Weltevrede R, Mulder A. Development and scale-up of an aerobic biofilm airlift suspension reactor. Wat. Sci. Technol. 1993; 27:253–261.

[16] Frijters CTMJ, Eikelboom DH, Mulder A, Mulder R. Treatment of municipal wastewater in a CIRCOX airlift reactor with integrated denitrification. Wat. Sci. Technol. 1997; 36-1:173–181.

[17] Nakhla G, Zhu J, Cui Y. Liquid-solid circulating fluidized bed wastewater treatment system for simultaneous removal of carbon, nitrogen, and phosphorus. US patent no. 6,716,244, Int'l PCT patent awarded Aug. 2005.

[18] Cui Y, Nakhla G, Zhu J, Patel A. Simultaneous carbon and nitrogen removal in anoxic-aerobic circulating fluidized bed biological reactor (CFBBR). Environ. Technol. 2004; 25:699-712.

[19] Patel A, Zhu J, Nakhla G. Simultaneous carbon, nitrogen and phosphorus removal from municipal wastewater in a circulating fluidized bed bioreactor. Chemos. 2006; 65:1103-1112.

[20] Cui Y, Liu H, Bai C. Circulating fluidized bed biological reactor for nutrients removal. Front. Environ. Sci. Eng. 2008; 2-3:349-353.

[21] APHA; AWWA; WEF. Standard methods for the examination of water and wastewater. 20th Edition, American Public Health Association, Washington D.C. 1998.

[22] Patel A, Nakhla G, Zhu J. Detachment of Multi Species Biofilm in Circulating Fluidized Bed Bioreactor. Biotech. Bioeng. 2005; 25:427-437.

[23] U. S. EPA. Guidelines for water reuse. EPA-625/R-04-92-004, U.S. Environment Protection Agency and U.S. Agency for International Development, Washington, DC. 2004.

[24] Chowdhury N, Nakhla G, Zhu J, Islam M. Pilot-scale experience with biological nutrient removal and biomass yield reduction in a liquid-solid circulating fluidized bed bioreactor. Wat. Environ. Res. 2010; 82-9:772-781.

[25] Felmy AR, Girvin DC, Jenne EA. MINTEQ- A computer program for calculating aqueous geochemical equilibria. EPA-6001 /3-84-032. US. Govt. EPA. Athens, GA 1985.

8 Evaluation of BNR from Wastewater by TCFBBR Using a Predictive Fluidization Model and AQUIFAS APP

8.1 Introduction

Along with increasing interests in biofilm processes, there have been also numerous efforts towards their analytical and numerical mathematical modeling. The analytical approach simplifies the set of differential equations, but requires more assumptions, such as knowledge of the rate-limiting substrate in each cell within a reactor and the limiting substrate in the layers within the biofilm. [1,2, and 3] One-dimensional (1D) biofilm models, such as the stratified dynamic multispecies model as the simplest numerical model, introduced [4,5] and implemented in the AQUASIM software [6], are widely used to describe macroscopic conversions in biofilm systems and to predict biofilm processes in a quantitative way. [7] AQUIFAS software [8,9, and 10] is another 1d dynamic model that has the ability for modeling integrated fixed-film activated sludge (IFAS) such as moving bed bioreactors (MBBRs), which are more complex than pure biofilm processes. Currently, the AQUIFAS APP solves 19 equations out of the 21 equations presented in IWA ASM2d [11] and is one of the most comprehensive models for biofilms. The detail rates of equation are illustrated in **Appendix B**. There has been few other commercially available software such as Biowin (EnviroSim Associated Ltd., ON Canada), GPS-X (Hydromantis, Inc., ON Canada), Simba (Ifak GmbH, Magdeburg, Germany), Pro2D (CH2M HILL, Inc., Colorado US), STOAT (WRc, Wiltshire, England) and WEST (MOST for WATER, Kortrijk, Belgium) with capability of 1d modeling of biofilm processes with heterogeneous biomass distribution. However, none of the aforementioned models is developed for fluidized bed bioreactors specifically.

Multi-dimensional modeling approaches also have been intensively investigated to explore the complex structural heterogeneity of the biofilms in different reactor types such as aerobic, anoxic and anaerobic [7, 12, 13, 14, and 15]. However, the complexity of the multi-dimensional biofilm models, dedicating more attention to the microenvironment and structure of the biofilm than to the macro-kinetic behavior, in addition to the

diversity of biofilm models in the literature, has segregated the biofilm research from engineering practice in the biofilm modeling community. [16] This gap becomes even broader when the biofilm model is applied in fluidized bed bioreactors (FBRs) due to the dependency of the specific surface area, the volume of the reactor, biofilm thickness and recirculation flows to each other.

In a fluidized bed bioreactor, there are changes in the biofilm thickness and the circulation flows. Due to these changes, the regime of fluidization, the volume of expanded bed as well as the specific surface area etc. also change, significantly affecting the performance of a FBR. Since none of the afore-mentioned software has integrated the effect of fluidization on the volume of the reactor and specific surface area (SSA), a comprehensive, predictive, and practical fluidization model has been developed in this research work, which has been linked to the popular commercial fixed film software AQUIFAS APP.

8.2 Materials and Methods

8.2.1 Specific Surface Area of Biofilm-Coated Particles

In order to facilitate computation of biofilm surface area, the number of particles and specific surface area as a function of size and porosity had to be determined. Number of different particles versus their weight were counted in different size ranges and depicted in **Figure 8.1a**.

Linear regression results in different experimental equations for each case with which the number of particles based on their weight under operational conditions can be calculated. In **Figure 8.1a,** the numbers of two different sizes of irregular-shape lava rock are depicted versus their weight in order to observe the dependency of the number of particles on the average size at the same weight. To analyze the dependency of the number of particles on weight and shape, spherical glass beads at the same size as lava rock with a diameter of 1300 μm as well as irregular-shaped zeolite at the same size as lava rock with a diameter of 425-610 μm are also depicted. With knowledge of biofilm thickness, average bare particle diameter, and the number of particles, the SSA of the bio

particle can be determined as one of the outputs of the fluidization model developed in **Figure 8.2**.

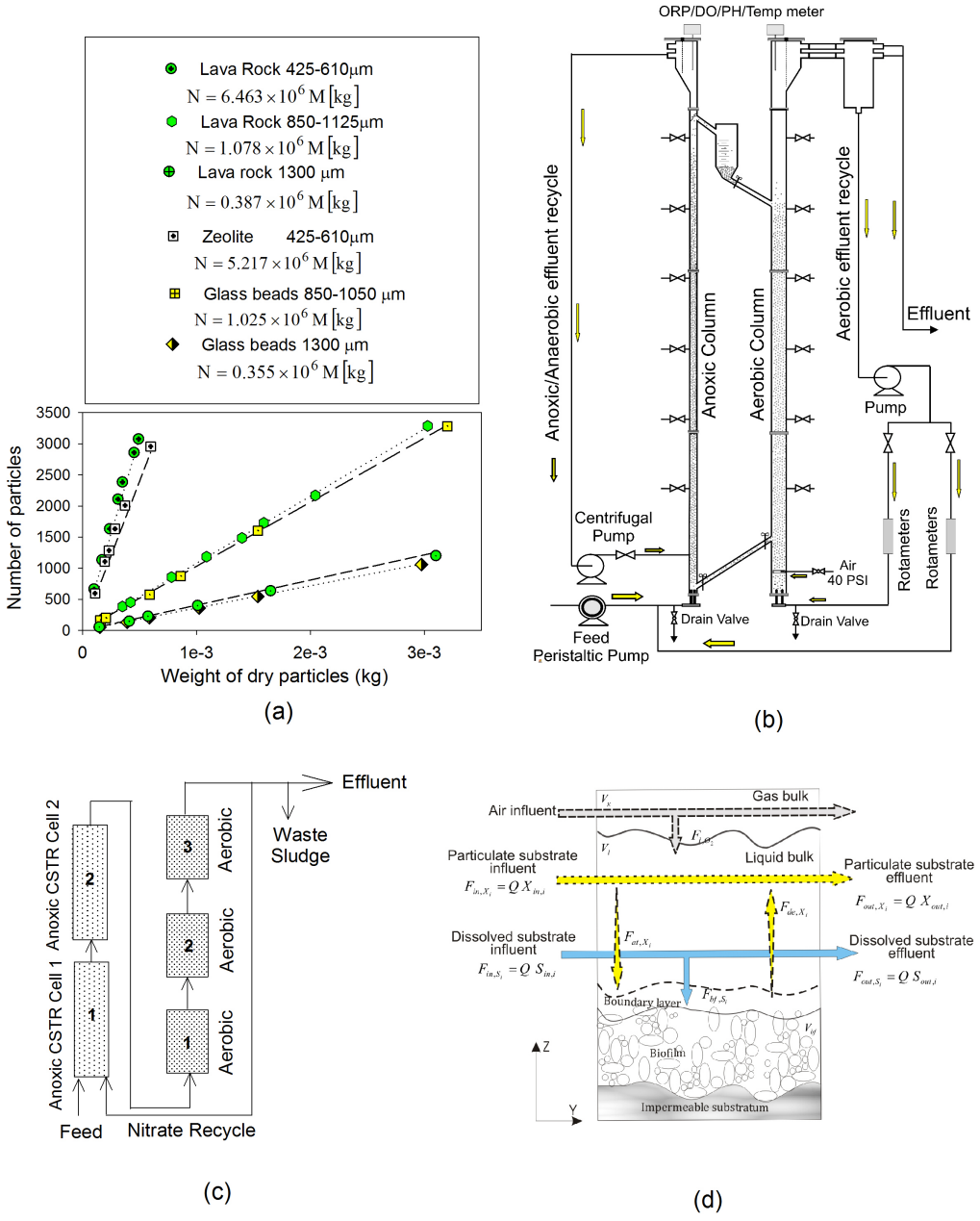

Figure 8.1. (a) Linear regression of particles versus weight (b) Schematic of TCFBBR (c) Reactor arrangement of the TCFBBR in AQUIFAS comprises of two anoxic and three aerobic fixed film CSTRs (d) The element of the AQUIFAS APP mathematical model

8.2.2 Twin Circulating Bed Bioreactor (TCFBBR)

The TCFBBR, **Figure 8.1b**, comprised of two plexi-glass columns operated as anoxic (5 cm x 5 cm) and aerobic (5 cm x 8.5 cm) FBRs with an overall height of 3.8 m each, was employed to investigate its BNR capability from municipal wastewater treatment. Nitrification predominantly occurred in the aerobic column of the TCFBBR (downer) and denitrification in the anoxic column (riser). Feed was injected at the bottom of the riser and a flow recirculation from downer to the riser was provided to ensure denitrification. Lava rock particles with an average size of 1000 μm were used in both columns as a carrier media. The design empty bed contact times (EBCTs) were 0.22 h in the anoxic column and 0.71 h in the aerobic column in phases I and II (**Table 8.1**), corresponding to particle masses of 2.5 kg in the riser and 8 kg in the downer which were initially estimated based on the specific nitrification rates (SNRs) of 0.09-0.14 g NH_4-N/g VSS/d, specific denitrification rates (SDNRs) of 0.033-0.243 g NO_x-N/g VSS/d and the attached biomass per g media of 10-30 mg VSS/g media, reported in the literature for the circulating fluidized bed bioreactor. [17] In the riser, heterotrophic bacteria grew on the media and the biofilm became thicker. At a certain biofilm thickness, depending on the superficial liquid velocity, the biofilm-coated particles reached the height where they can be transferred to the downer through an inclined pipe. An intermediate graduated container was placed between the two columns, as shown in **Figure 8.1b,** to monitor the particle transfer rate. Particles from the bottom dense phase of the downer with a thin biofilm (< 40 μm) were transferred back to the riser manually to make up the particles in the riser. Particle transfer cycles were observed to occur every 17 days.

Table 8.1. Operating parameters in TCFBBR

		Phase I	Phase II
Influent flow, Q_{in} (l/d)		262±8.2	260±5
Organic loading (kg COD/(m^3·d))		2.7±0.8	4.3±0.5
Nitrogen loading (kg N/(m^3·d))		0.3±0.1	0.51±0.06
Phosphorus loading (kg P/m^3·d))		0.032	0.06
R-R recirculation ratio ($Q_{r\text{-}r}/Q_{in}$)		10.7±3	9.4±3.1
D-R recirculation ratio ($Q_{d\text{-}r}/Q_{in}$)		4.5±2.1	6±2
D-D recirculation ratio ($Q_{d\text{-}}/Q_{in}$)		16.2±4	21±5
EBCT (h)= $V_{compact}/Q_{in}$	*Anoxic*	0.22	0.22
	Aerobic	0.71	0.71
HRT (h)	*Anoxic*	0.86	0.87
	Aerobic	1.43	1.44
Air flow (ml min^{-1})	(40 psig)	2060	2150
DO (mg/l)	*Aerobic*	5.4±0.7	4.3±0.5
	Anoxic	0.2±0.2	0.3±0.1
X (mg VSS/g lava rock)	*Anoxic*	25.1	29.5
	Aerobic	3.5	4.7
Biomass (g VSS)	*Anoxic*	113	145
	Aerobic	22.3	28.3
F/M ratio (g COD/(g VSS·d))		0.58	0.48
Detachment rates (1/d)	*Anoxic*	0.061	0.086
	Aerobic	0.18	0.2
Superficial liquid	*Anoxic*	1.3-1.9	1.3-1.9
Velocity, u_l(cm/s)	*Aerobic*	1.1-1.5	1.1-1.5
Estimated SRT (d)	*Anoxic*	32[a]	31
	Aerobic	7.6	6.8
	Overal	39.6[b]	37.4
Run time (d)		65	45

[a] based on equation (1), [b] based on equation (2)

8.2.3 Analytical Methods

Samples were collected from the feed tank, anoxic column top and the effluent. Total suspended solids (TSS), volatile suspended solids (VSS) and biochemical oxygen demand (BOD) were analyzed in accordance with Standard Methods 2540D, 2540E and 5210 [18] respectively. Dissolved oxygen (DO) and oxidation-reduction potential (ORP) were measured onsite using an Oakton DO 6 meter, and an Oakton ORPTestr 10 (Oakton, Singapore). HACH methods and testing kits (HACH Odyssey DR/2800) were used to analyze total and soluble chemical oxygen demand (TCOD and SCOD), total and soluble nitrogen (TN and STN) and total phosphorus (TP), NH_4-N, NO_2-N, NO_3-N, and

PO_4. Alkalinity was measured by titration with 0.01 N H_2SO_4 in accordance with the Standard Method no 2320 (APHA, 1998). The size of the bare and biofilm coated particles was measured using a Mastersizer 2000 laser analyzer (Malvern Instruments Inc., UK). and Visiongauge (Flexbar Machine Co, New York, USA) synchronized to a microscope (Mitutoya, Sakada, Japan) coupled with a camera (Leica DC 300, Germany), at a magnification of 50X. Based on Standard Method no 2540G (APHA, 1998), the attached biomass on the carrier media was measured and expressed as mg VSS/g clean particles. Approximately 10-20 g bioparticles were taken from columns, suspended in a 100 mL vial, and sonicated for 3 h at 30°C in an Aquasonic sonicator (SK 1200H Kupos, China) with a rated power of 45 Watts. After sonication, the TSS and VSS content of the detached biomass was determined following Standard Methods no 2540D and 2540E. [18]

8.2.4 Statistical Analysis

The student t-test was used to test the hypothesis of quality at a 95% confidence level. The null hypothesis was defined to be no difference between the two groups tested versus the alternative hypothesis if there is a statistical difference between the two groups.

8.3 Modeling and Simulation

8.3.1 Carrier Media

Lava rock particles were used in both columns with an average diameter (d_m) of 850-1125 μm, a total porosity (ψ_T) of 62% (44% external and 18% internal), a dry bulk particle density (ρ_{md}) of 1012 kg/m, a true particle density (ρ_{mt}) of 2628 kg/m^3 and a specific surface area (SSA) determined by BET (Micromeritics ASAP 2010, Micromeritics Co., USA) of 0.48 m^2/g for bare particle. The relatively high specific surface area of lava rock particles is due to the high porosity and non-uniformity. However after developing biomass on the media, the bio-particles can be considered spherical with a surface area of a sphere with diameter of d_p. **Figure 8.1a** shows the experimental numbers of lava rock particles with average diameters of 850-1050 μm, versus their weight. The linear regression demonstrates an experimental equation with which the number of particles can be estimated based on their weight with an accuracy of R^2=0.98. For instance, 1 g of lava rock with the sieved size range of 850-1125 μm

consists of 1078. **Figure 8.1a** also illustrates the effect of particle size on the particle numbers at constant weight for lava rock with internal porosity of 18% and glass beads without any internal porosity. It is clearly shown in **Figure 8.1a** that smaller particles correspond to a much higher number of particles.

Particle SSA is also a function of its size and porosity. **Figure 8.1a** demonstrates the relationship between particle numbers and weight of lava rock with SSA of 0.48 m^2/g, zeolite with SSA of 24.9 m^2/g and glass beads with SSA of 0.0038 m^2/g. Interestingly, the internal porosity in different size ranges has a small effect on the quantity of the particles. A porous media is more conducive for biomass attachment to smooth particles in the start-up phase of a fluidized bed bioreactor and less favorable for its brittleness and high shear forces by particle attrition. However, at steady state, porosity has a negligible effect on the bio-particle surface area and performance. As depicted in the fluidization model algorithm (**Figure 8.2,** Box 1), the number of particles are used to determine the total surface of biofilm in the simulated reactors for substrate diffusion.

8.3.2 Fluidization Model

A predictive model for two and three phase fluidized bed bioreactors was developed to determine the pertinent system parameters such as SSA, bed height, overall liquid gas and solids hold up and biomass quantity based on process parameters such as reactor dimensions, particle properties and flow rates and a guesstimated biofilm thickness as input variables. The flow chart of the model is shown in **Figure 8.2** with the input variables listed in Box 1. The method of computations for the fluidization model is explained in detail in 8.3.3.

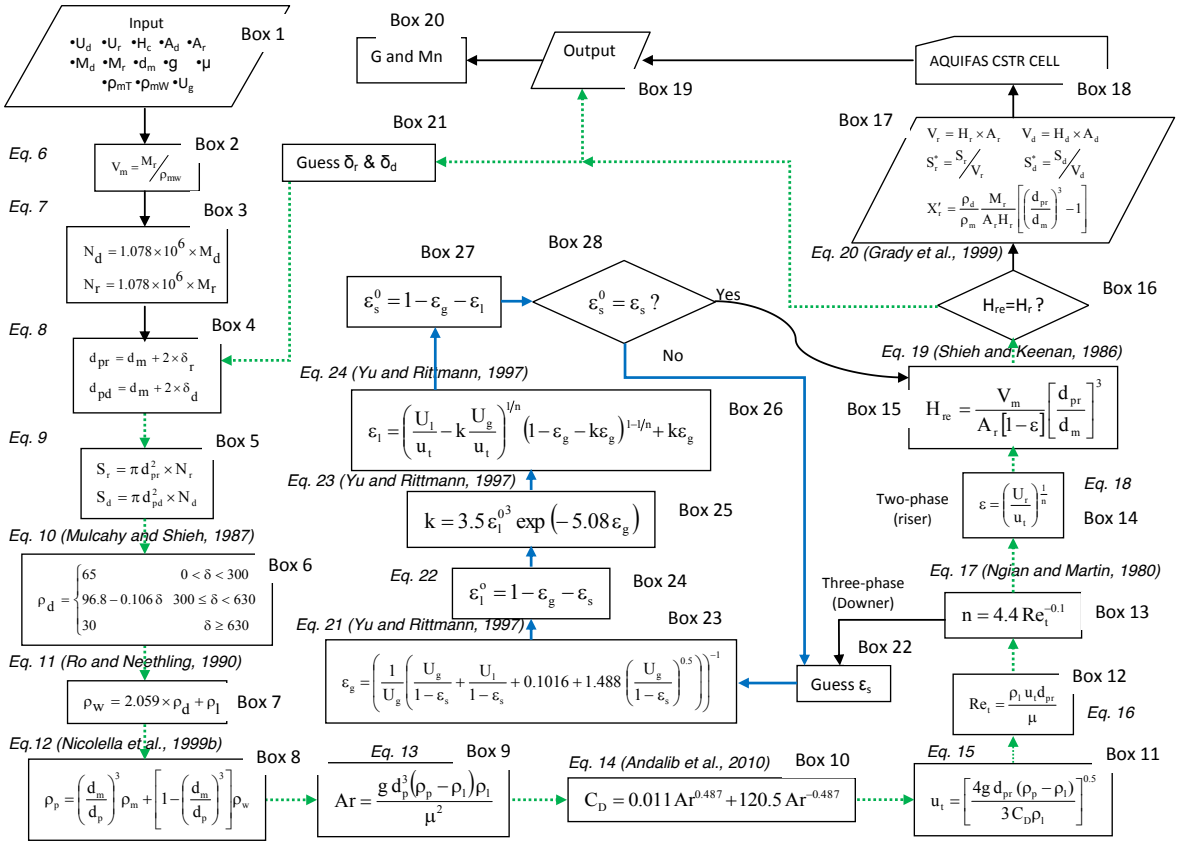

Figure 8.2. Algorithm of the fluidization model

As depicted in **Figure 8.2**, with a guessed biofilm thickness in each column, the bed height and biofilm specific surface area are calculated in two and three phase regimes. The model keeps iterating the biofilm thickness until the bed heights are equal to the nominal designed bed heights. At this point, the volumes of cells and biofilm SSA, as some of the output of the fluidization model, were used in the AQUIFAS APP model. AQUIFAS APP computes the biofilm thickness based on detachment rates and substrate uptake kinetics. The calculated biofilm thickness from AQUIFAS APP will be the new biofilm thickness in the fluidization model to correct the simulated bed heights. This loop converges at a specific biofilm thickness when the reactor volumes and biofilm specific surface area are used for AQUIFAS APP modeling. As seen in **Figure 8.2**, it's noteworthy to mention that:

a. Drag coefficient used in this model, is a function of Archimedes and explicit to terminal velocity proposed by Andalib et al. (2010). [19]

b. Richardson and Zaki's equation was used to predict bed voidage of two phase flow. [20]

c. For the three-phase fluidization, a wake model proposed by Yu and Rittmann (1997) was applied to predict liquid hold up while the solids hold up was obtained by iteration based on material balance. [21]

d. To predict bed heights and biomass quantity, **Eq. (19)** Box 1 and **Eq. (20)** Box 17 in **Figure 8.2**, proposed by Shieh and Keenan (1986) and Grady et al. (1999) respectively were found the most accurate in the literature. [22, 23]

8.3.3 Detailed Explanation of the Fluidization Model

Input variables of the model such as superficial liquid velocity in the riser (U_r) and downer (U_d), superficial gas velocity in the downer (U_g), overall height of the columns (H_c), cross sectional area of the riser (A_r) and the downer (A_d), average diameter of the bare media particle (d_m), true particle density ρ_{mt}, wet density of the media ρ_{mw}, and density and viscosity of the liquid, are listed in Box 1.

Box 3 depicts the result of linear regression of the number of the particles based on their weight, shown in **Figure 8.1a**, in this case lava rock with 825-1050 μm average diameter. With the total number of particles in the riser and the downer and guessing the thickness of the biofilm in the riser and downer in Box 21, the overall surface area of the particles in each column are calculated in Box 5. Along with development of biofilm on the surface of media, even irregular shape, bio-particles exposed to liquid shear force naturally intend to maintain spherical shape in order to reduce the liquid shear force on their surface. As a result, assumption of spherical bio-particles in Box 5 to calculate the overall surface area is plausible. The biofilm dry and wet densities are calculated in using **Eq. (10)** Box 6 and **Eq. (11)** Box 7 in **Figure 8.2** proposed by Mulcahy and Shieh (1987) and Ro and Neethling (1990) [24, 25], found the most accurate in the literature (Andalib et al., 2010). Overall bio-particle density is calculated using **Eq. (12)** Box 8. [26]

Archimedes number of bio-particles then after can be calculated using **Eq. (13)** Box 9) with which the drag coefficient, as an explicit function of terminal settling velocity, as well as terminal settling velocity of bio-particles were calculated using **Eq. (14)** Box 10

proposed by Andalib et al., (2010) and **Eq. (15)** Box 10. Reynolds number of terminal settling velocity for bio-particles is calculated in Box 12 and the bed expansion index can be calculated using Richardson and Zaki, **Eq. (17)** Box 13.

After Box 13, if the column is a two-phase liquid-solid fluidized bed (such as anoxic bioreactors), bed voidage is calculated using Richardson and Zaki **Eq. (18)** Box 14 and if the column contains a three-phase gas-liquid-solid fluidization (such as aerobic or anaerobic bioreactors), gas, solids and liquid hold-ups are calculated using a wake-model proposed by Yu and Rittmann (1997). This model was proposed to predict liquid hold up while the solids hold up was obtained by iteration based on material balance as following. The solid hold-up is guessed in Box 22 and the gas hold-up is calculated using **Eq. (21)** Box 23. Having solid and gas hold up, the liquid hold up can be calculated using equations 22, 23 and 24 proposed by Yu and Rittmann (1997). With the new liquid hold-up, the new solid hold-up is calculated in Box 27, the iteration will stop when the loop indicated by the blue bold arrows converges.

With the calculated solid and liquid hold-ups in the two phase fluidized bed and solid, liquid and gas hold-ups in the three phase fluidized bed, the height of the expanded bed can be calculated using **Eq. (19)** Box 15 proposed by Shieh and Keenan (1986) in Box 15. The new guess for biofilm thickness in both the riser and downer are applied in Box 21 until the calculated bed heights equal to the targeted values in the loop indicated using green dotted arrows.

In order to calibrate the AQUIFAS APP model, the values of G and Mn in the first run should be adjusted to predict the final biofilm thicknesses calculated in Box 21. This calibration is valid as long as there is no change in the hydrodynamics of the system. If the simulation is for a different type of wastewater, AQUIFAS APP will calculate new biofilm thicknesses in the riser and the downer with which new bed heights and expanded volume of the bioreactor are calculated. It is worth mentioning that with each change in the loop the model predicts new specific surface areas of biofilm in Box 5 as well as volume of the bioreactors in Box 17 to be used as inputs for AQUIFAS APP.

Biomass concentrations in the bioreactors can also be calculated using **Eq. (20)** Box 17 proposed by Grady et al. (1999) and compared to experimental data in order to verify the credibility of the calculated biofim thickness.

8.3.4 AQUIFAS APP Model

AQUIFAS APP is developed to model maximum of twelve continuous mixed liquor cells with integrated biofilm in either parallel or series layout and with different electron acceptor environments (aerobic, anoxic and anaerobic). As shown in **Figure 8.1d**, each cell is comprised of bulk liquid, which is completely mixed, and substratum to carry biofilm with substrate concentration gradient inside it in the Z direction. Based on IWA ASM2d model, nineteen reaction rates including biological phosphorus removal are included in the model with nine soluble and seven particulate components. The definition and values of the kinetic parameters of reactions as well as rate of the biological reactions used in AQUIFAS APP model are based on IWA ASM2d and is listed in detail in **Appendix B, C**.

Mass balances for each soluble component in the bulk liquid of each cell (**Figure 8.1d**) are as follows:

$$V_L \frac{\partial S_{out,i}}{\partial t} = Q\left(S_{in,i} - S_{out,i}\right) - J_{F,i} A_F \qquad (8.1)$$

The model computes the biofilm flux (j_F) of COD, dissolved oxygen, NH_4-N, NO_x-N, PO_4-P, and biomass from one layer (d_z) to the next layer and integrates the values over the thickness of the biofilm (L_F), as follows:

$$\begin{cases} J_{F,i} = \int_0^L r_{F,i}\, dz = D_i \dfrac{dS_i}{dz} & (8.2) \\ \dfrac{\partial S_i}{\partial t} = D_i \dfrac{\partial^2 S_i}{\partial z^2} + r_{F,i} & (8.3) \end{cases}$$

To alleviate numerical calculation, the model breaks the biofilm into 12 layers and a stagnant liquid layer. The flux rates, estimated using a finite difference technique, are governed by the diffusion between layers; COD, ammonium-nitrogen (NH_4-N), dissolved

oxygen, oxidized nitrogen (NO_x-N) utilized in each layer; and biomass and inert suspended solids generation and decay in each layer. Detailed equations are expanded elsewhere. [8, 9, 10, and 27] The biomass balance at steady state for the biofilm process in each cell in AQUIFAS APP is as following adapted from (Sen et al 2007, Boltz et al, 2009) where the biofilm diffusion model computes the biomass generated in each layer of the biofilm with thickness of δ (m) based on the substrate and electron acceptor concentrations in the layer: [27, 28]

$$r_{de,Xi} = J_{F,i}.Y_i = k_{n,i}\left(\frac{G}{Mn}\right)X_{F,i}(\delta)^n \qquad (8.4)$$

Where the left term is the production of biomass (Y_i is the yield biomass/substrate, M_X/M_S) and the right term represents the decrease in biomass due to inactivation, endogenous respiration and detachment. However, the detachment term is mostly dominant. The detachment rate ($r_{de,xi}$) of biofilm for biomass component of x_i ($g/m^2.d$) is computed from the flux rate into the biofilm. Factor G was used to adjust the shear for the hydrodynamic regime and factor Mn was considered as a modifier for the type of media surface. Mn value increased with surface roughness of the surface from 1 to 5.

For n=1, the unit of $k_{de,i}$ is in 1/d and for n=2 the unit of $k_{de,i}$ is m/d. The value of n is dependent on the shape of the particles and where the biofilm develops. In general, n=2 is used if the biofilm is on the outside of the particle (as in the case of a sphere), where the liquid velocities and shear increase as the thickness increases. n=1 is used if the biofilm is on the inside of hollow cylinder of a moving bed system, where the liquid velocities through the inside of the cylinder decreases relative to the velocity at which the particle is moving when the biofilm thickness increases and closes off more of the annular space within the cylinder.

In this instant, biofilm detachment and sloughing take place off the outermost biofilm layer as a result of biofilm sheared from the surface or breakage of biofilm off the innermost layer. The mechanism of biofilm detachment is extremely complicated especially when the particle attrition is involved. In general, the detachment rate is a function of the biofilm yields for heterotrophs and autotrophs, liquid shear force, particle

attrition, the brittleness of particles and the levels of electron acceptor such as COD, DO, NH_4-N and NOx in each cell.

Based on **Equation (8.4)**, the biofilm thickness is a function of the substrate concentrations in the mixed liquor, the average concentration of biomass in the biofilm denoted by the model as MLVSS of the biofilm, hydrodynamic shear force factor (G) and media shape factor (Mn).

8.3.5 Model Implementation and Calibration

To simulate the two columns of the TCFBBR, a cell arrangement comprised of two anoxic continuous stirred tank reactors (CSTR) in series and three aerobic CSTRs in series are considered in the AQUIFAS APP, as depicted in **Figure 8.1c**. The feed influent is injected at the bottom of the riser column, cell 1, and the flow stream from top of the anoxic column, cell 2, enters at the bottom of the aerobic column, cell 3. The nitrate recycle stream transfers nitrates from the top of the aerobic column, cell 5, to the bottom of the anoxic column, cell 1, similar to that in the TCFBBR. In this cell arrangement, a clarifier is not considered and the effluent suspended solids calculated in the model are indeed the actual suspended solids before clarification. The bed voidage, solid retention time, and flow regime in the two anoxic cells are assumed identical and similarly for the aerobic cells. The cross sectional area of anoxic and aerobic cells, were considered equal to the actual cross sectional area of the column whereas the height of each cell and the biofilm surface area available per volume of each cell as input variables for the AQUIFAS APP, are calculated from the fluidization model (**Figure 8.2)**. The DO set points for the anoxic and aerobic cells are similar to those measured onsite of 0.2 mg/L and 4.3-5.4 mg/L respectively. As explained in section 3.3 and **Equation (8.4)**, the AQUIFAS APP predicts the value of the biofilm thickness based on kinetics, substrate concentrations as well as the hydrodynamics of the system, governed predominantly by G and Mn in the range of 0-5. These values (G and Mn) were calibrated based on the biofilm thickness output from the fluidization model for the first run (synthetic wastewater) as G and Mn equaled to 1 and 0.1 respectively for the anoxic column and 5 and 0.1 for the aerobic column. For the second phase the aforementioned values for G and Mn were maintained to simulate the biofilm thickness.

8.4 Results and Discussion

8.4.1 Modeled Fluidization Characteristics

Figure 8.3 depicts the results of the numerical solution of the fluidization algorithm presented in **Figure 8.2** for two and three phase fluidized bed bioreactors with lava rock as carrier media with average size of 1000 μm. **Figure 8.3a** and **Figure 8.3b** depict the bed height and SSA of biofilm particles versus superficial liquid velocity (U_L) and biofilm thickness in liquid-solid fluidized beds. It can be seen that at the constant biofilm thickness, by increasing U_L, the bed height increases while the SSA decreases. It can also be concluded that at constant U_L, an increase in biofilm thickness would result in an increase in bed height and a decrease in SSA. **Figure 8.3c** and **Figure 8.3d** show the bed heights and SSA versus U_L and biofilm thickness in a gas-liquid-solid fluidized bed while the superficial gas velocity (U_g) is constant at 1.09 cm/s (similar to the operational condition for U_g in the TCFBBR). The same trend as two-phase flow was also observed in a three phase fluidized bed bioreactor. However the dependency of the bed height on U_L is more linear in the three-phase flow than the two-phase flow. **Figure 8.3e** and **Figure 8.3f** show the dependency of bed height and SSA in a three phase fluidized bed on the U_g and biofilm thickness at a constant superficial liquid velocity of 1.55 cm/s. As shown, the bed height increases when U_g decreases at constant biofilm thickness and the SSA increase with a rise in U_g, contrary to liquid superficial velocity effect on the fluidization, due to a decrease in the overall density of gas-liquid fluid.

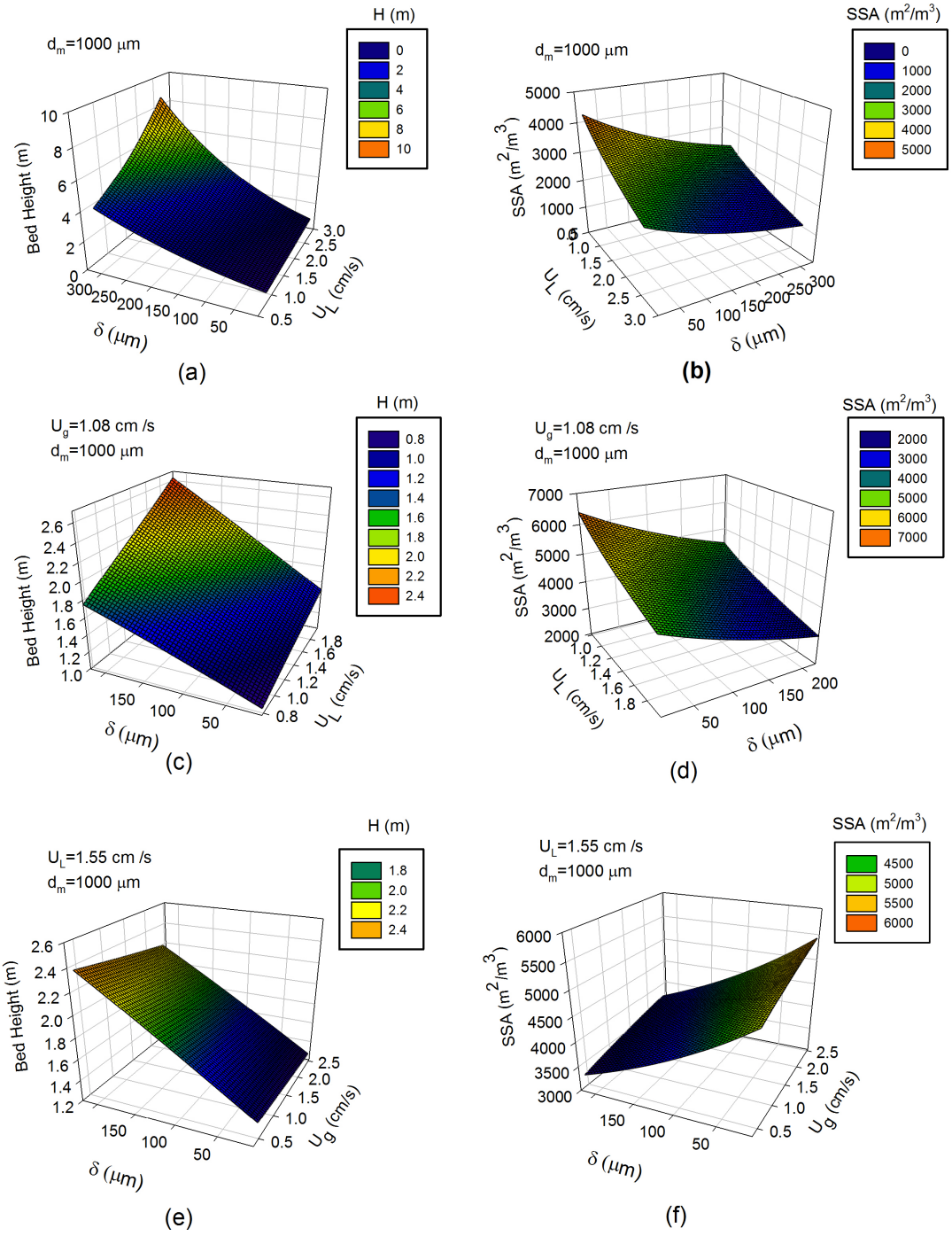

Figure 8.3. (a) Bed Height as a function of δ and U_L in two phase flow (b) *SSA* as a function of δ and U_L in two phase flow (c) Bed Height as a function of δ and U_L in three phase flow with a constant U_g (d) SSA as a function of δ and U_L in three phase flow with

a constant U_g (e) Bed Height as a function of δ and U_g in three phase flow with a constant U_L (f) *SSA* as a function of δ and U_g in three phase flow with a constant U_L

Based on the average operational conditions of the TCFBBR in the two phases (**Table 8.1**), the model predicted a bed height of 3.55 m in the riser with biofilm thickness of 270 μm, SSA of 2067 m^2/m^3, voidage of 0.55, solids holdup of 0.44 and total surface of particles of 20.1 m^2 for U_L of 0.0139 m/s in the riser. For the gas-liquid-solid fluidized bed downer, the bed height was 1.75 m with SSA of 4786 m^2/m^3, voidage of 0.45, solids hold up of 0.52, gas hold up of 0.03 and total surface of particles of 37.7 m^2 for U_L of 0.0155 m/s and U_g of 0.011 m/s. According to the aforementioned calculations, at steady state, the height of cells 1 and 2 in the AQUIFAS APP layout modeling is 1.77 m each and the height of cells 3, 4 and 5 are 0.59 m each (**Figure 8.1c**).

8.4.2 Nutrient Removal from Wastewater

The experimental data from the TCFBBR treating an average flow rate of 260 L/d of synthetic (phase I) and real municipal wastewater (phase II) for 65 and 45 days respectively, was used for the model evaluation. **Table 8.2a** shows the performance of the TCFBBR with respect to chemical oxygen demand (COD), attached and suspended solids (SS), nitrogen (N) and phosphorus (P) removal efficiencies and the simulated values for both riser and effluent in each phase. The composition of metal in the influent of municipal wastewater is shown in **Table 8.2b**. As noticed from **Table 8.1**, the coefficient of variation (COV) for attached biomass in the aerobic and anoxic columns in phase II are 8.9% and 4.8% respectively. Moreover the nitrification and denitrification activity per gram media based on batch tests shown **Table 8.1** demonstrate that the SNR and SDNR coefficients of variation in Phase II are 5.7% and 7.3%. Therefore, the attached biomass and biomass activity reached steady state and attainment of steady state conditions in the system in ensured.

Table 8.2. (a) Influent and effluent characteristics, experimental and modeled, in phases I and II (b) Metal composition of the influent municipal wastewater

(a)

	Phase I (Synthetic)					Phase II (Municipal)				
	Feed	Riser Exp.	Riser Simulated	Eff. Exp.	Eff. Simulated	Feed	Riser Exp.	Riser Simulated	Eff. Exp.	Eff. Simulated
TCOD (mg/L)	278±31[a]	60±18	**67**	31±16	**40.1**	398±52	101±40	**97.4**	50±21	**59.6**
SCOD (mg/L)	252±35	27±14	**28.3**	14±4	**15.8**	118±24	31±8	**36.1**	22±5	**19.8**
SBOD (mg/L)	189±26	20±10	**18.5**	9±5	**9.5**	72±14	18±4	**20.2**	11±3	**10.2**
$SCOD_{nbio}$	4					8				
TN (mg/L)	31±3.1	6.7±1.2	**7.7**	5.4±1.3	**6.0**	48±5.8	11.4±4	**10.8**	8±1.6	**9.6**
STN (mg/L)	29.6±3	4.6±1.2	**5.2**	3.9±0.8	**4.2**	31±5	7.6±2.3	**7.4**	6.1±2.1	**6.7**
NH_3-N (mg/L)	29.1±3	4.1±1.1	**4.6**	0.7±0.4	**0.43**	30±4.5	4.1±0.4	**4.0**	0.9±0.4	**0.72**
NO_3-N (mg/L)	0.5±0.2	0.5±0.2	**0.6**	2.6±0.5	**3.1**	0.8±0.3	3.2±1.9	**3.3**	5.1±1.6	**5.8**
NO_2-N (mg/L)	0.01	0.01	**0.0**	0.6±0.5	**0.7**	0.03	0.3±0.2	**0.1**	0.1±0.1	**0.2**
Alkalinity[b]						250±10	160±15	**170**	135±20	**127**
TP (mg/L)	3.1±0.3		**3.1**	2.4±0.4	**2.9**	6.5±1.4			3.2±0.6	**6.0**
PO_4-P (mg/L)	2.9±0.3	2.4±0.3	**2.6**	2.3±0.3	**2.5**	3.4±0.7	3±0.5	**5.5**	3±0.5	**5.5**
TSS (mg/L)	18±6	35±17	**34**	26±14	**34**	214±41	62±30	**51.2**	33±14	**54**
VSS (mg/L)	13±5	28±12	**28**	16±10	**23**	183±30	50±27	**43.8**	24±10	**37**
C:N:P			9:1:0.1					8:1:0.12		

[a] All the experimental values are presented as; Average ± Standard Deviation, [b] as mg $CaCO_3$ equivalent per liter

(b)

	Al(mg/L)	Ca(mg/L)	Fe(mg/L)	K(mg/L)	Mg(mg/L)	Na(mg/L)	Zn(mg/L)	S(mg/L)
Influent	0.76	59.8	5.5	12.0	12.9	64.4	0.4	0.3

As illustrated in **Table 8.2a**, TCOD removal efficiencies of 90% and 87% at a total empty bed contact time (EBCTs) of 0.93 h and organic loading rates (OLR) of 2.7±0.8 kg COD/m^3.d and 4.3±0.5 kg COD/m^3.d were observed which translate to the effluent TCOD of 31 mg/L and 50 mg/L in phases I and II respectively while the simulated TCOD in phases I and II were 40 mg/L and 59.6 mg/L. Based on the soluble effluent organic matter, simulated COD removal efficiency was 95% as compared with observed 96% in phases I and II, with effluent SBOD during both phases < 11 mg/L. As shown, the simulated final SCOD effluent in the phases I and II had less than 2% deviation from the experimental data. Comparison between the simulated and experimental TCOD and SCOD in phases I and II respectively (**Figure 8.4a** and **Figure 8.5a**), clearly show that the model prediction was within a 5% error. The two-sided t test method was conducted to compare the experimental and modeled effluent TCOD and SCOD in phases I and II.

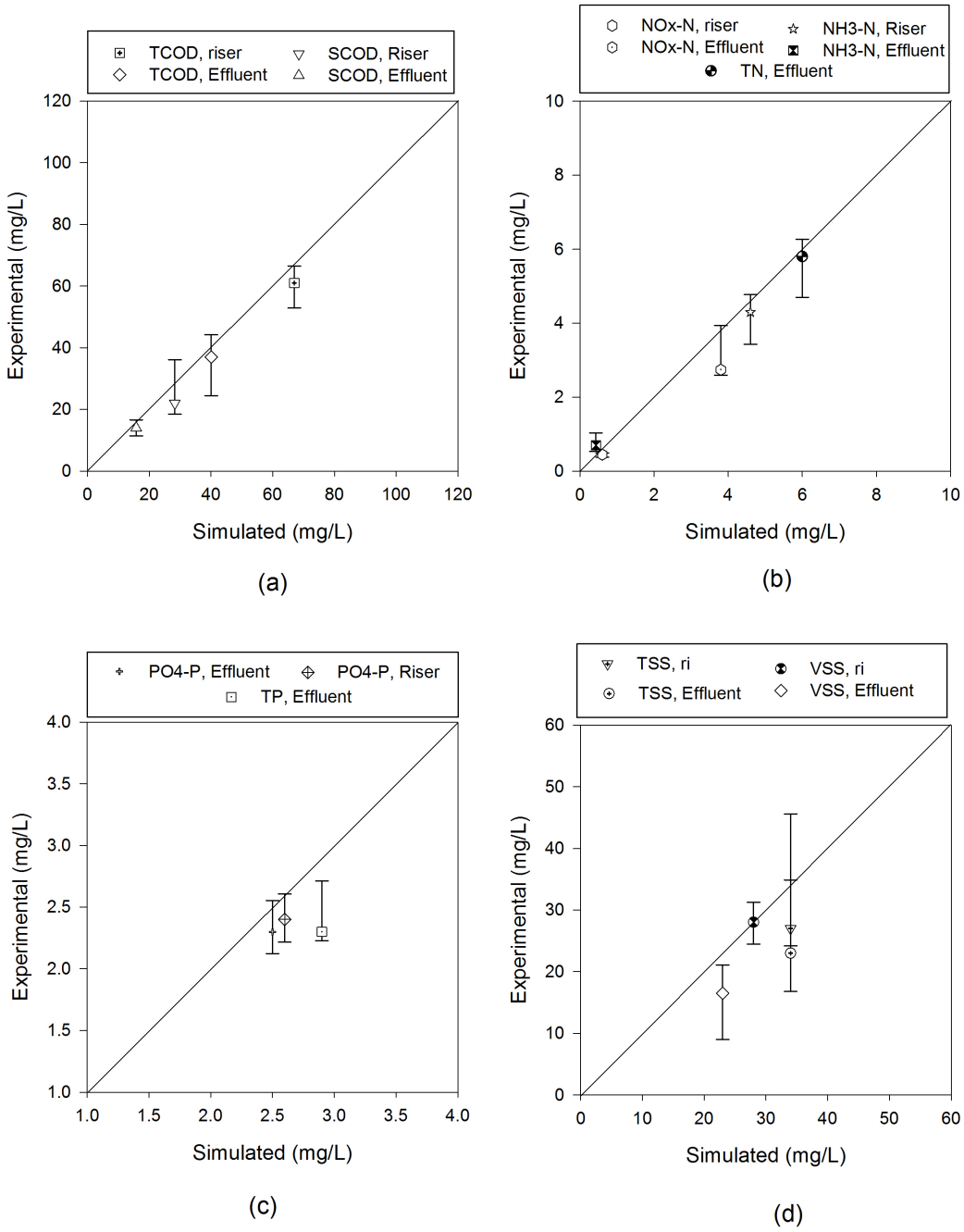

Figure 8.4. Comparison of the simulated data at top of the riser and effluent with the experimental results in phase I (synthetic wastewater) for (a) Total and soluble COD (b) Ammonia and NOx nitrogen (c) Ortho and total phosphorus (d) Total and volatile suspended solids

The null hypothesis, i. e., there are no differences between the modeled and experimental TCOD in phases I and II and SCOD in phases I and II, have been accepted on the basis of the calculated t values (2.17, 2.22 for TCOD and SCOD in phases I and II) and p values of (0.22, 0.48 for TCOD and 0.16, 0.24 for SCOD in phase I and II respectively) at a 95% confidence level. Thus, it can be concluded that there was no statistically significant difference between the experimental TCOD and SCOD, and the modeled values. Although the prediction of suspended solids in pure biofilm systems is very complicated, AQUIFAS APP simulated the VSS and TSS in the riser and downer reasonably well without an interference of a clarifier, as VSS in phase I in the riser and the downer were measured 28 mg/L and 16 mg/L whereas the simulated data was 28 mg/L and 23 mg/L. **Figure 8.4d** and **Figure 8.5d** illustrate the acceptable simulated TSS and VSS value versus the experimental value in the riser and effluent.

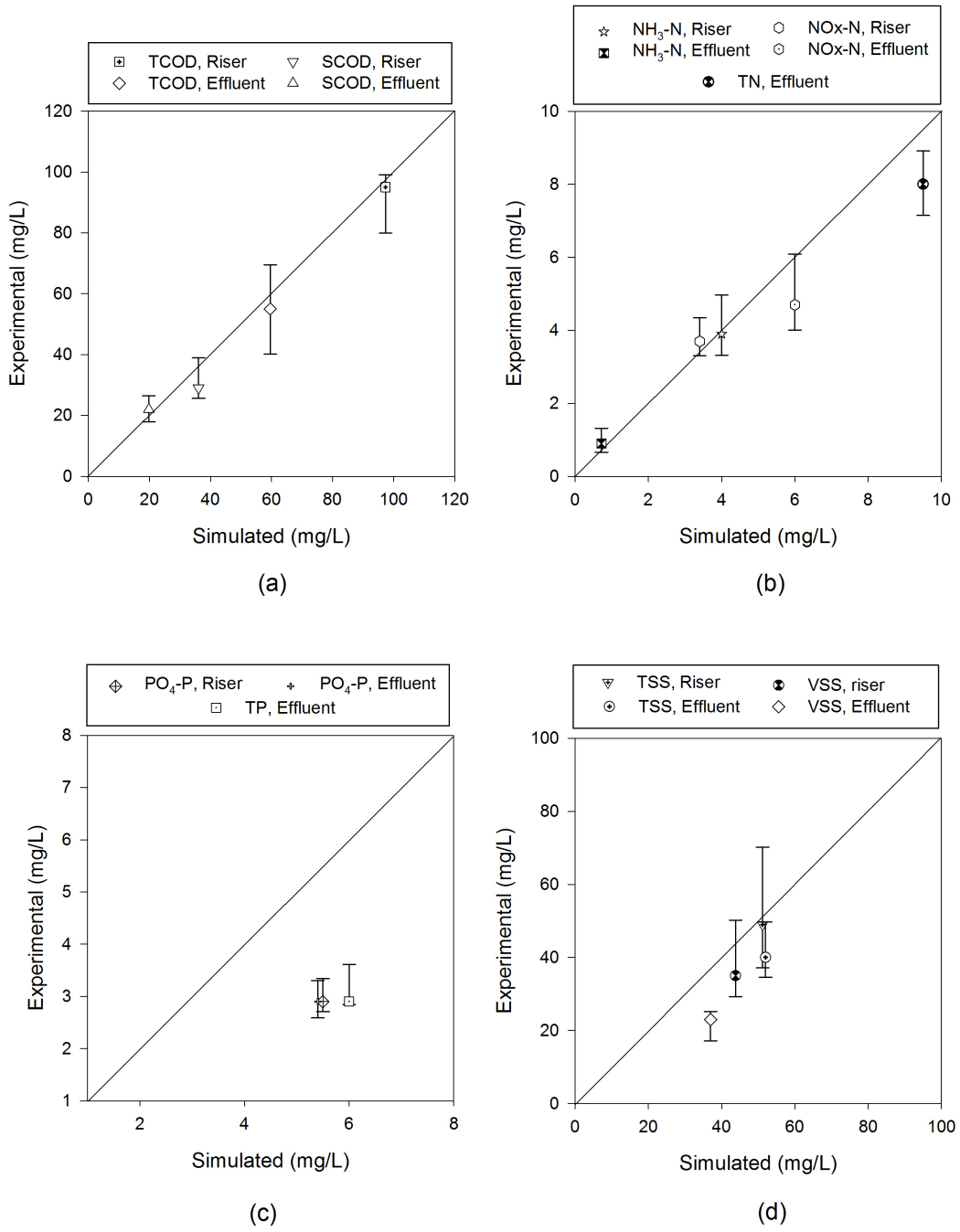

Figure 8.5. Comparison of the simulated data at top of the riser and effluent with the experimental results in phase II (synthetic wastewater) for (a) Total and soluble COD (b) Ammonia and NOx nitrogen (c) Ortho and total phosphorus (d) Total and volatile suspended solids

As shown in **Table 8.1** and **Table 8.2a**, at nitrogen loading rates (NLR) of 0.3 and 0.51 kg N/(m^3.d) in phases I and II respectively, the system achieved 84.5±1.3% TN removal in phases I and II with STN of < 4 mg/L and <6.1 mg/L in phases I and II, which met the tertiary standard limit of 10 mg/L. Interestingly the simulated data demonstrates 81%-83% nitrogen removal with effluent STN of 4.2 mg/L and 6.7 mg/L in phases I and II. As nitrogen removal is a multi cycle process including nitrification/denitrification in the downer and riser, the simulated values of NH_3-N and NO_x-N in the riser and downer distinctively show the capacity of the model to simulate the nitrogen removal of the system. The produced nitrate in the downer was recycled to the riser (anoxic column) with a recirculation flow to the feed flow ratio of 4.5-6. At an empty bed contact time of 0.22 h, effluent NO_x-N concentrations of 3.2 mg/L and 5.2 mg/L were observed in phases I and II with nitrite concentrations of 0.1-0.6 mg/L. As shown in **Table 8.2a**, **Figure 8.4b** and **Figure 8.5b**, NH_3-N and NO_x-N in the riser and effluent in phases I and II were simulated with less than 0.7 mg/L and 0.5 mg/L deviation from the experimental data. The two sided t test method was conducted with the null hypothesis, i. e., there are no differences between the modeled and experimental effluent NH_3-N in phases I and II and effluent NO_x-N in phases I and II, have been accepted on the basis of the calculated t values (2.54, 2.44 for NH_3-N and 2.17, 2.30 for NO_x-N in phases I and II respectively) and p values of (0.57, 0.67 for NH_3-N and 0.11, 0.26 for NO_x-N in phase I and II respectively) at a 95% confidence level which demonstrates that there was no statistically significant difference between the experimental NH_3-N and NO_x-N and the modeled values.

Total and ortho-phosphorus (OP) removals in phases I and II are shown in **Table 8.2a**. Approximately, 18±7% and 55±8% phosphorus removal efficiencies were observed in phases I and II at phosphorus loading rates of 0.032 and 0.06 kg P/m^3.d respectively. OP release in the riser, as the phosphorus accumulating microorganisms (PAO's) activity indicator, was insignificant, at 0.1 to 0.13 g/d throughout the tests (**Table 8.3**). As apparent from **Table 8.2a, Figure 8.4c** and **Figure 8.5c**, the model predicted OP of 2.6 mg/L and 2.5 mg/L in the riser and downer respectively while the experimental data shows 2.4 mg/L and 2.3 mg/L. The lack of PAOs and OP release is consistent with AQUIFAS APP, which did not predict the phosphorus removal while treating real

municipal wastewater. The additional phosphorus removal was found to be as a result of precipitation by predominantly calcium existing in the wastewater (**Table 8.2b**) in accordance with **Equation (8.5)**. While ASM2d model include precipitation and resolution of OP via the addition of metal salts (reactions 20 and 21 of the model) without characterizing the type of metal salt and precipitate form (Henze et al., 2000), and cannot account for precipitation with cations already present in the influent, the AQUIFAS APP ask the user to provide information the molar ratio of cation added to P precipitated. If the cation is already presented in the raw influent, the user still needs to enter the molar ratio of cation added from the influent to P precipitated, and this molar ratio can be < 1 because of the presence of cations in the influent. Because the aforementioned molar ratio was not applied in the simulation, the model failed to simulate the precipitation of OP while treating municipal wastewater.

$$10\,Ca + 6\,PO_4^{3-} + 2\,OH^- \leftrightarrow Ca_{10}(PO_4)_6(OH)_2 \qquad (8.5)$$

As mentioned before, AQUIFAS APP simulates 1d diffusion of substrate into the biofilm and biofilm thicknesses. The detailed diffusional simulation of TCFBBR runs is further discussed in 8.4.5.

8.4.3 Simulated Biomass Yield

A very low observed yield of 0.093 g VSS/g COD was observed in phase I with an average effluent VSS concentration of 16 mg/L while treating synthetic wastewater. Although there was a 38% increase in the OLR in phase II to 4.3 kg COD/(m^3.d), the observed yield increased marginally to 0.11 g VSS/g COD, a 7.8% increase compared to phase I. The long SRT of 37.8-39.6 d and also up to 54.4-62.7% influent COD consumption in the anoxic column (as shown in **Table 8.3**) rationalize the very low yield in the TCFBBR. Based on AQUIFAS APP simulation, 7.8 g VSS/d and 13.46 g VSS/d biomass were generated in phases I and II respectively. Accounting for the aforementioned produced sludge and the simulated COD removal of 68.172 g COD/d and 98.332 g COD/d in phases I and II , the simulated biomass yield were calculated 0.11 g VSS/g COD and 0.13 g VSS/g COD in phases I and II respectively approximately 15% higher than observed experimentally.

Table 8.3. Nutrient mass balance in Phases I and II

(g/d)	Mass in Inf.	Mass consumed	Mass Utilized	Mass in Eff.	Mass wastage	Percent closure
		Anoxic	Aerobic			
Phase I-Synthetic WW (260 L/d)						
TCOD	69.8±2.5			6±1.4	0.9[a]±0.01	98.0[1]
(sCOD)	64.6±1.1	38.6±3.5 (17.8)[d]	22.9±3.1	2.7±1.0		
TN	7.8±0.6	(17.5)[e]		1.45±0.3	0.12[b]±0.0	90.6[2]
NH_4-N	7.6±0.6	0.9±0.6 (0.17)[f]	5.6±0.9	0.15±0.8		
NO_3-N	0.18±0.03	5.4±0.3	-5.5±0.2	0.78±0.3		
NO_2-N	0.0±0.0	0.15±0.02	-0.18±0.03	0.04±0.01		
TP	0.8±0.1			0.66±0.1	0.021[c]±0.01	92.7[3]
PO_4-P	0.74±0.04	-0.1±0.1	2.5±0.7	0.5±0.02		
Phase II-Municipal WW (260 L/d)						
TCOD	108.8±10			12.1±3.4	2.48[a]±0.2	97.8[1]
(sCOD)	33.5±6.9	50.1±9.3 (26.6)[d]	42±11.2	5.0±0.5		
TN	11.4±2.1	(18.5)[e]		1.87±0.5	0.21[b]±0.05	89.6[2]
NH_4-N	7.8±1.4	1.2±0.08 (0.26)[f]	8.0±1.1	0.3±0.1		
NO_3-N	0.15±0.07	7.6±0.4	-7.7±0.35	1.1±0.5		
NO_2-N	0.0±0.0	-0.34±0.3	0.3±0.3	0.03±0.02		
TP	1.89±0.3			0.85±0.1	0.034[c]±0.01	50.1[3]
PO_4-P	1.0±0.04	-0.13±0.03	2.4±0.6	0.78±0.03	0.8[j]	89.1[5]
Alkalinity	64±1.4	-26.8[h]±1.3	55.4[i]±8	44±3.7		93.3[4]

[a,b,c] COD equivalent, Nitrogen (N) and phosphorus (P) content of 1 g biomass were measured 1.48±0.08, 0.094±0.01 and 0.018±0.05 g respectively.

[d] SCOD consumption through denitrification based on equation (6); for example Phase I $= 5.4 \times \frac{2.86}{1 - 1.42 \times 0.093}$

[e] Aerobic SCOD consumption in the riser; for example Phase I $= \frac{\Delta O_2}{\Delta t} \times (1 - Y_H)^{-1} = 0.0018 \frac{g O_2}{l} \times (10.7 + 1 + 4.5) \times 260 \frac{l}{d} \times (1 - 0.4 \times 1.42)^{-1}$

[f] Nitrogen assimilated for denitrification; for example Phase I $= 5.4 \times \frac{2.86}{1 - 1.42 \times 0.093} \times 0.093 \frac{gVSS}{gSCOD} \times 0.1 \frac{g\,N}{g\,VSS}$

[h] Alkalinity generated in the anoxic column; for example Phase II $= 7.7\,g\,N_{denitrified} \times 3.57 \frac{g\,Alk_{generated}}{g\,N}$

[i] Alkalinity consumed in the aerobic column; for example Phase II $= 7.7\,g\,N_{nitrified} \times 7.14 \frac{g\,Alk_{consumed}}{g\,N}$

[j] The value of phosphorus precipitated based on MINTEQ software (Felmy et al., 1985)

[1] COD % closure $= \frac{38.6 + 22.9 + 6 + 0.91}{69.8} \times 100$ [2] Nitrogen % closure $= \frac{1.45 + 5.5 + 0.12}{7.8} \times 100$

[3] Phosphorus % closure $= \frac{0.66 + 0.021}{0.8} \times 100$ [4] Alkalinity % closure $= \frac{64 - (55.4 - 26.8)}{44} \times 100$

[5] Phosphorus % closure with precipitation $= \frac{0.85 + 0.034 + 0.8}{1.89} \times 100$

8.4.4 Specific Nutrient Uptake Rate by Biomass

Table 8.3 illustrates the steady state mass balances for COD, TN, NH_3-N, NO_3-N, NO_2-N, TP, PO_4-P and alkalinity for phases I and II where positive values indicate removal and negative values denote generation. The mass balances were based on the

experimental data for the influent, anoxic and final effluent characteristics, recirculation flows and the sludge wastage for each phase individually. As shown in **Table 8.3**, mass balance closures of 98.0% and 97.8% for COD, 90.6% and 89.6% for nitrogen, 92.7% and 97.8% for phosphorus and 93.3% for alkalinity were observed in phases I and II respectively.

COD consumption the anoxic riser on was observed to account for 53%-58% of overall removal. The relatively high percentage of COD removal in the anoxic column (as compare to 25 to 40% in an activated sludge plant) was due to the denitrification process COD uptake as well as aerobic utilization as a result of DO recirculation from the aerobic column whereas the predominant COD removal in the aerobic zone was due to aerobic heterotrophic utilization. The measured COD consumption in the riser in phases I, II agree with the calculated COD consumption (**Table 8.3**) within 90.1%-94.5% accuracy. **Figure 8.6a** and **Figure 8.6b** show the simulated COD uptake rates by biofilm in different cells of phases I and II versus the average of mass balanced. The simulated overall COD uptake rate in the anoxic column were 37 g COD/d and 40 g COD/d in phase I and II whereas the mass balance show 32 g COD/d and 41.7 g COD/d. The simulated COD uptake in aerobic column in phases I and II were 30 g COD/d and 49 g COD/d whereas the mass balance showed 29 g COD/d and 43 g COD/d (**Table 8.3**).

As shown in **Figure 8.6c** and **Figure 8.6d**, the simulated nitrification rate in the biofilm was as 0.7 g NH_3-N/d and 0.8 g NH_3-N/d in the riser in phases I and II and the mass balance show 0.9 g NH_3-N/d and 1.2 g NH_3-N/d Nitrification in the riser (**Table 8.3**). The model calculates an overall biofilm nitrification rate of 6.2 g NH_3-N/d and 8.7 g NH_3-N/d in phase I and II in agreement with the mass balance which show 5.6±0.9 g NH_3-N/d and 8.0±1.1 g NH_3-N/d in phase I and II respectively. The simulated denitrification rates (**Figure 8.6e** and **Figure 8.6f**) in phases I and II (5.1 g N/d and 7.0 g N/d) also agreed with the mass balance values of 5.4±0.3 g NO_3-N/d and 7.6±0.4 g NO_3-N/d (**Table 8.3**).

Phosphorus removal was found to be due mainly to the biomass assimilation. However as mentioned earlier, additional phosphorus removal was observed while

treating the municipal wastewater. As a result, the phosphorus mass balance closure in phase II as shown in **Table 8.3** dropped to 50.1%.

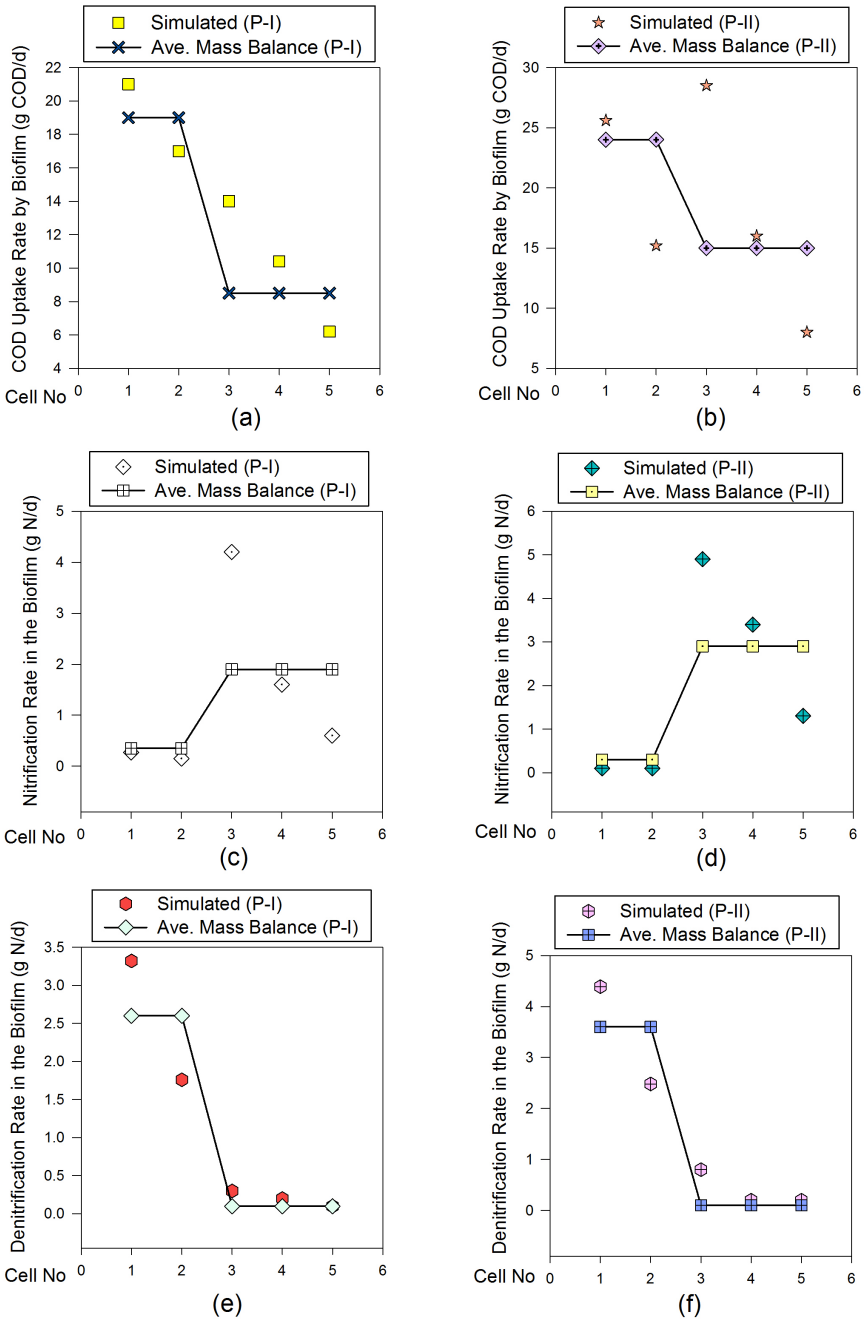

Figure 8.6. Comparison between simulated COD uptake, nitrification and denitrification rates in each cell and that calculated based on overall mass balance demonstrated in **Table 8.3**.

The phosphorus precipitated in the columns and on the carrier media and was not accounted while doing mass balance so the mass balance showed 50% closure (**Table 8.3**). It is worth mentioning that no significant changes in total solids and attached biomass of the TCFBBR were noticed in this study. The precipitation of the inorganic metal phosphates and its strong adherence to media resulted in an accumulation of P in the system, unaccounted for in the mass balance. Assuming the entire unaccounted soluble phosphorus (approximately 1.7 mg/L) was removed by the calcium, based on equation (5) it would have generated around 2.3 g of $Ca_{10}(PO_4)_6(OH)_2$ per day, translating to approximately 270 g of solids over the study period or <2.5% of the media mass.

8.4.5 Simulated Substrate Profiles Inside the Biofilm

Figure 8.7 shows the simulated concentration gradients of NH_4-N, NO_x-N, DO, $SCOD_{bio}$ in the biofilm in different cells of phases II as well as the biofilm thicknesses in each cell. The overall biofilm was divided into twelve layers to simulate the substrate concentrations in each layer. It is clear in both phases that a much higher concentration gradient is observed for different substrate in cells 1 and 2 where the biofilm thickness is significantly higher. Moreover, it can be seen that NOx-N is limited substrate inside the anoxic biofilm (cells 1 and 2) whereas there is not any substrate limitation observed inside the aerobic biofilms (cells 3, 4 and 5). The trend of nitrate production in the aerobic biofilm is noticeable in cells 3, 4 and 5 whereas the concentration of ammonia in the anoxic biofilm remains almost the same (cells 1 and 2).

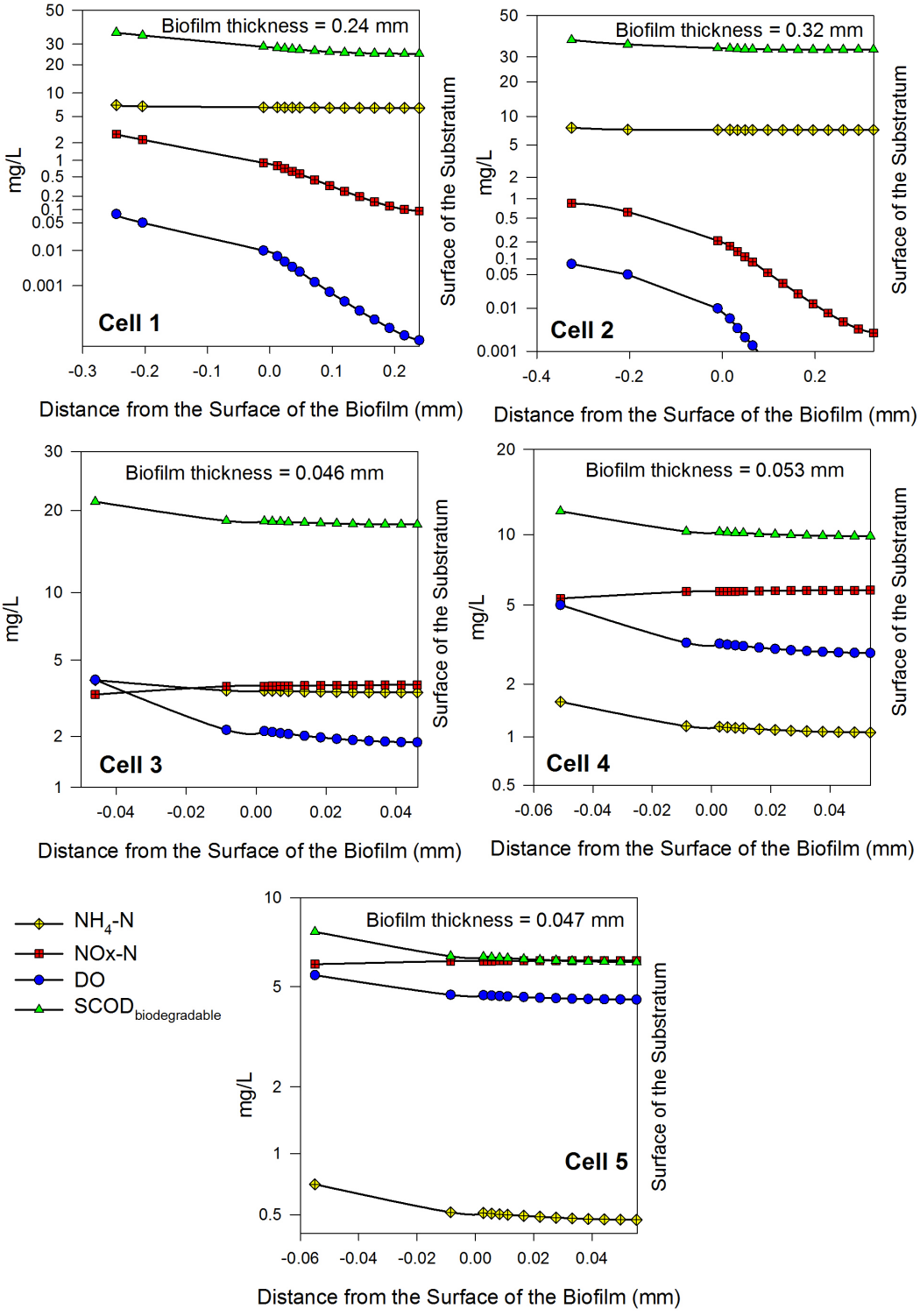

Figure 8.7. Substrate concentration profile within the biofilm in different cells

8.5 Conclusions

A two and three-phase fluidized bed model which predict SSA and the volume of the expanded bed based on changes in the biofilm thickness and the operational data, was applied and linked to AQUIFAS APP to simulate the nutrient removal efficiencies in fluidized bed bioreactors. The proposed model and its credibility were examined and verified using a twin circulating fluidized bed bioreactor comprises of an aerobic and an anoxic column for nutrient removal from municipal wastewater. Two-sided t test showed that there were no statistically significant difference between the experimental and the modeled TCOD, SCOD, NH_3-N, NO_x-N. A comparison between the experimental mass balance and the simulated carbon and nitrogen uptakes through nitrification and denitrification in each column further demonstrated the plausibility of the AQUIFAS APP integrated with the fluidization model.

8.6 References

[1] Atkinson AB, Davis DL. The Overall Rate of Substrate Uptake (reaction) by Microbial Films –Part I - A Biological Rate Equation. Chem. Eng. Res. Des. 1974; 52:248-254.

[2] Shieh WK, Keenan JD. Fluidized bed biofilm reactor for wastewater treatment, Adv. Biochem. Eng. Biotechnol. 1986; 33:131-169.

[3] Bae W, Rittmann BE. A structure model of dual-limiting kinetics. Biotechnol. Bioeng. 1996; 49:683-689.

[4] Wanner O. A multispecies biofilm model. Biotechnol. Bioeng. 1986; 28:314-328.

[5] Wanner O, Gujer W. Competition in biofilms. Wat. Sci, Tech. 1984; 17:27-44.

[6] Reichert P. AQUASIM- a tool for simulation and data analysis of aquatic systems. Wat. Sci. Tech. 1994; 30:21-30.

[7] Xavier JB, Picioreanu C, van Loosdrecht MCM. A framework for multidimensional modeling of activity and structure of multispecies biofilms. Environ. Microb. 2005; 7-8:1085-1103.

[8] Sen D, Randall CW. Improved computational model (AQUIFAS) for activated sludge, integrated fixed-film activated sludge and moving bed biofilm reactor systems, part 1: Semi-empirical model development, Wat. Environ. Res. 2008a; 80:439-453.

[9] Sen D, Randall CW. Improved computational model (AQUIFAS) for activated sludge, integrated fixed-film activated sludge and moving bed biofilm reactor systems, part II: Multilayer biofilm diffusional model, Wat. Environ. Res. 2008b; 80:624-631.

[10] Sen D, Randall CW. Improved computational model (AQUIFAS) for activated sludge, integrated fixed-film activated sludge and moving bed biofilm reactor systems, part III: Analysis and verification, Wat. Environ. Res. 2008c; 80:633-645.

[11] Henze M, Gujer W, Mino T, van Loosdrecht MCM. Activated Sludge Models ASM1, ASM2, ASM2d and ASM3.Scientific and Technical Report No. 9. IWA Publishing, London. 2000.

[12] Picioreanu C, van Loosdrecht MCM, Heijnen JJ. Mathematical modelling of biofilm structure with a hybrid differential-discrete cellular automaton approach. Biotechnol. Bioeng. 1998; 58**:**101–116.

[13] Picioreanu C, van Loosdrecht MCM, Heijnen JJ. Effect of diffusive and convective substrate transport on biofilm structure formation: a two-dimensional modeling study. Biotechnol. Bioeng, 2000b; 69:504–515.

[14] Picioreanu C, Kreft JU, van Loosdrecht MCM. Particle-based multidimensional multispecies model. Appl. Environ. Microbiol. 2004: 70:3024–3040.

[15] Lee MW, Park JM. One-dimensional mixed-culture biofilm model considering different space occupancies of particulate components. Wat. Res. 2007; 41:4317-4328.

[16] Plattes M, Henry E, Schossler PM. A zero-dimensional biofilm model for dynamic simulation of moving bed bioreactor systems: Model concepts, Peterson matrix and application to a pilot-scale plant. Biochem. Eng. J. 2008; 40:392-398.

[17] Chowdhury N, Nakhla G, Zhu J. Load maximization of a liquid-solid circulating fluidized bed bioreactor for nitrogen removal from synthetic municipal wastewater. Chemosphere, 2008; 71:807-815.

[18] APHA; AWWA; WEF. Standard methods for the examination of water and wastewater. 20th Edition, American Public Health Association, Washington D.C. 1988.

[19] Andalib M, Zhu J, Nakhla G. Terminal Settling Velocity and Drag Coefficient of Biofilm-Coated Particles at High Reynolds Numbers. AICHE, 2010; 56-10:2598-2606.

[20] Ngian KF, Martin WRB. Bed expansion characteristics of liquid fluidized particles with attached microbial growth. Biotechnol. Bioeng. 1980; 22:1843–1856.

[21] Yu H, Rittmann BE. Predicting bed expansion and phase holdups for three-phase fluidized-bed reactors with and without biofilm. Wat. Res. 1997; 31-10:2604-2616.

[22] Shieh WK, Mulcahy LT, LaMotta EJ. Mathematical model for the fluidized bed biofilm reactor. 1982; 4:269-275.

[23] Grady Jr. CPL, Daigger GT, Lim HC. Fluidized bed biological reactors, in: Biological wastewater treatment, Second ed., Marcel Dekker Inc., New York, pp. 809-842. 1999.

[24] Mulcahy LT, Shieh WK. Fluidization and reactor biomass characteristics of the denitrification fluidized bed biofilm reactor. Wat. Res. 1987; 21:451-458.

[25] Ro KS, Neethling JB. Terminal settling velocity of bioparticles. Res. J. Water Pollut. Cont. Fed. 1990; 62:901–906.

[26] Nicolella C, van Loosdrecht MCM, Di Felice R, Rovatti M. Terminal settling velocity and bed expansion characteristics of biofilm-coated particles. Biotechnol. Bioeng. 1999; 62:63–70.

[27] Sen D, Randall CW, Copithorn RR, Huhtamaki M, Farren G, Flournoy W. Understanding the importance of aerobic mixing, biofilm thickness control and modeling on the success or failure of IFAS systems for biological nutrient removal. Wat. Prac. 2007; 1-5:1-18.

[28] Boltz JP, Johnson BR, Daigger GT. Modeling integrated fixed-film activated sludge (IFAS) bioreactors I: mathematical treatment and model development. Wat. Enviro. Res. 2009; 81:555-562.

9 Comparative Modeling of BNR from Landfill Leachate Using CFBBR

9.1 Introduction

Landfill leachate is very complex due to large recalcitrant organic molecules, long leachate age, and low biodegradable organics concentration, high COD and ammonium content, low carbon to nitrogen ratio, and the presence of heavy metals and toxic components. [1, 2, 3, 4] Compared to conventional physical, chemical, and biological treatment processes for industrial wastewater, the circulating integrated fluidized bed bioreactor (CFBBR) system has numerous advantages including small footprint with elimination of clarifiers, high biomass retention resulting in long solids residence time (SRTs) and relatively short hydraulic retention time (HRTs), enhanced mass transfer, and lower sludge production rate.

Biological nutrient removal (BNR) from municipal wastewater and landfill leachate has been reported by Nakhla and coworkers [5, 6] using pilot-scale CFBBR. The CFBBR employs attached microbial films resulting from biodegradation of both organics and nutrients within an integrated system comprising an anoxic column in a fast fluidization regime and an aerobic column in a conventional fluidization regime. This new promising patented technology combines the compactness and efficiency of a fixed-film process with excellent organics, nitrogen, and phosphorus removal efficiencies of 85%, 80%, and 70%, respectively, and reduced sludge yields of 0.15 g VSS/g COD as compared with 60%-70% COD and 70%-74% nitrogen removal efficiencies achieved by upflow anaerobic sludge blanket (UASB) and moving bed bioreactor (MBBR), respectively. [7, 8, 9, 10, 11, 12]

Several mathematical mixed culture biofilm models have been published and presented over the past 20 years. [13, 14] These models vary in complexity from simple analytical models to multi and three-dimensional (3D) dynamic models in order to solve the mass balance differential equations between the biofilm and various particulate and

dissolved components of microbial cells, extracellular polymeric substance, organic and inorganic particles, nutrients, electron acceptors, and electron donors as a function of transport and transformation processes. [13] For the specific purpose of engineering design and analysis, a balance between the simplified and complex mechanistic approach is required. One-dimensional (1-D) fully dynamic and steady state simulation models are widely used to simulate the full-scale wastewater treatment plant (WWTP) such as the stratified dynamic multi-species model introduced and implemented in the AQUASIM software [13, 15, 16, 17, 18] and Activated Sludge Models (ASM1, ASM2, ASM2d, ASM3) introduced by International Water Association (IWA). [19] The IWA model is available in several user-friendly forms, the most common of which are the Simba® (Ifak GmbH, Magdeburg, Germany), ASIM® (EAWAG, Switzerland), EFOR® (DHI Inc., Denmark), BioWin® (Envirosim Associates Ltd., Burlington, ON), GPS-X® (Hydromantis Inc., Hamilton, ON), AQUIFAS® (Aquaregen, Mountain View, CA), Pro-2D® (CH2M HILL, Inc., Colorado, US), STOAT® (WRc, Wiltshire, England), and WEST® (Mostforwater, Belgium). However, Simba®, ASIM®, and EFOR® are only developed for the suspended growth municipal wastewater treatment plants while BioWin®, GPS-X®, AQUIFAS®, Pro-2D®, STOAT®, and WEST® are developed for both suspended and attached growth systems.

BioWin® and AQUIFAS® developed a fixed film model and successfully simulated the integrated fixed-film activated sludge (IFAS) process, moving bed biofilm reactor (MBBR), and biological aerated filter (BAF) systems for municipal wastewater treatment plants using a wide range of BOD loadings and biofilm thicknesses. [20, 21, 22, 23, 24, and 25] The developed models improved the accuracy of diffusional models by evaluating results against semi-empirical data based on experimental measurements from different full-scale WWTPs. For example, fluxes and thicknesses computed by biofilm diffusional modeling could be corrected based on the experimental measurements.

In a fluidized bed bioreactor, simulating the effective volume of the reactor (expanded bed) as a function of biofilm thickness and recirculation flows is challenging due to the complex hydrodynamics involving changing biofilm thicknesses, varying detachment and attrition rates whereas in the IFAS and MBBR detachment and attrition effects are

minimal. Moreover, the characteristics of wastewater have a considerable effect on the growth rate of attached biomass and biofilm thickness. Particularly, in case of landfill leachate with C/N ratio of 3:1, total chemical oxygen demand to violate suspended solids (TCOD/VSS) ratio of 8:1 and total biochemical demand to total chemical oxygen demand (TBOD/TCOD) of 0.44, simulation of biological nutrient removal using fluidized bed bioreactors is challenging as a result of biodegradable carbon limitation and biofilm growth limitations. However, none of the aforementioned software is designed to model fluidized bed bioreactors as a function of effective volume of the reactor, biofilm thickness limitation, and recirculation flows. In addition, the comprehensive literature review using web of Science® and Google Scholar®, as a search engines, with a keywords of landfill leachate, biological nutrient treatment, and modeling demonstrated that no models are readily available that can accurately predict biological nutrient removal from landfill leachate in a biofilm systems.

Thus, comparative modeling of CFBBR system treating landfill leachate was performed using calibrated BioWin® and AQUIFAS ® software. The primary goal of this study was to develop a model to simulate the CFBBR system during the treatment of landfill leachate. In addition to evaluating and comparing the CFBBR performance using both commercially available simulation models during the treatment of a high ammonia and very low carbon to nitrogen landfill leachate. This study also aimed at evaluating the biofilm and biomass prediction in the anoxic and aerobic columns and verifying the calibrated models by increasing the loading rates, reducing the empty bed contact time (EBCT), and decreasing the hydraulic retention time.

9.2 Materials and Methods

9.2.1 Liquid Solid Circulating Fluidized Bed Bioreactor

Experiments were conducted in a pilot-scale CFBBR with an anoxic compartment (riser) followed by aerobic compartment (downer) and recirculation lines between downer and riser as shown in **Figure 9.1** to treat landfill leachate collected from the W12A Landfill in London, Ontario, Canada. **Table 9.1** illustrates the leachate,

characterized predominantly by a carbon to nitrogen ratio of 3:1, TCOD/VSS ratio of 8:1 and TBOD/TCOD of 0.44.

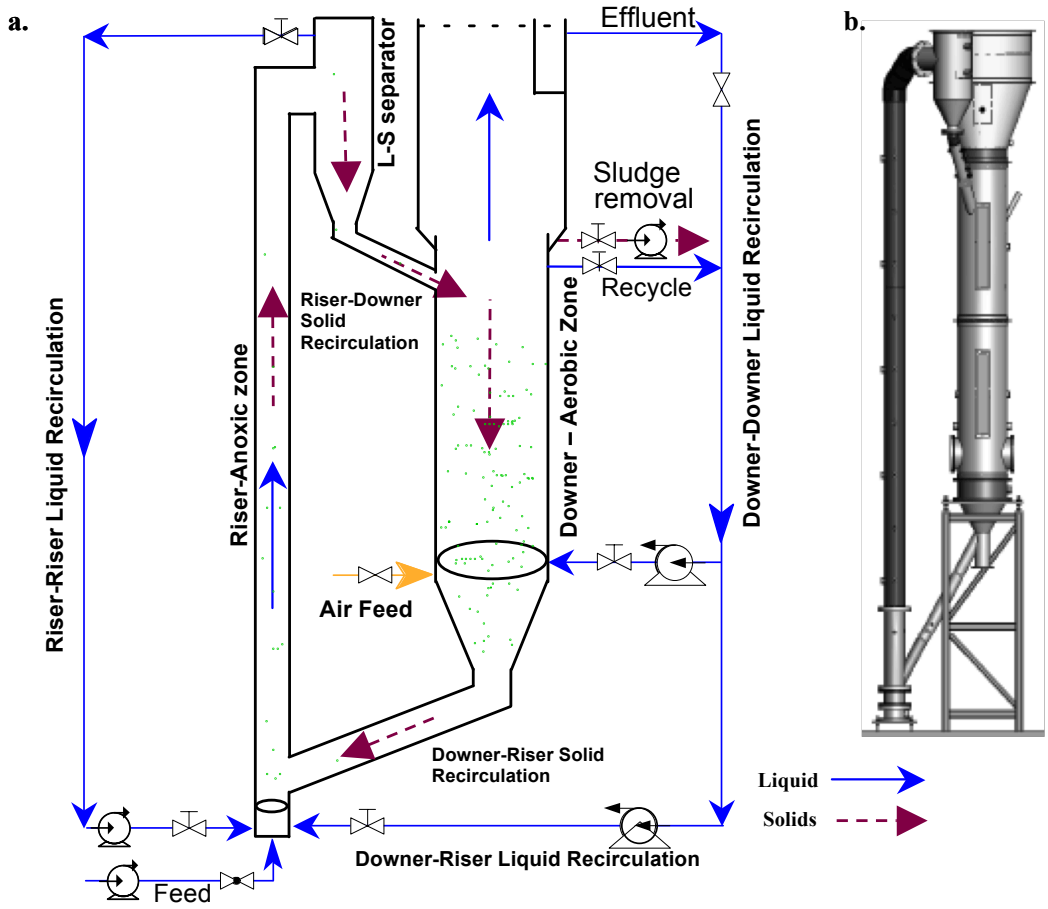

Figure 9.1. (a) Schematic and (b) 2-D view of the pilot-scale CFBBR

Table 9.1. Influent and effluent characteristics for different phases

Parameter	Experimental influent characteristics*	BioWin® model influent characteristics**	Effluent*	
			Phase I	Phase II
pH	7.9-8.8	**8.40**	7.2-8.2	7.6-8.1
Alkalinity**	1619±52	**1619**	323±71	296±57
COD (mg/L)	1259±77	**1300**	197±46	302±98
SCOD (mg/L)	1025±27	**1058**	153±43	245±85
NH_4-N (mg/L)	360±59	**349**	35.4±13.1	54.7±11.2
NO_3-N (mg/L)	3.1±1.5	**3.1**	59.9±31.1	63.9±10.3
TKN (mg/L)	392±64	**392**	49±15	92±23
PO_4-P (mg/L)	3.4±1.1	**3.8**	1.0±0.2	1.2±0.5
TP (mg/L)	6.2±1.3	**7**	1.7±0.3	2.0±0.6
TSS (mg L)	263±42	**270**	60±13	58±8
VSS (mg/L)	156±30	**163**	37±5	44±8
BOD (mg/L)	565±121	**687**++	83±13	98±18
SBOD (mg/L)	402±83	**684**++	35±8	40±12

*Average ± SD of a number of samples 8-12 with a frequency of a sample every 4 days;
**(mg $CaCO_3$/L)
++ Higher than the experimental data due to the BioWin® influent specifier limitations

The pilot-scale facility was developed based on the lab-scale experiments reported by Cui et al., 2004 [26], Patel et al. 2006 [27], and Chowdhury [28] et al. 2008. **Table 9.2** shows the detailed operational conditions and reactor design parameters of the CFBBR; further details of the reactor and operational conditions are presented elsewhere. [6, 28]

Lava rock particles with an average diameter of 600 μm (300-1000 μm) were used as the carrier media for biofilm attachment in the CFBBR. The particle porosity was about 33% and the total porosity (particle porosity and voids between particles) was 61%. The bulk density (considering packed media filled with water) of particles was approximately 1720 kg/m^3, with true density (the ratio of sample mass to its true volume) of 2560 kg/m^3 and a high specific surface area of 10,950 m^2/m^3.

Table 9.2. Operating conditions

		Phase I	Phase II
Influent flow, Q_{in} (L/d)		720±35	864±35
Average organic loading (kg COD/(m^3·d))		2.15	2.60
Average nitrogen loading (kg N/(m^3·d))		0.68	0.81
Average phosphorus loading (kg P/(m^3·d))		0.014	0.016
Riser-Riser recirculation ratio ($Q_{r\text{-}r}/Q_{in}$)		62	52
Downer-Riser recirculation ratio ($Q_{d\text{-}r}/Q_{in}$)		31	26
Downer-Downer recirculation ratio ($Q_{d\text{-}d}/Q_{in}$)		70	58
Empty Bed Contact Time (d)*	Anoxic	0.11	0.09
	Aerobic	0.38	0.32
Nominal HRT (d)**	Anoxic	0.07	0.06
	Aerobic	0.25	0.21
Avg. attached biomass (mg VSS/g lava rock)	Anoxic	16.3	18.7
	Aerobic	5.9	7.3
Biomass (g VSS)	Anoxic	2037.5	2337.5
	Aerobic	2504.9	3081.7
Food/microorganisms ratio (g COD/g VSS·d)		0.20	0.21
Detachment rates (d^{-1})	Anoxic	0.127[a]	0.132
	Aerobic	0.122[a]	0.127
Estimated SRT (d)	Anoxic	17[b]	13
	Aerobic	21	18
	Overall	38[c]	31

*EBCT = Vcompact/Q; **Nominal HRT = EBCT × (1- compact bed porosity)

[a] $Detachment\ \ rates(b^{'}) = \frac{QX_1}{MX_m}$

[b] $SRT_{anoxic} = SRT_{Total}\frac{M_{anoxic}X_{anoxic}}{M_{aerobic}X_{aerobic}+M_{anoxic}X_{anoxic}}$

[c] $SRT_{Total} = \frac{M_{aerobic}X_{aerobic}+M_{anoxic}X_{anoxic}}{Q_{effluent}VSS_{eff}+X_{wastage}}$

The CFBBR was started with 125 and 421 kg of fresh lava rock particles with the corresponding compact bed volumes of 80 L and 277 L in the riser and the downer respectively. The amount of particles was determined considering the observed nitrification-denitrification rates of 0.14 g N/g VSS·d and 0.62 g N/g VSS·d respectively and attached biomass of 15-39 mg VSS/g lava rock in the lab-study. [28, 29] The observed

attached biofilm thicknesses on the aerobic and anoxic biofim-coated particles in the pilot-study were 120 and 600 µm. The comparatively thin biofilm of the aerobic particles was mainly due to the higher abrasion and agitation generated by air, injected at the bottom of the aerobic column. The overall volume of the anoxic reactor, aerobic reactor, liquid-solids separator, and final clarifier were 0.19, 0.58, 0.06, and 0.30 m^3 respectively. The pilot-scale reactor was inoculated with enriched nitrifiers, acclimatized in the lab using return activated sludge from the Adelaide Pollution Control Plant, London, Canada, with further startup details presented elsewhere. [28, 29]

9.2.2 Analytical Methods

Influent, anoxic bed effluent, and final effluent samples were collected in airtight bottles twice a week, and refrigerated at 4°C prior to analysis. Total suspended solids (TSS), volatile suspended solids (VSS), 5-days biological oxygen demand (BOD), and total Kjeldahl nitrogen (TKN) were analyzed according to the Standard Methods. [30]

Dissolved oxygen (DO) in the CFBBR downer was measured using Thermo Orion (810 A+) meter. HACH methods and testing kits (HACH Odyssey DR/2500) were used to measure TCOD, soluble chemical oxygen demand (SCOD), and total phosphorus (TP). NH_4, NO_2, NO_3, and PO_4 were measured using ion chromatography (IC, Dionex 600, USA) equipped with CS16-HC and AS9-HC columns. The biofilm thickness of the CFBBR particles was measured using a microscope (SteREO Discovery V8, Carl Zeiss, Inc, Germany) coupled with a camera (Axio Cam HR, 13 MP, Carl Zesis, Germany), at a magnification of 80X.

Attached biomass on the support media was examined according to Standard Methods (APHA, 1998) and expressed as mg VSS/g clean particles. Approximately 4-5 g biofim-coated particles were taken from each of the two columns, suspended in a 50 mL vial, and sonicated for 3 h at 30°C in an Aquasonic sonicator (Model 75HT, ETL Laboratory Testing, Inc., New York). After sonication, the VSS content of the detached biomass was measured using Standard Methods [30] and the sonicated particles were cleaned and weighted after drying at 550°C for 1 h. The paired student t-test was conducted to

determine the statistical significance of the observed differences between the experimental data at the 95% confidence level.

9.3 Modeling and Simulation

The experimental results of the pilot-scale CFBBR were modeled and calibrated using BioWin® (3.0) software developed by Envirosim Associates Ltd. (Burlington, ON, Canada) and AQUIFAS® (AQUANET) software developed by Aquaregen (Mountain View, CA, US). Modeling of particulate attached growth systems using both software for simulation of the complex interactions that occur in the anoxic riser and aerobic downer biofilm reactors [19] was based on general Activated Sludge models i.e. ASM1, ASM2d, and ASM3. [31, 32, 33]

9.3.1 Modeling Using BioWin®

BioWin® is developed to model biofilm systems as 1-D fully dynamic and steady-state simulations using a wide range of BOD loading, biomass, and biofilm thickness evaluated against semi-empirical data based on experimental measurements from a full-scale WWTPs. The influent characteristics of the landfill leachate, simulated using the influent specifier associated with BioWin® revealed the carbonaceous and nutrient fractions summarized in **Table 9.1** and **Table 9.3** illustrating the simulated landfill leachate characterization compared to the experimental leachate characterization confirm the validity of the specification of various organic and nutrient fractions (**Table 9.3**) as reflected by the close agreement between all water quality parameters of COD and BOD.

Table 9.3. Carbonaceaous and nutrient fraction estimated for wastewater and assumed for landsill leachate in BioWin

Fraction (abbreviation)	Unit	Default[a]	Input[b]
Readily biodegradable (F_{bs})	gCOD/g TCOD	0.16	**0.694**[1]
Acetate (F_{ac})	gCOD/g rbCOD	0.15	**0.15**
Non-colloidal slowly biodegradable (F_{xsp})	gCOD/g sbCOD	0.75	**0.05**[2]
Unbiodegradable soluble (F_{us})	gCOD/g TCOD	0.05	**0.12**[3]
Unbiodegradable particulate (F_{up})	gCOD/g TCOD	0.13	**0.185**[4]
Ammonia (F_{na})	gNH_3-N/gTKN	0.66	**0.89**[5]
Particulate organic nitrogen (F_{nox})	gN/g Organic N	0.5	**0.25**[6]
Soluble unbiodegradable TKN (F_{nus})	gN/gTKN	0.02	**0.02**
N:COD ratio for unbiodegradable part. COD (F_{upN})	gN/gCOD	0.035	**0.035**
Phosphate (F_{po4})	gPO_4-P/gTP	0.5	**0.548**[7]
P:COD ratio for influent unbiodegradable part. COD (F_{upP})	gP/gCOD	0.011	**0.011**
Non-poly-P heterotrophs (FZ_{bh})	gCOD/g TCOD	0.0001	**0.0001**
Anoxic methanol utilizers (FZ_{bm})	gCOD/g TCOD	0.0001	**0.0001**
Ammonia oxidizers (FZ_{aob})	gCOD/g TCOD	0.0001	**0.0001**
Nitrite oxidizers (FZ_{nob})	gCOD/g TCOD	0.0001	**0.0001**
Anaerobic ammonia oxidizers (FZ_{amob})	gCOD/g TCOD	0.0001	**0.0001**
PAOs (FZ_{bp})	gCOD/g TCOD	0.0001	**0.0001**
Propionic acetogens (FZ_{bpa})	gCOD/g TCOD	0.0001	**0.0001**
Acetoclastic methanogens (FZ_{bam})	gCOD/g TCOD	0.0001	**0.0001**
H_2-utilizing methanogens (FZ_{bhm})	gCOD/g TCOD	0.0001	**0.0001**

[a] Default of municipal wastewater fractions

[b] Calibrated using the experimental data

[1] Fraction of TCOD which is readily biodegradable [(soluble readily biodegradable complex COD (S_{bsc}) + soluble readily biodegradable volatile fatty acid COD (S_{bsa})) / TCOD]

[2] Fraction of slowly biodegradable influent COD which is particulate [Slowly biodegradable particulate COD (X_{sp}) / (slowly biodegradable colloidal COD (X_{sc}) + slowly biodegradable particulate COD (X_{sp}))]

[3] Fraction of TCOD which is soluble Unbiodegradable [$SCOD_{eff}$ / $TCOD_{inf}$]

[4] Fraction of TCOD which is particulate Unbiodegradable [calibrated using the influent specifier associated with the model and equal to (1- F_{bs}-F_{us})]

[5] Fraction of influent TKN which is ammonia

[6] Fraction of influent biodegradable organic nitrogen which is particulate

[7] Fraction of influent TP which is phosphate

It must be asserted that BioWin® model is COD based and calculates TSS, VSS, and BOD (total and soluble) based on the specification of non-biodegradable particulate and non-colloidal slowly biodegradable fractions, which are not readily measured. In order to account for the much higher soluble fraction of the organic matter in the landfill leachate relative to typical municipal wastewater using the influent specifier, non-biodegradable

particulate (F_{up}) and non-colloidal slowly biodegradable (F_{xsp}) were adjusted to 0.185 g COD/g TCOD and 0.05 g COD/g sbCOD, respectively. It is noteworthy to mention that the adjusted parameters were out of the typical range considered for municipal wastewater in BioWin®. As depicted in **Table 9.4**, the various kinetics parameters for autotrophs and heterotrophs used in all modeling runs were set to default values.

Table 9.4. Kinetic parameters used for landfill leachate in BioWin

Name [unit]	Default	Input[a]	Arrhenius
Ammonia-Oxidizing Bacteria (AOB)			
Max. spec. growth rate [1/d]	0.90	**0.90**	1.072
Substrate (NH_4) half sat. [mgN/L]	0.70	**0.70**	1.00
Aerobic decay rate [1/d]	0.17	**0.17**	1.029
Anoxic/anaerobic decay rate [1/d]	0.08	**0.08**	1.029
$KiHNO_2$ [mmol/L]	0.005	**0.005**	1.00
Nitrite-Oxidizing Bacteria (NOB)			
Max. spec. growth rate [1/d]	0.70	**0.70**	1.06
Substrate (NO_2) half sat. [mgN/L]	0.10	**0.10**	1.00
Aerobic decay rate [1/d]	0.17	**0.17**	1.029
Anoxic/anaerobic decay rate [1/d]	0.08	**0.08**	1.029
$KiNH_3$ [mmol/L]	0.075	**0.075**	1.00
Ordinary Heterotrophic Organisms (OHOs)			
Max. spec. growth rate [1/d]	3.20	**3.20**	1.029
Substrate half sat. [mgCOD/L]	5.00	**5.00**	1.00
Anoxic growth factor [-]	0.50	**0.50**	1.00
Aerobic decay [1/d]	0.62	**0.62**	1.029
Anoxic/anaerobic decay [1/d]	0.30	**0.30**	1.029
Hydrolysis rate (AS) [1/d]	2.10	**2.10**	1.029
Hydrolysis half sat. (AS) [-]	0.06	**0.06**	1.00
Anoxic hydrolysis factor [-]	0.28	**0.28**	1.00
Anaerobic hydrolysis factor [-]	0.50	**0.50**	1.00
Adsorption rate of colloids [L/(mgCOD d)]	0.80	**0.80**	1.029
Ammonification rate [L/(mgN d)]	0.04	**0.04**	1.029
Assimilative nitrate/nitrite reduction [1/d]	0.50	**0.50**	1.00
Fermentation rate [1/d]	3.20	**3.20**	1.029
Fermentation half sat. [mgCOD/L]	5.00	**5.00**	1.00
Anaerobic growth factor (AS) [-]	0.125	**0.125**	1.00
Hydrolysis rate (AD) [1/d]	0.10	**0.10**	1.05
Hydrolysis half sat. (AD) [mgCOD/L]	0.15	**0.15**	1.00

[a] Calibrated using the experimental data

9.3.2 Modeling Using AQUIFAS®

AQUIFAS® is developed to model fixed film process using semi-empirical equations and a 2-dimensional biofilm model [20, 21, 22]. The model equations are based on the kinetics of COD uptake, nitrification, denitrification, and biological phosphorus removal by biofilm carrier particles, as measured under different substrate conditions within the length of a biological reactor. The equations incorporate Monod kinetics with mass flux to simulate the variation in substrate uptake rates, as a result of changes in external substrate concentrations, and associated changes in the biofilm thickness and fraction of nitrifiers in the biofilm that develop in a different cell reactors. The detailed model equations are presented elsewhere. [20, 21, 22]

The biofilm diffusion model breaks the biofilm into 12 layers and a stagnant liquid layer. COD, Do, biomass, nitrogen, and phosphors fluxes from a concentric layer to the next deeper layer are the net uptake and release in the layer and the flux from the concentric outer layer to this layer. This model adopted the model equations and stoichiometric relationships used in AQUIFAS® to compute the substrate uptake and biomass generation in each layer of the biofilms. The model sums up the substrate uptake and biomass generation over the 12 default model layers to compute the substrate and biomass flux for the biofilm in each cell of the reactor. Multiplication of substrate and biomass flux with the surface area in each cell gives the uptake for the cell. Unlikely BioWin® which requires detailed fractionation of COD as despites in **Table 9.3**, AQUIFAS® input was limited to the typical composite parameters i.e. BOD (total and soluble), COD (total and soluble), TSS, VSS, TN (total and soluble), and TP.

9.3.3 Model Implementation and Calibration

The CFBBR was modeled using basic reactors available in BioWin® and AQUIFAS®, i.e. influent, un-aerated media bioreactor, aerated media bioreactor, nitrate recirculation, clarifiers, effluent, and sludge wastage effluent as shown in **Figure 9.2**. The riser was simulated using two media bioreactors followed by three aerated media bioreactors as a downer and a solid-liquid separator to collect the excess biomass from the system. The influent enters into the riser with a downer-riser liquid and nitrate recirculation collected

from the last downer of aerated reactor. The combined fluid flows from riser to the downer. Finally, the effluent from the downer goes to the downer solid-liquid separator, shown as a clarifier, with the provision for sludge wastage. The cross sectional areas of anoxic and aerobic reactors were considered equal to the actual cross sectional area of the column in the pilot-scale. To ensure proper nitrifying-denitrifying conditions in the CFBBR, the DO set points in the anoxic riser and aerobic downer are similar to those measured onsite of 0.4 mg/L and 2-3.1 mg/L, respectively.

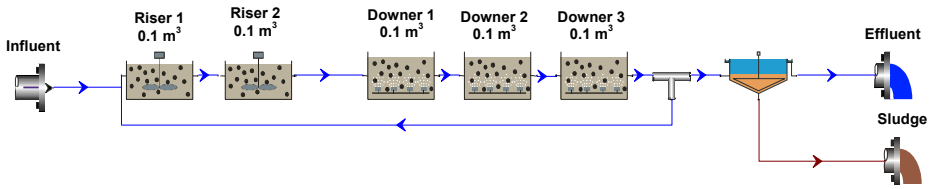

Figure 9.2. BioWin and AQUIFAS schematic flow diagram of CFBBR model

Lava rock particles with an average size of 600 µm were used as a carrier media in both the anoxic and aerobic reactor. The maximum possible surface area (SSA_{max}) in the anoxic and aerobic reactors was calculated considering zero void ratio and biofilm thickness of 500 µm and 120 µm diameter and a bare lava rock particles of 600 µm diameter as 3750 m^2/m^3 and 7060 m^2/m^3, respectively. Considering bed porosity, spherical lava rock particles occupy 44% of the total reactor volume at 100% fill, translating into a possible surface area for the anoxic and aerobic reactors of 2100 m^2/m^3 and 3950 m^2/m^3, respectively. Thus, the total surface area of the carrier media for the entire anoxic and aerobic reactors considering the compact bed was 166 m^2 ($2100\frac{m^2}{m^3}\times 0.11d(EBCT_{Ano}\ in\ Table\ 2)\times 0.72\frac{m^3}{d}$) and 1080 m^2 ($3950\frac{m^2}{m^3}\times 0.38d\ EBCT_{Aer}\ in\ Table\ 2)\times 0.72\frac{m^3}{d}$), respectively.

In order to simulate the fluidization regime of CFBBR system and the change of biofilm thickness, the shear factor was calibrated separately in each reactor with respect to expanded fluidized bed by a detachment rate coefficient in BioWin® model and hydrodynamic shear factor (G) in AQUIFAS® as shown in **Table 9.5** and **Table 9.6**. It is interesting to note that the properties and the weight of the carrier media such as

roughness, porosity, and chemical adsorption in BioWin® and AQUIFAS® models are not explicitly defined but implicitly as SSA, % fill, and biofilm volume fraction (BVF).

Table 9.5. Calibrated BioWin parameters

Parameters	Reactor	Default Values	Used Values[a]
Detachment rate ($g/m^3.d$)			
	Anoxic 1	8×10^4	8×10^4
	Anoxic 2	8×10^4	8×10^4
	Aerobic 1	8×10^4	2×10^6
	Aerobic 2	8×10^4	1.8×10^6
	Aerobic 3	8×10^4	1.8×10^6

[a] Calibrated using the experimental data

Table 9.6. Calibrated AQUIFAS parameters

Parameters	Reactor	Default Values	Used Values[a]
Hydrodynamic shear coefficient (G)			
	Anoxic 1	0-5	0.2
	Anoxic 2	0-5	0.2
	Aerobic 1	0-5	4
	Aerobic 2	0-5	3
	Aerobic 3	0-5	3

[a] Calibrated using the experimental data

9.4 Results and Discussion

The CFBBR was tested and evaluated at two different loading rates, empty bed contact times (EBCTs), and hydraulic retention time by adjusting the influent flow rate from 720 L/d (Phase I) and 864 L/d (Phase II). All volumetric loadings expressed in **Table 9.2** have been calculated based on the total CFBBR volume of 0.77 m^3 comprised of 0.19 m^3 anoxic riser, and 0.58 m^3 aerobic downer. The models were first calibrated with phase I data and then validated for phase II.

9.4.1 CFBBR Performance

Two different EBCTs of 0.49 and 0.41 d were examined to optimize the organic removal efficiency of the CFBBR. The raw leachate characteristics depicted in **Table 9.1** reflect a COD:N:P ratio of 3:1:0.0155. The CFBBR had to meet sewer use by-law criteria of 350 mg TSS/L, 300 mg BOD_5/L, 50 mg NH_4-N, and 10 mg TP/L. [34] The CFBBR proved to be a reliable integrated technology for biological nutrient removal from landfill leachate at a low carbon to nitrogen ratio of 3:1. The system was operated at loading rates of 2.2-2.6 kg COD/m^3·d, 0.68-0.81 kg N/m^3·d, and 0.014-0.016 kg P/m^3·d. The system efficiently removed nutrients at a flow rate of 720 L/d corresponding to an EBCT of 0.49 d and loading rate of 2.15 kg COD/m^3.d, 0.68 kg N/m^3.d, and 0.014 kg P/m^3.d.

The CFBBR removed approximately 85% organic, 80% nitrogen, and 70% phosphorus at nutrients loading rates of 2.15 kg COD/(m^3·d), 0.68 kg N/(m^3·d), and 0.014 kg P/m^3·d, as compared with 60%-70% COD and 70%-74% nitrogen removal efficiencies achieved by upflow anaerobic sludge blanket (UASB) and moving bed bioreactor (MBBR), respectively. [7, 8, 9, 10, 11, 12] The CFBBR effluent characterized by ≤35 mg SBOD/L, <35 mg NH4-N/L, <1.0 mg PO4-P/L, and 37 mg VSS/L, as shown in **Table 9.1**, sufficiently met sewer use by-law requirements for the City of London (Canada) without using any chemicals for phosphorus removal. Remarkably low yields of 0.15 and 0.16 g VSS/g COD were observed at long biological solids retention time (SRT) of 31-38 d.

Overall mass balances indicated COD closures of 96% and 85% in phases I and II, respectively, and alkalinity mass balances closed within 5%-8%, confirming data reliability. In order to ensure attainment of the steady-state conditions in the system, the suspended and attached biomass in the aerobic and anoxic columns were measured. As depicted in **Figure 9.3**, the coefficient of variation (COV) for attached biomass in the aerobic and anoxic columns during this study are 9% and 11%, respectively. Although it is arguable that suspended VSS concentrations varied more widely, as reflected by COV of 13% and 18% (**Figure 9.4**), this process is indeed a fixed-film system and 99.99% of the biomass inventory in the system is in the form of attached biomass. Therefore, the

attached biomass and biomass activity remained constant during the study, reflecting attainment of steady-state conditions.

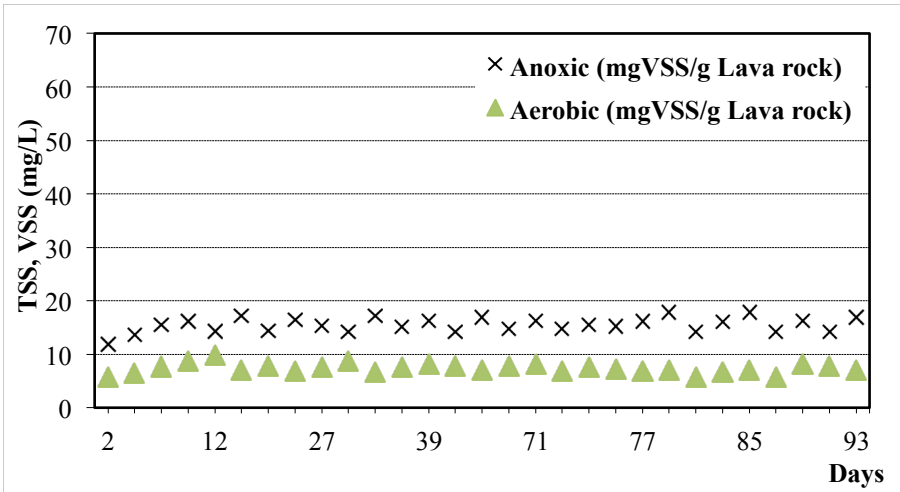

Figure 9.3. Temporal variation of attached biomass in the anoxic and aerobic reactors

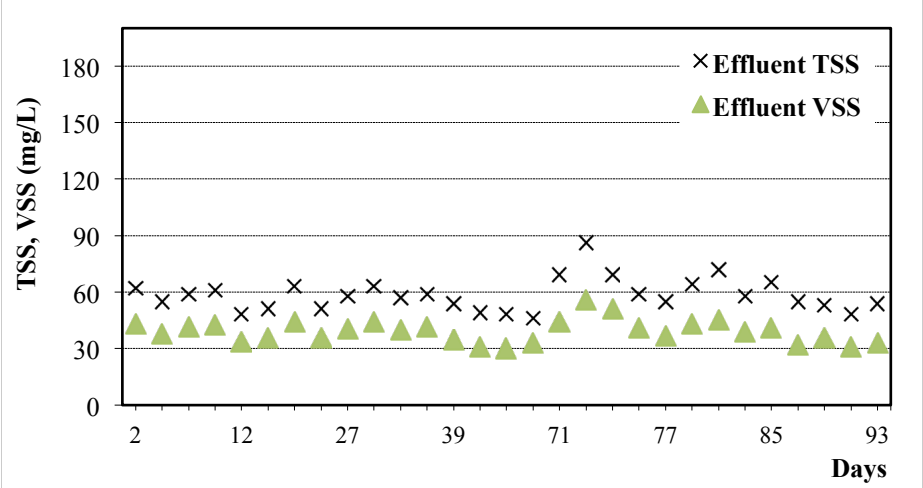

Figure 9.4. Temporal variation of the CFBBR effluent VSS concentrations

9.4.2 Model Calibration

The models were calibrated with the experimental data at the optimum loading rate of the pilot-scale CFBBR of 2.2 kg COD/m^3·d, 0.68 kg N/m^3·d, and 0.014 kg P/m^3·d corresponding to 720 L/d and were subsequently validated using the other set of

experimental data at the higher loading rate of 2.6 kg COD/m^3·d, 0.81 kg N/m^3·d, and 0.016 kg P/m^3·d. The simulations were started with the default values of the model, which were later adjusted to match the observed pilot-scale CFBBR results. **Table 9.5** shows the parameters adjusted during BioWin® calibration. Considering the effect of the perforated coarse bubble distributor in the aerobic reactor and its low oxygen transfer efficiency, the detachment rate was used to maintain the biofilm thickness as observed in the pilot-scale CFBBR system. Moreover, the percentage of the reactor occupied by the media was adjusted to simulate the changes in the expanded bed bioreactor. In AQUIFAS®, the hydrodynamic shear coefficient and the BVF defined as the fraction of liquid tank volume displaced by biofilm, were adjusted to simulate additional turbulence in fluidized beds as shown in **Table 9.6**. It is noteworthy to mention that the percentage of the reactor fill ratio used by BioWin® considered the volume of reactor occupied by clean media only while the BVF ratio used by AQUIFAS® considers only the biofilm attached to the lava rock media.

9.4.3 Steady State CFBBR Model

The steady-state CFBBR models using BioWin® and AQUIFAS® were focused on various aspects of process performance i.e. reactor effluent characteristics, nutrient removal rates, biofilm thickness, total biomass in the reactor, and process yields as well as the COD uptake, nitrification, and denitrification rates.

BioWin® Model

Table 9.7 shows a comparison between model prediction and experimental data for both phases using BioWin®. In phase I, the model predicted effluent NH_4-N of 33.7 mg/L, NO_3-N of 61.1 mg/L, and TKN of 46.6 mg/L compared well to observed NH_4-N of 35.4±13.1 mg/L, NO_3-N of 59.9±31.1 mg/L, and TKN of 49±15 mg/L, in the pilot-scale CFBBR system while in phase II the model predicted effluent NH_4-N of 54.7 mg/L, NO_3-N of 58.4 mg/L, and TKN of 67.3 mg/L closely matched observed NH_4-N of 54.7±11.2 mg/L, NO_3-N of 63.9±10.3 mg/L, and TKN of 92±23 mg/L.

Table 9.7. Experimental and simulated effluent quality

Parameter	Influent*	Phase I			Phase II		
		Simulated		Exp.*	Simulated		Exp.*
		BioWin	AQUIFAS		BioWin	AQUIFAS	
pH	7.9-8.8	**7**	**----**	7.2-8.2	**7.2**	**----**	7.6-8.1
Alkalinity**	1619±52	**311**	**338**	323±71	**323**	**338**	296±57
COD (mg/L)	1259±77	**236**	**174**	197±46	**235**	**203**	302±98
SCOD (mg/L)	1025±27	**169**	**128**	153±43	**169**	**166**	245±85
NH_4-N (mg/L)	360±59	**33.7**	**35.9**	35.4±13.1	**54.7**	**56.3**	54.7±11.2
NO_3-N (mg/L)	3.1±1.5	**61.1**	**69.4**	59.9±31.1	**58.4**	**57.5**	63.9±10.3
TKN (mg/L)	392±64	**46.4**	**36.5**	49±15	**67.3**	**69.8**	92±23
PO_4-P (mg/L)	3.4±1.1	**0.8**	**0.9**	1.0±0.2	**1**	**1**	1.2±0.5
TP (mg/L)	6.2±1.3	**1.5**	**1.6**	1.7±0.3	**1.8**	**1.8**	2.0±0.6
TSS (mg L)	263±42	**60**	**62**	60±13	**58**	**62**	58±8
VSS (mg/L)	156±30	**45**	**45**	37±5	**44**	**50**	44±8
BOD (mg/L)	565±121	**19**	**40**	83±13	**20**	**45**	98±18
SBOD (mg/L)	402±83	**1**	**18**	35±8	**1.3**	**19**	40±12

*Average ± SD of a number of samples 8-12 with a frequency of a sample every 4 days;
**(mg $CaCO_3$/L)

As despite in **Table 9.7**, the average percentage error (APE) in phase I, calculated as the summation of the absolute difference between the experimental and predicted values divided by the experimental values, averaged over the number of data points, revealed that the discrepancy between predicted and measured final effluent alkalinity, SCOD, NH_4-N, NO_3-N, TKN, TP, PO_4-P, and TSS was 1-10%. Comparatively, a higher APE of 20% was observed between simulated and measured final effluent TCOD and VSS in phase I. In phase II, the BioWin® model over-predicted SCOD, TKN, and PO_4-P by 20% while the other final effluent characteristics were in agreement with the experimental data. Furthermore, while the model over-predicted the final effluent VSS in phase I by 20%, it predicted the effluent VSS accurately in phase II reflecting lack of systematic prediction errors. Due lack of consideration of soluble microbial products (SMPs), the model significantly under-predicted the effluent BOD and SBOD in both phases by APE of 77% and 97%, respectively. However, predicted model results were within the range of the average plus or minus standard deviation of the effluent characteristics as shown in

Figure 9.5. The model accurately predicted effluent soluble nutrients. The APE for the effluent in both phases with respect to SCOD, ammonia, nitrates, and orthophosphates were 20%, 5%, 6%, and 9%, respectively. In general, the predicted effluent characteristics by BioWin® model in both phases were in good agreement (APE<22%) with the experimental but the effluent BOD and SBOD were under-predicted for various runs by 77% to 97%.

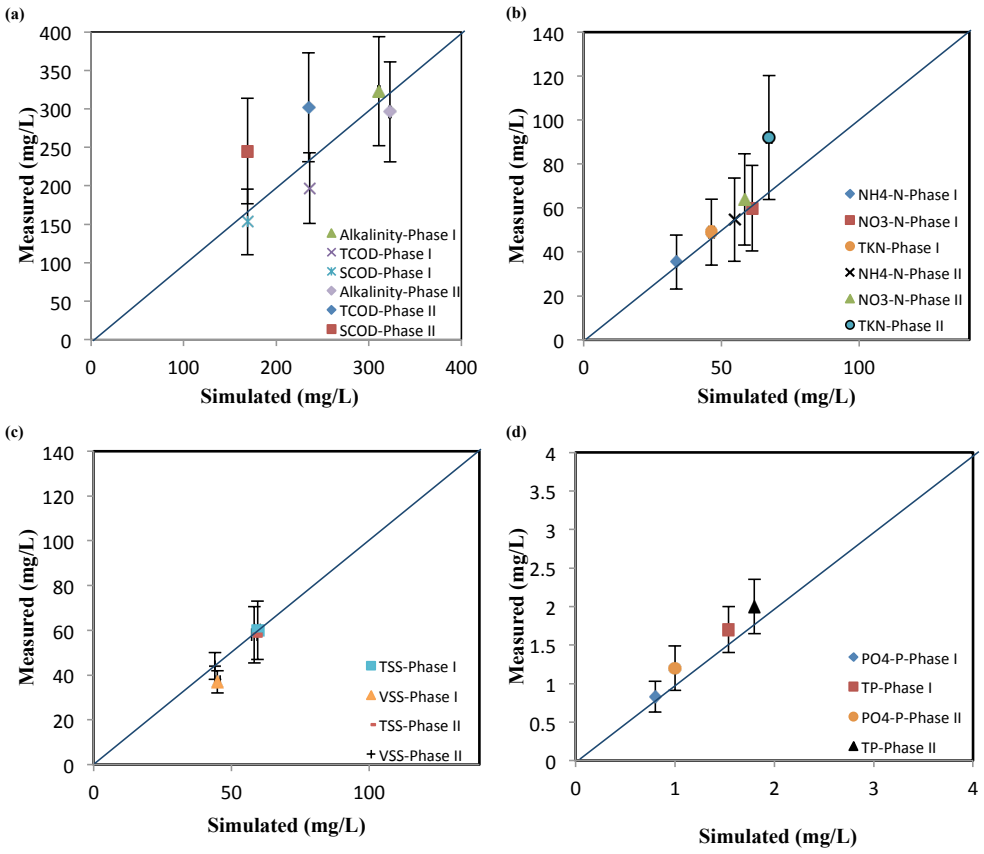

Figure 9.5. Comparison between predicted and measured parameters for phases I and II with BioWin

AQUIFAS® Model

Comparison between model prediction and experimental data using AQUIFAS® (**Table 9.7**) shows the discrepancy of 1%-13% between predicted and measured final effluent alkalinity, TCOD, NH_4-N, NO_3-N, TP, PO_4-P, and TSS, while a higher APE of

21% was observed between simulated and measured final effluent SCOD and VSS. In phase I, the model predicted effluent NH_4-N of 35.9 mg/L and NO_3-N of 69.4 mg/L compared to measured NH_4-N of 35.4±13.1 mg/L and NO_3-N of 59.9±31.1 mg/L, while in phase II the model predicted effluent NH_4-N of 56.3 mg/L and NO_3-N of 57.5 mg/L matched NH_4-N of 54.7±11.2 mg/L and NO_3-N of 63.9±10.3 mg/L. In both phases, the model under-predicted final effluent TKN with an APE of 24%. Moreover, the AQUIFAS ® model in phase I predicted TCOD and SCOD within APE of 10% and 16% respectively whereas in phase II, under-predicted TCOD and SCOD by 32% APE, reflecting lack of systematic prediction errors. Furthermore, the AQUIFAS® predictions for BOD and SBOD in both phases were more accurate than BioWin® with an APE of 50%. Model- predictions were within the range of the average plus or minus standard deviation of the effluent characteristics as shown in **Figure 9.6**. In general, the AQUIFAS® model- predictions for all effluent characteristics (excluding BOD), in both phases were in good agreement (APE<19%) with the experimental data but the BOD and SBOD were under-predicted for various runs by 50%.

The high discrepancy between the predicted and experimental BOD values by both the models may be due to soluble microbial products (SMPs) in the effluent. In fixed-film wastewater systems with longer sludge retention times, the effluent soluble BOD is predominantly more than effluent SBOD in suspended growth systems as a result of release of SMPs. None of the ASM models accounts for SMPs which is not really substantial in short SRT systems such as activated sludge but maybe important in long SRT systems such as CFBBR. [35]

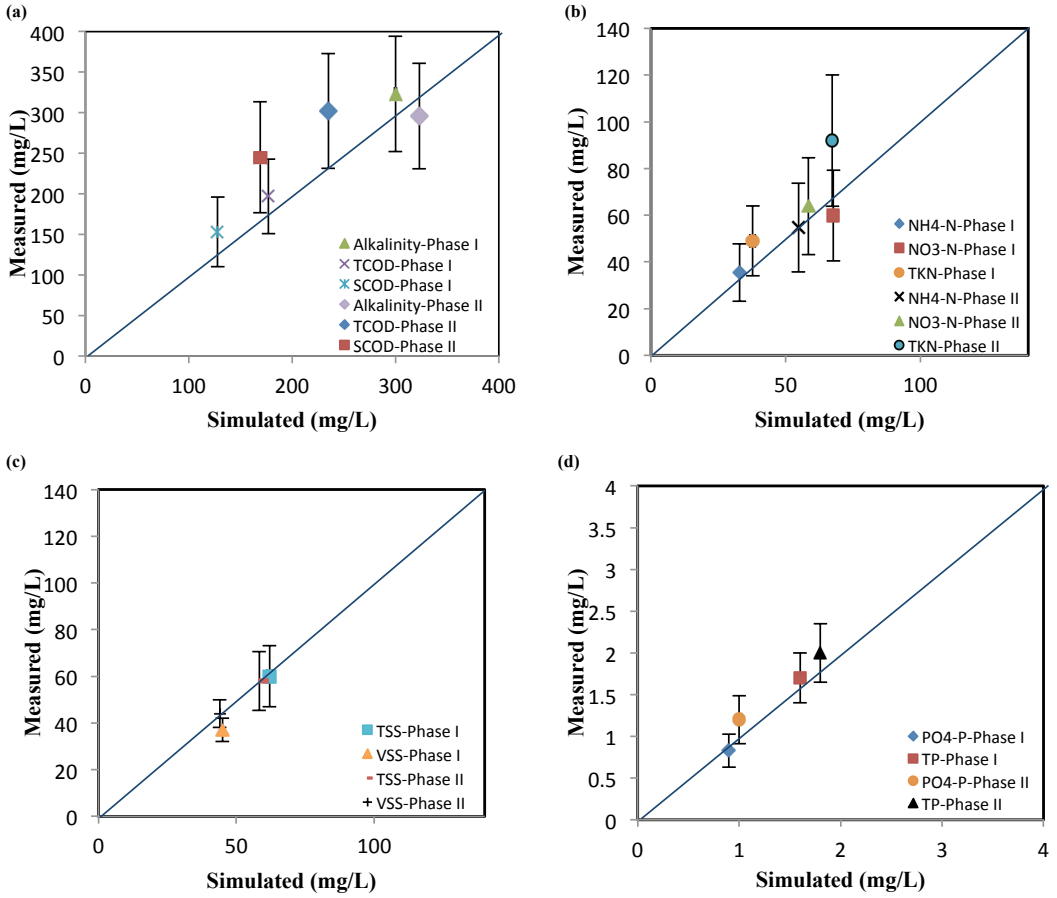

Figure 9.6. Comparison between predicted and measured parameters for phases I and II with AQUIFAS

9.4.4 Simulated Biomass Yield

Biomass yield in the pilot-scale CFBBR calculated as the sum of the net change in attached biomass, sludge wastage, and effluent solids divided by the total COD consumed in the process was 0.15 and 0.16 g VSS/g COD in phases I and II, respectively with overall sludge production of 146 g VSS/d and 164 g VSS/d. BioWin® predicted that 32 g VSS/d and 32.4 g VSS/d biomass were lost in the effluent of CFBBR system with an overall sludge wastage of 175 g VSS/d and 213 g VSS/d in phases I and II, respectively. Considering the aerobic and anoxic nutrient mass removal rates, the mean cell residence time, decay coefficient, and the simulated COD removal of 888 g COD/d and 1063 g COD/d in phases I and II, the simulated biomass yields with BioWin® were calculated as

0.23 g VSS/g COD and 0.24 g VSS/g COD in phase I and II, respectively which are approximately 50% higher than those observed experimentally.

As reported in **Table 9.8**, for AQUIFAS®, considering the effluent biomass of 32 g VSS/d and 46 g VSS/d and sludge production of 132 g VSS/d and 133 g VSS/d with a COD removal of 930 g COD/d and 1109 g COD/d in phases I and II, respectively leads to a simulated biomass yield of 0.17 g VSS/g COD and 0.16 g VSS/g COD in phases I and II, respectively, approximately 6% (on average) higher than experimental. AQUIFAS® biomass yields were thus much closer to the observed yields than BioWin®.

Table 9.8. Simulated results and measured parameters for nutrient removal rates

Parameter	Phase I			Phase II		
	Simulated		Exp.*	Simulated		Exp.*
	BioWin	AQUIFAS		BioWin	AQUIFAS	
Anoxic COD consumption (kg/d)	0.83	0.70	0.71±0.05	0.97	0.77	0.72±0.05
Aerobic COD consumption (kg/d)	0.08	0.18	0.08±0.05	0.10	0.29	0.15±0.05
Yield (g VSS/g COD)	0.23	0.17	0.16±0.04	0.24	0.16	0.16±0.02
Anoxic N removal (kg/d)	0.24	0.24	0.24±0.05	0.27	0.27	0.25±0.06
Aerobic N removal (kg/d)	0.20	0.18	0.19±0.04	0.23	0.21	0.19±0.04

*Average ± SD of a number of samples 8-12 with a frequency of a sample every 4 days

Although the predicted aerobic and anoxic attached biomass thicknesses of 160-200 and 500-580 μm respectively using BioWin® and AQUIFAS® were in close agreement with the experimental values of 120 and 600 μm in anoxic and aerobic, the total biomass in both models was under-predicted by 20% and 33% in phase I and II, respectively. In phase I, the total biomass using BioWin® in the anoxic and aerobic reactors was 1371 g VSS and 1886 g VSS, compared to measured of 2037 g VSS and 2505 g VSS, respectively, while in phase II model biomass was 1471 g VSS and 2057 g VSS, versus experimental anoxic and aerobic biomass of 2337 g VSS and 3081 g VSS, respectively with an APE of 30%. The total anoxic and aerobic biomass in phase I using AQUIFAS® was 1801 g VSS and 1882 g VSS, compared to anoxic and aerobic biomass of 2057 g VSS and 2505 g VSS, respectively while in phase II biomass was 1984 g VSS and 2004 g VSS as compared to anoxic and aerobic biomass of 2337 g VSS and 3081 g VSS, respectively with an APE of 20%.

Both models ignore the accumulation of the influent non-biodegradable VSS (nbVSS) in the system, which is usually about 10% [36] translating to 16 g nbVSS/d in phases I and II or a total of 1472 g nbVSS over the 92-day study duration.

9.4.5 Nutrient Uptake Rates

Anoxic COD removal by AQUIFAS® in phases I and II (**Table 9.8**) were close to the experimental data with an APE of 1.4% and 7% respectively whereas BioWin® over-predicted COD removal values by an APE of 17% and 35% respectively. However, aerobic COD consumption predicted by BioWin® with APE of 0% and 33% in phases I and II were much more precise than aerobic COD removal simulated by AQUIFAS®.

Nitrification and denitrification rates of 0.24-0.27 kg N/d and 0.2-0.23 kg N/d, respectively, predicted by BioWin® were comparable with the observed nitrification and denitrification rates, estimated from the amount of nitrogen nitrified and denitrified. AQUIFAS® nitrification and denitrification rates in phases I and II were in close agreement with the experimental data within APE of 0-10%.

As mentioned previously, the biomass yield predicted by BioWin® was 50% higher than measured due to shorter simulated SRTs of 15.7 d and 14 d in phases I and II respectively. In AQUIFAS®, the biomass yield predicted in the model was in close agreement with the observed experimental yield with an APE of 6%. AQUIFAS® predicted SRTs of 22 d and 20 d compared to measured (based on VSS) of 38 d and 31 d in phases I and II respectively. The SRT predicted by BioWin® and AQUIFAS® is based on the biomass only i.e. ignores accumulation of non-biodegradable influent VSS. Considering the specific nitrification rate (SNR) and specific denitrification rate (SDNR) of the attached and detached biomass of 0.14 gNH_4-N/gVSS.d, 0.19 gNO_3-N/gVSS.d, 1.57 gNH_4-N/gVSS.d, and 1.57 gNO_3-N/gVSS.d demonstrates that the established active SRT was 18 d in both phases compared to overall SRT of 38 d and 31 d in phase I and II, respectively.

As shown in **Figure 9.5**, the predicted orthophosphate and TP by BioWin® matched those measured with an APE of 10% in both phases. AQUIFAS® also predicted

orthophosphate and TP well with an APE of 10%. Phosphorous removal by both models was predominantly governed by biomass assimilation accounting for 70% of phosphorus removal based on the 2% phosphorous content of sludge produced.

9.5 Summary and Conclusions

Comparison between the calibrated BioWin® and AQUIFAS® models and the experimental data from the pilot-scale CFBBR shows that the modeling of landfill leachate along with attached growth systems was challenging due to the complex hydrodynamics involving changing biofilm thicknesses, varying detachment and attrition rates, and the complexity of leachate characteristics with C/N ratio of 3:1, TCOD/VSS ratio of 8:1 and TBOD/TCOD of 0.44.

BioWin® and AQUIFAS® predicted the soluble parameters with an APE of 10%. However, effluent SBOD and BOD were predominately underpredicted due to soluble microbial products (SMPs) in the effluent as a result of long SRTs in the CFBBR.

AQUIFAS® predicted the total biomass and biomass yield as well as the anoxic COD, anoxic N, and aerobic N removal rates in the CFBBR systems more accurately than BioWin®. Whereas BioWin® predicted aerobic COD uptake more accurately. The challenges faced during the modeling by BioWin® and AQUIFAS® were:

- The influent specifier associated with BioWin® was only limited for municipal wastewater simulation only whereas the AQUIFAS® has no influent specifier and the influent characteristics were adjusted in the model.
- The biomass detachment rates in a fixed-film system cannot be controlled by setting a desired SRT in the entire system.
- Although the media fill and SSA in the reactor can be adjusted, the models do not provide the users with the weight of media, which is essential for system design.
- Each column can be only aerobic, anoxic or anaerobic whereas in real fixed-film systems biofilms perform differently throughout the inner layers. As a result simultaneous nitrification and denitrification which may occur in the same reactor cannot be simulated by any of the two models.

9.6 References

[1] Park S, Choi KS, Joe KS, Kim WH, Kim HS. Variations of landfill leachate properties in conjunction with the treatment process, Environ. Technol. 2001; 22:639–645.

[2] Renou S, Givaudan JG, Poulain S, Dirassouyan F, Moulin P. Landfill leachate treatment: review and opportunity, J. Hazard. Mater. 2008; 150:468–493.

[3] Gálvez AL, Giusti L, Zamorano M, Ramos-Ridao AF. Stability and efficiency of biofilms for landfill leachate treatment, Bioresource Technology. 2009; 100:4895–4898.

[4] Foo KY, Hameed BH. An overview of landfill leachate treatment via activated carbon adsorption process, J. Hazard. Mater. 2009; 171:54–60.

[5] Nakhla G, Zhu J, Cui Y. Liquid-solid circulating fluidized bed wastewater treatment system for simultaneous removal of carbon, nitrogen, and phosphorus, US patent no. 7,261,811 (2004), Int'l PCT patent awarded (2005).

[6] Eldyasti A, Chowdhury N, Nakhla G, Zhu J. Biological nutrient removal from leachate using a pilot liquid–solid circulating fluidized bed bioreactor (LSCFB), Journal of Hazardous Materials, 2010; 181:289–297.

[7] Kettunen RH, Hoilijoki TH, Rintala JA. Anaerobic sequential anaerobic–aerobic treatments of municipal landfill leachate at low temperatures, Biores. Technol. 1996; 58:31–40.

[8] Kettunen RH, Rintala JA. Performance of an on-site UASB reactor treating leachate at low temperature, Water Res. 1998; 32:537–546.

[9] Kennedy KJ, Lentz EM. Treatment of landfill leachate using sequencing batch and continuous flow upflow anaerobic sludge blanket (UASB) reactors, Water Res. 2000; 34:3640–3656.

[10] Kettunen RH, Rintala JA. Sequential anaerobic–aerobic treatment of sulphur rich phenolic leachates, J. Chem. Technol. Biotechnol. 1995; 62:177–184.

[11] Horan NJ, Gohar H, Hill B. Application of a granular active carbon-biological fluidized bed for the treatment of landfill leachates containing high concentrations of ammonia, Water Sci. Technol. 1997; 36:369–375.

[12] Welander U, Henrysson T, Welander T. Nitrification of landfill leachate using suspended-carrier biofilm technology, Water Res., 1997; 31:2351–2355.

[13] Wanner O, Reichart P. Mathematical modeling of mixed-culture biofilm, Biotechnol Bioeng, 1996; 49:172-184.

[14] Wanner H, Hainan G, Dorn S. Nutritional value of floral nectar sources for flight in the parasitoid wasp Cotesia glomerata, Physiological Entomology, 2006; 31:127-133.

[15] Wanner O, Gujer W, Competition in biofilms, Water Science Tech. 1984;17:27-44.

[16] Wanner O. A multispecies biofilm model, Biotechnol. Bioeng. 1986; 28:314-328.

[17] Reichert P. AQUASIM-a tool for simulation and data analysis of aquatic systems, Water Science Tech. 1994; 30:21-30.

[18] Xavier JB, Picioreanu C, van Loosdrecht MCM. A framework for multidimensional modeling of activity and structure of multispecies biofilms, Environ. Microb. 2005; 7:1085-1103.

[19] Henze M, Gujer W, Mino T, Matsuo T, Wentzel MC, Marais GVR. Activated Sludge Model No. 2. IAWQ Scientific and Technical Report No. 3, IAWQ, London, England. 1995.

[20] Sen D, Randall CW. Improved computational model (AQUIFAS) for activated sludge, integrated fixed-film activated sludge, and moving-bed biofilm reactor systems, Part I: Semi-empirical Model Development, Water Environ. Res. 2008a; 80:439-453.

[21] Sen D, Randall CW. Improved computational model (AQUIFAS) for activated sludge, integrated fixed-film activated sludge, and moving-bed biofilm reactor systems, Part II: Multilayer Biofilm Diffusion Model. Water Environ. Res. 2008b; 80:624-632.

[22] Sen D, Randall CW. Improved computational model (AQUIFAS) for activated sludge, integrated fixed-film activated sludge and moving bed biofilm reactor systems, part III: Analysis and verification, Water Environ. Res., 2008c; 80:633-645.

[23] Phillips HM, Maxwell M, Johnson T, Barnard J, Rutt K, Seda J, Corning B, Grebenc JM, Love N, Ellis S. Optimizing IFAS and MBBR designs using full-scale

data, Proceedings of the Water Environment Federation 81ST Annual Technical Exhibition & Conference, Chicago, IL, USA, 2008.

[24] McGehee M, Gellner J, Beck J, White C, Bruton T, Howard D. BioWin Modeling of a Three Reactor IFAS System, Proceedings of the Water Environment Federation 82nd Annual Technical Exhibition & Conference, Orlando, FL, USA, 2009.

[25] Rupp H, Roy G, Tautic B, Bushey J. Pilot study confirms design of IFAS system for nitrogen reduction in Connecticut, Water Environment Federation Specialized Conference on Nutrient Removal, Washington, DC, 2009.

[26] Cui Y, Nakhla G, Zhu J. A. Patel, Simultaneous carbon and nitrogen removal in anoxic-aerobic circulating fluidized bed biological reactor (LSCFB), Environ. Technol. 2004; 25:699-712.

[27] Patel A, Zhu J, Nakhla G. Simultaneous carbon, nitrogen and phosphorus removal from municipal wastewater in a circulating fluidized bed bioreactor, Chemosphere. 2006; 65:1103-1112.

[28] Chowdhury N, Nakhla G, Zhu J. Load maximization of a liquid-solid circulating fluidized bed bioreactor for nitrogen removal from synthetic municipal wastewater, Chemosphere. 2008; 71:807-815.

[29] Chowdhury N, Nakhla G, Zhu J, Islam M. Pilot-scale experience with biological nutrient and biomass yield reduction in a liquid-solid circulating fluidized bed bioreactor, Water Environ. Res. (2009) DOI: 10.2175/WER 09-11-1541.

[30] APHA, AWWA, WEF. Standard Methods for the examination of water and wastewater. 20th Edition, American Public Health Association, Washington D.C., US. 1998.

[31] Barker PS, and Dold PL. General model for biological nutrient removal activated-sludge systems: model presentation, Water Environ. Res. 1997: 69-5:969–984

[32] Comeau Y, and Taka I. Schematic Representation of Activated Sludge Models. Proceedings of the Water Environment Federation Technical Exhibition and Conference. Chicago, IL, USA, 2008; 3:266–328

[33] Boltz JP, Morgenroth E, Sen D. Mathematical modeling of biofilms and bio-film reactors for engineering design, Water Science And Technology, 2010; 62-8:1821-1836.

[34] Waste Discharge By-law-16, City of London, Ontario, Canada (2007).

[35] Barker DJ, and Stuckey DC. A review of soluble microbial products (SMP) in wastewater treatment systems, Water Research, 1999; 33:3063-308.

[36] Metcalf, Eddy, Wastewater Engineering: Treatment and Reuse, 4th Ed., McGraw-Hill, New York, (2003) 622-623.

10 Simultaneous Denitrification and Methanogenesis (SDM): Review of Two Decades of Research

10.1 Introduction

Anaerobic digestion has proven to be the best alternative to aerobic processes for the treatment of high strength wastes due its lower sludge yields and energy consumption. High strength wastes produced by fertilizer production, explosive manufacturing and recovery of nuclear fuels either contain nitrogen in the forms of nitric and nitrous acid or in the form of ammonia, such as land fill leachate. In food processing, wastewaters also contain a high ammonia concentration and are often as a result of protein digestion. Since the nature of the aforementioned wastes requires an anaerobic biological process, the simultaneous denitrification and methanogeneis (SDM) in a single anaerobic reactor for the removal of nitrogen, has been studied as an area of interest during the last two decades. [1,2, and 3] The SDM process is also called anaerobic respiration. In anaerobic respiration, organic substrate or hydrogen is oxidized and an electron acceptor other than oxygen, such as nitrate, nitrite, sulphur, ferric iron and carbon dioxide are reduced. During this process, which is also called electron-transport phosphorylation, energy is conserved via an electrochemical proton and/or sodium ion gradient. [4] Side streams including the reject streams from the membrane, dewatering process and supernatant liquid from sludge digesters also contain a significant load of nutrients. Estimates of the nitrogen load from this side stream return range between 15% and 30% of the total nitrogen load on a process. [5] Several relatively new processes have been developed to remove nitrogen in high-concentration side streams from biosolids processing prior to recycling to the headwork of the publicly owned treatment works (POTWs); SHARON®, ANAMMOX®, CANON®, InNitri® [6], and BABE® [7]. In SHARON® process ammonia oxidizing bacteria (AOB) are encouraged and nitrite oxidizing bacteria (NOB) hindered by operating at higher temperature of 25-40 °C, SRT of 1-2d and lower oxygen concentrations of 1-2 mg/L. The products of SHARON® process are approximately 50% ammonia and 50% nitrite to be further denitritified by ammonia as electron donor in

ANAMMOX® and CANON® processes or heterotrophic bacteria in SHARON® process. Nonetheless, nitrogen removal in all the aforementioned processes takes place in two stages of nitrification and denitrification which could be eliminated in the case of the simultaneous denitrification in the anaerobic digester by returning the nitrite to the anaerobic digester after the first stage of SHARON® process.

Integration of heterotrophic denitrifiers, along with methanogenesis, provides a competitive environment between the two cultures for up take of the electron donors i.e. organic carbon. Del Pozo and Diez (2003) suggested the minimum bsCOD/NO_3-N based on the following equation: [8]

$$\frac{g\,bsCOD}{g\,NO_3 - N} = \frac{2.86}{(1 - Y_{H,NO_x}) + (1 - f_{X_I})Y_{H,NO_x}} \qquad (10.1)$$

Where $Y_{H,NOx}$ is the anoxic yield coefficient and f_{XI} is the fraction of inert COD (chemical oxygen demand) generated in biomass lysis.

Anaerobic Digestion Model No.1 (ADM 1) suggested that nitrate reduction, simultaneously in methanogenic systems, can have the following effects without addressing which one is a strong effect or a negligible effect, and whether these effects can be nullified at different operational conditions:

I. Channeling of electron equivalents (eeq) away from methanogenesis.
II. Decrease in the methane content of the biogas as a result of the production of N_2 and additional CO_2, as well as alkalinity and/or NH_4^+ production.
III. Competition between microbial groups for the same substrate(s).
IV. Inhibition of methanogenesis by nitrogen oxides. [9]

Denitrification and methanogenesis are mediated by different microbial populations requiring distinct environmental conditions and consequently, an integration of these processes might be problematic. [2] One of the challenges of coupling the denitrification and anaerobic process is indeed the carbon utilization pathway. In traditional treatment, the effluent from an anaerobic digester goes to aerobic treatment to nitrify ammonia

along with utilizing the remained COD aerobically. If the process has to meet tertiary effluent quality, it has to be denitrified to nitrogen gas as well. Since there is insufficient carbon available for heterotrophic denitrifiers, an additional carbon source will be required for the process of denitrification. Thus, it seems that coupling of denitrification and anaerobic digester in a single reactor will result in savings of substrate costs as well as material, energy consumption and space.

There has been a considerable effort to couple denitrification and methanogenesis in a single reactor in both suspended and attached growth systems. However, the occurrence of denitrification in methanogenic systems is not well documented [10] and requires a thorough literature review to reveal the extent of different inhibitory effects, as well as operational conditions. Moreover, contradictions in the literature, in this regard, also encourage a critical review that may lead researchers to a clearer direction.

10.2 History of Integrated Removal of Carbon and Nitrogen in Anaerobic Systems

During wastewater treatment, a common strategy proposed for combined C and N removal involves a sequential treatment of the wastewater in an anaerobic reactor followed by an aerobic post-treatment with upfront recycle of the final effluent to the anaerobic reactor, to promote denitrification of NOx – formed during post treatment. [11] Moreover, further treatment of anaerobically treated wastewaters is often required to meet sewer use by-laws.

Different system configurations found their application in the study of SDM, including batch fermentation [12, 13], completely stirred anaerobic digesters [1, 14], a mixed culture system co-immobilised in gel beads [15, 16], anaerobic upflow filter-UBF [17, 18], upflow anaerobic sludge blanket-UASB [19, 20, 21, 22, 23, 27] or combination of some UASB in series called anaerobic baffled reactor-ABR [24, 25] and etc. An overview of systems proposed to accomplish SDM in the literature along with some operational specifications is listed in **Table 10.1**. As seen, the hydraulic retention time (HRT) of all attached growth systems is shorter than 2 days and suspended growth up to 10 days, in order to achieve anaerobic COD removal. Suspended growth anaerobic digesters are usually designed and operated

without return sludge in which the HRT is equal to the sludge residence time (SRT). In case of fixed film systems however, HRT and SRT are decoupled. In the case of short SRTs for suspended growth systems [14, 15], either the anaerobic COD removal is not complete or the complete COD removal occurred in low COD/N ratios when the COD removal was predominantly due to carbon uptake through heterotrophic denitrifiers. Rustrian et al. (1997) applied a minimum SRT of 12.5 hr in a CSTR for SDM throughout the experimental period based on a study by Halling-Sorensen and Jorgensen (1993) that suggests the minimum SRT calculated for acidogenic populations was 3.3 hrs, whereas for denitrifiers it was 12 h. [26] In the aforementioned study, the acidogenic and methanogenic stages were decoupled in two series CSTR and the feasibility of simultaneous denitrification and acidogenesis was studied. The maximum denitrification and acidification rate were reported as 68% and 53% respectively where acidification rate was defined as the ratio percentage of the COD equivalent of produced fatty acids to feed COD concentration, at an organic loading rate (OLR) of 10 kg COD/m^3·d and NLR of 0.027-1 kg N/m^3·d. Rustrian et al. (1997) suggested that during a period of inhibition, the prevailing microorganisms growth rate is forced to decrease and the minimum SRT required to accommodate this growth rate increases, which could explain the inhibitory transients provoked by NO_3-N increase loads. It should be noted that in order to study the biomass yield of SDM systems and metabolic activity of denitrifiers and methanogens, knowledge of the SRT is required. In order to calculate SRTs in the attached growth systems, the amount of active and inactive attached and detached biomass should be measured. In the attached growth systems, listed in **Table 10.1**, however, rarely is the aforementioned information available.

Table 10.1. Integrated anaerobic-denitrification systems

No	Process	Type of waste	OLR (kg COD/m^3/d)	NLR (kg NO_3-N/m^3/d)	$\frac{COD}{NO_3 - N}$	Denitrification (%)	Methanogenic activity (%)	$Q_n Q_{in}$ (%)	Anae. HRT (d)	References
1	EGSB	Distillery	0.38-3.91	0.03-0.84	2.9-11.5	92-100	92-97	-	0.18-0.54	Zhang, 2003
2	UBF	Glusoe, Nitrate	-	-	7-30	99.8-65	97	-	-	Shin et al., 2002
3	CSTR	Glucose, Nitrate	0.53	0.005-2.5	2.35-107	1-64	0-96	-	10	Akuna et al., 1992
4	CSTR (acidogenesis)	Glucose, Nitrate	10	0.027-1	10-361	47-68	4-53	-	0.5	Rustrian et al, 1997
	Batch	Methanol						-	-	Chen and Lin, 1993
5	Batch	Molasses	-	-	38.9-65.6	97-99	1	-	-	Percheron et al., 1998
6	CSTR (immobilized)	Methanol, Nitrate	1.3-10	0.58-4.7	1-3.4	60-99.9	99	-	0.165	Chen et al., 1997 Lin and Chen 1995
7	Batch	Methanol, acetate Glucose, Benzoic	-	-	0-60	9-100	-	-	-	Her and Huang 1995
8	UASB	VFAs+ Nitrate	4.2	0.28	15	99	96	-	0.71	Hendriksen and Ahring, 1996
9	UBF	Methanol+ Nitrate	0.68-1.58	0.31-0.33	2.19-6.5	65-100	1-2.5	-	0.167	Hanaki and Polprasert, 1989
10	UASB (ANAMMOX)	synthetic	0.6-1.2	0.6	1-2	80-94	0	-	2	Sumino et al., 2006
11	UBF	Fish cannery	1-1.25	0.1-0.22	2.0-3.0	100	80	-	0.75-1.65	Mosquera –corral et al., 2001
12	MUF+BAS	Adhesive-formaldehyde	2	0.36-1.77	2.1-3.5	80	-		0.3-1.0	Garrido et al., 2001
13	UBF+MBR	Glucose	< 7.2	< 0.5	14.5-32.5	46	99	300	1.0	Ahn et al., 2007
14	UASB	Phenol, Cresol, sucrose	1.9	0.25-0.6				-	1.0	Fang et al., 1999
15	MBBR+CSTR	Aniline	3.48	0.48	7.2	90	96.1-97.8	0-800	1-3	Chen et al., 2009
16	ABR	Sucrose, Protein	4.8	1.2	4	82-96	100		0.83	Barber and Stucky, 1999
17	UASB+JLR	Sucrose, Peptone	0.59	0.068	8.6	86	92	400	1.0	Tai et al., 2006
18	UASB+CSTR	Municipal Leachate	1.6	0.11	14.0	98	58	300	4	Im et al., 2003
19	AGBR	Brewery	3.5	0.04 (0.13)*	21	99	98	200	1	Baloch et al., 2006
20	UASB/MBR	Glucose,VFA, meat extract, peptone	0.4-0.5	0.16-0.29	4	83	98	400	0.15	An et al., 2008
21	UASB+AS	Pre-settled piggery	3.1	0.640	5	54-77	97	300	0.63	Huang et al., 2007
22	UASB+BR	Landfill leachate	~12.5	1.7	7.3	81-93	70	200	1.5-4.1	Peng et al., 2008
23	FBB+FBB	Poultry slaughterhouse	0.39	0.064-0.14	2.7-6	84-95	92	600	1.2-6.1	Del Pozo and Diez 2003
24	UASB+UBAF	Industrial Wastewater	1.27-2.76	0.08-0.17	13-17	51-91	95	670	3.3	Lacalle et al., 2001
25	AABR	Aniline wastewater	4.2	0.6	7	90	96-97	600	3.3	Chen et al., 2009
26	UASB	Peptone+Nitrate	7.5	0.075-7.5	1-100	0-98	0-96	-	0.27	Ruiz et al., 2006
27	SBR+SBR	Piggery	0.5-2.5 (TOC)	0.25	10	85-91	81-91	100-300	1	Bernet et al., 2000

UASB: Upflow Anaerobic Sludge Blanket, EGSB: Expanded Granular Sludge Bed, UBF: Upflow Biofilter, CSTR: Continuous Stirred Tank Reactor, UBAF: Upflow Biological Aerated Filter, MUF: Multi-fed Upflow Filter, ABR: Anaerobic Baffled Reactor, MBBR: Moving Bed Bioreactor, MBR: Membrane Bioreactor, JLR: Jet Loop Reactor, FBB: Fixed film bioreactor, AABR: anaerobic aerobic biofilm reactor, BAS: biofilm airlift suspension., FBR: Fluidized bed bioreactor, AGBR: anaerobic baffled granular sludge bed reactor.

In biofilm processes, where diffusion gradients can evolve, resulting in distinct environmental conditions, methanogenesis and denitrification have reportedly been observed to co-exist. In a co-immobilized mixed culture system of denitrifying bacteria and methanogenic microbes contained in polyvinyl alcohol gel beads (Lin and Chen 1995), it was demonstrated that methanogenesis was active inside the beads where nitrate is absent, but denitrifiers grew on the surface of the beads. Hendriksen and Ahring (1996a) investigated removal of nitrate and carbon in an upflow sludge blanket (UASB) reactor with nitrate as nitrogen source and acetate as carbon source, at pH of 7 and temperature of 35 °C. [27] The system resulted in 96% denitrification and 99% COD simultaneously under OLR of 4.2 kg COD/m^3·d and nitrogen loading rate (NLR) of 0.28 kg NO_3-N/m^3·d corresponding to COD/N ratio of 15 and HRT of 0.71 d. In a 2001 study by Mosquera-Corral et al. (2001) it was noted that conducting anaerobic digestion and denitrification in one unit was possible when the carbon source is easily assimilated and an adequate C/N ratio is available in order to avoid methanogenesis inhibition. [28]

Hanaki and Polprasert (1989) investigated the potential of SDM in an upflow filter treating nitrate and methanol at COD/N ratio of 4.05 and OLR of 0.9-3.6 kg COD/m^3·d and resulted in 98-99.9% denitrification along with 95-97% COD removal through COD uptake by mostly denitrifiers and marginally methanogenic activity. [17] In the aforementioned system, the denitrification occurred in the bottom of an upflow anaerobic filter, but the methanogenesis happened in the top section of the filter, emphasizing on the accomplishment of SDM when the two activities are segregated within a single system.

In one study, a synthetic wastewater containing sucrose and peptone was treated with a UASB followed by an airlift reactor with a very low organic and nitrogen loading rates of 0.6 kg COD/m^3·d and 0.068 kg NO_x-N/m^3·d, respectively. [20] The denitrification and methanogenesis removal efficiencies of the integrated system were reported to be 86% and 92% at a COD/N ratio of 8.6, when the recycle ratio was 400%. In another study with low OLR of 3.1 kg COD/m^3·d and NLR of 0.64 kg NO_x-N/m^3·d, a pre-settled piggery wastewater was treated in a UASB activated sludge (AS) system, in which nitrified effluent of the AS reactor was recycled to the UASB at a recycle ratio of 300%. [29] The combined reactor system achieved efficient removal of COD (96–97%) and total nitrogen removal of (54–77%) although at a very low OLR for a UASB, where methanogenesis occurred with nearly complete denitrification in the UASB reactor. [29] All the above-mentioned SDM systems were running at OLR less than 5 kg COD/m^3·d, which is considered as a low organic loading rate. Furthermore, landfill leachate was treated in a two-stage UASB reactor followed by post treatment in an anoxic-oxic baffled reactor for nitritation. SDM with nitrite as the electron acceptor was observed in the first UASB reactor; where a maximum NO_2^--N removal rate of 3000 mg N/L·d was obtained. [30] Ruiz et al. (2006) stated that although it was possible to perform SDM in a UASB treating peptone at an OLR of 7.5 kg COD/m^3·d and NLR of 0.075-7.5 kg NO_x-N/m^3·d, feasible loading rates would be limited by the available activities. Therefore, in many cases separate reactors will be more suitable, where the denitrification occurs in a distinct anoxic environment.

Ahn et al. (2007) combined an anaerobic upflow bed filter with a membrane-aerated bioreactor to investigate simultaneous organic and nitrogen removal in the anaerobic system. Besides 99% organic removal as well as 46% nitrogen removal at OLR of <7.2 kg COD/m^3/d and COD/N of 14.5-32.5, a significant increase in membrane fouling was reported. [18] Transmembrane pressure (TMP) of the combined process was about 9 times higher than that of a unit MBR under the same operational conditions. The reason for this severe fouling in the combined system was postulated as increased extracellular polymeric substance (EPS) due to longer SRT of an anaerobic system and hydrophobicity.

Recycling of NO_2^- back to the anaerobic reactor can also result in the anaerobic reactor becoming enriched with ANAMMOX® bacteria, which use ammonia and nitrite to produce dinitrogen gas. [31] Also, Zhang (2003) studied the integration of methanogenesis and denitrification, with nitrite as the nitrogen and sucrose and glucose as the carbon source in an expanded granular sludge bed (EGSB) reactor at different OLR of up to 3.9 kg COD/m^3/d. As shown in **Table 10.1**, the system reached a complete denitrification of 97-100% with anaerobic COD reduction of 92-97%. [32]

An anaerobic baffled reactor (ABR), initially named as a modified sludge blanket reactor, comprises a series of UASBs. If the granular sludge is formed in this type of reactors, they are referred to anaerobic baffled granular sludge bed reactor (AGBR). One of the advantages of these types of reactors is reported to be separation of different microbial communities in different compartments along the reactor which results in a better resilience to organic and hydraulic shock loads as well as an ability to separate acidogenesis and methanogenesis longitudinally down the reactor. [24] The aforementioned advantages may be applicable when SDM process is occurring in the ABR reactor. Barber and Stucky (1999) reported an 82%-96% nitrogen removal through denitrification and 100% carbon removal through methanogenesis in a ABR at OLR of 4.8 kg COD/m^3·d and NLR of 1.2 kg N/m^3·d. However, denitrification predominantly occurred in the first two compartments and nitrogen oxide was eliminated before entering the methanogenesis zone in compartments 3 to 6.

Furthermore, a brewery wastewater with average COD of 10720 mg/L was treated in a 5-compartment AGBR, with five distinct compartments, followed by a nitrification unit. With an effluent recycle of 200%, OLR of 3.57 kg COD/m^3·d and NLRs of 0.04 kg NO_x-N/m^3·d and 0.13 kg NH_3-N/m^3·d, 97% COD removal due to methanogenesis and complete denitrification, were observed. [25] Interestingly, the concentrations of nitrate and nitrite in compartment 2 at different NO_x recycle to influent ratios varied from 0 mg N/L to 25 mg N/L and 0 mg N/L. Because the overall COD removal in this system was studied and it was not clear whether the anaerobic COD removal occurred in the first two compartments or not, an incomplete methanogenesis might have happened in compartment 2 and complete methanogenesis in compartments 3 to 5.

As seen in **Table 10.1**, among different system configurations, generally the biofilm and immobilized SDM systems as well as systems with different compartments such as ABR where the denitrifiers and methanogenic bacteria are located in different depth of biofilm or segregated in different compartments, have shown a better performance for simultaneous nitrogen and carbon removal.

It is also essential to measure nitrogen assimilatory uptakes by biomass in the SDM systems as well, in order to be subtracted from the overall nitrogen removal. Since the information regarding the observed biomass yield in different SDM systems is not provided, the nitrogen uptake by the biomass cannot be calculated. Although the biomass observed yields in anaerobic systems are low, at high OLRs and low NLRs assimilatory nitrogen removal by biomass synthesis could be significant.

10.3 Nitrogen Pathways

The discovery of new organisms is making the nitrogen cycle increasingly complicated, to the point that traditional descriptions of nitrification (ammonia is oxidised to nitrate via nitrite), denitrification (conversion of nitrate and nitrite to nitrogen gas), and nitrogen fixation are rather simplistic and insufficient for explanation of nitrogen pathways in real life. [7] **Figure 10.1** depicts the combination of nitrogen pathway and anaerobic digestion integrated from different references. [1, 7, and 33].The reactions occurring in **Figure 10.1** have been summarized in **Table 10.2**. It can be seen

from **Figure 10.1** that theoretically, methanogenesis should begin only after denitrification and at the excess amount of carbon; there should not be any inhibitory effect on methanogenesis or denitrifiers. In practice, however, the results are not quite the same as expected. For example, at high COD/NO_3-N ratios both acidogenesis and denitrification were reportedly hindered. [1, 14]

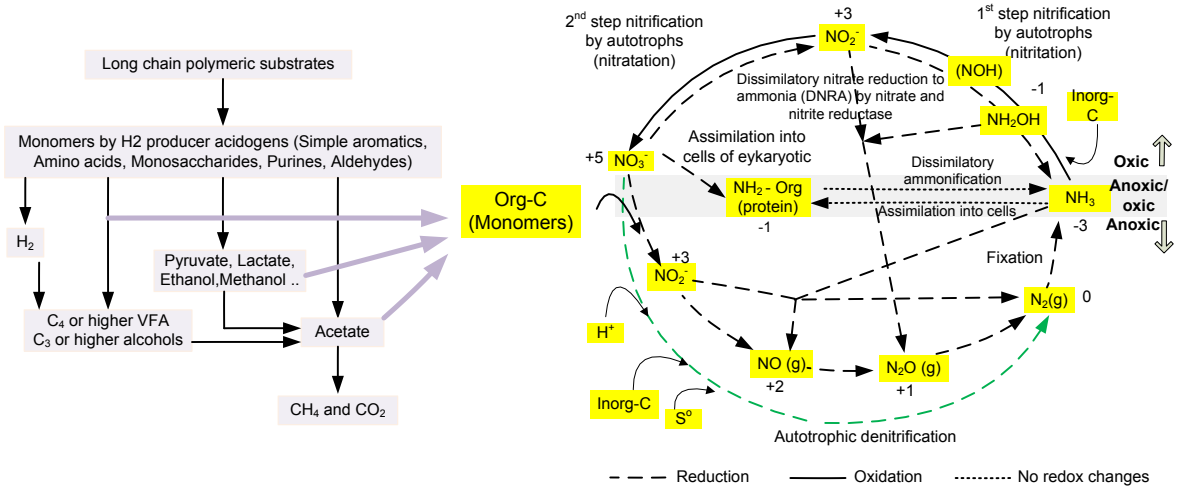

Figure 10.1. Inter relation of nitrogen pathway in an aqueous environment with microbial reactions in an anaerobic digestion.

In an anaerobic digester with the presence of nitrate, as the reactions shown in **Table 10.2**, the nitrate may be denitrified, reduced to the form of ammonia or converted to organic nitrogen. The biological nitrate reduction can be either a respiratory pathway, which is also called dissimilatory ammonification, or assimilatory ammonification, which denotes the reduction of nitrate to ammonia for the biosynthesis of nitrogenous compounds. These two pathways differ: 1- The enzymes of the respiratory pathways dissimilatory nitrate reduction to ammonia (DNRA) are integrated in cytoplasmic membranes or located in the periplasm (a space between the inner cytoplasmic membrane and external outer membrane of Gram-negative bacteria or the equivalent space outside the inner membrane of Gram-positive bacteria , and their synthesis is repressed by oxygen, whereas 2- The biosynthesis pathways use soluble enzymes, the synthesis of

which is repressed by ammonia. [4] According to Tiedje et al. (1988), DNRA is a major nitrate pathway in anaerobic digesters in which the nitrate reductase enzymes are within the cytoplasm. Several other researchers have also concluded that added nitrate was mainly reduced to ammonia, while only a minor fraction was recovered as nitrogen gas. [35] A number of obligate and facultative anaerobic, and microaerophilic, bacteria perform dissimilatory nitrate reduction to ammonium; mainly in carbon rich and low electron acceptor environments such as nitrate. Relative abundance of fermentative and obligate anaerobes such as ammonium formers, discovered in anaerobic environments is responsible for DNRA. [36] Assimilatory nitrate reduction occurs directly to eukaryotes, as shown in **Figure 10.1**. Also, organic nitrogen may be used further by bacteria and fungi to form ammonia (ammonification). Several authors have shown that high carbon to nitrogen ratios which are normally found in anaerobic digesters favor dissimilatory nitrate reduction to ammonia [1], while others found that a high COD/NO_3 did not favor dissimilatory reduction of nitrate to ammonia. [76] Rustrian et al. (1997) reported that the reduction of nitrate to ammonia was dominant at low nitrate loads (high COD/NO_3-N ratios: 361, 220 and 130) with 50% assimilation of nitrogen in biomass at COD/NO_3-N of 361.

As shown in **Table 10.2,** the Gibbs free energy for denitrification and DNRA reactions are significantly lower than methanogenic reactions. Assuming that neither denitrification nor methanogenesis is comparatively favored, reactions with lower Gibbs free energy have a much higher equilibrium constant (K_{eq}) at the same temperature, and consequently higher conversion rates.

$$K_{eq} = e^{\left(-\frac{\Delta G}{RT}\right)} \qquad (10.2)$$

Table 10.2. List of reactions occur in a SDM process

No	Reactions	ΔG^o (kJ/mol e donor)	Reference
	Methanogenesis		
1	$H_2 + 0.25\ HCO_3^- + 0.25\ H^+ \rightarrow 0.25CH_4 + 0.75H_2O$	-8.5	Van Lier et al., 2008
2	$CO_2 + 2\ CH_3CH_2OH \rightarrow CH_4 + 2\ CH_3COO^- + 2\ H^+$	-111 (mol CH_4)	Lengeler et al., 1999
3	$4\ HCOO^- + 4\ H^+ \rightarrow CH_4 + 3\ CO_2 + 2\ H_2O$	-144 (mol CH_4)	Lengeler et al., 1999
4	$4\ CO + 2\ H_2O \rightarrow CH_4 + 3\ CO_2$	-448 (mol CH_4)	Lengeler et al., 1999
5	$CH_3COO^- + H_2O \rightarrow CH_4 + HCO_3^-$	-31	Van Lier et al., (2008)
6	$4CH_3CH_2COO^- + 6H_2O \rightarrow 7CH_4 + CO_2 + 4HCO_3^-$	-57	Tugtas (2007)
7	$C_6H_{12}O_6 \rightarrow 3CH_4 + 3CO_2$	-428	Tugtas (2007)
8	$4CH_3OH \rightarrow 3CH_4 + CO_2 + 2H_2O$		Nishio et al., 1984
9	$CO_2 + 4H_2 \rightarrow CH_4 + 2\ H_2O$ (hydrogenotrophic)	-131	Henze et al., 2008
	Denitrification (Heterotrophs)		
10	$5H_2 + 2NO_3^- + 2H^+ \rightarrow 6H_2O + N_2(g)$	-224	Tugtas, 2007
11	$NO_2^- + 4H^+ + 3e^- \rightarrow 2H_2O + 0.5N_2(g)$	277	Gao et al., 2010
12	$5CH_3COO^- + 8NO_3^- + 8H^+ \rightarrow 9H_2O + 5CO_2 + 5HCO_3^- + 4N_2(g)$	-797	Tugtas, 2007
13	$5CH_3CH_2COO^- + 14NO_3^- + 14H^+ \rightarrow 17H_2O + 10CO_2 + 5HCO_3^- + 7N_2(g)$	-1398	Tugtas, 2007
14	$5C_6H_{12}O_6 + 24NO_3^- + 24H^+ \rightarrow 42H_2O + 30CO_2 + N_2(g)$	-2657	Lengeler et al., 1999
15	$C_6H_{12}O_6 + 8NO_2^- + 8H^+ \rightarrow 10H_2O + 6CO_2 + 4N_2(g)$	-3144	Lengeler et al., 1999
16	$5CH_3OH + 6NO_3^- \rightarrow 3N_2 + 5CO_2 + 6OH^- + 7H_2O$		Timmermans, 1983
	Denitrification (Autotrophs)		
17	$8NO_3^- + 5MeS + 6H_2O \rightarrow 2H^+ + 4N_2(g) + 5SO_4^{2-} + 5Me(OH)_2$		Cardoso et al., 2006
18	$NO_3^- + H^+ + 2.5\ H_2 \rightarrow 0.5N_2(g) + 3H_2O$	-560.3 kJ/reaction	Banihani et al., 2009
19	$3NO_3^- + 5NH_4^+ \rightarrow 4N_2(g) + 9H_2O + 2H^+$	-297	Mulder et al., 1995
	DNRA (Heterotrophs)- Respiratory ammonification		
20	$4H_2 + 2NO_3^- + 4H^+ \rightarrow 6H_2O + 2NH_4^+$	-150	Tugtas, 2007
21	$CH3COO^- + NO_3^- + 2H^+ \rightarrow CO_2 + HCO_3^- + NH_4^+$	-500	Tugtas, 2007
22	$8CH_3CH_2COO^- + 14NO_3\text{-} + 28H_+ \rightarrow 2H_2O + 16CO_2 + 8HCO_3^- + 14NH_4^+$	-878	Tugtas, 2007
23	$C_6H_{12}O_6 + 3NO_3^- + 6H^+ \rightarrow 3\ NH_4^+ + 3H_2O + 6CO_2$	-1767	Lengeler et al., 1999
24	$C_6H_{12}O_6 + 12NO_3^- \rightarrow 12\ NO_2^- + 6H_2O + 6CO_2$	-1767	Lengeler et al., 1999
25	$C_6H_{12}O_6 + 4NO_2^- + 8H^+ \rightarrow 4\ NH_4^+ + 2H_2O + 6CO_2$	-1713	Lengeler et al., 1999
	Aerobic deammonification		
26	$NH_2OH + NO_2^- \rightarrow N_2O(g)$		Henze et al., 2008
27	**Nitrification**		
28	$NH_4^+ + 1.5O_2 \rightarrow NO_2^- + 2H^+ + H_2O$	-277.68	Gao et al., 2010
29	$NO_2^- + 0.5O_2 \rightarrow NO_3^-$	-74.14	Gao et al., 2010
30	(overall) $NH_4^+ + 2O_2 \rightarrow NO_3^- + 2H^+ + H_2O$	-349	Mulder et al., 1995
	Nitrogen Fixation		
31	$N_2 + 8H^+ + 8e^- + 16ATP \rightarrow 2NH_3 + H_2 + 16ADP + 16Pi$		Henze et al., 2008
	Anoxic ammonia oxidation		
32	$NO_2\text{-} + NH_4^+ \rightarrow NO(g)$		Schmidt, 2002
	Anaerobic ammonia oxidation (Anommox)		
33	$1.3NO_2^- + NH_3^+ \rightarrow 1.02N_2(g) + 0.26\ NO_3^- + 2H_2O$	-357	Mulder et al., 1995

Since in the SDM process the two cultures are consuming a common carbon source, the reactions with lower Gibbs free energy are prone to suppression under limited carbon source.

Some researchers suggested that nitrate reduction to ammonium in methanogenic species also depends upon the nature of the available carbon source. [2] This reduction may be due to a boost in fermentative and obligate anaerobes in the presence of a fermentable substrate. Ammonification was reported to be the main pathway of nitrate reduction in a pure acidogenic system tested at high COD/NO_3-N ratios with 50% nitrate reduction to ammonia while glucose and glycerol were the substrates, and 100% nitrate denitrified to N_2 when acetate or lactate were the carbon sources. [13, 14, 37, and 38] However Shin (2002) suggested that acidogenesis favors nitrate reduction to ammonia, at alkalinity

below 2000 mg $CaCO_3$/L and after increasing the alkalinity up to 2400 mg $CaCO_3$/L the nitrogen cycle tends to favor denitrification to dinitrogen gas.

An anaerobic system due to its nature may be prone to ammonium anaerobic oxidation in the presence of electron acceptors such as nitrite. Simultaneous nitrite denitrification to N_2 and ammonium anaerobic oxidation (ANAMMOX®) was reported in an EGSB at COD/N ratios of 2.9-11.5 and maximum OLR of 3.9 kg COD/m^3·d using sucrose and glucose as the carbon sources and alkalinity of 1200 mg as $CaCO_3$/L (Zhang 2003). In addition, Sumino et al. (2006) integrated ANAMMOX® and denitrification in an upflow reactor treating synthetic wastewater at NLR of 0.6 kg N/m^3·d and C/N of 1 and reached 80%-94% nitrogen removal of which 50%-64% was contributed by ANAMMOX®. In the aforementioned report, the dissimilatory reduction of nitrite to ammonium was not observed and nitrogen removal occurred through nitrate reduction to nitrite in granular sludge at the bottom of the reactor and anaerobic ammonium oxidation with nitrite as electron acceptor by ANAMMOX® sludge attached to nonwoven-carrier at the top part of the single reactor. [31] It is worth mentioning that even though a methanogenic granular seed was used initially in the bottom part of the reactor to enrich denitrifiers, methanogenic activity was not reported after denitrification was completed on day 42.

10.4 Interactions of Methanogenesis and Denitrification

In an anaerobic digestion, carbon is eliminated through sequential steps of hydrolysis, acidogenesis, and methanogenesis. In some cases, hydrolysis and acidogenesis are decoupled with methanogenesis in two series of anaerobic reactors. Despite the phylogenetical diversity of methanogens, they have the ability to utilize a few simple compounds such as formate, CO_2, CO, methyl substrates such as methanol, methylamine, methylmercaptant and acetyl substrate such as acetate. [39]

Depending on the substrate, and the layout of the process, denitrifiers may interact with hydrolysis and acidogenesis along with methanogenesis in a single reactor or separately in series of anaerobic reactors. In the second case, VFAs, the products of the first two steps of hydrolysis and acidogenesis, can be used as readily biodegradable carbon source for heterotrophic denitrification. On the other hand, when denitrifiers and

methanogens are in the same habitat, they seem to be in competition for carbon uptake. However, it has been repeatedly stated in the literature that substrate competition was not the main mechanism for the suppression of methanogenesis. In fact, inhibition of methanogenesis by N-oxides has been implicated as the main mechanism involved in the suppression of methanogenesis. [40, 41]

Moreover, methanogenesis takes place in the absence of oxygen or other electron acceptors. Addition or presence of other, energetically more favorable electron acceptors than CO_2 such as nitrate, nitrite, sulphate, usually results in the reduction of these electron acceptors instead of methane production. [9]

As shown in **Table 10.2,** Tugtas and Pavlostathis (2007) stated that as a result of higher energy yield during denitrification; the bacterial yield is higher, as compared to that for methanogenesis. In addition, since stoichiometrically, complete nitrate reduction to nitrogen gas requires 5 electron equivalents per mol of nitrate, co-existence of fermenters/methanogens and denitrifiers may cause channeling of electrons away from methanogenesis, which may result in decrease in the overall methane production. [10]

Besides other important parameters such as organic and nitrogen loading rates (OLR, NLR), oxidation reduction potential (ORP), pH, COD/NO_3-N ratio and alkalinity have significant effects on the rate of SDM. The inhibitory effect of NO_x on methanogenesis has also been proposed by different researchers [9, 42], but a clear explanation of the inhibitory causes is still lacking.

10.4.1 Bacterial Consortium

Methanogens are of the domain, *Archaea* and are either *cocci* or *bacilli* shape. All are anaerobic and are important in the digestion of the waste products of other bacteria present in the same environment. Denitrifiers are bacteria that metabolize nitrogenous compounds and are also affected by environmental parameters such as pH and temperature in any anaerobic process. However, up until recently, methanogens were only reported to be involved in the catabolism of excess hydrogen and other fermentation products. Nitrate in an anaerobic system is either reduced to ammonia by nitrate reducing

bacteria such as *Pseudomonas denitrificans*, *Bacillus* (ammonification) or is denitrified to nitrogen by *Achaea* organisms. [43]

The demonstration of methanogens in denitrifying bioreactor ecosystems shown in **Table 10.1**, would mean, first, that methanogens and denitrifiers can be compatible and exist at comparably high redox potential. Second, the presence of methanogens would indicate a syntrophy between the denitrifying bacterial consortium producing hydrogen and hydrogen-consuming methanogens. [44] Zellner et al. (1995) studied syntrophy of a denitrifying consortium and methanogens in a fixed film reactor when methanol was the electron acceptor. An analysis of the biofilm identified methanogens and some bacteria responsible for denitrification using microscopy and immunologic analysis, antigenic fingerprinting technique. Zellner et al. (1995) used antibody probes for 17 methanogens and six *Pseudomonas stutzeri* to immunologically characterize the bacterial biofilm population. As shown in **Table 10.3**, the bacterial biofilm population of the denitrifying reactor was complex with distinct morphotypes of denitrifying, methylotrophic cells belonging to *Pseudomonas stutzeri*, *Methylobacterium spp*. and *Hyphomicrobium spp*. and of methanogens belonging to *Methanobrevibacter spp*. and *Methanosarcina spp.* [44] *Hyphomicrobium spp*. was also found to be one of the dominating organisms, along with *Alcaligenes denitrificans*. [44]

Table 10.3. Common bacteria and Archaea species involved in SDM

Genus	Metabolic Process	Number of Cells In mL of dispersed biofilm	Morphology	references
Pseudomonas stutzeri ATCC 17593	Denitrification	1.10E6	Gram (-) rod	Zellner et al., 1995
Pseudomonas stutzeri AN11	Denitrification	1.33E8	Gram (-) rod	Zellner et al., 1995
Methanobrevibacter smithii PS	Methanogenesis	3.20E4	Gram (+) coccoid	Zellner et al., 1995
Methanobrevibacter arboriphilus DH1	Methanogenesis	1.96E5	Gram (+) coccoid	Zellner et al., 1995
Methanobrevibacter smithii AL1	Methanogenesis	1.08E5	Gram (+) coccoid	Zellner et al., 1995
Methanobrevibacter arboriphilus AZ	Methanogenesis	4.37E6	Gram (+) coccoid	Zellner et al., 1995
Methanobrevibacter arboriphilus DC	Methanogenesis	9.27E7	Gram (+) coccoid	Zellner et al., 1995
Alcaligenes denitrificans	Denitrification	-	Gram (-) rod	Zellner et al., 1995
Methylobacterium spp.	Denitrification	-	Gram (-) rod	Zellner et al., 1995
Methanosarcina spp.	Methanogenesis	-	Gram (+) coccoid	Lin &Chen 1995 Zellner et al., 1995
Hyphomicrobium spp.	Denitrification	-	Gram (-) rod	Lin &Chen (1995) Zellner et al., 1995

In an attached growth system, it has been shown that denitrifiers with less biofilm density and faster growth rate tend to grow along the outer surface of the media, whereas

dense anaerobic methanogenesis, with slower growth rate, accumulate in the interior of the media. Using a phase contrast microscope, Lin and Chen (1995) studied a co-immobilized mixed culture using gel beads as carrier, at pH of 7 fed with 800 mg/L methanol and 100 mg/L NO_3-N and revealed that *Methanosarcina* bacteria and *Hyphomicrobium spp.* were able to grow simultaneously as they occupy different regions of the gel beads. *Hyphomicrobium spp.* bacterium grew mainly on the peripheral surface while *Methanosarcina spp.* bacterium grew in the inner part of the gel beads, shown in **Table 10.3**. Therefore the methanogens would enable the denitrifiers to grow on methanol by removing hydrogen if nitrate was absent or methanol (or another organic electron donor) was in excess of nitrate.

It can be concluded that *Pseudomonas stutzeri*, *Methylobacterium spp*., *Hyphomicrobium spp*., *Methanobrevibacter spp*., *Methanosarcina spp*., and *Alcaligenes denitrificans* are the dominant organisms in fixed-film SDM and that they can co-exist using methanol as the electron donor the complete the processes.

10.4.2 Nitrogenous Compounds Inhibition

The reports of SDM are indeed intriguing, as methanogenesis is reported to be inhibited by denitrification (the reason is not very clear) at different COD/N ratios. In fact, methanogenic activity was reportedly completely suppressed in a co-immobilized mixed culture system until the nitrite and nitrate concentration in the bulk were almost negligible. [2, 16] The inhibitory effect of denitrification on methanogenesis is complicated due to the different degree of inhibition by various denitrification intermediates such as NO, N_2O, NO_2^-, NO_3^-.

Ammonia toxicity can be a problem in feedstocks with high protein content. Ammonia is rapidly formed in a digester by dissimilatory ammonification of protein constituents. Free ammonia has been found to be much more toxic to methanogens than ammonium ion, and thus ammonia toxicity thresholds are very sensitive to pH below 7.0. [45] In general, free ammonia levels should be kept below 80 ppm, to prevent inhibition. [45] However, a much higher concentration, about 1500 - 3000 ppm, ammonium ion can be

tolerated.[46] Concentrations of free ammonia and ammonium ion are related by equilibrium reactions and pH.

The inhibitory effects of N compounds on methanogenesis seem to be caused by several mechanisms:[9] (1) the toxic effect of N compounds on members of the methanogenic microbial community; (2) the competition between denitrifiers and methanogenesis for H_2 substrate; (3) temporary accumulation of sulphate and Fe_3^+ produced during denitrification, which consequently allow sulphate reducers and Fe_3^+ reducers to become active and compete for H_2 substrate with methanogenesis. It has been shown that addition of nitrate, nitrite and nitrous oxide (N_2O) decreased the H_2 concentration (partial pressure) below the threshold of methanogens, thus not allowing exergonic production of methane ($\Delta G>0$). Although CH_4 production was inhibited, addition of NO caused a decrease in H_2 concentration, which made exergonic methanogenesis from H_2/CO_2 always possible ($\Delta G<0$).[9, 47] Methanogenic activity did not resume until all the electron acceptors were reduced and consequently H_2 had reached the methanogenic threshold again. Thus, the competition between methanogens and denitrifiers for H_2 is not significant. Roy and Conrad (1999) concluded that the main mechanism involved in the suppression of CH_4 production by nitrate is the inhibition of methanogenic intermediates rather than the competition between denitrifiers and methanogenesis for substrates.

Akunna et al. (1992) studied the effect of different influent NO_3-N and NO_2-N concentration on COD removal in a CSTR with influent COD of 5319 mg/L and C/N ratios of 2-100. The lowest effluent COD was observed at nitrate and nitrite loads of 0.01-0.08 kg NO_3-N/m^3·d (100-800 mg influent N/L) and 0.06-0.08 kg NO_2-N/m^3·d, respectively. Akunna et al. (1992) stated that higher influent COD removal was compensated by denitrification process when the COD removal by methanogenesis was lower. However, COD uptake through denitrification, when influent nitrate is 100 mg/L, is insignificant compared to influent COD concentration of 5310 mg/L. At nitrate and nitrite influent concentrations of 2500 mg NOx-N/L, methane production and ammonification stopped while denitrification decreased considerably, indicating a global inhibition induced by the high influent nitrate and nitrite. Chen et al. (1997) studied the

effect of nitrate loading in a CSTR co-immobilized denitrification and methanogenesis with methanol as carbon source, and concluded that even at a high influent concentration of nitrate up to 774 mg N/l and COD/N ratio of up to 3.4, denitrification efficiencies were stable at >99% with methanol removal efficiencies >98%.

As shown in **Table 10.4a**, Kluber and Conrad (1998) reported the nitrogen oxide inhibition of methanogenesis is as follows: $NO>NO_2>N_2O>NO_3^-$. As seen in **Table 10.4a,** the inhibitory effect of nitrogenous compounds on methanogenesis varies largely and depends on the methanogenic species and their metabolic substrates. [9] It was concluded that NO is the strongest inhibitor, being effective even at 10 μg/L, with irreversible effect as separation of NO from the culture head space did not result in resumption of methanogenesis. [9, 40] It was also concluded that N_2O inhibitory effect was partially reversible, as removal of N_2O from the headspace caused partial methanogenesis revitalization. The inhibition imparted by NO_3^- was also reported in the literature as not due directly to NO_3^- itself, but instead due to reduced intermediates such as NO_2^- formed during the denitrification process [11, 48], as an inhibition of methanogenesis in a lag phase of one day following nitrate injection was not observed in a SDM. Although Percheron et al. (1999) demonstrated that some methanogenic species can grow at a NO_3-N concentration as high as 630 mg/L, Kluber and Conrad 1998 reported that nitrate inhibited *Methanobacterium bryantii* at a NO_3-N of 420 mg/L. Elsewhere, accumulation of intermediate nitrites was observed when insufficient carbon was supplied to an SDM system with C/N <1.5, which further inhibited the methanogenic activity. [13] Nitrite accumulation was higher with glucose as the carbon source, and lower with benzoic acid.

Inhibitory effects of methane production caused by nitrogen oxides may be due to enzyme inhibition and/or changes in the redox potential. [12] Seifritz et al., (2002) found that in the presence of nitrate *Moorella thermoacetica* lacked a membranous b type cytochrome, which was present in cells grown in the absence of nitrate. On the other hand, the toxicity of NO may be due to its reaction tendency with transition metal protein enzymes and oxygen, and its ability to form adducts with amines and thiols of varying stability. [50] The direct inhibitory effect of nitrate/nitrite reductase enzymes on methanogenic activity, however, has not been studied.

Table 10.4. (a) Concentration of N-compounds causing 50% and 100% inhibition of methanogenesis (adapted from Clarens et al, 1998; Kluber and Conrad, 1998; Zhang 2003) (b) Short and long inhibitory effect of nitrogen oxides on methanogenesis (adapted from Tugtas et al., 2007)

N-oxides	*Methanogarcina mazei* In acetate substrate		*Methanogarcina barkeri* In the H_2/CO_2 substrate		*Methanobacterium bryantii* In the H_2/CO_2 substrate	
	50%	100%	50%	100%	50%	100%
NO_3^--N (mg/L)	560	>>980	72	>>720	350	>>420
NO_2^--N (mg/L)	1.4	≥2.8	0.7	≥1.4	14	-
NO-N- (µd/L)	-	-	12.6	≥23.8	4.2	≥11.2
N_2O-N (mg/L)	-	≥12.04	3.64	>26.6	0.84	≥2.66

Table 4b. Short and long inhibitory effect of nitrogen oxides on methanogenesis (adapted from Tugtas et al., 2007)

		N-Oxide reduction	Methane Production		
Culture Series	COD/N	Time (day)[a]	Recovery Time (day) [b]	Initial Rate (mL/L-day) [c]	Normalized Rate (%) [d]
NO_3^- (mg/L)					
0	-	0	0	182±21	100
10	166	0.6	0	179±13	98
30	55	1.2	0	166±17	91
75	22	1.2	0.9	157±7	86
150	11	1.2	1.2	95±0	52
350	5	4.3	4.3	34±13	18
NO_2^- (mg/L)					
0	-	0	0	136±5.4	100
17	97	0.1	0.1	102±7	75
50	33	0.8	0.8	27±2	20
125	13	1.6	1.6	26±7	19
250	7	2.8	10	18±1	14
500	3	10	18	2.6±0.9	2
NO (mg/L)					
0	-	0	0	136±21	100
0.02	83000	ND	0	143±14	105
0.16	10400	ND	0	64±14	47
0.8	2070	16.5	ND	0	0
N_2O (mg/L)					
0	-	0	0	207±28	100
19	87	1.2	0.17	100±7	48
48	35	1.2	0.9	107±14	53
96	17	1.2	1.17	121±7	58
191	9	2.0	1.2	93±7	45

ND, not detected

[a] Time required for the complete N-oxide reduction to N_2.

[b] Incubation time at which methane was first detected.

[c] Results of linear regression (mean±stdev; n ≥3) of single culture data starting at the recovery time.

[d] Normalized to the initial methane production rate of the control culture observed at each assay.

Most of the experiments done by researchers to study the inhibitory effects of nitrogen oxides were conducted in batch tests and concluded that the methanogenesis were either very slow during the denitrification or completely hindered until the nitrogen oxides disappeared. [9, 11, 12, 32, 40, 51, and 76] In particular, Tugtas and Pavlostathis, (2007) studied the short and long term inhibitory effect of nitrogen oxides, as shown in **Table 10.4b**, at different COD/N ratios. Simultaneous methane production and N-oxide reduction was observed in the 10 and 30 mg N/L nitrate and 0.02 mg N/L aqueous NO-amended cultures. However, addition of N-oxides resulted in immediate cessation of methanogenesis in all other cultures. Methanogenesis completely recovered, subsequent to the complete reduction of N-oxides to nitrogen gas in all N-oxide amended cultures, with the exception of the 500 mg N/L nitrite and 0.8 mg N/L aqueous NO amended cultures in different recovery times, shown in **Table 10.4b**. Partial recovery of methanogenesis was observed in the 500 mg N/L nitrite-amended culture, in contrast to complete inhibition of methanogenesis in the 0.8 mg N/L aqueous NO-amended culture. Accumulation of volatile fatty acids was observed in both cultures at the end of the incubation period. There have been some reports [11] indicating the significance of the type of substrates on the inhibitory degree of nitrogen oxides. Hydrogen as the substrate for methanogenic activity reduced NO_2^- slowly, such that NO_2^- accumulated more, and as a result the toxicity was greater compared to acetate as a substrate. [11, 51]

In contrast to the literature, Barber and Stucky, (2000) reported 67% increase in methane production in the front compartment of an anaerobic baffled reactor treating glucose/protein at OLR of 4.8 kg COD/m^3·d (**Table 10.1)**, when nitrate and nitrite were present in the system with concentrations of 176 mgN/L and 43 mgN/L, respectively. An increase in pH, due to release of hydroxyl ions during denitrification, was mentioned as a cause of methanogenesis improvement as well as dissimilatory nitrate reduction to ammonia (DNRA), which was explained to be responsible for the improved methane production in two ways:

1- DNRA reaction has a very high hydrogen demand (4 moles of hydrogen required per mole of nitrate reduced), which reduced hydrogen to levels low enough to allow syntrophic reactions to proceed and this resulted in a build-up of methane precursors.

2- Ammonium ion released during DNRA was reported to possibly improve methane production due to an enhanced availability of reduced nitrogen as a nutrient to methanogens.

In the case of a continuous system all successful SDMs are all reported at lower COD/N << 15 and OLR<< 10 kg COD/m^3·d. [1, 2, 3, 17, 27, and 32]

The mechanisms of nitrogen oxide inhibition of methanogenesis in anaerobic digesters can be considered far from solved, and are probably complex comprising of toxicity, competition, and indirect stimulation of other respiring bacteria by oxidation of reduced electron acceptors such as ferrous iron and sulphide. [52]

10.4.3 Effects of Various Carbon Sources and C/N Ratio

The nature of carbon source and the carbon to nitrogen ratio (C/N) are important parameters in the operation of denitrification systems at optimal conditions from both, technical and economic points of view. [28] Coupled anaerobic digestion and denitrification in one unit is reportedly possible when the carbon source is easily assimilated and an adequate C/N ratio is available in order to avoid methanogenesis inhibition. [1, 17] Roy and Conrad (1999) reported that in SDM the duration of the suppression of methanogens by nitrate electron acceptor was closely related to the ratio of electron donor (COD) to electron acceptor. The greater this ratio, the shorter the suppression, indicating that nitrate and its potentially toxic denitrification intermediates nitrite, NO and N_2O, were then faster reduced to non-toxic N_2.

Some researchers suggested that the nature of substrate in anaerobic sludge impacts nitrogen pathways. Volatile fatty acids, such as acetic acid reportedly favored denitrification, while fermentative substrates such as glucose and glycerol were preferred for ammonification. [52] Akunna et al., (1995) stated that dissimilatory nitrate reduction to ammonia took place in anaerobic digestion only during fermentation and that nitrate conversion to ammonia was greatly minimized with non-fermentable organic carbon sources i.e. VFAs. **Figure 10.2a** shows the carbon flux in an anaerobic digestion/NO_x reduction system proposed by Akunna et al. (1995), which also suggest that the

proportion of nitrate transformable to ammonia during fermentation would be relatively high when influent COD/NO_3-N ratio was large. Akunna et al., (1993) studied the NO_x reduction pathway in batch digested sludge in the presence of five different carbon sources: glucose, glycerol, acetic acid, lactic acid, and methanol and concluded that nitrogen reduction pathway depend on the nature of organic substrate present in the medium at C/N ratio of 3.8-5.4.

Ammonium accumulation was found in glucose and glycerol media as a result of 50% dissimilatory nitrate and nitrite reduction to ammonia; the rest were denitrified. In the media containing these glucose, glycerol and VFAs, particularly acetic acid, were produced and ammonification was higher than denitrification only when glucose and glycerol were still present in the media. Ammonium production was higher in nitrite cultures than in nitrate cultures for the glucose and glycerol media, when in the culture media with acetic and lactic acids and methanol, ammonium was not detected. Thus, nitrate/nitrite reduction in acetic and lactic acids media was essentially due to denitrification. Moreover, COD requirements for nitrate and nitrite reductions were generally lower in cultures with acetic and lactic acids than in glucose and glycerol cultures. The methanol culture media showed a very small reduction rate for the N-NO_x indicating minimal quantities of bacteria capable of denitrifying with this substrate. On the other hand, Shin et al. (2002) conducted a SDM with glucose and acetic acid as different carbon sources, and concluded that the denitrification/ammonification ratio is a function of alkalinity regardless of the kind of substrate as the carbon source. **Figure 10.2b** proposed by Shin et al. (2002) shows a modified carbon flux in an aerobic/NOx reduction system based on the alkalinity in the system.

For denitrification with methanol as carbon source, COD required for denitrification ranging from 2.7 to 5.34 g sCOD/g NO_3^--N have been reported. [12, 17, 53, and 54] The COD demand was found to be less (2.5-3.9 g sCOD/g NO_3^--N) when ethanol was the carbon source. [55] According to Reaction (10) **Table 10.2**, denitrifying 1 g of NO_3^--N chemically requires 2.86 g of COD, because each mole of hydrogen is equivalent to 16 g of COD ((5/2) x (16/14)=2.86). The actual required COD, however, would be greater than 2.86 due to COD required for cell growth.

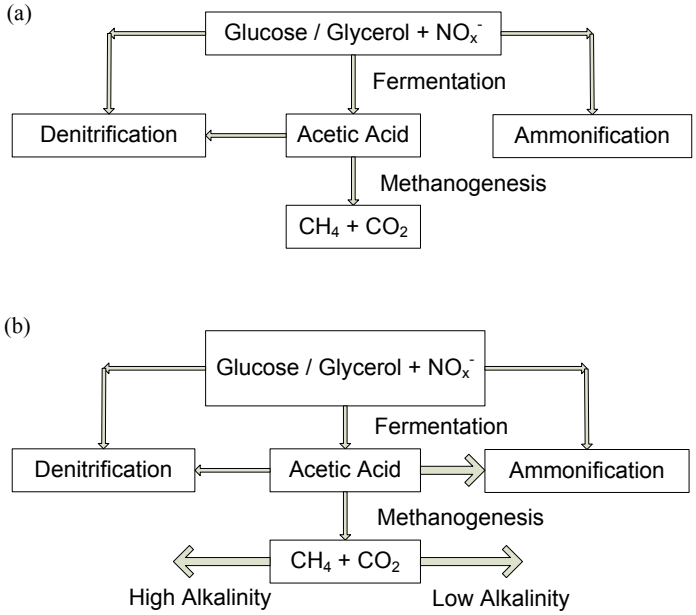

Figure 10.2. (a) Carbon flux in an aerobic digestion/NOx reduction system (Adapted from Akunna, 1995) (b) Modified carbon flux in an anaerobic digestion/NOx reduction system. (Adapted from Shin et al., 2002)

Chen and Lin (1993) concluded that in a batch system although at CH_3OH/N of higher than 2.7 (COD/N of 1.8), methanol was maintained in the system after accomplishment of denitrification, at CH_3OH/N of up to 3.97 corresponding to COD/N ratio of 5.9; methane formation was completely suppressed as long as the presence of nitrogen oxides was sustained. Complete methane production was then observed at CH_3OH/N of 5.25 corresponding to COD/N of 7.8. However, when nitrogen oxide in the culture was consumed by denitrification process, they could no longer effectively suppress methanogenesis. The necessary external electron donor (methanol) was found insufficient for complete denitrification in the case of CH_3OH/N ratio of 1.6 corresponding to COD/N of 2.4. Complete denitrification in an anaerobic UASB treating phenol took place when the COD/ NO_3^--N was as low as 3.34, while there was no methane production indicating that all COD was consumed for denitrification alone. [19]
Figure 10.3 shows denitrification and methanogenesis activity (%) versus the COD/NO_3-N ratio at different alkalinities in batch and continuous-flow systems under different

OLRs and NLRs proposed by different researchers. Percheron et al. (1998), using batch treating sulphide-rich molasses at pH of 7.4 and T of 34°C, stated that at COD/NOx-N ratios up to 65 nitrogen oxides were completely reduced to nitrogen gas. The effect of alkalinity, however, was not considered in their studies. Rustrian et al. (1997) reported that VFAs were produced with nitrate and glucose as substrates in a acidogenesis CSTR without denitrification at COD/N-NO_3 ratios > 220; denitrification and VFA production at 88.5 ≤ COD/N-NO_3 ratios ≤ 220, and denitrification and smallest VFA rates at COD/N-NO_3 ratios < 44.3. At COD/N-NO_3 ratios > 130, nitrate assimilation appeared to be the main nitrate reduction pathway. The degree of acidification (the ratio of volatile fatty acids as COD to initial substrate COD) increased from 4% at COD/NO_3-N ratio of 10 to the maximum of 53% at COD/NO_3-N of 88. However, the degree of acidification decreased from 53% to 27% with increasing the COD/NO_3-N ratio from 88.5 to 360. The lowest concentration of VFA in the outlet was obtained at COD/NO_3-N ratios < 20.

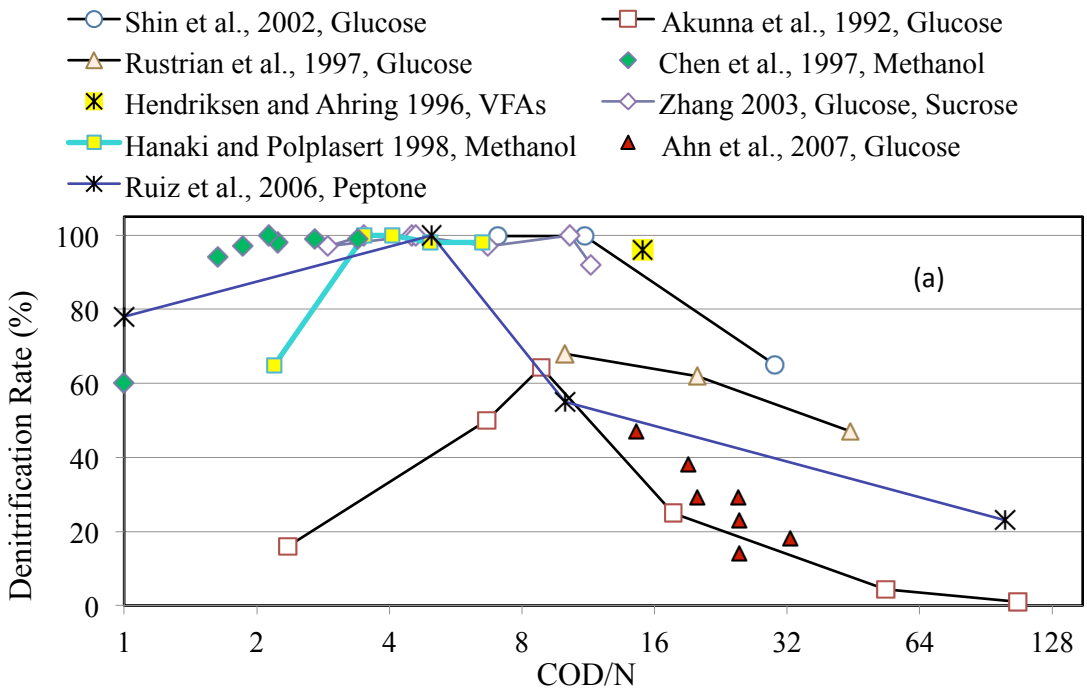

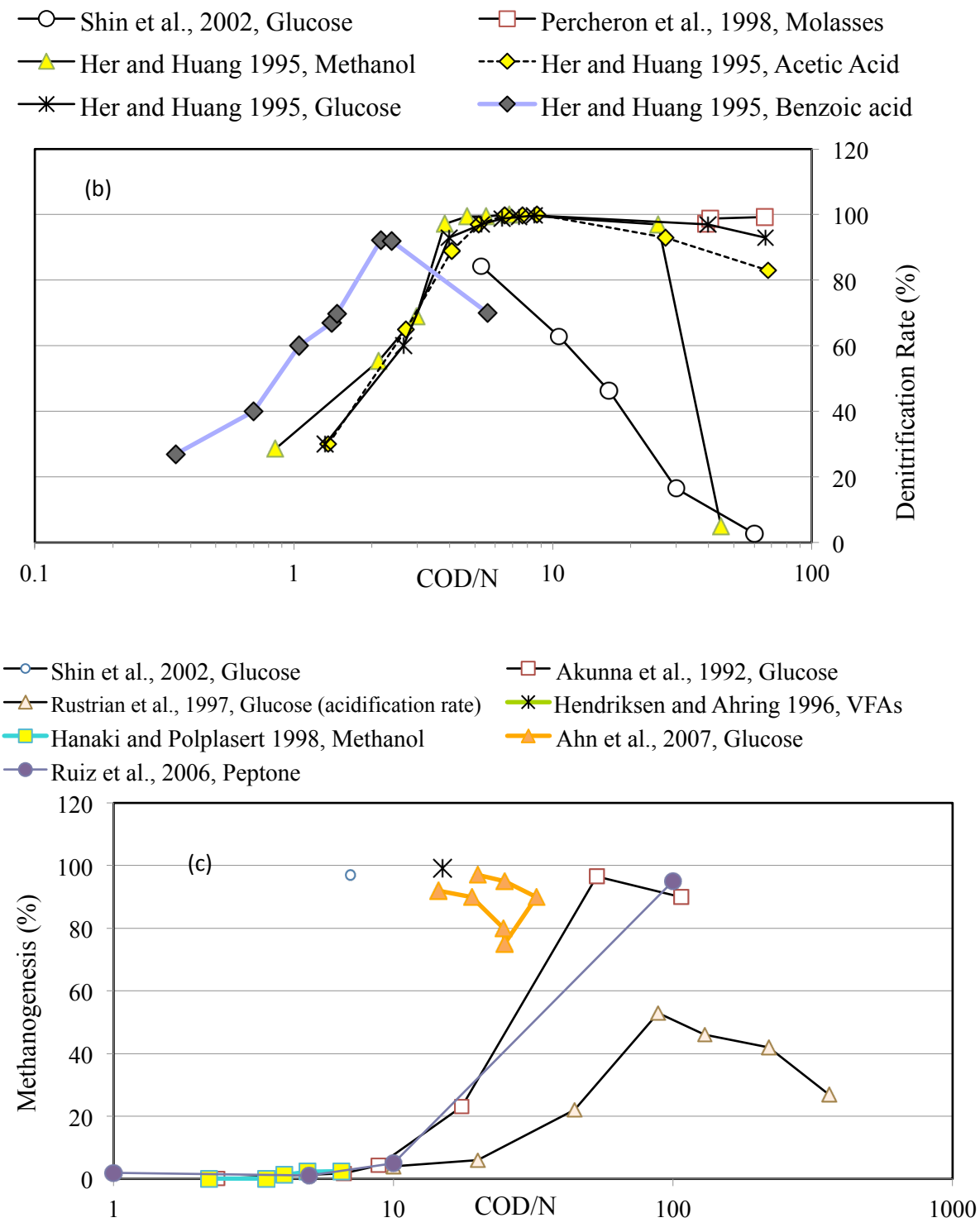

Figure 10.3. (a) Denitrification activity versus COD/N ratio in continuous SDM systems (b) Denitrification activity versus COD/N ratio in batch SDM systems (c) Methanogenic activity versus COD/N ratio in continuous SDM systems

Akunna et al. (1992) reported methane production without denitrification at COD/N-NO_X > 53 with glucose as substrate in a CSTR of combined acidogenesis and methanogenesis; denitrification and methane production at 8.86 ≤ COD/N-NO_X≤ 53 and only denitrification at COD/N-NO_X < 8.86. At COD/N-NO_X > 53, ammonification was also reported to be the main nitrate and nitrite reduction pathway, and at COD/N-NO_X > 106, a 100% reduction of nitrate and nitrite to ammonia was observed. As depicted in **Figure 10.3c**, methanogenesis rate decreased as the COD/NO_3-N was decreased. The maximum methane percentage of 55% (96.5% methanogenesis) was recorded at a COD/NO_3-N ratio of 53. At COD/NO_3-N ratio of 2.13, methane production ceased entirely.

As depicted in **Figure 10.3**, Hanaki and Polprasert (1998) also studied the effect of COD/N ratio at different OLR while treating methanol by an upflow filter and confirmed three different zones (already proposed by Her and Huang, 1995) of COD/N< 3.45 where incomplete denitrification occurs, named as zone 1, 3.45 ≤ COD/N < 3.97 complete denitrification without methane production and zone 3 with COD/N > 4 where methane production initiated. In Hanaki's work the experiments were conducted for COD/N < 6.5 and at maximum OLR of 2.0 kg COD/m^3·d.

Her and Huang (1995) investigation of the influence of carbon source and C/N ratio on denitrification in anaerobic batch systems concluded that the minimum C/N ratio required for nearly complete denitrification using an aromatic carbon source (benzoic acid) was significantly higher that non aromatic carbon sources, and therefore the minimum C/N ratio required for nearly complete denitrification increased with an increase in molecular weight. However, normalizing C/N ratio to COD/N for benzoic acid resulted in a lower minimum COD/N ratio compared to the other sources for complete denitrification. The Minimum COD/N ratio for methanol, acetic acid, glucose and benzoic acid were reported as 3.8, 4.1, 3.9 and 2.1, respectively corresponding to the C/N ratios of 0.9, 1.9, 1.5 and 3.1.The appropriate C/N for nearly complete denitrification when nitrate was the nitrogen source for different carbon sources of methanol, acetic acid, glucose and benzoic acid were 0.9-10, >1.9, >2.0 and 3.0-3.6, respectively corresponding to the COD/N ratios of 3.6-42, 6.5-8.7, 6.4-8.5 and 1.5-2.4. When nitrite

was the nitrogen source, the C/N ratios for the aforementioned substrates, respectively changed to 0.6-10, >1.3, >1.6 and 2.6-3.6. Increasing the C/N ratio to 15 in the case of methanol and benzoic acid as the carbon source, hindered denitrification to as low as 4%, whereas C/N ratio up to 25 did not hinder denitrification when acetate and glucose were the carbon sources.

The same trend for the effect of the C/N ratio was also observed in an immobilized denitrifiers and methanogens in gel beads in a CSTR system at NLR of 0.6 kg $NOx/m^3 \cdot d$. [15] At COD/N<1.74, the denitrification was incomplete due to the limitation of the methanol supply as carbon source. A complete denitrification with nitrogen removal efficiency of 99% was achieved at COD/N of >1.74. At 1.74 < COD/N < 3.4 methanogenic activity was reported to be responsible for carbon removal. In this study, it was also indicated that methanogenic activity occurred only after nitrate or nitrite were completely depleted.

The effect of COD/N ratio on the SDM seems to be different in biofilm processes, as Hendriksen and Ahring (1996a) reported 96% denitrification rate at COD/N of 15 using an UASB treating VFAs at 1500 mg $CaCO_3$/L alkalinity. Hanaki and Polprasert (1998) also observed 98% denitrification rate while treating alcohol with alkalinity of 1400 mg $CaCO_3$/L and COD/N of 6.5 by an up-flow filter. As shown in **Figure 10.3**, Zhang (2003) reported a 97%-100% denitrification rate with COD anaerobic reduction of 92-97% at COD/N of 10.3 using an EGSB treating sugar (glucose and sucrose) at alkalinity of 1000 mg CaCO3/L, when nitrite was the initial electron acceptor.

10.4.4 Effects of Alkalinity, pH, Temperature and ORP

Alkalinity has a vital role in anaerobic digestion and the pH of the microbial culture. A 16% decrease in organic removal efficiency in a UBF treating synthetic wastewater was reported when the alkalinity was decreased to 3000 mg $CaCO_3$/L from the initial 4000 mg $CaCO_3$/L. [18] Shin et al. (2002) studied the effect of the alkalinity on the denitrification and ammonification ratio in SDM, and came up with a modified carbon flux model in an anaerobic digestion/NO_x reduction system, as shown in **Figure 10.2b** concluding that alkalinity played an important role on ammonification and denitrification

in anaerobic sludge regardless the type of substrate. However, the effect of changes in denitrification and ammonification rates on methanogenesis and how they affected the system ORP was not reported in this study.

Shin et al (2002) reported a complete denitrification when acetate was the carbon source with COD/NOx-N ratio of 25 to 30 and alkalinity of 2400 mg as $CaCO_3$/L. When alkalinity was decreased from 2400 to 600 mg $CaCO_3$/L, denitrification was hindered completely and ammonification occurred. Again, raising the alkalinity to 3000 mg $CaCO_3$/L resulted in complete denitrification and a similar phenomenon was observed while using glucose as a substrate with COD/N ratio of 25-30. Following the decrease of alkalinity from 2400 mg $CaCO_3$/L to less than 1000 mg $CaCO_3$/L, the ammonification increased to 100% and an increase of alkalinity up to 2000 mg $CaCO_3$/L converted most of the nitrate to nitrogen gas. It should be mentioned that in the case of glucose as the substrate both ammonification and denitrification fluctuating during the test.

The pH and temperature are reported in the literature as important parameters that affect the behavior of denitrifiers and methanogens in an anaerobic process. Chen and Lin (1993) examined the correlation between denitrifiers and methanogenesis in a mixed culture system of wastewater sludge, with the main focus being the substrate competition between the organisms. They noted that the optimum conditions for denitrification were pH of 7.0-8.0 and 30-35°C, while for methanogenesis they were pH of 6.5-7.5 and 30-35°C.

Methanogenesis has been known to proceed, only under strict anaerobic conditions at a redox potential (ORP) below -330 mV [56, 57] and denitrification proceeds at a higher redox potential of -100 mV. [58]

The suppression of methanogenesis by N-oxides was first attributed to the increase in the redox potential due to nitrate addition. [40] However, studies conducted under controlled redox conditions revealed that the suppression of methanogenesis was not related to changes in the redox potential. [59, 60] Tai et al. (2006) found that ORP as high as -250 mV for sole methanogenic activity has been reported in a UASB synthetic wastewater, which further increased to -26 mV during the early stage of the recycled

period of nitrate following a drastic reduction in biogas and methane production. Furthermore, Fetzer and Conrad (1993) have shown that rates of methane production were not significantly affected when the redox potential value of an anoxic medium ranged -100 to -420 mV. [61] This indicated that ORP is possibly not the factor affecting methanogenesis in a mixed culture system involving both heterotrophic denitrifiers and methanogens, since the reactor had turned into an anoxic reactor, and the condition was no longer strictly anaerobic. [20] Akunna et al. (1998) and Chen and Lin (1993) used cultures containing cysteine solution and Ti(III) citrate as reducing agents respectively which lowered the redox potential to about -300 mV and -340 mV to -530 mV. Although cysteine enhanced methanogenesis for cultures not containing nitrate, as well as denitrification rate from 3.5 to 7 mg NO_3-N/g VSS· h in a single denitrifying batch system, the inhibition of methanogenesis at ORP of -300 mV persisted and stopped only after the total reduction of all nitrogen oxides. In the case of Ti(III) citrate, inhibition of methane formation, however, was still observed to occur in the presence of nitrogen oxides.

Even though nitrite ions exerted a stronger inhibitory effect on methanogenesis as compared to nitrate at the same concentration, it elevated the ORP of the culture less than nitrate did. [12] In a co-immobilized SDM, redox potential was observed at -100 mV at COD/N<1, where partial denitrification occurred. [15] A substantial amount of nitrate and nitrite in the system reportedly resulted in ORP higher than -200 mV, and when the methane production resumed with COD/N>2, the system was running under a strict anaerobic state with ORP< -415 mV.

10.5 Metabolic Interactions

As shown in **Table 10.2**, Tugtas and Pavlostathis (2007) stated that as a result of higher energy yield during denitrification, the bacterial yield is higher, as compared to that for methanogenesis. Thus it is obvious that nitrate reducers should outgrow methanogenesis, which has been verified in a few natural environments. [9]

In the reactor treating nitrate containing wastewater, denitrifiers and methanogens compete for electrons producing nitrogen and methane, respectively, according to the following reduction half-equations, where electrons e^- are obtained from the oxidation

half-reactions, in which hydrogen and organic substrate, such as acetate, are oxidized to H^+ and CO_2:

Denitrification (Reaction 10 **Table 10.2**-Half reac.) $2NO_3^- + 12H^+ + 10e^- \rightarrow N_2 + 6\ H_2O$

$5H_2 \rightarrow 10H^+ + 2e^-$

Methanogenesis (Reaction 1 **Table 10.2**-Half react.) $HCO_3^-_- + 9H^+ + 8e^- \rightarrow CH_4 + 3\ H_2O$

$4H_2 \rightarrow 8H^+ + 8e^-$

Methanogenesis (Reaction 5 **Table 10.2**) $CH_3COO^- + 9H^+ + 8e^- \rightarrow 2\ CH_4 + 2H_2O$

$CH_3COO^- + 2H_2O \rightarrow 2\ CO_2 + 7H^+ + 8e^-$

Reaction (10) **Table 10.2** shows that denitrifying one mole of NO_3^- consumes $5e^-$. Based on the estimation by Gujer and Zehnder (1983), producing one mole of CH_4 would consume $5.2e^-$ (0.3x8 + 0.7x(8/2) = 5.2). Therefore, fractions of electron flow to methanogenesis and denitrification can be estimated from the amount of nitrate denitrified and methane produced. In the strict anaerobic degradation of organic matter, 30% of the carbon source for methanogenesis was from bicarbonate (Reaction 1 **Table 10.2**) and 70% from acetate (Reaction 5 **Table 10.2**). [63] Since stoichiometrically, complete nitrate reduction to nitrogen gas requires 5 electron equivalents per mole of nitrate, co-existence of fermenters/methanogens and denitrifiers may cause channeling of electrons away from methanogenesis, which may result in decrease in the overall methane production. [10]

Ruiz et al. (2006) showed that COD/N ratio has a strong influence on biomass activity, and therefore on the metabolic pathways of nitrate and organic matter utilization. Low COD/N values generated high denitrifying activities, and high COD/N value elevated methanogenic activities. Fang and Zhou (1999) demonstrated that electron flows to methanogenesis and denitrification were dependent on the COD/NO_3^--N ratio. At the COD/NO_3^--N ratio of 3.34, all electrons were utilized by denitrification, as evidenced by the cessation of methane production. The fraction of electron flow to methanogenesis increased, with the COD/NO_3^--N ratio, from nil at the ratio of 3.34 to 21.2% at 5.23.

Batch specific denitrification rate (SDNR) of mixed denitrifying and methanogenic cultures is a function of different parameters such as the quantity of different species in the mixed culture, type of substrates, COD/N ratio and all operational conditions such as temperature and pH. A change in, for instance, temperature may have a significant effect on the culture, as methanogenic activity is very sensitive to thermal fluctuations. A direct comparison of specific denitrifying activities with reported values is rather complex since the nature of the biomass i.e., the fractions of the various populations, used in the different studies are unknown. Also, the initial nitrate concentration, or loading of the system, seems to play an important role. [2] In the literature, a range of reference values for specific methanogenesis activity of 1-2 g COD/ g VSS·d [64], and SDNR of 0.04 g NOx-N/g VSS·d to 0.42 g NOx-N/ g VSS·d has been reported. [65] Ruiz et al. (2006) reported different specific methanogenic activities (SMA) and denitrifying activities (SDNR) at different COD/N ratio, as depicted in **Figure 10.4**. The obtained results confirmed that the maximum activity of denitrifying microorganisms (low COD/N) seriously affect the activity of methanogenic bacteria. Even though both activities can be found at a COD/N ratio of around 10, their values are much lower than those that would be found in fully methanogenic or denitrifying reactors. [23] This means that if both processes are going to be performed in a single stage, low loading rates should be applied. Indeed, low organic and nitrogen loads are, in general, a common characteristic of all SDM reported in the literature, as seen in **Table 10.1**.

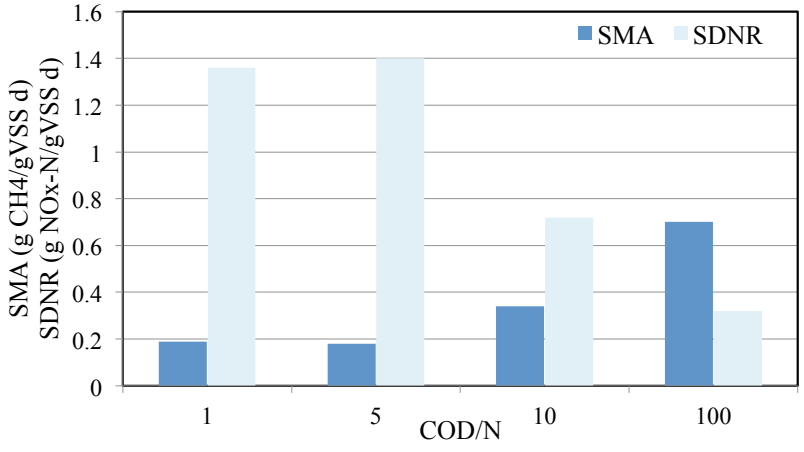

Figure 10.4. Dependency of SMA and SDNR on COD/N ratio

Denitrification is also reported to shift the distribution of volatile fatty acids in a SDM system. Barber and Stucky (2000) reported a significant reduction in propionate and butyrate concentrations in an anaerobic baffled reactor treating glucose/protein, whilst acetate increases significantly which could be a result of a greater inhibitory effect on methanogenic bacteria compared to acetogenic bacteria

The specific rates of denitrification and methanogenic activity in a simultaneous environment have been investigated in two forms of suspended growth mixture and attached biomass. Experiments by Chen & Lin (1993) using a mixture of sludge separately acclimated to denitrification and methanogenesis, respectively, showed that the methanogenic COD removal rate (calculated per g VSS of methanogens added) decreased in the mixed system, whereas the denitrifying COD removal rate (calculated per g VS of denitrifiers added) was the same. Rustrian et al., (1997) reported SDNR of 684 mg NOx-N/g VSS·d at nitrate loading rate of 1.0 kg NO_3-N/m^3·d and COD/NO_3-N of 10. At a very low COD/NO_3-N ratio of 4.8, Bernet et al., (1996) reported a SDNR of 782.4 mg NOx-N/g VSS·d at nitrate loading rate of 2.2 kg NO_3-N/m^3·d, with a wine distillery effluent. [66] Tai et al. (2006) reported the SMA of 1.3 g CH_4–COD/g VSS·day for the granular methanogenic sludge in an UASB at an OLR of 4.8 kg COD/m^3·d before recycling nitrate. However, after several months of recycling, SMA of the granular sludge decreased as much as 30%-40% to 0.8-0.9g CH_4–COD/g VSS·d at the end of the study, despite different OLRs of 0.7 kg COD/m^3·d, 0.9 kg COD/m^3·d, and 1.4 kg COD/ m^3·d.

10.6 Modeling Inhibition

ADM1 categorized the form of inhibition kinetics by different inhibitory parameters on methanogenic activities in different forms: (a) reversible forms; (b) direct impact of the inhibitors on the microbial yield and decay; (c) Empirical forms for pH inhibition; (d) competitive uptake such as butyrate and valerate competition for C_4 (not considered as inhibition); (e) secondary substrate Monod kinetics. [10] The inhibitory models of groups (a) and (e) are both reversible. In ADM1, three different non-competitive inhibitors such as free ammonium and hydrogen, uncompetitive inhibitors and competitive inhibitors,

equations are proposed. However, none of the aforementioned equations were applied in ADM1. The inhibitory effect of nitrogen reduction in a methanogenic system can fit in category (a) if the inhibitory mechanism is due to presence of nitrogen oxide or enzymes and/or (e) if the carbon uptake competition is considered and an inhibitory effect.

Most of the anaerobic digestion process models employ the Monod equation as follows:

$$\mu_j = \frac{\mu_{\max} S}{K_s + S} \tag{10.3}$$

where μ is rate of reaction j, μ_{max} is rate of reaction at substrate saturation, K_s is half saturation constant and S is substrate concentration.

Batstone et al. (2002) suggested that the effect of different forms of inhibition can be integrated into the Monod equation in the following form to allow for easy substitution or addition of inhibition terms:

$$\mu_j = \frac{\mu_{\max} S}{K_s + S} \cdot I_1 \cdot I_2 \cdots I_n \tag{10.4}$$

where $I_{1\cdots n} = f(S_{1\cdots n})$ are the inhibition functions.

Five different reaction forms describing the inhibition occurrence on enzyme-catalysed reactions were proposed in the literature: [10, 67, 68]

1. Irreversible inhibition resulting from damage of parts of the enzymatic catalysis system. Very high concentrations of end products such as VFAs and alcohols damage biological materials.

$$I = 1 - \frac{S_I}{\mu_{\max} \cdot K_I} \tag{10.5}$$

where K_I is inhibition factor and S_I is concentration of inhibiting compound (product)

2. Reversible non-competitive inhibition, resulting from interaction between end products such as free ammonia and hydrogen and allosteric control site of the enzyme

catalyzing the reaction which retards some reactions for the overall metabolism optimization.

$$I = \frac{1}{1 + S_I / K_I} \tag{10.6}$$

3. Reversible, competitive inhibition resulting from the competition between the inhibitory compound and the substrate for the same catalytic side of the enzyme.

$$I = \frac{K_S + S}{K_S\left(1 + S_I / K_I\right) + S} \tag{10.7}$$

4. Reversible, uncompetitive inhibition

$$I = \frac{K_S + S}{S\left(1 + K_I / S_I\right) + K_S} \tag{10.8}$$

5. Competitive uptake inhibition resulting from butyrate and valerate competition for C_4.

$$I = \frac{1}{1 + S_I / S} \tag{10.9}$$

Tugtas et al., (2006 and 2010) incorporated nitrate reduction processes into the IWA Anaerobic Digestion Model No. 1 (ADM1) in order to account for the effect of such processes on fermentation and methanogenesis. The inhibitory effect of N-oxides on the methanogens was accounted for by the use of reversible non-competitive inhibition functions. Model simulations were compared with experimental data obtained with a batch, mixed fermentation and methanogenic culture amended with various initial nitrate concentrations. Huilinir et al. (2008) applied the proposed equation by Tugtas et al., (2006) to model SDM in a continuous Upflow-Packed-Bed Biofilm reactor and concluded that the inclusion of the inhibition of methanogenesis by nitrogen compounds did not improve the predictions.

10.7 Conclusions

The cause of inhibition of methanogenesis in the literature by simultaneous nitrogen oxide reduction has been reported to be from different reasons such as an increase in ORP, electron channeling, carbon uptake competition between denitrifiers and methanogenesis, toxic effects of nitrogen oxides as well as reductase enzymes in nitrogen cycle. However, denitrification and methanogenic activity can be integrated in a single anaerobic system under certain conditions. Among different system configurations, the biofilm and immobilized SDM systems as well as ABRs where the denitrifiers and methanogenesis are located in different depth of biofilm or distinct compartments, have shown a better performance for simultaneous nitrogen and carbon removal. At different COD/N ratios, the inhibitory factors are different. At COD/N ratio of 2, both denitrification and methanogenic activity are inhibited due to carbon deficiency. At COD/N ratios of 2-10, denitrifiers are thermodynamically favored and thus denitrification occurs as a result of electron channeling to denitrifiers. In this region methanogenesis are either completely or partially hindered. At COD/N ratio of greater than 10, there will not be an inhibitory effect on methanogenesis due to carbon competition or electron channeling. On the other hand experimental results show an inhibitory effect on denitrifiers that could be as a result of inverse electron channeling at very high COD/N ratios of greater than 20 as a result of methanogenic reaction dominance in the system. In the all above cases, if concentrations of nitrogen oxides in the system are above certain values (**Table 10.4**) methanogenesis is inhibited. Thus the main inhibitory factor for methanogenesis in a SDM system is the nitrogen oxide toxicity. This condition occurs at the lag phase of denitrification activity (beginning of the process) when still the concentration of nitrogen oxides in the system is high. It has been reported that after the nitrogen oxide concentrations decrease, the methanogenesis is revitalized while still the same amount of electrons are transferred to denitrifiers with ΔG reaction significantly lower than methanogenesis. ORP less than -300 mV is conducive to a better methanogenic activity while denitrification happen in higher ORPs (-150 to -100) although ORP cannot be considered as effectively inhibiting methanogenesis factor as experimental results show than the addition of cysteine that resulted in ORP of -300 mV did not affect the performance of denitrifiers and methanogenesis in a SDM system.

ORPs value in a SDM simultaneous system depends strongly on the carbon and nitrogen loading rates as well as the efficiency of each process.

It should be noted that, as shown in **Table 10.1**, successful SDM occurred when systems were under very low organic and nitrogen volumetric loading rates of <5 kg COD/m^3·d and <1 kg NOx-N/m^3·d respectively.

The nature of substrate and COD/N ratio in a SDM system reportedly impact the nitrogen fate to either denitrification or DNRA. Fermentable substrate such as glucose and glycerol were reported to encourage DNRA with increasing COD/N ratio. On the other hand VFAs were reported to facilitate denitrification. However, Shin et al. (2002) suggested that the nitrogen cycle is independent of the nature of substrate and is a function of alkalinity. At alkalinity >2400 mg $CaCO_3$/L, the system was conducive to accomplish denitrification and at low alkalinity of <1000 mg $CaCO_3$/L was favorable to DNRA.

10.8 References

[1] Akunna JC, Bizeau C, and Moletta R. Denitrification in anaerobic digesters: possibilities and influence of wastewater COD/N-NOx ratio. Environmental Technology. 1992; 13:825-836.

[2] Vang Hendriksen H, and Ahring BK. Combined removal of nitrate and carbon in granular sludge: Substrate competition and activities. Antonie van Leeuwenhoek. 1996b; 69:33-39.

[3] Shin HS, Kim KY, Lee CY, Kang SK. Effect of alkalinity and substrate on simultaneous denitrification and methanogenesis. WEF Proceeding: 2002.

[4] Lengeler JW, Drews G, Schlege HG. Biology of the prokaryotes. ISBN: 3-13-108411-1 1999.

[5] Solley D. Upgrading of large wastewater treatment plant for nutrient removal. Churchill Fellowship 2000 report. The Winston Churchill Memorial trust of Australia 2000.

[6] Warakomski A, van Kempen R, and Kos P. Microbiology/Biochemistry ofNitrogen Cycle Innovative Process Applications. International Water Association proceedings, Moncton, New Brunswick, Canada 2006.

[7] Henze M, van Loosdrecht MCM, Ekama GA, and Brdjanovic D. Biological wastewater treatment: Principle, modeling and design. IWA publishing 2008. ISBN: 1843391880.

[8] Del Pozo R, and Diez V. Organic matter removal in combined anaerobic–aerobic fixed-film bioreactors. Wat. Res. 2003; 37:3561–3568.

[9] Kluber HD, and Conrad R. Effects of nitrate, nitrite, NO, and N2O on methanogenesis and other redox processes in anoxic rice field soil. FEMS Microbiol. Ecol. 1998; 25:301-318.

[10] Batstone DJ, Keller K, Angelidaki I, Kalyuzhenyi SV, Pavlostathis SG, Rozzi A, Sanders WTM, Siegrist H, and Vavilin VA. Anaerobic Digestion Model No. 1. IWA publishing: 2002.

[11] Banihani Q, Sierra-Alvarez R, and Field JA. Nitrate and nitrite inhibition of methanogenesis during denitrification in granular biofilms and digested domestic sludges. Biodeg. 2009; 20:801–812.

[12] Chen KC, Lin YF. The relationship between denitrifying bacteria and methanogenic bacteria in a mixed culture system of acclimated sludges. Wat. Res. 1993; 27-12:1749-1759.

[13] Her JJ, and Huang JS. Influences of carbon source and C/N ratio on nitrate/nitrite denitrification and carbon breakthrough. Bioresearch Technol. 1995; 54:45-51.

[14] Rustrian E, Delgenes JP, Bernert N, and Moletta R. Nitrate reduction in acidogenic reactor: Influence of wastewater COD/N-NO_3 ratio on denitrification and acidogenic activity. Environ. Technol. 1997; 18:309-315.

[15] Chen KC, Lin YF, and Houng JY. Performance of a continuous stirred tank reactor with immobilized denitrifiers and methanogens. Wat. Environ. Res. 1997; 69-2:233-239.

[16] Lin YF, and Chen KC. Denitrification and methanogenesis in a co-immobilized mixed culture system. Wat. Res. 1995; 29-1:35-43.

[17] Hanaki K, and Polprasert C. Contribution of methanogenesis to denitrification with an upflow filter. Journal WPCF. 1989; 61-9:1604-1611.

[18] Ahn YT, Kang ST, Chae SR, Lee CY, Bae BU, and Shin HS. Simultaneous high-strength organic and nitrogen removal with combined anaerobic upflow bed filter and aerobic membrane bioreactor. Desal. 2007; 202:114–121.

[19] Fang HHP, and Zhou GM. Interactions of methanogens and denitrifiers in degradation of phenols . J. Environ. Eng. 1997; 57-63.

[20] Tai CS, Singh KS, and Grant SR. Combined Removal of Carbon and Nitrogen in an Integrated UASB-Jet Loop Reactor Bioreactor System. J. Environ. Eng. 2006; 624-637.

[21] Im JH, Woo HJ, Lee TH, Lee HI, and Kim CW. Feasibility for application of methanogenesis/denitrification process to municipal leachate treatment. Environ. Eng. Res. 2003; 8-5:229-235.

[22] An Y, Yang F, Wong FS, and Chua HC. Simultaneous Bioenergy (CH_4) Production and Nitrogen Removal in a Combined Upflow Anaerobic Sludge Blanket and Aerobic Membrane Bioreactor. Energy & Fuels. 2008; 22:103–107.

[23] Ruiz G, Jeison D, and Chamy R. Development of denitrifying and methanogenic activities in USB reactors for the treatment of wastewater: Effect of COD/N ratio. Process Biochemistry. 2006; 41:1338–1342.

[24] Barber WP, and Stuckey DC. Nitrogen removal in a modified anaerobic baffled reactor (ABR): 1, denitrification. Wat. Res. 2000; 34-9:2413-2422.

[25] Baloch MI, Akunna JC, and Collier PJ. Carbon and nitrogen in a granular bed baffled reactor. Environ. Technol. 2006; 27:201-208.

[26] Halling-Sorensen B, and Jorgensen SE. The removal of nitrogen compounds from wastewater. Studies in Environmental Sciences. Elsevier Eds: The Netherlands, 1993; 54:119-138.

[27] Vang Hendriksen H, and Ahring BK. Integrated removal of nitrate and carbon in an upflow anaerobic sludge blanket (UASB) reactor: Operating performance. Wat. Res. 1996a; 30-6:1451-1458.

[28] Mosquera-Corral A, Sanchez M, Campos JL, Mendez R, and Lema JM. Simultaneous methanogenesis and denitrification of pretreated effluents from a fish canning industry. Wat. Res. 2001; 35-2:411-418.

[29] Huang JS, Chou HH, Chen CM, and Chiang CM. Effect of recycle-to-influent ratio on activities of nitrifiers and denitrifiers in a combined UASB–activated sludge reactor system. Chemosphere. 2007; 68:382–388.

[30] Peng Y, Zhang S, Zeng W, Zheng S, Mino T, and Satoh H. Organic removal by denitritation and methanogenesisvand nitrogen removal by nitritation from landfill leachate. Wat. Res. 2008; 42:883-892.

[31] Sumino T, Isaka K, Ikuta H, Saiki Y, and Yokota T. Nitrogen removal from wastewater using simultaneous nitrate reduction and anaerobic ammonium oxidation in single reactor. J. Biosci. Bioeng. 2006; 102-4:346-351.

[32] Zhang DJ. The integration of methanogenesis with denitrification and anaerobic ammonium oxidation in an expanded granular sludge bed reactor. J. Environ. Sci. 2003; 15-3:423-432.

[33] Metcalf and Eddy, Wastewater Engineering: Treatment and reuse. 4th ed., McGraw-Hill: 2003.

[34] Tiedje JN. Biology of Anaerobic Microorganisms, by Zehnder, A.J.B. Wiley Publishing:New York, 1988; 179-244.

[35] King D, and Nedwell DB. The influence of nitrate concentrations upon the end-products of nitrate dissimilation by bacteria in anaerobic salt march sediment. FEMS Microbiology Ecology. 1985; 31:23-28.

[36] Kasper HF, Tiedje JM, Firestone RB. Denitrification and dissimilatory nitrate reduction to ammonium in digested sludge. Can. J. Microbiol. 1981; 27:875-885.

[37] Akunna JC. Denitrification in anaerobic digesters: a review of recent studies. 50th Purdue Univ. Ind. Waste. Conference Proceedings, Purdue: 1995.

[38] Akunna JC, Bernet N, and Moletta R. Nitrate and nitrite reductions with anaerobic sludge using various carbon sources: glucose, glycerol, acetic acid, lactic acid and methanol. Wat. Res. 1993; 27-9:1303-1312.

[39] Ferry JG. Methane from acetate. J. Bacteriol. 1992; 174:5489-5495.

[40] Tugtas AE, and Pavlostathis SG. Inhibitory Effects of Nitrogen Oxides on a Mixed Methanogenic Culture. Biotechnol. Bioeng. 2007; 96-3:444-455

[41] Roy R, and Conrad R. Effect of methanogenic precursors (acetate, hydrogen, propionate) on the suppression of methane production by nitrate in anoxic rice field soil. FEMS Microbiology Ecology. 1999; 28:49-61.

[42] Tugtas AE, Tezel W, and Pavlostathis SG. An extension of the Anaerobic Digestion Mode No.1 to include the effect of nitrate reduction processes. Wat. Sci. Technol. 2006; 54:41-49.

[43] Brock TD, Medigan MT, Martinko JM, Parker J. Biology of microorganisms. 7th edition 1997.

[44] Zellner G, Feuerhake E, Jordening HJ, Macario AJL, and Conway de Macario E. Denitrifying and methanogenic bacteria in the biofilm of a fixed-film reactor operated

with methanol/nitrate demonstrated by immunofluorescence and microscopy. App. Micro. Biotechnol. 1995; 3:566-571.

[45] Duarte AC, and Anderson GK. Inhibition modeling in anaerobic digestion. Wat. Sci. Technol. 1982; 14:749-763.

[46] McCarty PL. Anaerobic waste treatment fundamentals III: toxic materials and their control. Public Works. 1964; 91-94.

[47] Scheid D, Stubner S, and Conrad R. Effects of nitrate and sulfate amendment on the methanogenic populations in rice root incubations. FEMS Microbiology Ecology. 2003; 43:309–315.

[48] Quevedo M, Guynot E, and Muxi L. Denitrifying potential of methanogenic sludge. Biotechnology Letters. 1996; 18-12:1363-1368.

[49] Seifritz C, Drake JM, Daniel SL. Influent of nitrate on oxalate- and glyoxylate-dependent growth and acidogenesis by *Moorella thermoacetica*. Arch. Microbiol. 2002, 178:457-464.

[50] Zumft WG. Cell biology and molecular basis of denitrification. Microbiol. Mol. Biol. Rev. 1997; 61-4:533-616.

[51] Tugtas AE, and Pavlostathis SG. Inhibitory effects of nitrate reduction on methanogenesis in the presence of different electron donors. Wat. Sci. Technol. 2008; 293-698.

[52] Stams AJM, Oude Elferink SJWH, Westermann P. Metabolic interactions between methanogenic consortia and anaerobic respiring bacteria. Adv. Biochem. Eng. 2003; 81:31-56.

[53] Narkis N, Rebhun M, and Sheindorf C. Denitrification at various carbon to nitrogen ratios. Wat. Res. 1979; 13:93-98.

[54] Liessens J, Germonpré R, Beernaert S, and Verstraete W. Removing nitrate with a methylotrophic fluidized bed: technology and operating performance. Journal of AWWA 1993; 85:144-154.

[55] Christenson M, Lie E, and Welander T. A comparison between ethanol and methanol as carbon sources for denitrification. Wat. Sci. Technol. 1994; 30-6:83-90.

[56] Wolf RS. Unusual coenzymes of methanogenesis. Tr. Biochem. Sci.1985; 10:396-399.

[57] Jee HS, Mano T, Nishio N, and Nagai S. Influence of redox potential on methanation of methanol by Methanosarcina barkeri in Eh-stat batch cultures. J. Fermen. Technol. 1988; 66:123-126.

[58] Zehnder AJB, Stumm W, Geochemistry and biochemistry of anaerobic habitats. Anaerob. Microbiol. Wiley New York 1988.

[59] Balderston WL, and Payne WJ. Inhibition of methanogenesis in salt marsh sediments and whole-cell suspensions of methanogenic bacteria by nitrogen oxides. App. Environ. Microbiol. 1976; 32:264-269.

[60] Roy R, Kluber HD, and Conrad R, Early initiation of methane production in anoxic rice soil despite the presence of oxidants. FEMS Microbiology and Ecology. 1997; 24:311-320.

[61] Fetzer S, Conrad R. Effect of redox potential on Methanogenesis by *Methanosarcina barkeri*. Arc. Microbiol. 1993; 160:108-113.

[62] Akunna JC, Bernet N, and Moletta R. Effect of nitrate on methanogenesis at low redox potential. Environ. Technol. 1998; 19:1249-1254.

[63] Gujer W, and Zehner AJB. Conversion process in anaerobic digestion. Wat. Sci. Technol. 1983; 127-167.

[64] Visser A, Alphenaar PA, Gao Y, van Rossum G, and Lettinga G. Granulation and immobilisation of methanogenic and sulfatereducing bacteria in high-rate anaerobic reactors. App. Microbiol. Biotechnol. 1993; 40:575-581.

[65] Henze M. Capabilities of biological nitrogen removal processes from wastewater. Wat. Sci. Technol. 1991; 23:669-679.

[66] Bernet N, Delgenés N, and Moletta R. Denitrification by anaerobic sludge in piggery wastewater. Environ. Technol. 1996; 17:293-300.

[67] Lehninger AL, Nelson DL, and Cox MM. Principles of biochemistry (Second edition), Worth, New York. 1993 ISBN 0-87901-500-4.

[68] Zubay G. Biochemistry (third edition). Brown, Dubuque, Iowa. 1993 ISBN 0-697-14267-5**.**

[69] Tugtas AE, Tezel U, and Pavlostathis SG. A comprehensive model of simultaneous denitrification and methanogenic fermentation processes. Biotechnol. Bioeng. 2010; 105-1:98-108.

[70] Chen S, Sun D, and Chung J. Simultaneous methanogenesis and denitrification of aniline wastewater by using anaerobic–aerobic biofilm system with recirculation. Journal of Hazardous Materials 2009; 169:575–580.

[71] Garrido JM, Mendez R, and Lema JM. Simultaneous urea hydrolysis, formaldehyde removal and denitrification in a multi-fed upflow filter under anoxic and anaerobic conditions. Wat. Res. 2001; 35-3:691-698.

[72] Bernet N, Delgenes N, Akunna JC, Delgenes JP, and Moletta R. Combined anaerobic-aerobic SBR for the treatment of pigerry wastewater. Wat. Res. 2000; 34-2:611-619.

[73] Lacalle ML, Villaverde S, Fdez-Polanco F, and García-Encina PA. Combined anaerobic/aerobic (UASB + UBAF) system for organic matter and nitrogen removal from a high strength industrial wastewater. Wat. Sci. Technol. 2001; 4:255–262.

[74] Clarens M, Bernet N, Delgenés JP, and Moletta R. Effects of nitrogen oxides and denitrifcation by Pseudomonas stutzeri on acetotrophic methanogenesis by Methanosarcina mazei. FEMS Microbiology Ecology 1998; 25:271-276.

[75] Huilinir C, Aspé E, and Roeckel M. Model of simultaneous denitrification and methanogenesis in an Upflow Packed-Bed Biofilm Reactor: Nitrogen Compounds' inhibition and pseudo two-dimensional biofilm model. J. Chem. Technol. Biotechnol. 2008; 84:254-268.

[76] Percheron G, Michaud S, Bernet N, and Moletta R. Nitrate and nitrite reduction of a sulphide-rich environment. J. Chem. Technol. Biotechnol. 1998; 72:213-220.

[77] Li J, Zhang ZH, Li ZH, Huang G, and Naoki A. Removal of organic matter and nitrogen from distillery wastewater by a combination of methane fermentation and denitrification/nitrification processes. J. Environ. Sci. 2006; 18-4:654-659.

11 High Rate BNR from High Strength Wastewater Using AF-CFBBR

The primary objective of this work was the investigation of simultaneous biological nitrogen removal from high strength wastewater and anaerobic biodegradation by a newly developed integrated anaerobic fluidized bed (AF) with circulating fluidized bed bioreactor called AF-CFBBR. Additionally, the inhibitory effect of nitrate on methanogenic activities in a high rate anaerobic fluidized bed with organic loading rate of above 35 kg COD/m^3·d was studied in order to evaluate the feasibility of simultaneous denitrification and methanogenic activities (SDM) in a high rate anaerobic system. The AF-CFBBR showed 99.7% COD removal, 84% nitrogen removal, with a very low sludge yield of 0.017 g VSS/g COD while treating a wastewater containing 10700 mg COD/L and 250 mg NH_3-N/L. The system was operated at an organic loading rate (OLR) of 35 kg COD/m^3·d based on the AF volume and 1.1 kg N/m^3·d based on the CFBBR at an overall HRT of less than 12 h in the AF-CFBBR.

In the SDM tests, methanogenesis was completely hindered when NO_3-N was fed at concentrations of 50 mg N/L and 250 mg N/L. As a result, the system failed due to organic overloading and a drop in pH in less than 48 hr. Methanogenesis inhibition effect by nitrates was found reversible when NO_3-N concentration in the feed was 50 mg/L and irreversible when NO_3-N in the feed was 250 mg/L.

11.1 Introduction

High strength wastes produced by fertilizer production, explosive manufacturing and recovery of nuclear fuels as well as landfill leachate contain in addition to organic matter, nitrogen in the forms of ammonia, nitric and nitrous acids. [1] Similarly, many food-processing wastewaters such as rendering also contain high ammonia concentrations as a result of protein digestion. Since the nature of the aforementioned high strength wastes requires anaerobic processes to recover energy and also nutrient removal is becoming mandatory in many places, biological treatment can be accomplish using either the

sequence of anaerobic, anoxic and aerobic systems or simultaneous denitrification and methanogenesis (SDM) in a single anaerobic reactor.

The anaerobic Digestion Model No.1 (ADM1) suggests that nitrate reduction simultaneously in methanogenic system can have different effects such as: [2] Channeling of electron equivalents (eeq) away from methanogenesis, decrease in the methane content of the biogas as a result of the production of N_2 and additional CO_2, as well as alkalinity and/or NH_4^+ production, competition between microbial groups for the same substrate(s) and inhibition of methanogenesis by nitrogen oxides. [3, 4] It seems however that the predominant inhibitory effect on methanogenic activity is the toxic effect of nitrogen oxides. [5, 6]

There has been a considerable effort to couple denitrification and methanogenesis in a single reactor in both suspended and attached growth systems, which has been extensively studied in Chapter 10. Although simultaneous denitrification and methanogenesis in a single reactor has been studied in the aforementioned literature, all the data were reported for low rate OLRs less than 5 kg COD/m^3·d and nitrogen loading rate (NLR) less than 0.8 kg N/m^3·d with four exceptions of 7.5 kg COD/m^3·d and 0.075-7.5 kg N/m^3·d in an Upflow Anaerobic Sludge Blanket (UASB) [7], 12.5 kg COD/m^3·d and 1.7 kg N/m^3·d in a UASB [8], < 7.2 kg COD/m^3·d in an Upflow Biofilter (UBF) [9] and 10 kg COD/m^3·d and 4.7 kg N/m^3·d in an immobilized beads [10] CSTR. The Circulating Fluidized Bed Bioreactor (CFBBR), introduced and developed by Nakhla and his coworkers [11], was tested for biological nutrient removal (BNR) from municipal wastewaters in both lab and pilot scales at OLR of 5 kg COD/m^3·d and NLR of 0.5 kg N/m^3·d. [12] The CFBBR consists of an anoxic riser and an aerobic downer with fast and conventional fluidization regimes respectively. More than 90% organic, 70%-80% total nitrogen and 50%-70% phosphorous removal were reported, with hydraulic retention times (HRTs) of 2-3 h and an observed biomass yield of 0.12-0.16 g VSS/g COD. The CFBBR was reported to treat high strength wastewater such as landfill leachate as well with the aforementioned OLR and NLR. [13] However, in order to accomplish high rate biological nutrient removal from high strength waste containing nitrogen, a newly developed bioreactor referred to henceforth as anaerobic fluidized-circulating fluidized

bed bioreactor (AF-CFBBR) was designed and operated to treat synthetic high strength wastewater with TCOD of 10600±270 mg/L, NH_3-N of 250±10 mg/L and pH of 4 while having the advantages of the CFBBR such as low yield and HRT. The pH of the synthetic feed with COD of 10600 mg/L was maintained at 4, similar to some food waste streams such as thin stillage. Furthermore, this study investigated the inhibitory effect of nitrate on methanogenesis at different nitrogen loadings and OLR of up to 35 kg COD/m^3·d when the system was treating acidic high strength wastewater and also whether the inhibitory effect of nitrate was reversible which demonstrated the feasibility of the simultaneous denitrification and methanogenesis in a single reactor under high organic loading rates of feed with pH of 4.

11.2 Materials and Methods

11.2.1 System Description and Operating Conditions

The AF-CFBBR (**Figure 11.1)** is comprised of a conventional strict anaerobic fluidized bed (AF) with overall height of 3.6 m followed by a CFBBR comprising an anoxic and aerobic fluidized bed bioreactors FBRs with heights of 2 m and 3.6 m respectively. Zeolite particles (3 kg) with an average diameter (d_m) of 425-610 μm were used as carrier media in the anaerobic column and 3 kg zeolite particles with average diameter of 610-825 μm, were circulated between the aerobic and anoxic fluidized bed columns of CFBBR. The amount of particles were initially estimated based on the specific nitrification rates (SNRs), specific denitrification rates (SDNRs), and specific methanogenesis activity (SMA) of 1.74 mg NH_3-N/g media·d and 2.73 mg NO_x-N/g media·d and 275 mg COD/g media·d, respectively reported in the literature for the TCFBBR and an anaerobic fluidized bed reactor. [17, 27] The particle weight hold up in the aerobic column of the CFBBR was maintained at 2.4 kg continuously. Zeolite characteristics were determined as follows: a total porosity (ψ_T) of 61% (44% external and 17% internal), a dry bulk particle density (ρ_{md}) of 885 kg/m, a true particle density (ρ_{mt}) of 2360 kg/m^3 and a external specific surface area and uniformity coefficient determined by BET (Micromeritics ASAP 2010, Micromeritics Co., USA) of 26.5 m^2/g and 1.85 respectively. In the riser, heterotrophic bacteria grow on the media and the biofilm becomes thicker. At a certain biofilm thickness, depending on the superficial

liquid velocity, the biofilm-coated particles reach the height where they can be transferred to the downer through the inclined pipe. However, similar to the TCFBBR, an intermediate graduated container was placed between the two columns, as shown in **Figure 11.1,** to monitor the particle transfer rate. After exposure to the high shear force in the gas-liquid-solid phase in the downer, the biofilm detaches and leaves the system along with the effluent. Particles from the bottom dense phase of the downer with a thin biofilm (< 100 μm) are transferred back to the riser manually to make up the particles in the riser.

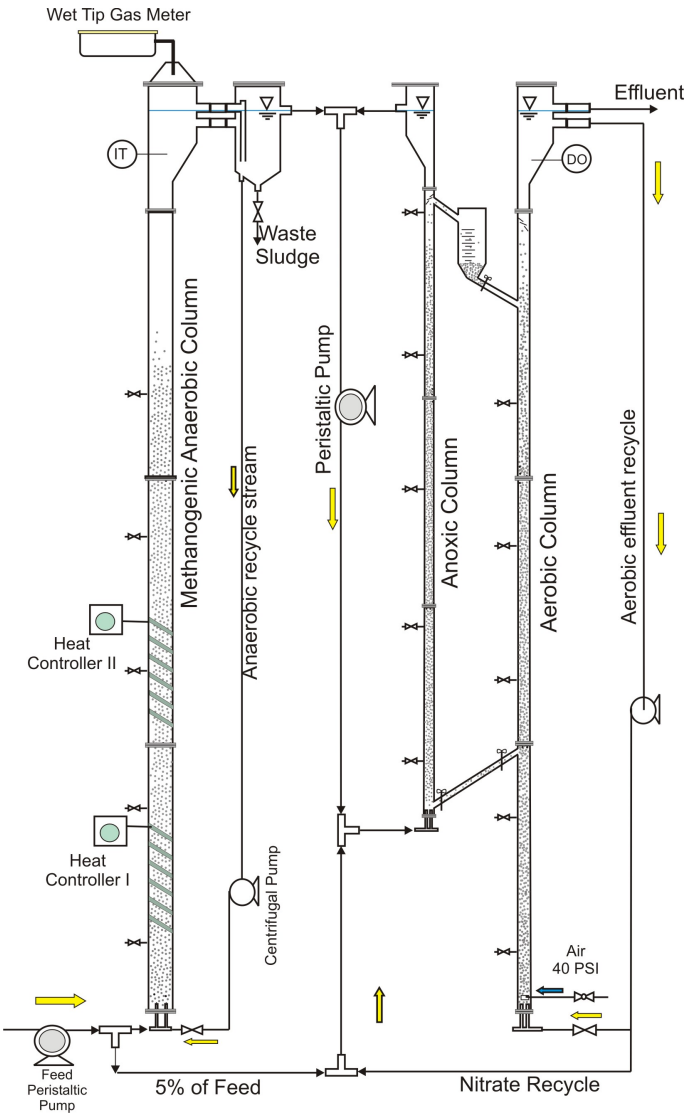

Figure 11.1. Schematic of Anaerobic Fluidized-Circulating Fluidized Bed Bioreactor (AF-CFBBR)

Table 11.1 shows the operating conditions of the overall system in different modes and phases. The feed solution was pumped into the bottom of the anaerobic and anoxic columns by a peristaltic pump (Masterflex I/P, Masterflex AG, Germany) with the volumetric ratio of 95% and 5% respectively. To ensure fluidization, AF to AF, riser to riser and downer to downer recirculation flows to feed ratios of, 47:1, 105:1-109:1 and 59:1-64:1 were provided respectively at the maximum volumetric loading rate (Mode 3). All recirculation flows were maintained using two centrifugal pumps (IWAKI MD-40RT-115NL, IWAKI CO., Ltd. Japan) and monitored by rotameters (OMEGA FL-812 and OMEGA FL-5331G, Omega Engineering, Inc., Canada). Air, at 40 psi, was injected at the bottom of the aerobic column using a fine bubble diffuser at the rate of 2200-2500 mL/min. At the maximum volumetric loading rate (Mode 3), the system was operating with an overall hydraulic retention time (HRT) of 12.8 h, empty bed contact time (EBCT) of 3.2 h and AF and CFBBR estimated sludge retention times (SRTs) of 32d and 28d respectively.

Table 11.1. Operating Conditions of AF-CFBBR in Different Phases

	Anaerobic fluidized bed (AF) under operation (**Mode 1**)			AF- Aerobic fluidized bed under operation (**Mode 2**)		AF-CFBBR under operation (**Mode 3**)		
	Phase-I	**Phase-II**	**Phase-III**	**Phase-IV**	**Phase-V**	**Phase-VI-I**	**Phase-VI-II**	**Phase-VI-III**
Day	1-23	24-35	36-46	47-91	92-128	129-145	145-160	160-172
Feed flow rate (L/d)	1.8-4.2	7.6-8	13-14.5	25-28	34-39	47-55[a]	55[a]	55[a]
Anaerobic-Anaerobic circulation flow (Q/Q_{in})	1800	681	340	194	143	109	107	105
Anoxic-Anoxic Circulation flow (Q/Q_{in})	-	-	-	-	-	2	2	2
Aerobic-Aerobic circulation flow (Q/Q_{in})	-	-	-	135	96	64	59	64
Aerobic-Anoxic Circulation flow (Q/Q_{in})	-	-	-	-	-	2.3	4	6.2
OLR based on anaerobic reactor (kg COD/m^3.d)	2±0.8	5.3±0.2	9.8±1	18±0.7	25±1	33.3±1.5	33.5±1.2	34.5±0.8
NLR based on anaerobic reactor (kg N/m^3.d)	-	-	-	0.72±0.0	0.6±0.0	0.8±0.1	0.8±0.1	0.85±0.0
OLR based on CFBBR reactor (kg COD/m^3.d)	-	-	-	0.85±0.7	0.5±0.1	3.8±0.7	3.3±0.1	4.8±0.2
NLR based on CFBBR reactor (kg N/m^3.d)	-	-	-	1±0.1	0.7±0.2	1.11±0.0	1.12±0.0	1.15±0.0
Anaerobic EBCT (h)=$V_{compact}/Q_{in}$	44-19	10	5.5	2.9	2.1	1.6	1.6	1.6
Aerobic EBCT (h)=$V_{compact}/Q_{in}$	-	-	-	2.4	1.8	1.3	1.3	1.3
Anoxic EBCT (h)=$V_{compact}/Q_{in}$	-	-	-	-	-	0.27	0.26	0.26
Anaerobic HRT(d)	8.9-3.5	2±0.1	1.1±0.1	0.6±0.1	0.4±0.0	0.32	0.32	0.32
Aerobic HRT(d)	-	-	-	0.3±0.1	0.2±0.0	0.17	0.17	0.17
Anoxic HRT (d)	-	-	-	-	-	0.04	0.04	0.04
Anaerobic attached biomass (mg VSS/g media)	13.6±0.9	14.8±0.5	15.6±0.6	20±2	29.6±1.5	32±0.5	33±0.2	33±0.4
Aerobic attached biomass (mg VSS/g media)	-	-	3.5±1	12.3±2	14.5±0.6	16.5±1.7	20.6±0.5	20.5±0.5
Anoxic attached biomass (mg VSS/g media)	-	-	-	-	-	1-41	85±1.5	82.2±2
Total anaerobic attached biomass (g VSS)	40.7	44.4	46.8	61.2	88.5	96.4	100.2	99.3
Total aerobic attached biomass (g VSS)	-	-	8.1	29.3	33.2	37.9	47.5	47.8
Total anoxic attached biomass (g VSS)	-	-	-	-	-	0.3-24.6	51.2	49.5
F/M in AF (g COD/g VSS.d)	0.5-1	1.9	3.4	4.5	4.5	5.5	5.4	5.5
F/M in CFBBR (g COD/g VSS.d)	-	-	-	-	0.15	0.66	0.35	0.55
Anaerobic col. detachment rate (1/d)		0.031			0.033		0.035	
Aerobic col. detachment rate (1/d)	-	-	-	-	-		0.035	
Anoxic col. detachment rate (1/d)							0.02	
Air (40 PSIG) flow (mL/min)	-	-	-			2200-2500		
Aerobic DO (mg/L)	-	-	-	7.8±0.8	8.3±0.2	6.2±0.1	6.3±0.1	5.6±0.0
Anoxic DO (mg/L)	-	-	-	-	-	0.35±0.1	0.4±0.1	0.7±0.2
AF estimated SRT (d)		27			30		32	
CFBBR estimated SRT (d)	-	-	-	-	-		28	
Superficial liquid velocity in anaerobic col. (cm/s)					1.42±0.04[b]			
Superficial liquid velocity in aerobic col. (cm/s)	-	-	-			1.7±0.1		
Superficial liquid velocity in anoxic col. (cm/s)	-	-	-	-	-		1.2±0.1	
Specific nitrification rate (**SNR**) (g NH_3-N/g VSS·d)	-	-	-	-	0.25-0.27		0.25-0.31	
Specific denitrification rate (**SDNR**) (g NO_3-N/g VSS·d)	-	-	-	-	-			3.4-3.8

[a] 5% of overall feed was directly fed to the bottom of the anoxic column.
[b] The terminal settling velocity of Zeolite with d_m=600 µm and 1000 µm biofilm thickness is 2.8 cm/s , still significantly lower than the operating u_L (Andalib et al., 2010).

11.2.2 Acclimatization and Start-up

Initially, the clean media was fluidized in the anaerobic, anoxic and aerobic columns at superficial liquid velocities of 1.4 cm/s, 1.2 cm/s and 1.6 cm/s respectively. Acclimatization took place in two different stages. First, Mode 1, the anaerobic column was seeded with 16 L secondary anaerobic digester sludge (SDS) acquired from St. Mary treatment plant, Ontario, Canada, with TSS and VSS concentrations of 15900 mg/L and 12180 mg/L respectively. In the second stage, Mode 2, the CFBBR was seeded with enriched nitrifiers, acclimatized in the lab using 10 L of returned activated sludge (RAS) from the Adelaide Pollution Control Plant, London, Canada, with TSS and VSS concentrations of approximately 7000 and 4800 mg/L respectively. The injected SDS into the anaerobic column and the RAS were recirculated within the anaerobic column and CFBBR respectively for a week to transport and trap the bacteria from the bulk liquid on

the media surface and the pores. Thereafter, the continuous synthetic feed, with the composition shown in **Table 11.2a**, was initiated at a flow rate of 1.8 L/d into the anaerobic column at day eight corresponding to OLR 0.28 kg COD/m^3·d and NLR of 0.01 kg N/m^3·d. The loading rates were thereafter increased to reach the maximum capacity of the system in nutrient removal. On day 49, the anaerobic column effluent was connected to CFBBR for further treatment of nitrogen compound. On day 132, the anoxic column was reseeded with 2 L RAS for 3 days and the aerobic to anoxic flow was initiated in order to denitrify the nitrogen oxides produced in the downer column.

Table 11.2. (a) Composition of the synthetic wastewater (b) Steady-state characteristics of anaerobic, anoxic and aerobic effluent in Mode 1, Mode 2 and Mode 3

(a)

Feed composition [a]	CH_3COOH (mL/L_{Feed})	NH_4Cl (g/L_{Feed})	K_2HPO_4 (g/L_{Feed})	$MgSO_4.7H_2O$ (g/L_{Feed})	$CaCl_2.2H_2O$ (g/L_{Feed})	Yeast extract (g/L_{Feed})	$NaHCO_3$ (g/L_{Feed})	Trace element (mL/L_{Feed})
Concentrations	9.5	1.7 and 0.93	0.1	0.03	0.03	0.03	5.7-6.7	1
Trace element Composition	$FeCl_2.4H_2O$ ($mg/L_{Trace\ E}$)	$MnCl_2.4H_2O$ ($mg/L_{Trace\ E}$)	H_3BO_3 ($mg/L_{Trace\ E}$)	$ZnCl_2$ ($mg/L_{Trace\ E}$)	$CuCl_2$ ($mg/L_{Trace\ E}$)	$AlCl_3$ ($mg/L_{Trace\ E}$)	$CoCl_2.6H_2O$ ($mg/L_{Trace\ E}$)	$NiCl_2$ ($mg/L_{Trace\ E}$)
Concentrations	2000	500	50	50	30	50	50	50

[a] All the above reagent were ACS Grade, 99.5% min.

(b)

		Anaerobic fluidized bed(AF) operated (**Mode 1**)			AF- Aerobic fluidized bed operated (**Mode 2**)		AF-CFBBR operated (**Mode 3**)					
Parameter (mg/L)		**Phases I, II and III**			**Phases IV and V**		**Phase-VI-I to VI-III**	**Phase-VI-I**		**Phase-VI-II**		**Phase-VI-III**
Days (d)		*1-46*			*47-128*		*129-172*	*129-145*		*145-160*		*160-172*
	Influent	Anaerobic Effluent			Anaerobic Effluent	Aerobic Effluent	Anaerobic Effluent	Anoxic	Effluent	Anoxic	Effluent	Anoxic	Effluent
Produced biogas(L/d)	-	1 to 32	44 to 64	95 to 128	168 to 320	-	333 to 405	-	-	-	-	-	-
TCOD	10600 ± 270	894	498	392	181±71	59±17	390± 140	61±14	49±8	80±5	58±7	79±24	67±1
SCOD		218	261	260	124±76	21±11	181± 86	30±11	31±5	50±16	40±18	46±16	34±12
TSS	-	927	314	125	65±26	38±15	188±85	28±8	22±10	42±15	32±10	29±8	30±10
VSS	-	480	176	96	44±19	25±12	146±56	21±5	16±8	27±12	19±7	23±6	23±8
NH_3-N	250(427)[b]	398	401	405	213±10	0.9±0.6	215±8	70±1	3±1	45±12	1.3±0.3	57±19	3.1±0.6
NO_3-N	2	3	4	3	3.9±1.5	201±9	1.8±1	4.7±4	76±22	2±0.5	39±2	16±11	88±5
NO_2-N	1	1	2	2	0.2±0.4	3±0.8	1.3±1	1.3±0.6	0.9±0.1	2±0.5	2±0.5	38±2	20±2
TN	255(430)[b]	440	425	420	213±13	215±14	231±12	-	78±21	-	45±10	-	113±10
PO_4-P	26.3	-	-	-	-	-	23.5±2.6	19±0.5	18.8±0.8	20.5±2	20±2	21±1	19.3±0.5
Alkalinity[a]	-	3034±228				1464±460	3065±115	2115±21	1875±35	2630±180	2017±280	2095±100	1885±120
ORP(mV)	-	-157±9				92±22	-193±8	-	38±13	-	12±2	-	2±1
pH	4.6±0.1	7.1±0.1				8±0.4	7.09±0.0	8.2±0.1	8.4±0.1	8.2±0.2	8.4±0.1	8.1±0.1	8.3±0.0
Temp (°C)	20	35.7±0.8				22.4±0.1	35.7±0.8	22.4±0.1					
CH_4 (%)	-	47.8±1.3			45.6±1.2	-	49.1±1	-	-	-	-	-	-
H_2 (%)	-	0.12±0.0			0.12±0.0	-	0.14±0.0	-	-	-	-	-	-
N_2 (%)	-	0.8±0.1			0.9±0.1	-	0.9±0.1	-	-	-	-	-	-

[a] as mg $CaCO_3$/L [b] For Mode 1

Nitrogen and phosphorus content of biomass were measured 9±1.2% and 2.1±0.4% respectively

11.2.3 Analytical Methods

Samples from the feed tank, the anaerobic column, the anoxic column, and the final effluent were collected for analysis. Total suspended solids (TSS), volatile suspended

solids, (VSS) were analyzed in accordance with Standard Methods 2540D, 2540E respectively. [14] HACH methods and testing kits (HACH Odyssey DR/2800) were used to analyze total and soluble chemical oxygen demand (TCOD and SCOD), total nitrogen (TN), NH_4-N, NO_2-N, NO_3-N, and PO_4. Alkalinity was measured by titration with 0.01 N H_2SO_4 in accordance with the Standard Method no 2320 (APHA 1998). DO and ORP were measured onsite using an Oakton DO 6 meter, and an Oakton ORPTestr 10 (Oakton, Singapore). Based on Standard Method no 2540G [14], the attached biomass on the carrier media was measured and expressed as mg VSS/g clean particles. Approximately 10-20 g bio-particles were taken from each of the two columns, suspended in a 100 mL vials, and sonicated for 3 h at 30°C in an Aquasonic sonicator (SK 1200H Kupos, China) with a rated power of 45 watts. After sonication, the TSS and VSS content of the detached biomass was determined following Standard Methods no 2540D and 2540E. [14] The rate of biogas produced in the methanogenic column was measured by a gas wet tip gas meter connected to the top of anaerobic column. Methane, nitrogen gas, hydrogen gas were determined by injecting 0.5 mL of the biogas composition into a gas chromatograph (Model 310, SRI Instruments, Torrance, CA) equipped with a thermal conductivity detector (TCD) and a molecular sieve column (Molesieve 5A, mesh 80/100, 182.88 × 0.3175 cm). The temperatures of the column and the TCD detector were 90 and 105^{o}C, respectively. Argon was used as carrier gas at a flow rate of 30 mL/min.

11.2.4 Bacterial Community Analysis

Samples were taken from bottom and top of anoxic, anaerobic and aerobic columns and numbered 1and 2 for anoxic, 3 and 4 for anaerobic and 5 and 6 for aerobic column respectively. The total genomic DNA were extracted from each sample using the UltraClean Soil DNA Isolation Kit (MO BIO Labratories, Carlsbad, CA, USA). PCR amplification of a region of the 16S rRNA gene was performed with universal the primer set 349f-GC (5'-CGCC CGCC GCGC GCGG CGGG CGGG GCGG GGGC ACGG GGGG CCTA CGGG AGGC AGCA G-3') and 907rM (5'-CCGT CAAT TCMT TTGA GTTT-3', where M=A+C) [15] using a MyCycler thermal cycler (BioRad, Hercules, CA, USA). The PCR products were applied directly to a 6% (w/v) polyacrylamide gel with

20-50% denaturing gradient (100% denaturing gradient corresponds to 70M urea and 40% (v/v) formamide). Electrophoresis was run at a constant voltage of 130V at 58 °C for 6 h. The DNA templates from the bands of interest were re-amplified and the PCR products were purified with the QIAquick PCR purification Kit (QIAGEN Sciences, MD, USA). The fragments were sequenced at the Sequencing Facility at the Robarts Research Institute (The University of Western Ontario, London, Ontario, Canada) and comparing with available sequences from the GenBank database using the BLAST program.

11.2.5 Fed-Batch Experiments

Batch tests were carried out to test the maximum SNR and SDNR of the attached biomass in the system following the methods previously used for the CFBBR._Batch reactors (0.5 L working volume) equipped with magnetic stirrers were used for nitrification by injecting air and alkalinity or for denitrification by avoiding intrusion of air and injecting SCOD. The biomass attached to the media used in the SDNR and the SNR tests were in the range of 1500-4000 mg VSS/L and 240-500 mg VSS/L respectively, considering the amounts of biofilm in the anoxic and aerobic column of 25-50 mg VSS /g media and 4-6 mg VSS /g media, respectively. The initial acetate COD in the denitrification batch tests was set at 350-450 mg/L while the initial alkalinity used in the nitrification test was 250-350 mg/L as $CaCO_3$. For the SNR tests, the initial ammonia concentrations were 35-55 mg/L, added as ammonium chloride. The biofim-coated particles from anaerobic column were used for specific methanogenic activity (SMA) at 37°C, using 250 mL bottle capped with Teflon septum. Approximately 10 g anaerobic biofilm coated particles and 0.3-0.6 mL acetic acid were added together into the 125 mL-bottles containing sufficient nutrients and 3000 mg alkalinity per litre as $CaCO_3$. All the bottles were sealed after purging the headspace with nitrogen to eliminate the present of oxygen/air. The experiment was continued until the bottles stopped producing biogas. Daily biogas was measured by inserting needle attached to a syringe (100 mL and 20 mL). Methane composition was measured using Gas Chromatography (GC) SRI 310 °C with a packed column.

11.3 Results and Discussion

11.3.1 System Biomass Inventory

Figure 2a illustrates the buildup of attached biomass in the anaerobic, anoxic and aerobic columns. The process of biomass buildup comprises two steps: the attachment of biomass during acclimatization and the growth of biomass during the process. The biomass attachment during acclimatization under the same hydrodynamic conditions should result in relatively the same biomass attachment. As shown in **Figure 11.2a**, the attachment of biomass in anaerobic, anoxic and aerobic column, labeled as A, B and C, are 12.5 mg VSS/g media, 14 mg VSS/g 10.8 mg VSS/g media respectively. The aforementioned results are in agreement with the values of u_l in different columns. As shown in **Figure 11.2a**, the concentration of immobilized biomass in the anaerobic reactor increased slowly between days 1 and 120 as a result of the gradual start-up strategy adopted which limited the availability of substrate in the reactor and the low growth rate associated with the methanogenic bacteria, similar to the work reported by Hsu and Shieh (1993). As noticeable from **Figure 11.2a**, the coefficient of variations (COV) for attached biomass in the anaerobic, anoxic and aerobic columns between days 140 and 170 were 1.3%, 3.9% and 3.1% respectively which ensured attainment of the steady state conditions in the system. Moreover, relatively constant suspended biomass in different columns demonstrates the stability of the system in terms of biomass sloughing and detachments.

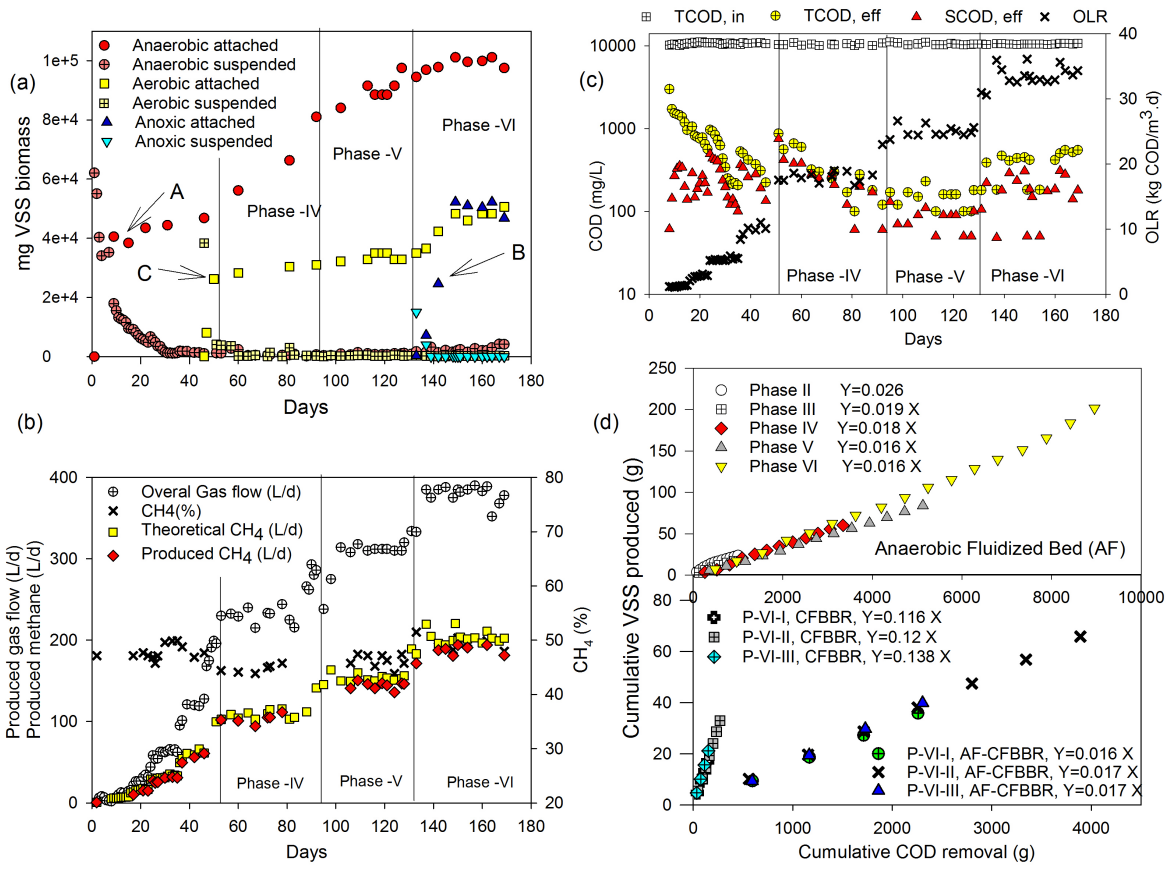

Figure 11.2. (a) Biomass inventory (b) methane production in AF (c) COD removal in AF (d) Biomass yield in AF, CFBBR, AF-CFBBR

11.3.2 Nutrient Removal

The anaerobic fluidized bed (AF) was operated as a mesophilic methanogenic reactor with temperature of 35.7±0.8 °C and alkalinity of 3034±228 as mg $CaCO_3$/L. As shown in **Table 11.2b,** although the pH of feed was 4.6, pH inside the AF remained constant at 7 throughout the experiment due to the high rate acetic acid degradation in the column. ORP was observed in the range of -158 mV to -193 mV.

Figure 11.2b illustrates the trend of biogas production in AF during phases I to VI. As shown in **Figure 11.2b**, the percent methane of the produced biogas fluctuated between 45% and 52% (**Table 11.2b**) resulting in methane production rates of 103±6 L/d, 144±5 L/d and 188±6 L/d in Phases IV, V and VI respectively. Based on CH_4 equivalent of

COD converted by aceticlastic methanogens at standard conditions (0°C and 1 atm), 0.35 L CH_4/g COD, the theoretical methane production was also calculated and depicted in **Figure 11.2b**. Discrepancies of 3.8%-6.4% between the values of theoretical and measured methane were observed. It should be noted that the ratio of biogas produced in the system to the volume of the reactor in Phase VI was 24 L_{gas}/L_{rea}.d, which was handled without using a separator at the top of the reactor.

Figure 11.2c depicts the COD removal rate in AF in different phases. As shown in **Table 11.2b**, the influent TCOD was constant throughout the experiments at concentration of 10600±270 mg/L. The effluent SCOD in phases I to IV when the anaerobic attached biomass was not fully developed was observed to be in the range of 218 mg/L to 260 mg/L. In phase IV, SCOD reduced to 124 mg/L at OLR of 26 kg COD/m^3·d. In Phase VI at maximum OLR of 35 kg COD/m^3·d the system reached 98.3% TCOD removal, with effluent SCOD increased to 180 mg/L. Total suspended solids concentration in the bulk liquid after seeding in phase I decreased gradually from 927 mg/L to the minimum level of 124 mg/L in Phase V at OLR of 26 kg COD/m^3·d. However, increasing the OLR to 35 kg COD/m^3·d in Phase VI resulted in an increase in TSS to 188 mg/L (**Table 11.2b**). **Figure 11.3a** shows the trend of COD removal in AF-CFBBR between Phases IV and VI, when the AF-CFBBR was operational. In overall HRT of 12 h, TCOD was decreased from 10600 mg/L to an average of 50±20 mg/L in the AF-CFBBR effluent throughout all phases, corresponding to the overall TCOD removal of 99.3%. The composition of the TCOD influent to the CFBBR comprised AF effluent, which was 181 mg/L and 390 mg/L in phases V and VI respectively, and 5% feed flow with TCOD of 10600 mg/L. As shown in **Figure 11.3a**, the TCOD influent to the CFBBR was 740±20 in phase VI mg/L corresponding to OLR of 3.3-4.8 kg COD/m^3·d based on the overall volume of the CFBBR in Phase VI (**Table 11.1**). The final effluent SCOD of the AF-CFBBR was 21±10 mg/L and 35±10 mg/L in phase V and VI respectively. **Figure 11.3b** illustrates the trend of volatile suspended solids concentrations in the bulk liquid of the three columns. In Phase IV, the suspended VSS in the anaerobic column averaged 45 mg/L, which increased to 65 mg/L, and 146 mg/L in Phases V and VI. The increase in the anaerobic effluent VSS as a result of higher VSS detachment rates in Phases V and VI (**Table 11.1**) coincided with higher OLRs in those

Phases. The aerobic and anoxic suspended VSS remained < 25 mg/L in Phases V and VI (**Table 11.2b**), which met the secondary effluent discharge quality, which are 30 mg TSS/L.

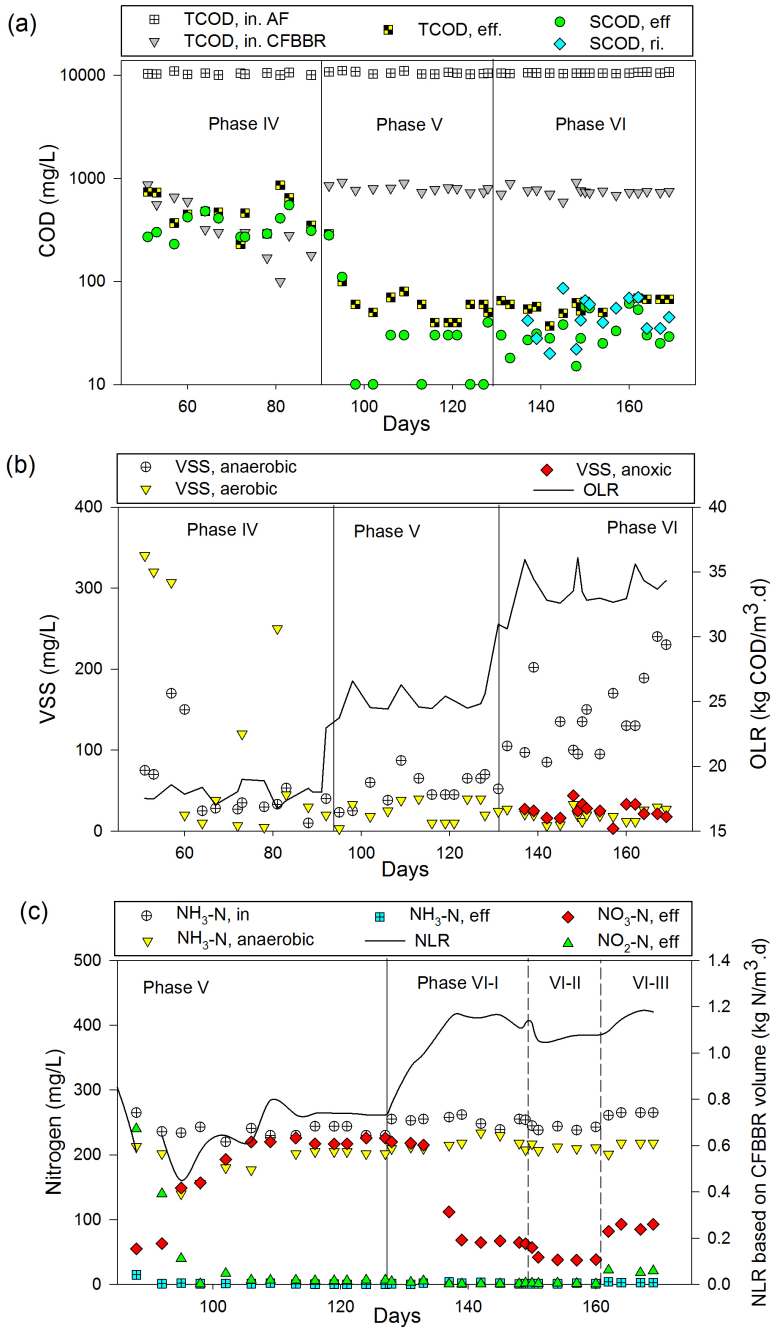

Figure 11.3. (a) COD removal in AF-CFBBR (b) VSS in different columns (c) Nitrogen removal in the system

Figure 11.3c depicts the nitrogen removal trend in AF-CFBBR during Phases V and VI. In Phase V, the anoxic column was not operational and nitrogen removal was solely based on biomass assimilation in the AF when NH_3-N decreased from 250 mg/L in the feed to 213±10 mg/L in the AF effluent and nitrification of ammonia in the aerobic column from 213±10 mg N/L to < 1 mg NH_3-N/L in the system effluent. Assuming the overall anaerobic yield of 0.016 g VSS/g COD and 9±1.1% nitrogen content of biomass (**Table 11.2b** and **Figure 11.2d**) the nitrogen assimilated into biomass was calculated as 20±3 mg /L. The nitrate and nitrite concentrations in AF remained below 3.9 m Ng/L and 0.2 mg N/L in Phase V respectively. The NH_3-N remaining in the AF effluent was sequentially completely nitrified in the aerobic column to an average concentration of 0.9±0.5 mg N/L at NLR of 0.7 kg N/m^3·d. SNR batch tests in Phase V showed nitrification rate of 0.25-0.27 g N/g VSS·d which confirmed the aerobic online nitrification rate within 10% discrepancy. The influent STN to the aerobic column in Phase V was 217±11 mg N/L in the form of NH_3-N and the effluent STN from the aerobic column was 205±9 mg/L in the of NO_x-N. Nitrogen assimilation in the aerobic biomass was estimated at 1.4 mg N/L in Phase V with OLR of 0.5±0.1 kg COD/m^3·d (**Table 11.2a**) and biomass nitrogen content of 9%, thus, indicating that a partial denitrification, of 10 mg N/L may have occurred simultaneously in the aerobic column. The anoxic column was operated with three aerobic to anoxic recirculation flows to feed ratios of 2.3, 4 and 6.2 in Phases VI-I, VI-II and VI-III respectively (**Table 11.1**). The influent NH_3-N and TN to CFBBR in Phase VI were 215 mg N/L and 232 mg N/L corresponding to NLR of 1.1 kg N/m^3·d. As shown in Figure 3a and Table 2a, the effluent NH_3-N throughout the Phase VI remained 1-3 mg N/L, in agreement with batch SNR value range of 0.25-0.31 g N/g VSS·d with 13% discrepancy. The recirculated nitrate to the anoxic column was denitrified to the effluent concentrations of 76±22 mg NO_3-N/L, 39±2 mg NO_3-N/L and 88±5 mg NO_3-N/L in Phases VI-I, VI-II and VI-III respectively. In Phase II when the effluent NO_3-N and NO_2-N were 39 mg N/L and 2 mg N/L, total nitrogen removal of 82.3% was achieved with NH_3-N effluent of 1.3 mg/L. The batch SDNR tests showed a value range of 3.4-3.8 g NO_3-N/g VSS·d. In Phase VI-III, when the aerobic to anoxic recirculation flows to feed ratio increased to 6.2, aerobic DO dropped to 5.6 mg O_2/L from the initial value of 6.3 mg O_2/L and anoxic DO

increased to 0.7 mg O_2/L in Phase VI-II, resulting in nitrite incomplete nitrification in the aerobic column as well as insufficient denitrification in the anoxic column. Therefore, effluent nitrite and nitrate increased to 20 mg N/L and 88 mg N/L respectively (**Table 11.2b**). The nitrification, denitrification and organic loading rates based on aerobic, anoxic and anaerobic biofilm surface area respectively in AF-CFBBR were 2.6 g N/m^2·d, 9.03 g N/m^2·d and 12.1 g COD/m^2·d, as demonstrated in Appendix E. Phosphorus removal occurred as a result of phosphorus biomass assimilation in the three columns. As shown in **Table 11.2a**, in Phase VI, 2.8±0.2 mg P/L and 3.0±0.3 mg P/L, were removed in AF and CFBBR respectively when the assimilation values were based on 1.8% biomass phosphorus content by weight of TSS, 3.3 mg P/L and 0.8 mg P/L.

11.3.3 Biomass Yield

Figure 2d illustrates the linear regression of cumulative VSS produced, based on the sum of the effluent biomass, the net change in attached biomass and biomass wasted, versus cumulative COD removed in anaerobic fluidized bed, CFBBR and AF-CFBBR. The highest observed yield for the AF utilizing acetic acid was 0.026 g VSS/g COD in phase II at OLR of 5.3±0.2 kg COD/m^3·d. Along with increasing the OLR to 34.5 kg COD/m^3·d in AF, the observed yield decreased to 0.016 g VSS/g COD. The very low observed yield of the anaerobic column was expected with the sludge retention time (SRT) in the column estimated at 27-32 days (**Table 11.1**) and the true yield for methanogenesis utilizing acetate is 0.05 g VSS/g COD. [16] Similar to the yields reported in the TCFBBR [17], very low observed yields of 0.116 g VSS/g COD to 0.138 g VSS/g COD were measured in Phase VI-I to VI-III in the aerobic/anoxic CFBBR. Due to the fact that 95% of the overall COD was consumed in the anaerobic fluidized bed, the overall observed yield of AF-CFBBR was measured 0.017 g VSS/g COD, close to the yield of AF.

11.3.4 SDM Experiment

Figures 11.4a and **11.4b** show the effect of nitrate at concentrations of 50 mg N/L and 250 mg N/L on the methanogenic activity in test (a) and (b) respectively. In test (a) the organic loading rate and methane production rate were 26 kg COD/m^3·d and 125 L/d

respectively when 50 mg NO_3-N/L was injected in the feed stream to the AF. As shown in **Figure 11.4a**, After 4 h when the concentration of NO3-N in the AF increased to 35 mg N/L from the initial value of 1.5 mg N/L, the methane production decreased to 108 L/d and SCOD rose to 800 mg/L. During this time, the pH in AF remained the same at 7.1. After 14 h when NO_3-N in AF was 32 mg N/L, methane production declined to 39 L/d and SCOD in the column increased to 3250 mg/L with a pH of 6.8. After 48 h, the system completely failed with SCOD of 9570 mg/L and pH of 5.5. Interestingly, unlike the literature report regarding the possible ammonification or denitrification of NO_3-N in a methanogenic environment [18, 19], in this study nitrates were not converted to ammonia or nitrogen during SDM test. An increase in NH_3-N effluent of 20 mg/L after 24 h could be as a result of a cease in assimilatory nitrogen uptake by inactivated biomass. After 120 h, the system was completely inactive with COD removal rate of 1%. The ORP also increased in test (a) from -200 mV at t=0 to -10 mV after 48 h. The system was recovered by replacing the liquid inside the reactor with water containing 3000 mg alkalinity/L as $CaCO_3$ and pH of 7 and feeding it at OLR of 2 kg COD/m^3·d to 35 kg COD/m^3·d stepwise in 200 h. In the second stage, after the system was recovered and operated under OLR of 35 kg COD/m^3·d, methane production rate of 160 L/d and pH of 7.1, 250 mg NO_3-N/L was added to the feed. The same trend as test (a) was observed in test (b) where the methane production rate declined to 43 L/d and SCOD inside the column increased to 4950 mg/L from the initial value of 130 mg/L. pH decreased to 5.7 and ORP increased to -100 mV from the initial value of -200 mV. After 48 h, the anaerobic column was operating with 8% of biogas production capacity when the SCOD inside the reactor was 9900 mg/L. Ammonification and denitrification in this phase were also not observed, as after 120 h the concentrations of ammonia and nitrate in the effluent remained the same as feed. Many industrial wastewater streams have very low pH such as food-industry wastewater. Therefore if a high rate anaerobic treatment system is used for treatment, stability of the system should be ensured. If a high rate anaerobic system fails to operate for any reason for a period of time, the pH inside the reactor drops and impedes the methanogenic activity. The drop in pH in the aforementioned tests was probably the most likely reason to hinder other microbial activity to accomplish ammonification or denitrification. A similar strategy as stage one was followed to recover the system.

However the system was revitalized after two weeks even at a very low OLR of 3 kg COD/m^3·d. Interestingly, the inhibitory effect of anaerobic methanogenic activity was reversible after 200 h of operating the system with feed NO3-N concentration of 50 mg/L, whereas after 200 h of operation under test (b) condition the methanogenic activity was completely irreversible, clearly showing on the toxic effect of NO_3 on the methanogenesis.

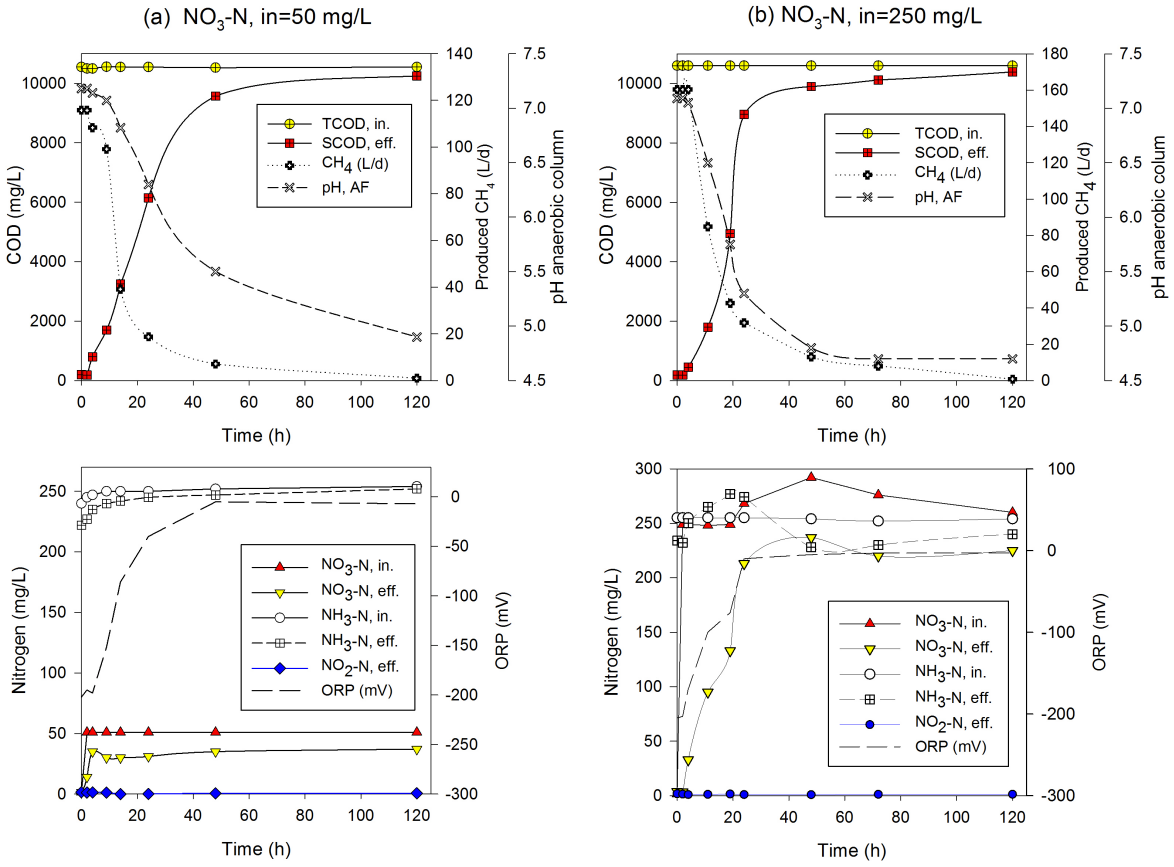

Figure 11.4. Simultaneous denitrification methanogenesis with (a) NO_3-N=50 mg/L (b) NO_3-N=250 mg/L.

11.3.5 Microbial Community and Nutrient Fate

In order to further investigate the predominant species in the three fluidized beds of the AF-CFBBR, the DNA of the attached biofilm from the bottom and top of each

column, were extracted and used for PCR-DGGE analysis. **Figure 11.5a** shows the DGGE profile of the 16S rDNA gene fragments in each column.

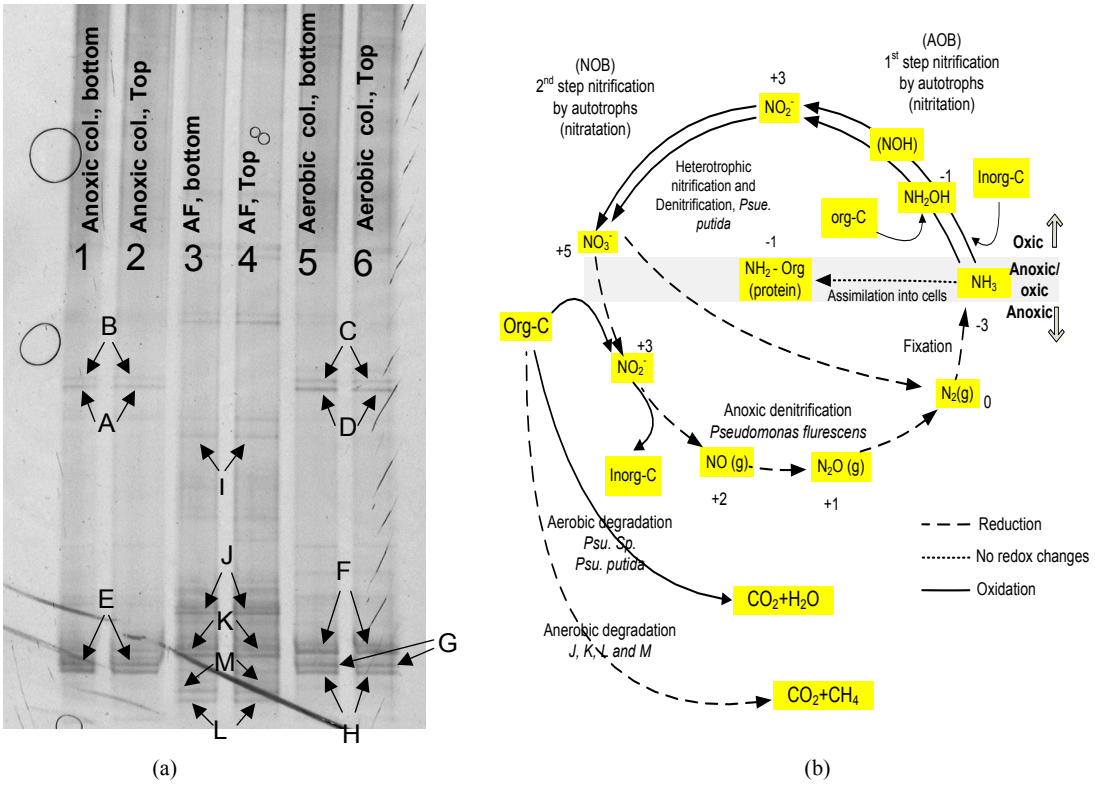

Figure 11.5. (a) DGGE profile of the 16SrDNA gene fragments from different columns (b) Diagram of C and N fate in the system (adapted in part from Kampschreur et al., 2009) [20]

Figure 11.5a clearly shows that the microbial community in each column is the same at the top and the bottom of the reactor and independent of the bed heights. Nitrification process took place predominantly in the aerobic column by ammonium and nitrite oxidizing bacterium (**Table 11.3**). However, the existence of AOB and NOB in the anoxic column demonstrates a partial nitrification process in the anoxic column by AOB and NOB. Denitrification occurred mostly through two different processes: 1- anoxic heterotrophic denitrification in the anoxic column by *Pseudomonas fluorescens* 2- Aerobic denitrification in the aerobic column by heterotrophic *Pseudomonas putida* (**Table 11.3**). *Pseudomonas fluorescens* as the main denitrifiers was only found in the

anoxic column where DO is less than 0.3 mg/L. Mc Kenney et al., (1994) reported that oxygen has an inhibitory effect on the growth and denitrification rates of *Pseudomonas fluorescens* which is the main reason why this species was found only in anoxic condition. [21] Aerobic denitrification is carried by just a few types of heterotrophic bacteria through removal of NH_4^+ to NO_2^- or NO_3^- (heterotrophic nitrification) and simultaneous aerobic conversion of the NO_3^- or NO_2^- to N_2O and/or N_2 (aerobic denitrification). *Pseudomonas putida,* which was observed in the aerobic column, has been reported to be one of the main aerobic denitrifiers in the literature. [22, 23, 24] *Pseudomonas spp.* observed in the aerobic column, were the predominant degraders of organics in the oxic zone. However, *Pseudomonas putida* and *Pseudomonas fluorescens* observed in both anoxic and aerobic columns were also reported to have the highest degradative potential among aerobic degrading bacteria. [25] Species K, L and M derived in **Figure 11.5a**, were responsible for acetic acid convergence to methane and CO2 as aceticlastic methangens (archae). *Petrimonas sp.* whose named was proposed by Grabowski et al. (2005), was also present in the anaerobic culture. This species was described as a mesophilic, anaerobic, fermentative bacterium. [26]

Table 11.3. Affiliation of denaturing gradient gel electrophoresis (DGGE) bands

Band	Affiliation (accession no.)	Similarity (%)
A	Uncultured ammonium and nitrite oxidizing bacterium (FJ529975)	99
B	*Flammovirgaceae* bact. (FJ516870)	92
C	*Flammovirgaceae* bact. (FJ516870)	92
D	Uncult. ammonium and nitrite oxidizing bact. (FJ529975)	78
	Flammovirgaceae bact. (FJ516870)	72
E	*Pseudomonas fluorescens*	95
F	Uncult. *Pseudomonas* sp. (FN994919.1)	94
G	*Pseudomonas putida* (AB543806.1)	96
H	Uncult. *Pseudomonas* sp. (GU000125.1)	91
I	Uncult. *Bacteroidetes* from fecal matter (GU959493)	80
	Prevotellaceae bacterium (GQ358273)	78
J	*Petrimonas* sp. (GU583827.1)	86
K	Uncult. methanogenic archaeon (FJ982725)	91
L	Methanosarcina mazeii (AF411469.1)	96
M	Methanosarcina mazeii (EU544030.1)	98

Figure 11.5b illustrates the carbon and nitrogen fate in the AF-CFBBR. Organic carbon removal takes place through aerobic degradation, anaerobic reduction, heterotrophic aerobic and anoxic uptake and assimilatory uptake by anaerobic, anoxic and aerobic microorganisms. Inorganic carbon in the form of alkalinity and minerals was consumed for autotrophic nitrification and produced by heterotrophic denitrifiers. Nitrogen was either assimilated within the anaerobic, anoxic and aerobic cells or converted to nitrate by heterotrophic and autotrophic nitrifiers and sequentially converted to N_2. A mass balance provides a better understanding of the aforementioned process.

11.3.6 Mass Balance

Table 11.4 illustrates the steady-state mass balance for COD, TN, NH_3-N, NO_3-N, NO_2-N, PO_4-P and alkalinity for phase VI-II in which the optimum conditions of nutrient removal occurred in this study for AF and CFBBR individually. The mass balances were based on experimental data of the anaerobic and anoxic influent, anaerobic, anoxic and final effluent characteristics, recirculation flows and the sludge wastage of each column.

As shown in **Table 11.4**, mass balance COD closures of 96.9% for AF and 96.7% for CFBBR, nitrogen closures of 93.3% for AF and 95.6% for CFBBR and alkalinity closure of 88.7% in CFBBR were calculated respectively.

An overall COD removal of 97% in the anaerobic column was observed. The aerobic and anoxic columns contributed to 27% and 73% of overall COD removal in the CFBBR corresponding to 9.3 g/d and 26.1 g/d respectively. Based on denitrified NO_3-N in the anoxic riser the COD consumed by heterotrophs in the riser was calculated 24.5 g/d which makes up for 94% of the overall COD removal in the riser. In addition, the average liquid flow recirculation from the aerobic column to the anoxic column of 9.9 L/h with a DO concentration of 5.5 mg/L contributed to 1.7 g/d aerobic COD removal in the riser which in negligible compared to the COD removed by denitrification.

Table 11.4. Nutrient mass balance in Phase VI-II

	Mass in influent (g/d)	Mass in Influent (g/d)	Mass consumed and in (effluent)* (g/d)	Mass consumed (g/d)	Mass consumed (g/d)	Mass in effluent (g/d)	Mass wastage (g/d)	Percent closure CFBBR (%)	Percent closure AF (%)
	Anaerobic	Anoxic	Anaerobic	Anoxic	Aerobic				
				Phase VI-II- SWW (55 l/d)					
TCOD	536±19	49±4	(16±6)*			3.0±0.3	9.1[a]±1.4	96.7[1]	96.9[4]
(sCOD)	536±19	29±7	529±21	26.1±4.5 (24.5)[d] (1.7)[e]	9.3±2.1	2±0.8			
CH_4 (L/d)			203±7						
TN	12.6±0.8	11.9±0.6	(11.7±0.4)*		7.8±0.5	2.2±0.1	0.9[b]±0.2	95.6[2]	93.3[5]
NH_4-N	12.5±0.7	11.3±0.5	1.7±0.4	0.9±0.4 (0.3)[f]	7.6±0.5	0.06±0.06			
NO_3-N	0.07±0.01	0.08±0.01	0.0±0.0	7.4±0.7	0.9±0.4	2±0.1			
NO_2-N	0.0±0.0	0.0±0.0	0.0±0.0	0.0±0.0	0.0±0.0	0.1±0.1			
PO_4-P	1.2±0.01	1.1±0.07	0.11±0.07	0.01±0.0	0.01±0.0	1.09±0.08			
Alkalinity		152±6	26.4[h]	54.2[i]		110±20		88.7[4]	

[a,b,c] COD equivalent, Nitrogen (N) and phosphorus (P) content of 1 g biomass were measured 1.44±0.03, 0.091±0.02 and 0.019±0.04 gr respectively.

[d] SCOD consumption through denitrification based on $\frac{\text{g SCOD}}{\text{g NO}_3-\text{N}} = \frac{2.86}{1-1.42\,Y_{obs}}$ For example Phase I $= 7.4\times\frac{2.86}{1-1.42\times 0.12}$

[e] Aerobic SCOD consumption in the riser; for example Phase I $= \frac{\Delta O_2}{\Delta t}\times(1-Y_H)^{-1} = 0.0018\frac{\text{g O}_2}{\text{l}}\times(2+1+4.5)\times 55\frac{\text{l}}{\text{d}}\times(1-0.4\times 1.42)^{-1}$

[f] Nitrogen assimilated for denitrification; for example Phase I $= 7.4\times\frac{2.86}{1-1.42\times 0.12}\times 0.12\frac{\text{gVSS}}{\text{gSCOD}}\times 0.1\frac{\text{g N}}{\text{g VSS}}$

[h] Alkalinity generated in the anoxic column; for example Phase II $= 7.7\,\text{g N}_{\text{denitrified}}\times 3.57\frac{\text{g Alk}_{\text{generated}}}{\text{g N}}$

[i] Alkalinity consumed in the aerobic column; for example Phase II $= 7.7\,\text{g N}_{\text{nitrified}}\times 7.14\frac{\text{g Alk}_{\text{consumed}}}{\text{g N}}$

[1] COD % closure $= \frac{26.1+9.3+3.0+9.1}{49}\times 100$ [2] N% closure $= \frac{2.2+(7.4+0.9)+0.9}{11.9}\times 100$ [3] Alk.% closure $= \frac{110}{152-(54.2-26.4)}\times 100$ For (CFBBR)

[4] COD % closure $= 203\frac{\text{L}_{CH4}}{\text{d}}\times\left(0.35\frac{\text{L}_{CH4}}{\text{gCOD}}\times\frac{273+36}{273}\right)^{-1}\times\left(529\frac{\text{gCOD}}{\text{d}}\right)^{-1}$ [5] N% closure $= 0.016\frac{\text{gVSS}}{\text{gCOD}}\times 33000\frac{\text{gCOD}}{\text{m}^3\text{.d}}\times 0.1\frac{\text{gN}}{\text{gVSS}}\times 0.016\,\text{m}^3\times(12.6-11.7)^{-1}$ (For AF)

Ammonia nitrogen was either assimilated in the biomass of AF or CFBBR or involved in nitrification-denitrification process in CFBBR. As shown in Table 3, nitrogen mass closure of 93.3% indicates that (11.7 g/d-12.6g/d) nitrogen reduction in the anaerobic column was due to biomass assimilation, as calculated in the footnotes of **Table 11.4**. Thereafter, as shown in **Table 11.4**, 7.6 g/d ammonia was utilized by nitrifiers in the downer and 0.9 g/d in the riser, 0.3 g/d of which is NH3-N assimilated in denitrifiers. **Table 11.4** clearly shows that although 90% of the overall nitrification occurs in the downer of CFBBR, partial nitrification in the riser was achieved. Overall mass balance for nitrate was based on nitrate consumption in each column. Table 4 shows that 7.4 g/d of nitrogen were denitrified in the riser as well as 0.9 g/d in the downer which indicates that 89% of denitrification was accomplished in the anoxic column by heterotrophs. However, 11% of nitrogen removal through denitrification occurred in the aerobic column at DO levels of > 5.5 mg/L. Due to the fact that biofilm thickness of aerobic biofilm-coated particles was less than 100 μm and the DO level was high, the 11% of

nitrogen removal happened under simultaneous nitrification denitrification (SDM) process. An alkalinity mass balance closure of 88.7% was calculated based on the amount of alkalinity consumed by autotrophic nitrifiers in the downer as well as alkalinity produced in the riser by the denitrifiers responsible for anoxic denitrification. Phosphorus removal of 10% in the system was observed as a result of biomass assimilation in the three columns.

11.4 Conclusions

- An integrated anaerobic fluidized bed and circulating fluidized bed bioreactor (AF-CFBBR) was designed, commissioned and operated for 180 days in order to investigate its carbon and nitrogen removal capability from high strength synthetic wastewater.
- The AF-CFBBR affected 99.7% COD removal, 84% nitrogen removal with a very low sludge yield of 0.017 g VSS/g COD while treating a wastewater containing 10700 mg COD/L as well as 250 mg NH_3-N/L. The superior system performance was at OLR of 35 kg COD/m^3·d based on AF and 1.1 kg N/m^3·d based on CFBBR with an overall HRT of less than 12 h.
- Microbial communities in the system were determined using DGGE test which confirmed the inter mixture of AOB and NOB in both aerobic and anoxic column and *Pseudomonas putida* responsible for simultaneous denitrification nitrification. Methanogenic activity was also observed to be led by archaeon rather than bacteria.

- The feasibility of simultaneous denitrification and methanogenic activity at a very high OLR and different NO_3-N concentrations was studied while the feed pH was 4 resemblances the food industry wastewater. Methanogenesis was completely hindered when NO_3-N was fed at concentrations of 50 mg N/L and 250 mg N/L. As a result the system failed due to organic overloading and a sharp drop in pH in less than 48 hr. Denitrification inhibition was reversible when NO_3-N was 50 mg/L and irreversible when NO_3-N in the feed was 250 mg/L.

11.5 References

[1] Chen KC, Lin YF. The relationship between denitrifying bacteria and methanogenic bacteria in a mixed culture system of acclimated sludges. Wat. Res. 1993; 27-12:1749-1759.

[2] Batstone DJ, Keller K, Angelidaki I, Kalyuzhenyi SV, Pavlostathis SG, Rozzi A, Sanders WTM, Siegrist H, and Vavilin VA. Anaerobic Digestion Model No. 1. IWA publishing: 2002.

[3] Kluber HD, Conrad R. Effects of nitrate, nitrite, NO, and N2O on methanogenesis and other redox processes in anoxic rice field soil. FEMS Microb. Ecol. 1998; 25:301-318.

[4] Percheron G, Michaud S, Bernet N, Moletta R. Nitrate and nitrite reduction of a sulphide-rich environment. J. Chem. Technol. Biotechnol. 1998; 72:213-220.

[5] Roy R, Conrad R. Effect of methanogenic precursors (acetate, hydrogen, propionate) on the suppression of methane production by nitrate in anoxic rice field soil. FEMS Microb. Ecol. 1998; 28:49-61.

[6] Tugtas AE, Pavlostathis SG. Inhibitory effects of nitrate reduction on methanogenesis in the presence of different electron donors. Wat. Sci. Technol. 2008; 293-698.

[7] Ruiz G, Jeison D, and Chamy R. Development of denitrifying and methanogenic activities in USB reactors for the treatment of wastewater: Effect of COD/N ratio. Proc. Biochem. 2006; 41:1338–1342.

[8] Peng Y, Zhang S, Zeng W, Zheng S. Mino, T.; Satoh, H. Organic removal by denitritation and methanogenesisvand nitrogen removal by nitritation from landfill leachate. Wat. Res. 2008; 42:883-892.

[9] Ahn YT, Kang ST, Chae SR, Lee CY, Bae BU, Shin HS. Simultaneous high-strength organic and nitrogen removal with combined anaerobic upflow bed filter and aerobic membrane bioreactor. Desal. 2007; 202:114–121.

[10] Chen KC, Lin YF, Houng JY. Performance of a continuous stirred tank reactor with immobilized denitrifiers and methanogens. Wat. Environ. Res. 1997; 69-2:233-239.

[11] Cui Y, Nakhla G, Zhu J, Patel A. Simultaneous carbon and nitrogen removal in anoxic-aerobic circulating fluidized bed biological reactor (CFBBR). Environ. Technol. 2004; 25:699-712.

[12] Chowdhury N, Nakhla G, Zhu J, Islam M. Pilot-scale experience with biological nutrient removal and biomass yield reduction in a liquid-solid circulating fluidized bed bioreactor. Wat. Environ. Res. 2010 Doi: WER 08-11-1541RR.

[13] Eldyasti A, Chowdhury N, Nakhla G, Zhu J. Biological nutrient removal from leachate using a pilot liquid–solid circulating fluidized bed bioreactor (LSCFB). J of Haz. Mat. 2010; 181:289–297.

[14] APHA; AWWA; WEF. Standard methods for the examination of water and wastewater. 20th Edition, American Public Health Association, Washington D.C. 1998.

[15] Muyzer G, de Waal EC, Uitterlinden AG. Profiling of complex microbial populations by denaturing gradient gel electrophoresis analysis of polymerase chain reaction-amplified genes coding for 16S rRNA. Appl. Environ. Microbiol. 1993; 59: 695-700.

[16] Metcalf and Eddy, Wastewater Engineering: Treatment and reuse, Fourth ed., McGraw-Hill, 2003.

[17] Andalib M, Nakhla G, Zhu J. Dynamic testing of the twin circulating fluidized bed bioreactor (TCFBBR) for nutrient removal from municipal wastewater. Chem. Eng. J. 2010; 162:616-625.

[18] Shin HS. Effect of alkalinity and substrate on simultaneous denitrification and methanogenesis. WEF Proceeding. 2002

[19] Akunna JC, Bizeau C, Moletta R. Denitrification in anaerobic digesters: possibilities and influence of wastewater COD/N-NOx ratio. Environ. Technol. 1992; 13:825-836.

[20] Kampschreur J, Temmink H, Kleerebezem R, Jetten MSM, van Loosdrecht MCM. Nitrous oxide emission during wastewater treatment. Wat. Res. 2009; 43:4093-4103.

[21] McKenney DJ, Drury CF, Findlay WI, Mutus B, McDonnell T, Gajda C. Kinetics of denitrification by *Pseudomonas fluorescens*: Oxygen effects. Soil Biol. Biochem. 1994; 26-7:901-908.

[22] Daum M, Zimmer W, Papen H, Kloos K, Nawrath K, Bothe H. *Physiological and molecular biological characterization of ammonia oxidation of the heterotrophic nitrifier* Pseudomonas putida, Curr. Microbiol. 1998; 37:281–288.

[23] Zhao B, Liang He H, Fan Zhang X. Nitrogen removal capability through simultaneous heterotrophic nitrification and aerobic denitrification by *Bacillus* sp. LY. Environ. Technol. 2010; 31-4:409-416.

[24] Kim M, Jeong S, Jeong Yoon S, Ja Cho S, Hun Kim Y, Ju Kim M, Yoen Ryu E, Lee S. Aerobic denitrification of *Pseudomonas putida* AD-21at different C/N ratios. J. of Biosci. Bioeng. 2008; 106-5:498–502.

[25] Jordening H, Winter J. Environmental biotechnology: Concepts and applications. Wiley VCH page 205, 2005.

[26] Grabowski A, Tindall BJ, Bardin V, Blanchet D. Petrimonas sulfuriphila gen. nov., sp. nov., a mesophilic fermentative bacterium isolated from a biodegraded oil reservoir. Int. J. Syst. Evol. Microbiol. 2005; 55:1113–1121.

[27] Hsu Y, Shieh WK. Startup of anaerobic fluidized bed reactors with acetic acid as the substrate. Bietechnol. Bioeng. 1993; 41:347-353.

[28] Andalib M, Nakhla G, Zhu J. Terminal settling velocity and drag coefficient of biofilm-coated particles at high Reynolds numbers. AIChE 2010 56-10:2598-2606.

12 General Discussions

12.1 Summary and Engineering Significance

Even though, the fluidized bed bioreactors were efficiently removing either organics or nutrients [1, 2] very few studies [3, 4] attempted to remove nitrogen and phosphorus simultaneously.

Nakhla and his colleagues [5-8] proposed and patented liquid solid circulating fluidized bed bioreactor (LSCFB) in 2004 comprises of an anoxic column (riser) and an aerobic column (downer). Since then biological nutrient capabilities of LSCFB in lab and pilot scale from municipal as well as some industrial wastewater such as landfill leachate and rendering wastewater have been under investigation.

In all the aforementioned application, the LSCFB demonstrated 90% organic, 80% total nitrogen, and 70% total phosphorus removal at nutrients loading rates of 4.12 kg COD/m^3·d, 0.26 kg N/m^3·d, and 0.051 kg P/m^3·d, and an empty bed contact time of 1.5 h. In general both lab and pilot studies confirmed that the LSCFB treated municipal wastewater effluent characterized by <1.0 mg NH_4-N/L, <5.0 mg NO_3-N/L, <1.0 mg PO_4-P/L, <10 mg TN/L, <10 mg SBOD/L, and 10-15 mg VSS/L, can easily meet the regulations for non-potable applications of treated wastewater without using any chemicals for phosphorus removal and secondary clarifier for suspended solids removal.

The observed yields in this study were 1/4 of the conventional treatment processes attributed to long solid retention times of 20-39 d and anoxic consumption of 40-50% influent COD.

LSCFB comprises a 6.5-m tall riser and a downer with overall height of 5 m. In addition, the smaller riser cross sectional area compared to the downer accelerated uncontrolled particle transfer rate from riser to downer. Although this technology showed promising results in treating some high strength wastewater such and landfill leachate, the nature of aerobic and anoxic treatment makes this system inappropriate in general to

treat high strength industrial wastewater where a strict anaerobic system is needed. Insufficient aeration system in the LSCFBR caused a high shear force and abrasion rate in the downer that resulted in very low biomass retention. Therefore, the system did not reach its maximum nitrogen loading rate capacity.

In this study, the general approach was to design and test a circulating fluidized bed with the same height of 3.6-4 m for both riser and downer and with rectangular cross sectional area. These specifications facilitate retrofitting of existing wastewater treatment tanks by dividing into compartments.

In the TFBBR, the size of the downer and the riser were the same with the same cross sectional area. Although the biological nutrient removal efficiency from synthetic municipal wastewater was the same as LSCFBR, the overall hydraulic retention time was less, 2.2 h. In addition greater cross sectional area of riser resulted in lower superficial liquid velocity and subsequently longer overall sludge retention time, 72-108 d. As a result lower sludge yield of 0.06-0.07 g VSS/g COD than the LSCFB of 0.12 g VSS/g COD was observed. Moreover, oxygen limitation in the riser of TFBBR caused an anaerobic zone in which sulfate reduction bacteria (SRB) reduced sulfate to H_2S gas. The fluidization regime in both riser and downer was conventional fluidization and particle recirculation took place through two electro-impellers. With particle recirculation using this technology, the particle transfer rate from riser to the downer and vice verse was controllable. However, the particle transfer in the dilute phase (riser to downer) was easier.

In TCFBBR, the same concept as TFBBR was applied with smaller riser (cross sectional area of 60% of downer). The particle recirculation was through inclined pipes and particle recirculation rate could be measured with a graduated vessel. The lab-scale TCFBBR operated at loading rates of up to 4.5 kg COD/m^3·d, 0.5 kg N/m^3·d and 0.041 kg P/m^3·d removed >96% organic matter, 84-88% nitrogen and 12-50% phosphorus at EBCT of 0.7, 1.2 and 0.9 h and overall hydraulic retention time of (HRT) 2h. TCFBBR achieved long SRT of 37-40 d, shorter than TFBBR, which still rationalized the relatively higher observed yield of 0.9-0.1 g VSS/g COD, than that the TFBBR.

High strength wastes produced by fertilizer production, explosive manufacturing and recovery of nuclear fuels as well as landfill leachate contain in addition to organic matter, nitrogen in the forms of ammonia, nitric and nitrous acids. The nature of the aforementioned high strength wastes requires anaerobic processes to recover energy. In addition, nutrient removal is becoming mandatory in many places. Therefore, A new integrated anaerobic fluidized bed (AF) with CFBBR called (AF-CFBBR) was developed to investigate simultaneous biological nitrogen removal from high strength wastewater and anaerobic treatment. Additionally, the inhibitory effect of nitrate on methanogenic activities in a high rate anaerobic fluidized bed at organic loading rates of above 35 kg COD/m^3·d was studied in order to evaluate the feasibility of simultaneous denitrification and methanogenic activities (SDM) in a high rate anaerobic system. The AF-CFBBR showed 99.7% COD removal, 84% nitrogen removal, with a very low sludge yield of 0.017 g VSS/g COD while treating a wastewater containing 10700 mg COD/L and 250 mg NH_3-N/L. The system was operated at an organic loading rate (OLR) of 35 kg COD/m^3·d based on the AF volume and 1.1 kg N/m^3·d based on the CFBBR at an overall HRT of less than 12 h in the AF-CFBBR. The very interesting concept in AF-CFBBR was a new aeration system that increased the nitrogen-loading rate to up to 1.1 kg N/m^3·d. In this method, two-stage aeration was applied, one at the bottom of the column and the second right at the top of the expanded bed. Both diffusers were fine bubble diffuser to reduce the effect of agitation and shear force in the aerobic column. The aeration through the first diffuser at the bottom was just enough to provide a DO of 1.5 mg/L in the liquid. The second diffuser aerated the liquid on top of the bed to the DO of 6 mg/L to be recirculated to the bottom of the column by the recirculation pump.

12.2 Scientific Contribution

I. Ar numbers particles were found to be a better parameter to define the drag coefficient of falling particles and bed expansion index.

II. A new equation for determining F_d as an explicit function of terminal settling velocity was proposed based on Archimedes numbers (Ar) of the biofilm coated particle. The proposed equation adequately predicted the terminal

settling velocity of other literature data at lower Re_t of less than 130, with an accuracy >85% as well as particles with Re_t of up to 300.

III. A new equation based on Archimedes number was proposed to calculate bed expansion index of biofilm-coated particles, which predicted the existing experimental data with less than 10% standard error. This equation is a new mathematical concept of defining bed expansion index in general and can be extended to rigid particles.

IV. A two-phase and three-phase predictive fluidization model based on the characteristics of a system such as media type and size, flow rates, and reactor cross sectional area was proposed to calculate bed expansion, solid, liquid and gas hold up, specific surface area of the biofilm particles. The model was subsequently linked to 1d AQUIFAS APP software (Aquaregen*)* to model two and three phase fluidized bed bioreactors. The credibility of the proposed model for biological nutrient removal was validated using the experimental data with less than 10% average error.

V. The TFBBR, TCFBBR and AF-CFBBR have embodied a complex anaerobic-anoxic-aerobic treatment train into a single unit with the advantages of liquid-solid circulating fluidized bed and attached biomass. The strong influence of liquid-solid recirculation on biofilm detachment maintains a smooth and strong biofilm, which is essential for efficient nutrient removal in a continuous process. The observed anaerobic conditions in thick biofilm even though no strict anaerobic arrangement was provided, primarily due to low concentrations and diffusion limitation of dissolved oxygen and nitrate.

VI. Denitrification in TCFBBR was found through two different processes: 1-anoxic heterotrophic denitrification in the anoxic column by *Pseudomonas fluorescens* 2- Aerobic denitrification in the aerobic column by heterotrophic *Pseudomonas putida,* which is the main species for aerobic denitrification. *Pseudomonas fluorescens* as the main denitrifiers was only found in the anoxic column when DO was less than 0.3 mg/L.

VII. In the simultaneous denitrification and methanogenesis (SDM) tests conducted in this work, nitrate concentration above 50 mg/L were found completely

inhibitory to methanogenesis in a high rate anaerobic system with OLR of > 35 kg COD/m^3·d.

VIII. The scientific explanation of nutrient removal processes, sludge reduction and model developed in this study provide invaluable insight into the behavior of the complex microbial consortium, which will benefit scientists and practitioners particularly in optimization of biological treatment processes.

12.3 References

[1] Shieh WK, Keenan DK. Fluidized bed biofilm reactor for wastewater treatment. In: Fiechter, A. (Ed.), *Advances in Biochemical Engineering/Biotechnology*. Springer-Verlag, Berlin, 1986; 132-168.

[2] Payraudeau M, Paffoni C, Gousailles M. Tertiary nitrification in an up flow biofilter on floating media: influence of temperature and COD load. *Water Sci. Technol*. 2000; 41:21-27.

[3] Feng Q, Yu A, Chu L, Xing XH. Performance study of excess sludge and simultaneous removal of organic and nitrogen by a combination of fluidized–and fixed-bed bioreactors with different structured macroporous carriers. *Biocehm. Eng. J.,* 2008; 39:344-352.

[4] Monti A, Hall ER, Dawson RN, Husain H, Kelly HG. Comparative study of biological nutrient removal (BNR) processes with sedimentation and membrane-based separation. *Biotechnol. Bioeng.*, 2006; 94:740-752.

[5] Nakhla G, Zhu J, Cui Y. Liquid-solid circulating fluidized bed wastewater treatment system for simultaneous removal of carbon, nitrogen, and phosphorus. 2004, US patent no. 6,716,244, Int'l PCT patent awarded Aug. 2005.

[6] Chowdhury N, Nakhla G, Zhu J. Load maximization of a liquid-solid circulating fluidized bed bioreactor for nitrogen removal from synthetic municipal wastewater. Chemosphere, 2008;71:807-815.

[7] Cui Y, Nakhla G, Zhu J, Patel A. Simultaneous carbon and nitrogen removal in anoxic-aerobic circulating fluidized bed biological reactor (CFBBR). Environ. Technol. 2004; 25:699-712.

[8] Patel A, Zhu J, Nakhla G. Simultaneous carbon, nitrogen and phosphorus removal from municipal wastewater in a circulating fluidized bed bioreactor. Chemos. 2006; 65:1103-1112.

13 Conclusions and Recommendations

13.1 Conclusions

The principal findings of this study were:

I. A new explanation of drag coefficient for wide ranges of Re_t and based on a biofilm-coated particle Archimedes number was defined. A new equation for drag coefficient of biofilm-coated particles was generated that was able to predict terminal-settling velocity with average error of less than 10% to the experimental data in the literature. This equation is explicit in terminal settling velocity and is valid within $310 < Ar < 2.5\times10^5$ and $7 < Re_t < 300$.

II. Bed expansion index (n) of fluidized biofilm-coated particles was defines as a function of *Ar* number. A new equation for (*n*) that predicted the entire experimental bed expansion index in the literature within less than 10% error was proposed. This equation is explicit with respect to particle settling velocity and just a function of biofilm-coated particle physical property, thus trial and error methods are not required.

III. A lab-scale TFBBR was developed with the same height of riser and downer and rectangular cross-sectional area to retrofit the existing conventional wastewater treatment tanks. The system operated at loading rates of 1.3-2.5 kg COD/m^3·d, 0.14-0.28 kg N/m^3·d and 0.024-0.041 kg P/m^3·d to study the performance of the system with respect to biological nutrient removal. The system removed >96% organic matter, 84% nitrogen and 12% phosphorus at EBCT of 0.7, 1.2 and 0.9 h. The TFBBR achieved tertiary effluent quality with BOD<6 mg/L, TN < 6 mg/L,

NO_3-N < 5 mg/L, NH_4-N < 1 mg/L and TSS < 20 mg/L at an overall HRT of less than 2.9 h.

IV. The newly developed lab-scale TCFBBR was operated at loading rates of 2.7-4.3 kg COD/m^3·d, 0.3-0.51 kg N/m^3·d, and 0.032-0.06 kg P/m^3·d to study nutrient removal efficiencies of the system at a very short HRT of 2.3 hrs. Approximately > 90% organic, >85% nitrogen, and 20%-51% phosphorus removal were experienced using the TCFBBR at nutrient loading rates of 4.3 kg COD/m^3·d, 0.51 kg N/m^3·d, and 0.06 kg P/m^3·d, and an EBCT as low as 1.0 h. Due to precipitation and assimilation 17%-51% of the influent phosphorus was removed without addition of any chemicals. The system did not show any considerable deterioration in nutrient removal efficiency during dynamic testing at a hydraulic peaking factor of 4 for 3 hours. A 50% loss of nitrification efficiency was observed during a carbon shock test due to DO limitations, washout of nitrifiers, and high COD concentrations in the aerobic downer.

V. A two and three-phase fluidized bed model which predicts particle specific surface area (SSA) and the volume of the expanded bed based on changes in the biofilm thickness and the operational data, was applied and linked to AQUIFAS APP to simulate the nutrient removal in the TCFBBR. Two-sided t-tests showed that there were no statistically significant differences between the experimental and the modeled TCOD, SCOD, NH_3-N, NO_x-N. A comparison between the experimental mass balance and the simulated carbon and nitrogen uptakes through nitrification and denitrification in each column further demonstrated the plausibility of the AQUIFAS APP integrated with the fluidization model.

VI. An integrated anaerobic fluidized bed and circulating fluidized bed bioreactor (AF-CFBBR) was designed, commissioned and operated for 180 days in order to investigate its carbon and nitrogen removal capability from high strength synthetic wastewater. The newly developed anaerobic fluidized bed and circulating fluidized bed bioreactor (AF-CFBBR) affected 99.7% COD removal,

84% nitrogen removal with a very low sludge yield of 0.017 g VSS/g COD while treating a wastewater containing 10700 mg COD/L as well as 250 mg NH_3-N/L. The superior system performance was at OLR of 35 kg COD/m^3·d based on AF and 1.1 kg N/m^3·d based on CFBBR with an overall HRT of less than 12 h. Microbial communities in the system were determined using the DGGE test, which confirmed the inter mixture of AOB and NOB in both aerobic and anoxic column and *Pseudomonas putida* responsible for simultaneous denitrification nitrification. Methanogenic activity was also observed to be led by archaeon rather than bacteria.

VII. The feasibility of simultaneous denitrification and methanogenic activity at a very high OLR and different NO_3-N concentrations was studied while the feed pH was maintained at 4 resembling the food industry wastewater. Methanogenesis was completely hindered when NO_3-N was fed at concentrations of 50 mg N/L and 250 mg N/L. As a result the system failed due to organic overloading and a sharp drop in pH in less than 48 hr. Denitrification inhibition was reversible when NO_3-N was 50 mg/L and irreversible when NO_3-N in the feed was 250 mg/L.

13.2 Limitations

Both TFBBR and TCFBBR showed excellent performances at high OLR and NLR with regards to biological nutrient removal from municipal wastewater with minimum production of excess sludge, which is a great advantage of these systems. AF-CFBBR also demonstrated very promising results in terms of biological nutrient removal from high strength wastewater at very high OLR of 35 kg COD/m^3·d and NLR of 1.1 kg N/m^3·d. However the nature of fluidization itself brings some limitations with it:

I. One of the limitations is the high recirculation rate of liquid to maintain a liquid superficial velocity of above minimum fluidization velocity. This rate may not cause a problem when the system is dealing with a low feed flow rate. However,

when the feed flow rate is high and as a result the cross sectional area of the system is large, the required energy could be significant which could be a major drawback of this technology. For anaerobic fluidized beds, where a high rate methanogenic activity can be reached and because the price of produced biogas is rising, this energy problem is less of a concern. The authors, however, have a recommendation to overcome this weakness in Chapter 13.4.

II. It is demonstrated that the method of aeration in the system is crucial. Inadequate oxygen transfer in TFBBR and CFBBR due to usage of coarse bubble aeration ring caused a lower aerobic biofilm concentration rather than when a finer diffuser was used in AF-CFBBR. As a result, proper maintenance of fine bubble diffuser disks in the downer is crucial.

III. The biofilm development in the riser and sequentially biofilm-coated particle transfer from riser to the downer can not be fully controlled because there has not been simply any comprehensive model proposed yet to understand all the parameters and functions that govern the phenomena.

IV. Biofilm formation on the carriers fully depends on the type of carrier media chosen for the system. However, carriers could pose problems leading to long start-up times, especially when microorganisms having low growth rates such as nitrifying and methanogenesis microorganisms.

V. The very short hydraulic retention time of the system causes the systems sharply responses to an increase in suspended solid concentrations in the feed flow.

VI. The very low sludge yield, although an advantage in general, nullifies the possibility of biological phosphorus removal from waste stream

13.3 Necessary Design Modifications

I. Fine bubble diffuser disc should be used in this technology to improve oxygen transfer efficiency and most importantly to reduce the shear force in the three-phase fluidization regime of the downer.

II. A carrier media with a high specific surface area and low density should be used. Lava rock had an acceptable SSA but the density was very high. Zeolite was lighter but with an ideal SSA.

III. Particle transfer from the riser to the downer should be controlled.

13.4 Recommendations

I. The liquid and air tubing and distributers are recommended to be hooked in the system from the top of the columns to facilitate the maintenance

II. Fine bubble aeration is strongly recommended.

III. A full scale retrofitting of an existing conventional treatment tank is recommended based on TFBBR design principles

IV. Different media with different densities and specific surface area (SSA) should be tested in the system in order to find the best carrier media for this technology with a low density, high SSA and low price.

V. An anaerobic column divided into two compartments for denitrification and methanogenesis connected to an aerobic column is recommended for high rate biological nutrient removal from high strength wastewater.

Appendices

Appendix A. BET results of lava rock and natural zeolite

Full Report Set

ASAP 2010 V5.01 E Unit 1 Serial # 1 Page 26

Sample: Lava Rock
Operator: Yan
Submitter:
File Name: C:\ASAP2010\DATA\000-527.SMP

Started: 7/30/2009 2:19:58PM Analysis Adsorptive: N2
Completed: 7/30/2009 4:17:15PM Analysis Bath: 77.35 K
Report Time: 7/30/2009 4:19:07PM Thermal Correction: No
Sample Weight: 1.1120 g Smoothed Pressures: No
Warm Freespace: 27.5367 cm³ Cold Freespace: 87.9433 cm³
MEASURED
Equil. Interval: 5 secs Low Pressure Dose: None

Summary Report

Some summary reports could not be produced because they require the Micropore option.

Area

Single Point Surface Area at P/Po 0.22032806 :	0.4760	m²/g
BET Surface Area:	0.4834	m²/g
Langmuir Surface Area:	0.6832	m²/g
Micropore Area:	0.1534	m²/g
External Surface Area:	0.3300	m²/g
BJH Adsorption Cumulative Surface Area of pores between 17.000000 and 3000.000000 A Diameter:	0.4608	m²/g
BJH Desorption Cumulative Surface Area of pores between 17.000000 and 3000.000000 A Diameter:	0.9503	m²/g

Volume

Single Point Adsorption Total Pore Volume of pores less than 778.9670 A Diameter at P/Po 0.97450681:	0.001772	cm³/g
Micropore Volume:	0.000067	cm³/g
BJH Adsorption Cumulative Pore Volume of pores between 17.000000 and 3000.000000 A Diameter:	0.002816	cm³/g
BJH Desorption Cumulative Pore Volume of pores between 17.000000 and 3000.000000 A Diameter:	0.002746	cm³/g

Pore Size

Adsorption Average Pore Diameter (4V/A by BET):	146.6072	A
BJH Adsorption Average Pore Diameter (4V/A):	244.4491	A

Full Report Set

ASAP 2010 V5.01 E Unit 1 Serial # 1 Page 26

Sample: Natural Zeolite
Operator: Yan
Submitter:
File Name: C:\ASAP2010\DATA\000-528.SMP

Started: 7/31/2009 9:07:44AM Analysis Adsorptive: N2
Completed: 7/31/2009 1:21:45PM Analysis Bath: 77.35 K
Report Time: 7/31/2009 1:21:47PM Thermal Correction: No
Sample Weight: 0.7800 g Smoothed Pressures: No
Warm Freespace: 27.6535 cm³ Cold Freespace: 89.4633 cm³
MEASURED
Equil. Interval: 5 secs Low Pressure Dose: None

Summary Report

Some summary reports could not be produced because they require the Micropore option.

Area

Single Point Surface Area at P/Po 0.20055019 :	30.7011	m²/g
BET Surface Area:	31.5406	m²/g
Langmuir Surface Area:	43.4287	m²/g
Micropore Area:	4.9965	m²/g
External Surface Area:	26.5441	m²/g
BJH Adsorption Cumulative Surface Area of pores between 17.000000 and 3000.000000 A Diameter:	28.3575	m²/g
BJH Desorption Cumulative Surface Area of pores between 17.000000 and 3000.000000 A Diameter:	38.6623	m²/g

Volume

Single Point Adsorption Total Pore Volume of pores less than 659.0104 A Diameter at P/Po 0.96974600:	0.066416	cm³/g
Micropore Volume:	0.002040	cm³/g
BJH Adsorption Cumulative Pore Volume of pores between 17.000000 and 3000.000000 A Diameter:	0.078718	cm³/g
BJH Desorption Cumulative Pore Volume of pores between 17.000000 and 3000.000000 A Diameter:	0.084119	cm³/g

Pore Size

Adsorption Average Pore Diameter (4V/A by BET):	84.2287	A
BJH Adsorption Average Pore Diameter (4V/A):	111.0369	A

Appendix B. Process equations used in AQUIFAS APP

Process rate equations used in AQUIFAS APP adopted from ASM2d.

j	Process	Process rate equation ρ_j
Hydrolysis processes:		
1	Aerobic Hydrolysis	$K_h \cdot \frac{S_{O2}}{K_{O2}+S_{O2}} \cdot \frac{X_S/X_H}{K_X+X_S/X_H} \cdot X_H$
2	Anoxic Hydrolysis	$K_h \cdot \eta_{NO3} \cdot \frac{K_{O2}}{K_{O2}+S_{O2}} \cdot \frac{S_{NO3}}{K_{NO3}+S_{NO3}} \cdot \frac{X_S/X_H}{K_X+X_S/X_H} \cdot X_H$
3	Anaerobic Hydrolysis	$K_h \cdot \eta_{fe} \cdot \frac{K_{O2}}{K_{O2}+S_{O2}} \cdot \frac{K_{NO3}}{K_{NO3}+S_{NO3}} \cdot \frac{X_S/X_H}{K_X+X_S/X_H} \cdot X_H$
Heterotrophic organisms: X_H		
4	Growth on fermentable S_F,	$\mu_H \cdot \frac{S_{O2}}{K_{O2}+S_{O2}} \cdot \frac{S_F}{K_F+S_F} \cdot \frac{S_F}{S_F+S_A} \cdot \frac{S_{NH4}}{K_{NH4}+S_{NH4}} \cdot \frac{S_{PO4}}{K_P+S_{PO4}} \cdot \frac{S_{Alk}}{K_{Alk}+S_{Alk}} \cdot X_H$
5	Growth on fermentation S_A,	$\mu_H \cdot \frac{S_{O2}}{K_{O2}+S_{O2}} \cdot \frac{S_A}{K_A+S_A} \cdot \frac{S_A}{S_F+S_A} \cdot \frac{S_{NH4}}{K_{NH4}+S_{NH4}} \cdot \frac{S_{PO4}}{K_P+S_{PO4}} \cdot \frac{S_{Alk}}{K_{Alk}+S_{Alk}} \cdot X_H$
6	Denitrification with fermentable S_F,	$\mu_H \cdot \eta_{NO3} \frac{K_{O2}}{K_{O2}+S_{O2}} \cdot \frac{K_{NO3}}{K_{NO3}+S_{NO3}} \cdot \frac{S_F}{K_F+S_F} \cdot \frac{S_F}{S_F+S_A} \cdot \frac{S_{NH4}}{K_{NH4}+S_{NH4}} \cdot \frac{S_{PO4}}{K_P+S_{PO4}} \cdot \frac{S_{Alk}}{K_{Alk}+S_{Alk}} \cdot X_H$
7	Denitrification with fermentation S_A,	$\mu_H \cdot \eta_{NO3} \frac{K_{O2}}{K_{O2}+S_{O2}} \cdot \frac{K_{NO3}}{K_{NO3}+S_{NO3}} \cdot \frac{S_A}{K_A+S_A} \cdot \frac{S_A}{S_F+S_A} \cdot \frac{S_{NH4}}{K_{NH4}+S_{NH4}} \cdot \frac{S_{PO4}}{K_P+S_{PO4}} \cdot \frac{S_{Alk}}{K_{Alk}+S_{Alk}} \cdot X_H$
8	Fermentation	$q_{fe} \cdot \frac{K_{O2}}{K_{O2}+S_{O2}} \cdot \frac{K_{NO3}}{K_{NO3}+S_{NO3}} \cdot \frac{S_F}{K_F+S_F} \cdot \frac{S_{Alk}}{K_{Alk}+S_{Alk}} \cdot X_H$
9	Lysis	$b_H \cdot X_H$
Phosphorus-accumulating organisms (PAO): X_{PAO}		
10	Storage of X_{PHA}	$q_{PHA} \cdot \frac{S_A}{K_A+S_A} \cdot \frac{S_{Alk}}{K_{Alk}+S_{Alk}} \cdot \frac{X_{PP}/X_{PAO}}{K_{PP}+X_{PP}/X_{PAO}} \cdot X_{PAO}$
11	Aerobic Storage of X_{PP},	$q_{PP} \cdot \frac{S_{O2}}{K_{O2}+S_{O2}} \cdot \frac{S_{PO4}}{K_{PS}+S_{PO4}} \cdot \frac{S_{Alk}}{K_{Alk}+S_{Alk}} \cdot \frac{X_{PP}/X_{PAO}}{K_{PP}+X_{PP}/X_{PAO}} \cdot \frac{K_{MAX}-X_{PP}/X_{PAO}}{K_{PP}+K_{MAX}+X_{PP}/X_{PAO}} \cdot X_{PAO}$
12	Anoxic storage of X_{PP},	$\rho_{12} = \rho_{11} \cdot \eta_{NO3} \cdot \frac{K_{O2}}{S_{O2}} \cdot \frac{S_{NO3}}{K_{NO3}+S_{NO3}}$
13	Aerobic growth of X_{PHA},	$\mu_{PAO} \cdot \frac{S_{O2}}{K_{O2}+S_{O2}} \cdot \frac{S_{NH4}}{K_{NH4}+S_{NH4}} \cdot \frac{S_{PO4}}{K_P+S_{PO4}} \cdot \frac{S_{Alk}}{K_{Alk}+S_{Alk}} \cdot \frac{X_{PHA}/X_{PAO}}{K_{PHA}+X_{PHA}/X_{PAO}} \cdot X_{PAO}$
14	Anoxic growth of X_{PP},	$\rho_{14} = \rho_{13} \cdot \eta_{NO3} \cdot \frac{K_{O2}}{S_{O2}} \cdot \frac{S_{NO3}}{K_{NO3}+S_{NO3}}$
15	Lysis of X_{PAO},	$b_{PAO} \cdot X_{PAO} \cdot S_{ALK}/(K_{Alk}+S_{Alk})$
16	Lysis of X_{PP},	$b_{PP} \cdot X_{PP} \cdot S_{ALK}/(K_{Alk}+S_{Alk})$
17	Lysis of X_{PHA},	$b_{PHA} \cdot X_{PHA} \cdot S_{ALK}/(K_{Alk}+S_{Alk})$
Nitrifying organisms (Autotrophic organisms): X_{AUT},		
18	Aerobic growth of X_{AUT},	$\mu_{AUT} \cdot \frac{S_{O2}}{K_{O2}+S_{O2}} \cdot \frac{S_{NH4}}{K_{NH4}+S_{NH4}} \cdot \frac{S_{PO4}}{K_P+S_{PO4}} \cdot \frac{S_{Alk}}{K_{Alk}+S_{Alk}} \cdot X_{AUT}$
19	Lysis of X_{AUT},	$b_{AUT} \cdot X_{AUT}$

Appendix C. Kinetic parameters used in AQUIFAS APP

Definition and values for the kinetic parameters used in AQUIFAS APP adopted from ASM2d.

Temperature:		20°C	10°C	unit
Hydrolysis of particulate substrates: X_S				
K_h	= Hydrolysis rate constant	3.0	2.0	d^{-1}
η_{NO3}	= Anoxic hydrolysis reduction factor	0.6	0.6	---
η_{fe}	= Anaerobic hydrolysis reduction factor	0.4	0.4	---
K_{O2}	= Saturation/inhibition coefficient for oxygen	0.2	0.2	g O_2 m^{-3}
K_{NO3}	= Saturation/inhibition coefficient for nitrate	0.5	0.5	g N m^{-3}
K_X	= Saturation/inhibition coefficient for particulate COD	0.1	0.1	g X_S (g X_H)$^{-1}$
Heterotrophic organisms: X_H				
μ_H	= Maximum growth rate on substrate	5.0	3.0	g X_S (g X_H)$^{-1}$$d^{-1}$
q_{fe}	= Maximum rate for fermentation	3.0	1.5	g S_F (g X_H)$^{-1}$$d^{-1}$
η_{NO3}	= reduction factor for denitrification	0.75	0.75	---
b_H	= Rate constant for lysis and decay	0.4	0.2	d^{-1}
K_{O2}	= Saturation/inhibition coefficient for oxygen	0.2	0.2	g O_2 m^{-3}
K_F	= Saturation coefficient for growth on S_F	4.0	4.0	g COD m^{-3}
K_{fe}	= Saturation coefficient for fermentation of S_F	4.0	4.0	g COD m^{-3}
K_A	= Saturation coefficient for growth on acetate S_A	4.0	4.0	g COD m^{-3}
K_{NO3}	= Saturation/inhibition coefficient for nitrate	0.5	0.5	g N m^{-3}
K_{NH4}	= Saturation coefficient for ammonia	0.05	0.05	g N m^{-3}
K_P	= Saturation coefficient for phosphate	0.01	0.01	g P m^{-3}
K_{Alk}	= Saturation coefficient for alkalinity (HCO_3^-)	0.1	0.1	mole HCO_3^- m^{-3}
Phosphorus-accumulating organisms (PAO): X_{PAO}				
q_{PHA}	= Rate constant for storage of X_{PHA}	3.0	2.0	g X_{PHA}(g X_{POA})$^{-1}$ d^{-1}
q_{PP}	= Rate constant for storage of X_{PP}	1.5	1.0	g X_{PP}(g X_{POA})$^{-1}$ d^{-1}
μ_{PAO}	= Maximum growth rate of PAO	1.0	0.67	d^{-1}
η_{NO3}	= reduction factor for anoxic activity	0.6	0.6	---
b_{PAO}	= Rate for lysis of X_{PAO}	0.2	0.1	d^{-1}
b_{PP}	= Rate for lysis of X_{PP}	0.2	0.1	d^{-1}
b_{PHA}	= rate for lysis of X_{PHA}	0.2	0.1	d^{-1}
K_{O2}	= Saturation/inhibition coefficient for oxygen	0.2	0.2	g O_2 m^{-3}
K_{NO3}	= Saturation coefficient for nitrate	0.5	0.5	g N m^{-3}
K_A	= Saturation coefficient for acetate SA	4.0	4.0	g COD m^{-3}
K_{PS}	= Saturation coefficient for phosphate in storage of PP	0.2	0.2	g P m^{-3}
K_{NH4}	= Saturation coefficient for ammonia	0.05	0.05	g N m^{-3}
K_P	= Saturation coefficient for phosphate	0.01	0.01	g P m^{-3}
K_{Alk}	= Saturation coefficient for alkalinity (HCO_3^-)	0.1	0.1	mole HCO_3^- m^{-3}
K_{PP}	= Saturation coefficient for poly-phosphate	0.01	0.01	g X_{PP}(g X_{POA})$^{-1}$
K_{MAX}	= Maximum ratio of X_{PP}/X_{PAO}	0.34	0.34	g X_{PP}(g X_{POA})$^{-1}$
K_{IPP}	= Inhibition coefficient for PP storage	0.02	0.02	g X_{PP}(g X_{POA})$^{-1}$
K_{PHA}	= Saturation coefficient for PHA	0.01	0.01	g X_{PHA}(g X_{POA})$^{-1}$
Nitrifying organisms (Autotrophic organisms): X_{AUT}				
μ_{AUT}	= Maximum growth rate of X_{AUT}	0.1	0.35	d^{-1}
b_{AUT}	= Decay rate of X_{AUT}	0.15	0.05	d^{-1}
K_{O2}	= Saturation coefficient for oxygen	0.5	0.5	g O_2 m^{-3}
K_{NH4}	= Saturation coefficient for ammonia	1.0	1.0	g N m^{-3}
K_{Alk}	= Saturation coefficient for alkalinity (HCO_3^-)	0.5	0.5	mole HCO_3^- m^{-3}
K_P	= Saturation coefficient for phosphorus	0.01	0.01	g P m^{-3}

Appendix D. Diffusion coefficient for biofilm diffusional model

Diffusion coefficients for biofilm diffusional model used in the simulation.

Diffusion Rates	Substrate	Temperature (°C)	Value Units ($cm^2\ d^{-1}$)	Source
$D_{L,S}$ [a]	Acetate in water	20	1.09	Perry and Chilton (1973)
$D_{L,N}$	NH_4N in water	20	1.2	Chen et al. (1989)
$D_{L,DO}$	DO in water	20	1.6	Williamson and McCarty (1976)
$D_{L,NO2}$	NO_2N in water	20	1.4	Williamson and McCarty (1976)
$D_{L,NO3}$	NO_3N in water	20	1.4	Williamson and McCarty (1976)
$D_{L,S}$	Acetate in water	12	0.82	Perry and Chilton (1973)[b]
$D_{L,N}$	NH_4N in water	12	0.9	Perry and Chilton (1973)
$D_{L,DO}$	DO in water	12	1.42	Perry and Chilton (1973)
$D_{L,NO2}$	NO_2N in water	12	1.05	Perry and Chilton (1973)
$D_{L,NO3}$	NO_3N in water	12	1.05	Perry and Chilton (1973)

[a] Diffusion coefficients are considered 80% of the above values for water
[b] 75% of value at 20°C based on ratio of solubilities at 20°C and 12°C

Appendix E. Calculation of OLR and NLR based on biofilm surface area

Nitrogen and organic loading rates based on biofilm surface area in Twin Circulating Fluidized Bed Bioreactor (TCFBBR) and Anaerobic Fluidized-Circulating Fluidized Bed Bioreactor (AF-CFBBR)

Assumptions:

1. Biofilm-coated particles are spherical
2. The size of the bare particle is the average of the range size
3. Nitrification occurs just in the aerobic column
4. Denitrification occurs just in the anoxic column
5. 30% of particles in the dense phase of the aerobic columns do not develop biofilm
6. 30% of particles in the dense phase of the anoxic column do not develop biofilm
7. The organic loading rate is based on the both heterotrophic anoxic carbon removal and aerobic respiration

TCFBBR

Number of particles (Lava rock 850-1125 μm) based on particle weight and according to experiments (Shown in **Figure 8.2**):

$N=1.078\times10^{6}[M(kg)]$

Weight of particles in the aerobic column of TCFBBR =5.5 kg (**Table 3.2**)

Effective weight of the particles in the aerobic column of TCFBBR=3.85 kg

Effective number of particles in the aerobic column of TCFBBR:

$1.078\times10^{6}\times3.8\ kg=4\times10^{6}$ number

Average biofilm thickness in the aerobic column of TCFBBR (**Table 3.2**)=30

Average diameter of biofilm-coated particles in the aerobic column=

900 μm+2×60μm=960 μm

Effective surface area of a biofilm-coated particle in the aerobic column:

$=4\pi r^2=4\pi\times(480\mu m)^2=2.8\times10^{-6}\ [m^2]$

Total surface area of biofilm-coated particles in the aerobic column of TCFBBR=

$2.8\times10^{-6}\ [m^2]\times4\times10^6$ number$=11.2\ m^2$

Volumetric NLR in the TCFBBR=0.55 kg $N/m^3\cdot d$ (Total volume of TCFBBR=26 lit)

→ Nitrogen loading in TCFBBR=14.2 g N/d

→ Nitrogen loading rate based on surface area of nitrifiers biofilm=

14.2 [g N/d]/11.2[m^2]=**1.26 [g $N/m^2\cdot d$]**

Weight of particles in the anoxic column of TCFBBR =2.2 kg (**Table 3.2**)

Effective weight of the particles in the anoxic column of TCFBBR=1.54 kg

Effective number of particles in the anoxic column of TCFBBR:

$1.078\times10^6\times1.5$ kg$=1.6\times10^6$ number

Average biofilm thickness in the anoxic column of TCFBBR (**Table 3.2**)=280

Average diameter of biofilm-coated particles in the anoxic column=

900 μm+2×280μm=1460 μm

Effective surface area of a biofilm-coated particle in the anoxic column:

$=4\pi r^2=4\pi\times(730\mu m)^2=6.7\times10^{-6}\ [m^2]$

Total surface area of biofilm-coated particles in the anoxic column of TCFBBR=

$6.7\times10^{-6}\ [m^2]\times1.6\times10^6$ number$=10.7\ m^2$

Volumetric NLR in the TCFBBR=0.55 kg $N/m^3\cdot d$ (Total volume of TCFBBR=26 lit)

→ Nitrogen loading in TCFBBR=14.2 g N/d

→ Nitrogen loading rate based on surface area of denitrifiers biofilm=

14.2 [g N/d]/10.7[m^2]=**1.32 [g N/m^2·d]**

Volumetric OLR in the TCFBBR=5 kg COD/m^3·d (Total volume of TCFBBR=26 lit)

→ Organic loading in TCFBBR=130 g COD/d

→ Organic loading rate based on surface area of total biofilm=

130 [g COD/d]/(10.7+11.2)[m^2]=**5.9 [g COD/m^2·d]**

TFBBR

Number of particles (Lava rock 850-1125 μm) based on particle weight and according to experiments (Shown in **Figure 8.2**):

$N=1.078\times10^6$[M(kg)]

Weight of particles in the aerobic column of TFBBR =4.7 kg (**Table 3.2**)

Effective weight of the particles in the aerobic column of TCFBBR=3.29 kg

Effective number of particles in the aerobic column of TFBBR:

$1.078\times10^6\times3.3$ kg=3.55×10^6 number

Average biofilm thickness in the aerobic column of TFBBR (**Table 3.2**)=30

Average diameter of biofilm-coated particles in the aerobic column=

900 μm+2×25μm=950 μm

Effective surface area of a biofilm-coated particle in the aerobic column:

$=4\pi r^2=4\pi\times(475\mu m)^2=2.8\times10^{-6}\ [m^2]$

Total surface area of biofilm-coated particles in the aerobic column of TFBBR=

$2.8\times10^{-6}\ [m^2]\times3.55\times10^{6}$ number$=9.94\ m^2$

Volumetric NLR in the TFBBR=0.28 kg $N/m^3\cdot d$ (Total volume of TFBBR=32 lit)

→ Nitrogen loading in TFBBR=9 g N/d

→ Nitrogen loading rate based on surface area of nitrifiers biofilm=

9 [g N/d]/9.94[m^2]=**0.905 [g $N/m^2\cdot d$]**

Weight of particles in the anoxic column of TFBBR =2.2 kg (**Table 3.2**)

Effective weight of the particles in the anoxic column of TCFBBR=1.54 kg

Effective number of particles in the anoxic column of TFBBR:

$1.078\times10^{6}\times1.5$ kg$=1.6\times10^{6}$ number

Average biofilm thickness in the anoxic column of TFBBR (**Table 3.2**)=380

Average diameter of biofilm-coated particles in the anoxic column=

900 μm+2×380μm=1660 μm

Effective surface area of a biofilm-coated particle in the anoxic column:

$=4\pi r^2=4\pi\times(730\mu m)^2=8.6\times10^{-6}\ [m^2]$

Total surface area of biofilm-coated particles in the anoxic column of TFBBR=

$8.6\times10^{-6}\ [m^2]\times1.6\times10^{6}$ number$=13.7\ m^2$

Volumetric NLR in the TFBBR=0.28 kg $N/m^3\cdot d$ (Total volume of TCFBBR=32 lit)

→ Nitrogen loading in TCFBBR=9 g N/d

→ Nitrogen loading rate based on surface area of denitrifiers biofilm=

9 [g N/d]/13.7[m^2]=**0.65 [g N/m^2·d]**

Volumetric OLR in the TFBBR=2.8 kg COD/m^3·d (Total volume of TFBBR=32 lit)

→ Organic loading in TFBBR=90 g COD/d

→ Organic loading rate based on surface area of total biofilm=

90 [g COD/d]/(13.7+9.4)[m^2]=**3.9 [g COD/m^2·d]**

AF-CFBBR

Number of particles (Natural zeolite 610-1050 μm) based on particle weight and according to experiments (Shown in **Figure 8.2**):

$N=1.025\times10^6$[M(kg)]

Weight of particles in the aerobic column of CFBBR =2.7 kg (**Table 3.2**)

Effective weight of the particles in the aerobic column of CFBBR=1.89 kg

Effective number of particles in the aerobic column of CFBBR:

$1.025\times10^6\times1.89$ kg=1.93×10^6 number

Average biofilm thickness in the aerobic column of CFBBR (**Table 3.2**)=100

Average diameter of biofilm-coated particles in the aerobic column=

700 μm+2×100μm=900 μm

Effective surface area of a biofilm-coated particle in the aerobic column:

$=4\pi r^2=4\pi\times(450\mu m)^2=2.54\times10^{-6}$ [m^2]

Total surface area of biofilm-coated particles in the aerobic column of TCFBBR=

2.54×10^{-6} [m^2] $\times1.93\times10^{6}$ number=4.9 m^2

Volumetric NLR in the CFBBR=1.15 kg N/m^3·d (Total volume of TCFBBR=11.0 lit)

→ Nitrogen loading in TCFBBR=12.7 g N/d

→ Nitrogen loading rate based on surface area of nitrifiers biofilm=

12.7 [g N/d]/4.9[m^2]=**2.6 [g N/m^2·d]**

Weight of particles in the anoxic column of CFBBR =0.3 kg (**Table 3.2**)

Effective weight of the particles in the anoxic column of CFBBR=0.21 kg

Effective number of particles in the anoxic column of CFBBR:

$1.025\times10^{6}\times0.21$ kg=0.21×10^{6} number

Average biofilm thickness in the anoxic column of CFBBR (**Table 3.2**)=380

Average diameter of biofilm-coated particles in the anoxic column=

700 μm+2×380μm=1460 μm

Effective surface area of a biofilm-coated particle in the anoxic column:

$=4\pi r^2=4\pi\times(730\mu m)^2=6.7\times10^{-6}$ [m^2]

Total surface area of biofilm-coated particles in the anoxic column of CFBBR=

6.7×10^{-6} [m^2] $\times0.21\times10^{6}$ number=1.4 m^2

Volumetric NLR in the CFBBR=1.15 kg N/m^3·d (Total volume of CFBBR=11 lit)

→ Nitrogen loading in TCFBBR=12.65 g N/d

→ Nitrogen loading rate based on surface area of denitrifiers biofilm=

12.65 [g N/d]/1.4[m^2]=**9.03 [g N/m^2·d]**

Number of particles (Natural zeolite 425-610 μm) based on particle weight and according to experiments (Shown in **Figure 8.2**):

$N=5\times10^6[M(kg)]$

Weight of particles in the anaerobic column of AF-CFBBR =3 kg (**Table 3.2**)

Effective weight of the particles in the aerobic column of AF-CFBBR=2.1 kg

Effective number of particles in the anaerobic column of AF-CFBBR:

$5\times10^6\times2.1$ kg=10.5×10^6 number

Average biofilm thickness in the anaerobic column of AF-CFBBR (**Table 3.2**)=320

Average diameter of biofilm-coated particles in the anaerobic column=

500 μm+2×320μm=1240 μm

Effective surface area of a biofilm-coated particle in the anaerobic column:

$=4\pi r^2=4\pi\times(620\mu m)^2=4.8\times10^{-6}$ [m^2]

Total surface area of biofilm-coated particles in the anaerobic column of AF-CFBBR=

4.8×10^{-6} [m^2] $\times10.5\times10^6$ number=50.4 m^2

Volumetric OLR in the anaerobic column (AF) of AF-CFBBR=38 kg COD/m^3·d (Total volume of AF=16 lit)

→ Organic loading in AF=608 g COD/d

→ Organic loading rate based on surface area of total biofilm=

608 [g COD/d]/(50.4)[m^2]=**12.1 [g COD/m^2·d]**

In order to give a comparison of nitrification loading rate based on biofilm surface area, the following graph (Adopted from Black and Veach, AMERICANA 2011, Montreal, Canada) is presented. As shown in the graph the maximum nitrification loading with 90% nitrification efficiency is accomplished when the nitrogen loading is below 0.9 g $N/m^2.d$ where as the maximum nitrogen loading rate in this thesis was 0.9 to 2.6 g $N/m^2.d$ with more than 97% nitrification rate.

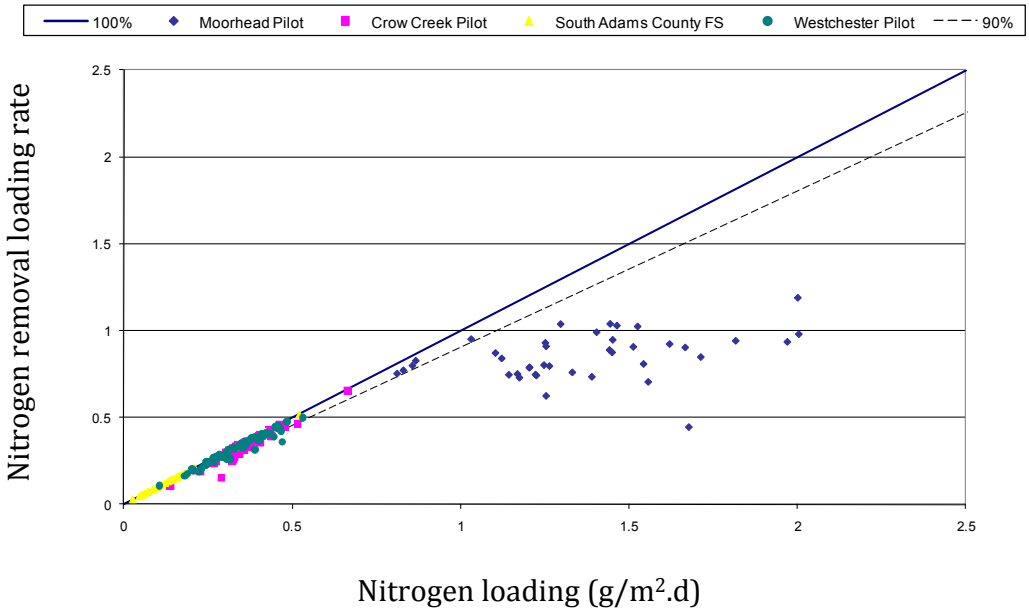

Figure adopted from Black and Veach, AMERICANA 2011, Montreal, Canada- NH3 loading versus Removal rate (g $N/m^2.d$) in MBBR systems.

Curriculum Vitae

Name: Mehran Andalib

Post-secondary Education and Degrees:

Sahand University of Technology
Tabriz, Iran
1995-1999 B.Sc.

Mazandaran University of Science and Technology
Babol, Iran
2000-2003 M.Sc.

The University of Western Ontario
London, Ontario, Canada
2008-2011 Ph.D.

Honours and Awards:

Ontario Graduate Scholarship for Science and Technology
2010-2011

The Ross and Jean Clark Scholarship
2010

The Graduate Thesis Scholarship 2011

Western Graduate Research Scholarship (WGRS)
2008-2011

Related Work Experience

Teaching Assistant
The University of Western Ontario
2008-2011

Technical Manager
IPT oil waste treatment co, Tehran, Iran
2003-2005

Publications:

1. Andalib M, Nakhla G and Zhu J-X, (2010) Dynamic testing of the twin circulating fluidized bed bioreactor (TCFBBR) for nutrient removal from municipal wastewater. Chemical Engineering Journal, 162(2), 616-625.

2. Andalib M, Nakhla G, Zhu J. (2010) Biological Nutrient Removal Using a Novel Laboratory-Scale Twin Fluidized-Bed Bioreactor. Chemical Engineering & Technology, 33 (7), pg. 1125-1136

3. Andalib M, Nakhla G, Zhu J. (2010) Terminal Settling Velocity and Drag Coefficient of Biofilm-Coated Particles at High Reynolds Numbers AIChE Journal Vol. 56, No. 10 2598-2606

4. Andalib M, Nakhla G, Sen D, Zhu J. (2011) Evaluation of Biological Nutrient Removal from Wastewater by Twin Circulating Fluidized Bed Bioreactor (TCFBBR) Using a predictive Fluidization Model and AQUIFAS APP. Bioresource Technology 102 (3), 2400-2410.

5. Eldyasti A, **Andalib M**, Hafez H, Nakhla G, Zhu J. (2010) Comparative Modeling of Biological Nutrient Removal from Landfill Leachate using a Circulating Fluidized Bed Bioreactor (CFBBR). (Accepted)

6. Andalib M, Nakhla G, McIntee E, Zhu J. (2010) Simultaneous methanogenesis and denitrification activity: An overview of two-decade research Submitted to Desalination

7. Andalib M, Zhu J, Nakhla G. (2010) Bed expansion index for biofilm coated particles. Submitted to Chemical Engineering Journal

8. Andalib M, Nakhla G, Zhu J. (2010) Simultaneous denitrification methanogenesis in a high rate biological nutrient removal fluidized bed. Submitted to ES&T

Conference Paper Presentations:

9. Andalib M, Nakhla G, Zhu J (2010) Nutrient Removal from Municipal Wastewater by Twin Circulating Fluidized Bed Bioreactor (TCFBBR)
Conference: Canadian Society of Chemical Engineering Conference, Saskatchewan, Canada

10. Andalib M, Eldayasti A, Nakhla, G, Zhu J. (2010). Modeling of Biological Nutrient Removal from Wastewater by Twin Circulating Fluidized Bed Bioreactor (TCFBBR) Using a predictive Fluidization Model and AQUIFAS APP. Second annual PTRC conference, London, Canada.

11. Eldyasti A, **Andalib M**, Hafez H, Nakhla G, Zhu J. (2010) Comparative Modeling of Biological Nutrient Removal from Landfill Leachate using a Circulating Fluidized Bed Bioreactor (CFBBR). WEFTECH 2011, LA California USA